

https://dspace.org/

Investigation into the magnitude and direction of ground stresses in the coalfields and their impact on safety and productivity

Muaka, Joseph Justin Mbenza

2013-07-19
http://hdl.handle.net/10539/12854

Downloaded from a DSpace repository. https://dspace.org/

INVESTIGATION INTO THE MAGNITUDE AND DIRECTION OF GROUND STRESSES IN THE COALFIELDS AND THEIR IMPACT ON SAFETY AND PRODUCTIVITY

Joseph Justin Mbenza Muaka

A research report submitted to the Faculty of Engineering and the Built Environment, University of the Witwatersrand, in fulfillment of the requirements for the degree of Master of Science in Engineering

Johannesburg, 2013

Declaration

I _____ (Student number: _____) am a student registered for _____ in the year _____. I hereby declare the following:

- I am aware that plagiarism (the use of someone else's work without their permission and/or without acknowledging the original source) is wrong.
- I confirm that the work submitted for assessment is my own unaided work except where I have explicitly indicated otherwise.
- I have followed the required conventions in referencing the thoughts and ideas of others.
- I understand that the University of the Witwatersrand may take disciplinary action against me if there is a belief that this is not my own unaided work or that I have failed to acknowledge the source of the ideas or words in my writing.

Signature: _____ Date: _____

Abstract

In situ stress is an important input for design in rock mechanics. It is often used as the boundary condition in numerical modeling. In coal mines, and particularly South African coal mines, stress has been granted very little attention. As a result, mine layouts have been designed with little consideration of stress. However instances of stress related falls of ground which lead to injuries, fatalities and production losses are reported.

The present study, through site visits and direct roof observations, has assisted in quantifying the impact of stress in the Witbank and Highveld coalfields. It was found that some mines experience severe stress-related problems. A hazard map was created based on observations and results of in situ stress measurements carried out in the Witbank and Highveld coalfields. This hazard map is intended to be used for estimating the potential of stress related problem in absence of accurate stress measurements.

A NNW-SSE direction of major horizontal compressive stresses was found to be consistent across the two coalfields, although a change to a NE-SW direction was also observed in the north-eastern part of the Witbank (Arnot Colliery). This change in stress direction was confirmed by both in situ stress measurements and underground mapping. While this change in direction has been attributed to local effects such as the presence of surrounding opencast mines or major structures (faults and dyke), this study has shown that the propagation southward of the east African rift can also be the cause.

Numerical modelling was carried out to demonstrate how ground stress is generated by geological processes such as erosion and sedimentation. Results of this analysis were found to correlate well with the in situ stress measurements. Therefore, it was concluded that the actual stress regime across the Witbank and the Highveld coalfields is the result of a complex process of erosion and sedimentation. Numerical modelling and observation have also confirmed that the k-ratio (horizontal stress) increases with the depth of weathering and that isopach maps of weathering can be used in prediction of stress related problem.

Various mitigating techniques are being used in the Witbank and Highveld coalfields to combat deleterious effects of horizontal stress. As part of this study, the reduction of the cutout distance, and the undercutting technique have been modeled in detail using a finite element

software package (Phase2). It was found that these mitigating techniques are more efficient for lower k-ratios than higher k-ratios. Therefore, they are expected to work better when mild stress problems are experienced rather than severe ones.

Acknowledgements

I am so grateful to God my creator and my redeemer for having ordered my steps until now. He gave me the strength that I needed to complete this research and stand firm in presence of adversities and discouragement.

I offer my profound gratitude to my supervisor, Professor Nielen van der Merwe for his guidance and advice. I also thank, from the bottom of my heart, Professor Thomas Richard Stacey for the review of this research report and his constructive criticism. I attribute the level of my Master's degree to their effort and without them this research report would not have been completed.

My sincere gratitude goes to the Coaltech committee, in particular to Mr. Johann Beukes for having entrusted me with such an important project and having financed this Master's degree.

This Master's degree is also the result of encouragement and managerial skills of Mr. David Minney who has coordinated all the site visits and aided me throughout the collection, analysis and interpretation of data without imposing on me a preconceived opinion.

Mr Alan Naismith, Partner at the geotechnical (Mining) department at SRK Consulting, is acknowledged for having proposed my name to Coaltech as a suitable candidate for the project. He is also thanked for his review and recommendations.

In the numerical modelling part of the project, SRK's licenses have been used and I have been very much aided by Thandile Dlokweni who taught me the basics of the finite difference analysis code, FLAC 3D.

During the site visits, I was led underground by Rock Engineers: Duncan Lees, Lelanie Prinsloo, Ernest Wevell, Wikus Mahne and Sandor Petho.

Beyond Rock engineering, I am grateful to my sister, Dr. Marie Mbenza Sukama, who has financed my coming to South Africa together with my Graduate Diploma in Engineering (GDE) at Wits University. I am also grateful to my Aunt and her husband, Seraphine and Ambroise Walemba, for having accommodated me in their home with care and affection during the time of my studies.

I would like to dedicate this report to my beloved wife Lilian Mariita, my handsome son John and my beautiful daughter Juliana for the love, stability and comfort that they bring into my life. You guys rock my world

TABLE OF CONTENTS

Declaration ..... **i**

Abstract ..... **ii**

Acknowledgements ..... **iv**

List of Figures ..... **x**

List of Tables ..... **xvi**

List of symbols ..... Error! Bookmark not defined.

List of Acronyms ..... **xix**

CHAPTER 1 ..... **1**

1. Introduction **1**
1.1 Background 1
1.2 Definition of the problem 1
1.3 Objectives 3
1.4 Methodology 4
1.5 Content of the report 5

CHAPTER 2 ..... **6**

2. Geology of the Witbank and Highveld Coalfields **6**
2.1 Coalfields 10

2.1.1 Coal Seams in the Witbank Coalfield 11

2.1.2 Coal seams in the Highveld Coalfield 12

2.2 Structural geology 12

CHAPTER 3 ..... **16**

3. Review of stress effects at shallow depth **16**
3.1 Survey of stress effects at shallow depth 16

3.1.1 United States of America 16

3.1.2 Australia 20

3.1.3 Horizontal shortening of the Roof under the influence of horizontal stress 25

3.1.4 Low Stress “Plug” Falls 26

3.1.5 Mid-Angled Discontinuities 27

3.1.6 South Africa 28
3.2 Review of theory related to stress origin 35
3.2.1 Poisson's effect Theory 35
3.2.2 Tectonic Stress Theory 36
3.3 Origin of in-situ stress in Southern Africa 36
3.3.1 Residual Stress Theory 39
3.3.2 Horizontal stress generated by magmatic intrusion 43
3.4 Influence of weathering 43
3.4.1 Theoretical model 43
3.4.2 Evidence of impact of weathering on Horizontal stress 50
3.5 Influence of topography 53
3.5.1 Hilly district formed by erosion 53
3.5.2 Hilly district formed by sedimentation 55
3.5.3 Basin formed by erosion 56
3.5.4 Basin filled by sedimentation 63
3.6 Induced stress around Mine excavations 67
3.6.1 Model set up 68
3.6.2 In situ stress 68
3.6.3 Material Properties 69
3.6.4 Results 69
3.7 Conclusion 73
CHAPTER 4 75
4. Coal Mining methods and their influence on stress 75
4.1 Generalities on Mining Methods 75
4.2 Mining method classification 76
4.3 Impact of mining method on stress 77
4.4 Mining methods used in the Witbank and Highveld 78
4.4.1 Bord and Pillar mining 79
4.4.2 Longwall Mining 82

4.5 Pillar extraction (stooping) 91
4.6 Multiple seam mining 97
4.7 Conclusion 98

CHAPTER 5 99

5. Review of stress data 99
5.1 Data Collected from Witbank and Highveld Collieries 99

5.1.1 In situ stress measurements 100

5.1.2 Stress Observation at Arnot Coal (Exxaro) 109

5.1.3 Analysis of data from Arnot Colliery 117

5.1.4 Stress Observation at Kenako shaft (AngloCoal) 123

5.1.5 Stress Observation at Brandspruit Colliery (Sasol South Africa) 131

5.1.6 Analysis of data from Sasol 135

5.1.7 Stress Observation at Coal of Africa (Mooiplaats) 147

5.1.8 Stress Observation at Khutala Colliery (BHP Billiton) 155

5.1.9 Stress Observation at Boschmans Colliery (Xstrata Coal) 157

5.1.10 Stress observation at Forzando (Total SA) 161

5.2 Review of stress measurement data 161

5.2.1 Description of stress measurement data 161

5.2.2 Validation and subjective quantitative grading of stress measurement data 174

5.3 Analysis of the stress measurement data 184

5.3.1 Stress Index 184

5.3.2 Correlation with depth 188

5.3.3 Correlation with topography 194

5.3.4 Topography of the Witbank and Highveld Coalfields 194

5.3.5 Analysis of the correlation between the stress orientations and the topography surface 196

5.3.6 Correlation with structural geology 201

5.3.7 Correlation with in situ stress measurement data from elsewhere 203

5.4 Review of stress mitigation strategies employed in the Coalfields 206
5.4.1 Increase roof bolt density 207
5.4.2 Change mechanical anchor bolts to full column resin grouted roof bolts 207
5.4.3 Changed orientation of the panel with respect to the orientation of the major horizontal 208
5.4.4 Sacrificial road 210
5.4.5 Use of a slot cut in the roof 210
5.4.6 Undercutting 210
5.4.7 Change of mining parameters 216
5.5 Conclusion.....221
CHAPTER 6 222
6. Conclusions and Recommendations 222
7. References 226
Appendix A Coalfields stress database 234
Appendix B Sasol Guttering database 239

List of Figures

Caption Page

Figure 2-1 Map showing the spatial position of the Witbank and Highveld coalfields.....7
Figure 2-2 Areal distribution (schematic) of lithostratigraphic units in the Main Karoo Basin modified (modified after Johnson et al., 1997) 8
Figure 2-3 Generalised stratigraphy and lithology of the Karoo Supergroup in the Main Karoo Basin (modified after Johnson et al., 1997) 9
Figure 2-4 Regional scale geological map showing position of dykes (after du Plessis 2008).....14
Figure 3-1 FLAC 3D results showing the spatial distribution of gutters in a simulated development layout. The Figure also indicates that direction of gutters (in dark blue) varies with the position where they occur within the Layout but that there is a general trend oriented perpendicular to the direction of the major horizontal Stress (SHmax) (Estherhuizen et al, 2008).....18
Figure 3-2 Roof guttering at a roof-pillar contact (Esterhuizen et al, 2008) 19
Figure 3-3 Horizontal stress induced failure between two pillars, arrows indicate the orientation of maximum horizontal stress (Esterhuizen et, 2008).....20
Figure 3-4 Large oval-shaped fall into the weaker overlying strata in a limestone mine (Esterhuizen et al, 2008) 20
Figure 3-5 Chart showing the time dependent behaviour of a static roof (Adams, 2002) ...22
Figure 3-6 Picture showing a buckling roof at Kenako shaft in South Africa 23
Figure 3-7 Chart showing variation of Load bearing capacity of an Euler beam versus vertical displacements for different beam thicknesses 24
Figure 3-8 Chart illustrating the variation of Load bearing capacity with vertical displacement at different values of eccentricities 25
Figure 3-9 Figure illustrating shortening of the roof with on-going displacement and low angle shearing across individual beds (Adams, 2002) 26
Figure 3-10 Sketch illustrating the formation of a low angled shear crack as the roof buckles (Adams, 2002) 26
Figure 3-11 Sketch illustrating Mid-Angled Discontinuities mechanism (Adams, 2002) 27
Figure 3-12 Graph of FOS vs. Roadway width.....28
Figure 3-13 Diagram showing mechanism of roof failure due to shear, the colours and the size of the arrows denote the magnitude of horizontal stress and displacements (Alan et al 2003).....30
Figure 3-14 Diagram showing failure mechanism when high horizontal stress is combined with a slip (Alan et al 2003).....32
Figure 3-15 map showing the configuration of tectonic plates as is today and the East Africa rift (Unkown 2010).....36
Figure 3-16 Map illustrating the anticipated configuration of tectonic plates 100 Ma into the future, NE movement of the Africa plate, The Euler pole and the NNW direction of the Wegner stress (Unknown 2010) 37
Figure 3-17 Anderson theory for determining orientation of rock stress.....38
Figure 3-18 Phase 2 model used to investigate the influence of erosion on the k-ratio 39
Figure 3-19 Graph illustrating how the k-ratio varies with depth on erosion.....40
Figure 3-20 Graph showing variation of k-ratio on sedimentation 41
Figure 3-21 Graph illustrating k-ratio versus depth for both sedimentation and erosion.....42
Figure 3-22 Elasto-plastic curves of k-ratio as a function of depth at a lateral pressure of 2 MN/m^2 and at a corresponding weathering depth of 40 m 46

Figure 3-23 Graph showing that increasing the depth of weathering implies an increase of lateral pressure 47
Figure 3-24 Graph showing how increase of lateral pressure leads to a corresponding increase of the weathering depth while keeping the maximum value of the stress-ratio unchanged 48
Figure 3-25 Figure illustrating the relationship between the depth of weathering and the Lateral Pressure for different values of friction angle of intact rock 49
Figure 3-26 Graph showing trend of K-ratios with the strength (friction) of the intact rock 49
Figure 3-27 Figure illustrating the elasto-plastic curves obtained by numerical modeling and analytically for a weathering depth of 40 m and a lateral pressure of 2MPa 50
Figure 3-28 Picture showing the site on the road to Bethal where a stress induced buckling in a shale layer was observed 51
Figure 3-29 Pictures illustrating measurement of dip direction with a compass 51
Figure 3-30 Probability density function of dip direction showing the extent of 95% confidence interval 52
Figure 3-31 Model geometry of the hilly district model (100 m high hill) 53
Figure 3-32 Stage 1 of the Hilly district Phase 2 model showing the mesh element density and boundary conditions 54
Figure 3-33 Stage 2 of the hilly district Phase 2 model 54
Figure 3-34 Contours of k-ratio after formation of the hilly district by erosion (100 m hill) 55
Figure 3-35 Contours of k-ratio after formation of the hilly district by sedimentation (100 m hill) 55
Figure 3-36 Contours of K-ratio for a basin width equal to 100 m 57
Figure 3-37 Contours of K-ratio for a basin width equal to 200 m 58
Figure 3-38 Contours of K-ratio for a basin width equal to 300 m 59
Figure 3-39 Contours of K-ratio for a basin width equal to 400 m 60
Figure 3-40 Profiles of k-ratio along the bottom of the basin 10 m below surface 62
Figure 3-41 Figure illustrating the maximum k-ration as a function of width of erosion 63
Figure 3-42 Figure illustrating k-ratio contours around a basin filled by sediments 64
Figure 3-43 Profiles of k-ratio along the bottom of the basin 10 m below surface (sedimentation) 66
Figure 3-44 Figure illustrating the maximum k-ratio as a function of width of sedimentation 66
Figure 3-45 Concentration of horizontal stress in the immediate roof 70
Figure 3-46 contours of σ1 around circular and horse shoe excavations for k-ratio of one and two 70
Figure 3-47 contours of σ1 around square and square with rounded corners excavations for k-ratio of one and two 71
Figure 3-48 contours of σ1 around circular, horse shoe, square and square with rounded corners excavations for k-ratio of four 71
Figure 3-49 Graph of horizontal stress in the immediate roof for different excavation shapes and k-ratio 72
Figure 3-50 Contours of vertical stress and its concentration in sidewalls 72
Figure 4-1 Infrastructures of a typical underground mine (Coal Mine.Art 2011) 76
Figure 4-2 Modified Scheme of coal mining method classification (after Galvin 1981) 77
Figure 4-3 Contribution of the different underground mining method to the total South African underground coal production (after Dougall 2009) 79

Figure 4-4 Typical multiple roadways longwall mining illustrating the chain pillar loading cycle (after Colwell et al 1999) 83
Figure 4-5 three dimensional representation of stress distribution around a longwall panel (after Whittaker 1974) 84
Figure 4-6 MINSIM model used to analyse the stress distribution around a longwall panel 85
Figure 4-7 Two and three dimensional plots showing the vertical stress in the hanging wall of a longwall panel as obtained following a MINSIM analysis 87
Figure 4-8 Graph illustrating angle between the major principal stress and roadway direction (after Gale and Blackwood 1987) 88
Figure 4-9 Conceptual curves of stress as a function of face advance (after van der Merwe and Madden 2010) 90
Figure 5-1 Regional location of Arnot Coal Mine 110
Figure 5-2 Typical stratigraphic Column at Arnot Coal Colliery 112
Figure 5-3 Plan showing the layout of 10 shaft at Arnot Colliery, the red arrows show the direction of the major horizontal stress and the blue ones the mining direction 114
Figure 5-4 Plan showing the layout of 8 Shaft at Arnot Colliery, the red arrows show the direction of the major horizontal stress and the blue ones the current mining direction 115
Figure 5-5 Plan showing occurrences of guttering in a section at Arnot, shaft 8 116
Figure 5-6 Rosette showing the direction of the maximum horizontal stress inferred from the direction of guttering at Arnot 117
Figure 5-7 Stereonet of strike direction of joints at Ptn 13, Arnot 118
Figure 5-8 Probability distribution of stress Magnitude at Arnot 119
Figure 5-9 Picture showing the tip of a gutter observed at a rib side at Arnot Colliery and how the guttered mudstone roof was re-supported by roof bolts 121
Figure 5-10 Picture showing guttering at Arnot Colliery and how metal straps are used in tandem with roof bolts in order to prevent the guttered roof from peeling off 122
Figure 5-11 Picture showing the tension failure on one side of a guttering in the mudstone roof at Arnot and how it is re-supported by straps and roof bolts after guttering 122
Figure 5-12 Regional location of Kenako shaft 124
Figure 5-13 Typical stratigraphic Column at Kenako Shaft, AngloCoal 126
Figure 5-14 Plan showing the layout of Kenako shaft at Greenside Colliery, the red arrows show the direction of the major horizontal stress as measured in the inclined shaft and in section 50/51 127
Figure 5-15 Picture showing a Multiple splits guttering at Kenako shaft resulting from a progressive slabbing of the laminated roof. Note that the bolts are still in place and do not seem to have been bent 129
Figure 5-16 Picture illustrating the principal failure mechanism of the roof at kenako, the weathered mudstone roof peels off progressively between the bolts 129
Figure 5-17 Picture showing a typical buckling of the mudstone roof and the low angled shear crack associated with it 130
Figure 5-18 Picture showing a guttered mudstone roof being re-supported with mine pole, strap and roof bolts 130
Figure 5-19 Picture showing mudstone roof being supported by w-straps and roof bolts in tandem, the roof seems to be quite stable 131

Figure 5-20 Regional location of Secunda and Brandspruit shaft 132
Figure 5-21 Map showing location of Brandspruit in Secunda 133
Figure 5-22 Typical stratigraphic Column of the Highveld Coalfield 134
Figure 5-23 Microsoft excel database built based on document 6 139
Figure 5-24 Filtered table constructed in order to determine the probability of stress effects when dyke and river are both present.....141
Figure 5-25 number of observations and number of guttering and floor heave per mine .142
Figure 5-26 Roof composition derived from the database at Bosjesspruit (left) and Brandspruit (right) 142
Figure 5-27 Probability of occurrence of guttering and floor heave per mine 143
Figure 5-28 graph illustrating number of observations, number of stress related problems and their probability of occurrence per roof type 144
Figure 5-29 Pie chart showing the number of occurrences that have failed within hours per roof type (left) and graph of probability of failure (right) 145
Figure 5-30 Pie chart showing the number of occurrences that have failed within days per roof type (left) and graph of probability of failure (right) 145
Figure 5-31 Pie chart showing the number of occurrence that have failed within years per roof type (left) and graph of probability of failure (right) 146
Figure 5-32 Regional location of Mooiplaats Colliery 148
Figure 5-33 Typical stratigraphic Column of Ermelo coalfield and Mooitplaats Colliery (after Greenshields, 1986).....149
Figure 5-34 Plan showing the layout of Mooiplaats Colliery 151
Figure 5-35 Mine Layout of Mooiplaats colliery showing guttering occurrences.....152
Figure 5-36 Guttering in a laminated Sandstone roof supported by a tandem roof bolt and metal straps at Mooiplaats 153
Figure 5-37 Picture showing the tip of guttering in a laminated Sandstone roof which is being re-supported by straps and roof bolts 154
Figure 5-38 Picture illustrating the used of cable anchor in addition to roof bolts and metal straps.....154
Figure 5-39 Regional location of Khutala colliery 156
Figure 5-40 Regional location Boschmans Colliery 158
Figure 5-41 Picture of a dyke and the way it is being supported by W-straps and roof bolts at Boshmans shaft (X-Strata Coal) 159
Figure 5-42 Picture of a coal face and the roof in the vicinity of a dyke at Boshmans Shaft (X-strata Coal) 160
Figure 5-43 Picture showing the dyke visited at Boshmans and the presence of dripping water in the roof (X-Strata Coal) 160
Figure 5-44 Pie showing the repartition of stress measurements by coal seam.....162
Figure 5-45 Plan showing orientation of major horizontal stress and results of mapping carried out at Arnot and Mooiplaats. Red arrows show the major horizontal stress and the rose diagrams give the results of the underground mapping. ...164
Figure 5-46 Map showing ratios of major horizontal stress to vertical stress (k1) 166
Figure 5-47 Map showing ratios of major to minor horizontal stress (K1/K3) 167
Figure 5-48 Graph illustrating variation of the major horizontal to vertical stresses ratios by collieries where in situ stress measurement were conducted 168
Figure 5-49 Polar Stereonet illustrating direction of principal stress obtained from stress measurement data.....170
Figure 5-50 Plot box summarizing stress measurement data 171
Figure 5-51 Statistical summary of magnitude of principal stress obtained from stress measurement data 172

Figure 5-52 Comparison of near vertical stresses calculated from overburden density (2500 MN/m^3) and measured in situ 174
Figure 5-53 Repartition of stress measurement included in the data set according to grade 175
Figure 5-54 Cumulative frequency curves versus deviation from average stress (Grade C) 178
Figure 5-55 Cumulative frequency curves versus deviation from average stress (Grade B) 179
Figure 5-56 Cumulative frequency curves versus deviation from average stress (Grade E) 180
Figure 5-57: Cumulative frequency curves versus deviation from average stress (Grade A) 181
Figure 5-58: Cumulative frequency curves versus deviation from average stress (Grade B) 182
Figure 5-59 Cumulative frequency curves versus deviation from average stress (Grade D) 183
Figure 5-60 Pie Chart showing repartition of group grade within the coal stress database 184
Figure 5-61 Contour map of stress indices in the Witbank and Highveld Coalfields 186
Figure 5-62 3D distribution of the stress index contours 188
Figure 5-63 Scatter plot of ratios of major horizontal stresses to vertical stress (K1) versus depth 189
Figure 5-64 Scatter plot of ratios of minor horizontal stresses to vertical stress (K3) versus depth 189
Figure 5-65 k-ratio versus depth graphs comparing the stress measurements with the sedimentation and erosion theoretical models 190
Figure 5-66 Plot of K1 ratios versus Vertical Stress 190
Figure 5-67 Trendline of K1 ratios function of vertical stress after removing an outlier 191
Figure 5-68 Regression line of maximum horizontal stresses versus depth 193
Figure 5-69 Surfer plot of the Topography of Witbank, Highveld and the surrounding regions derived from SRTM data. The size of bubbles on the map indicate magnitude of major horizontal stress 195
Figure 5-70 Surfer 3-dimensional surface of the topography of Witbank, Highveld and their surroundings 196
Figure 5-71 Map showing Major Horizontal stress direction and magnitude on the shaded relief map of the Witbank and Highveld 197
Figure 5-72 Elevations versus Stress Index 198
Figure 5-73 Graph showing correlation between elevation and stress index 198
Figure 5-74 Graph showing correlation between stress index and elevation 199
Figure 5-75 Hazard map as derived from topographical information and underground observations 200
Figure 5-76 Map showing direction and magnitude of SHmax on a structural geology map (after the Andreoli, 2011) 202
Figure 5-77 Map showing directions of principal horizontal stresses when combining data from Stacey and Wesseloo (in blue) with in situ stress data collected in the Witbank and Highveld Coalfield (in green) 204
Figure 5-78 Histogram and cumulative frequency curve of major horizontal stress directions in the North East region 205
Figure 5-79 Histogram of major horizontal stress directions in the South west region 206

Figure 5-80 Picture showing guttering in a thick laminated roof and the support system composed of roof bolts and straps used to mitigate the hazard 208
Figure 5-81 Map showing ratios of major to minor horizontal stress (K1/K3) 209
Figure 5-82 Phase2 Model set up to analyse effect of undercutting.....213
Figure 5-83 graph showing number of yielded elements versus k-ratio in the immediate roof 214
Figure 5-84 Results of the Phase2 undercutting Model.....215
Figure 5-85 Tunnel wall displacements as a function of distance from the face (after Hoek 1999).....218
Figure 5-86 Numerical modeling result showing wall (roof) displacement (m) as a function of % of field stress 219
Figure 5-87 Graph showing number of yielded element in the roof versus k-ratios at a distance of 3 m from the face and 15 m from the face 220

List of Tables

Caption Page

Table 2-1 Summary of the regional scale trend relationships relating dykes, sills or lineaments in the Witbank Coalfield (du Plessis 2008) 13
Table 3-1 Summary of the parameters used in the erosion model 39
Table 3-2 Summary of parameters used in the numerical and theoretical analysis 45
Table 3-3 Summary of dip direction measurements 52
Table 3-4 Summary of parameters used in the analysis 54
Table 3-5 Summary of excavation dimensions 68
Table 4-1 Summary of parameters and material properties used in the longwall stress analysis 86
Table 5-1 Summary of principal stress components at Arnot Coal Mine 101
Table 5-2 Summary of Horizontal and vertical stress component at Arnot 101
Table 5-3 Summary of principal stress components at Goedehoop Colliery 102
Table 5-4 Summary of principal stress components at Bank Colliery 102
Table 5-5 Summary of principal stress components at Nooitgedacht (today Kenako) 102
Table 5-6 Summary of Horizontal and vertical stress components at Goedehoop Colliery 103
Table 5-7 Summary of Horizontal and vertical stress components at Bank Colliery 104
Table 5-8 Summary of Horizontal and vertical stress components at Greenside (Nooitgedacht today Kenako shaft) 104
Table 5-9 Summary of principal stress component at Bosjesspruit 106
Table 5-10 Summary of Horizontal and vertical stress components at Bosjesspruit 107
Table 5-11 Summary of principal in-situ stress at Khutala Colliery 108
Table 5-12 Summary of principal horizontal stress at khutala Colliery 108
Table 5-13 Summary of coefficient of variation of k-ratios per colliery 168
Table 5-14 Grading system for individual stress measurement after Stacey and Wesseloo (1998) 175
Table 5-15 Summary of Multiple Regression Statistics using Cartwright formula 192
Table 5-16 Summary of material properties used in the numerical modeling 212

List of Symbols

No X seam	X^{th} coal seam counted from bottom up
Ga	1 billion years
Ma	1 Million years
N	North
S	South
E	East
W	West
P	Euler beam end-load (MN/m^2)
e	eccentricity (m)
I	Moment of Inertia (m^4)
E	Young's Modulus (GPa)
u	Lateral displacement (m)
L	Length of the beam (m)
FOS	Factor of Safety
σ_{bc}	Magnitude of maximum stress occurring at the ends of a beam (MPa)
γ	Unit weight (MN/m^3)
t	beam thickness (m)
σ_v	Vertical stress component (MPa)
σ_h	Horizontal stress component (MPa)
ν	Poisson's ratio
σ_1	Major principal stress (MPa)
σ_2	Intermediate principal stress (MPa)
σ_3	Minor principal stress (MPa)
K1	ratio of major horizontal to vertical stress
K3	ratio of minor horizontal to vertical stress
ΔZ	depth of erosion, sedimentation
Z	depth at which stress measurement is taken
C	Lateral Pressure (MPa)
H	depth (m) or mining height
Ø	Friction angle (°)
Φ	Friction angle (°), goaf angle (°)

CoV, CV	Coefficient of variation
L_c	Critical mining span
D	Depth of dolerite base
h	Pillar height
S_1	in situ coal strength
x	distance from the nearest rib
P	thickness of partings between coal seams
Std, Stdev	Standard deviation
Sx, Sy, Sy	component of stress parallel to x, y and z direction
R^2	Regression coefficient

List of Acronyms

SRTM	Shuttle Radar Topographical Mission
HGT	Shuttle Radar Topographical Mission files extension
HDR	Header files extension
DEM	Digital Elevation Model
ULXMAP	Upper-left pixel Coordinate Reference System X coordinates
ULYMAP	Upper-left pixel Coordinate Reference System Y coordinates
COP	Code of Practice
RMT	Rock Mechanics Technology

CHAPTER 1

Introduction

1.1 Background

Coaltech is a collaborative initiative in the South African coal industry between the minerals and energy industries, labour, the government, universities and research organisations. Its initiative is to develop technology and apply research findings in the Witbank and Highveld coalfields that will enable the South African coal industry to remain competitive, sustainable and safe well into the 21st century. As part of the Coaltech research programme, the working committee initiated a project into the investigation into the magnitude and direction of ground stresses in the Witbank and Highveld Coalfields.

Stress is a natural but intangible phenomenon which predates any mining activities. The vertical component of stress results largely from the mass of strata overlying mining workings. Horizontal stress components result from a combination of natural rock elasticity (the Poisson effect and tectonic forces). Both components of stress are modified during mining activities. When any stress component exceeds the strength of the rock mass in which it exists, rock failure occurs. Failure results in scaling of the sidewalls of excavations and pillars and fracture of roof strata with associated falls of ground. An understanding of the stress regimes present in a mining environment will facilitate the development of amelioration strategies to improve safety and productivity.

1.2 Definition of the problem

In situ stress is an important input for design in rock mechanics. It is often used as the boundary condition in numerical modeling. In the coal mines, and particularly the coal mines in South Africa, stress has hitherto been granted very little attention. Therefore, mine layouts have been designed with little consideration of stress, although stress induced falls of ground (guttering) are causing injuries, fatalities and production losses.

The Witbank and Highveld coalfields are major contributors to South African coal production. Both coalfields have been extensively mined out over the past 100 years and their resources have been depleted drastically. In order to prolong the production of these two valuable coalfields well into the 21st century, high extraction methods such as pillar

extraction are contemplated together with various methods aiming at extracting coal in challenging conditions. In this regard, reliable in situ stress data is an important part of the design process.

The World Stress Map project (WSM) provides a vital source of ground stress across the world. However, there were not enough measurements coming from the Witbank and Highveld coalfields included in the database from which reliable in situ stress estimation can be derived. The lack of reliable ground stress data in virtually all the southern Africa region motivated Wesseloo and Stacey (2006) to create a stress database based on stress measurements and observations conducted on various civil engineering and mining projects. The present study was aimed at upgrading this existing database with more stress measurement data and observations from the Witbank and Highveld coalfields.

1.3 Objectives

This research project has been based on existing information and evaluates and collates stress measurements and other observations to provide a visual representation of stress fields existing in the Witbank and Highveld Coalfields together with a qualitative assessment of the impact on safety and productivity. The scope of work was as follows:

Site visits:

Introduction and exposure of the postgraduate student to practical coal mining and ground stress problems through a series of site visits to Exxaro, Anglo Coal, Total SA, Sasol and BECSA.

Literature survey and review:

- Survey of stress effects observed in near surface (<500m) civil and mining excavations internationally to quantify the "shallow" depth stress problem.
- Review of the theory relating to stress origin, temporal development, magnitude and direction including tectonic stress components, stress adjustments due to mining activities and the contribution of extension strain and shear to rock failure. Numerical modeling was used to illustrate stress adjustments arising from simplified, typical mining geometries.
- Overview of the geological nature of the Witbank and Highveld Coalfields including seam depth, overburden type and palaeo-basement configuration.
- Review of the extent of existing and planned surface and underground coal mining in the Witbank and Highveld Coalfields including the location of underlying (gold) and other mining environments.
- Summary of coal mining methods applied and their influence on surrounding stress magnitudes and distributions.

Data collection and analysis:

Review of all stress measurements made in the Coalfields, assessment of the quality, rotation into appropriate components (vertical and horizontal), preparation of a stress data base, graphic presentation of individual measurements and generation of a stress "flux" plan.

Collection of tangible evidence of stress induced damage in coal mine workings through underground inspections, accident records and reports of (stress-affected) fall of ground incidents.

- Review of stress amelioration strategies employed in the Coalfields.
- Guidelines in managing stress hazards:
- Consideration of the operational significance of horizontal stress in terms of both the mining processes and ground support methods in use.
- Generation of guidelines for the future use of horizontal stress mapping for operational strata management.
- Generation of guidelines as to how any deleterious effects of horizontal stress could be further mitigated within the practicalities of the mining methods in use.

1.4 Methodology

The research methodology used during this study is based on a comprehensive approach proposed by Stephansson (2003) for estimation of virgin state of stress and determination of final rock stress model. This method makes use of both measurement and observations (geology, structures, guttering and rock falls) to derive orientation and magnitude of stress.

In this study the following information is used:

- Morphology
- Topography
- Lithology
- Structural geology
- Soil cover (weathering)
- Palaeo floor
- Miscellaneous Observations (guttering)

- In situ rock stress measurements.

1.5 Content of the report

The report has been subdivided into 6 chapters. The next chapter presents the geology of the Witbank and Highveld coalfields. Chapter 3 reviews stress effects at shallow depths observed in coal mines in United States of America, Australia and South Africa. Theories explaining the origin of ground stresses are also presented and demonstrated using finite element analysis. Distribution of stress around excavations of various shapes was also studied in this chapter. In Chapter 4, the underground mining methods used in the Witbank and Highveld coalfields are presented with emphasis placed on their impact on the magnitude and direction of ground stresses. Chapter 5 presents the stress measurements collected from the mines. The analyses carried out on the data together with the results are also presented in this chapter. The mitigating techniques used in the Witbank and Highveld to combat stress effects are also documented in this chapter, and Chapter 6 concludes this research report. Details of the stress database created from the information collected from the mine are summarized in Appendices.

CHAPTER 2

Geology of the Witbank and Highveld Coalfields

The material of this section was included for completeness of the report and therefore has used mostly the direct wording, which is shown within inverted commas.

"The Witbank Coalfield is located in the province of Mpumalanga in South Africa in the northern sector of the main Karoo basin" (Johnson, et al. 2006). Figure 2-1 shows the spatial positions and the boundaries of the Witbank and the Highveld coalfields.

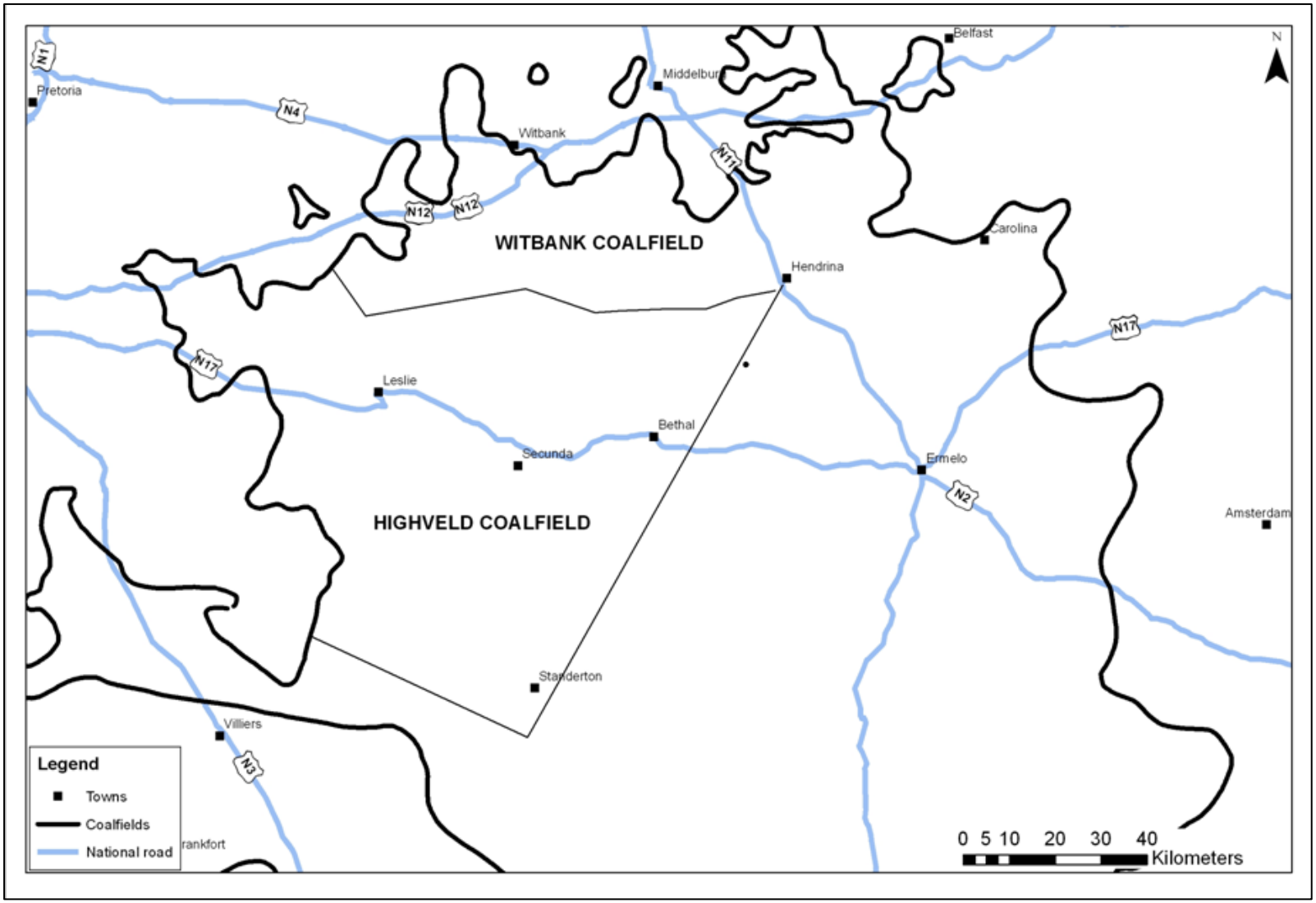


Figure 2-1 Map showing the spatial position of the Witbank and Highveld coalfields

"The Karoo Supergroup in South Africa consists of various formations which range in age from Late carboniferous to Middle Jurassic and attains a cumulative thickness as much as 12 km in the southern portion of the so called main Karoo basin. Spatially, the Karoo Supergroup in South Africa is composed of 5 basins: the main basin and a suite of much smaller basins (Ellisras basin, Tshipise basin, Springbok Flat basin, Tuli basin). The main basin covers an area of about 700000 km^2 and has the most economic value by far" (Johnson et al., 2006). Figure 2-2 shows the areal distribution of the lithostratigraphic units in the main Karoo Basin, whereas Figure 2-3 shows the generalised stratigraphic and lithologic column of the Karoo Supergroup in the main Karoo Basin (Johnson et al., 1997).

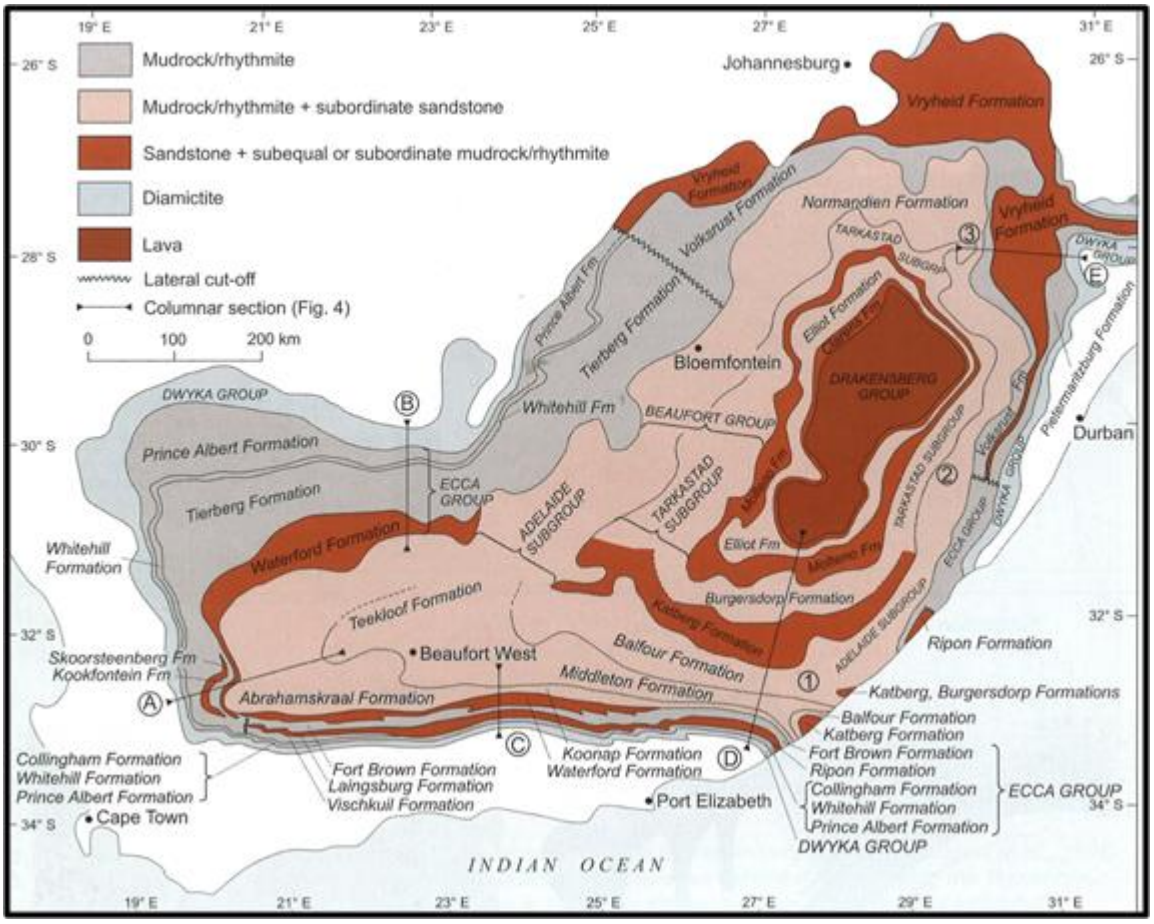


Figure 2-2 Areal distribution (schematic) of lithostratigraphic units in the Main Karoo Basin modified (modified after Johnson et al., 1997)

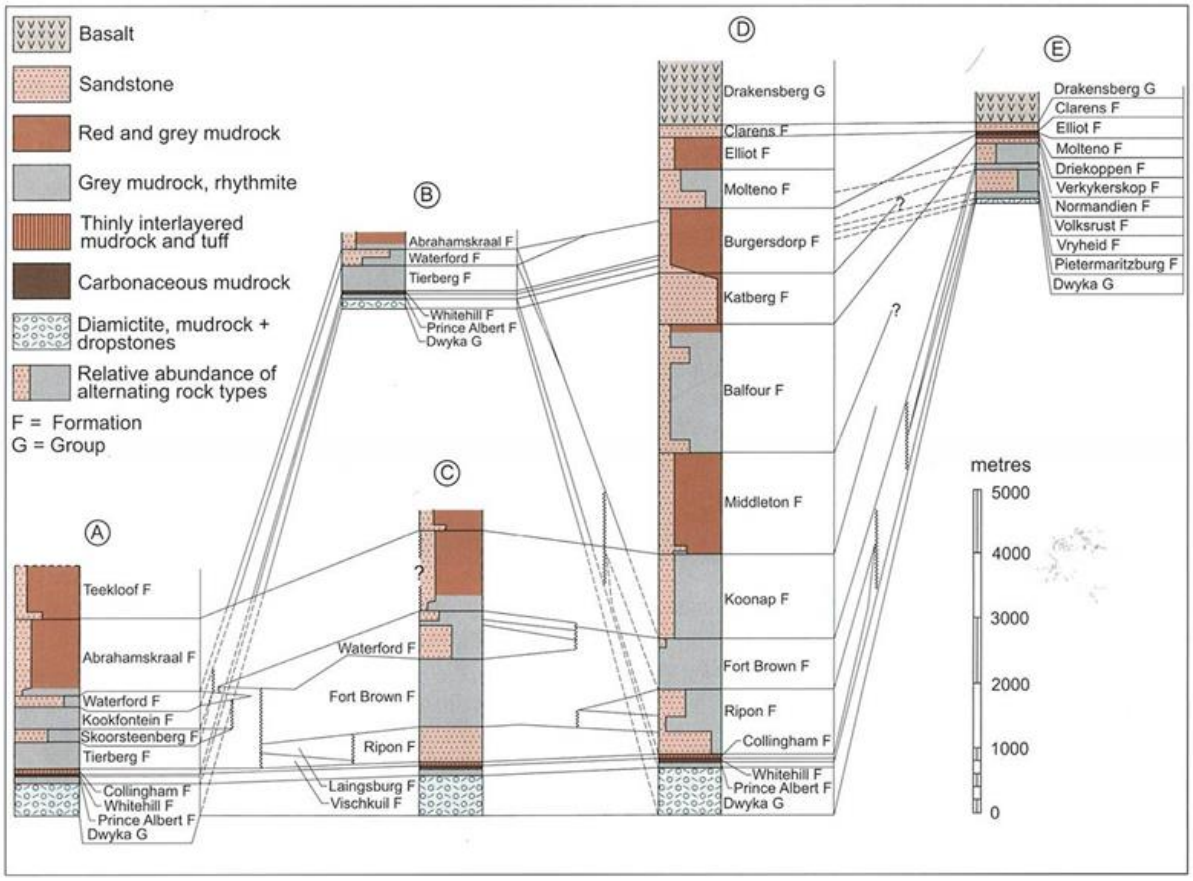


Figure 2-3 Generalised stratigraphy and lithology of the Karoo Supergroup in the Main Karoo Basin (modified after Johnson et al., 1997)

"The main Karoo basin is underlain by a stable floor, comprising the Kaapvaal craton in the north and the Namaqua metamorphic belt to the south and is bounded to the south by a fold-thrust belt , Cape Fold belt" (Johnson, et al. 2006). "The main Karoo craton is said to constitute a retro-arc foreland basin since it contains a flysh-molasse succession which wedges northwards over the adjacent craton, but it is also situated behind an inferred magmatic arc and associated fold thrust belt produced by a northward subduction" (Dickinson 1974).

"The Permian Ecca group is the most economic coal bearing group in South Africa. It is composed of 16 formations, reflecting the lateral changes that characterise its succession. The individual formations can be gathered into three groups (southern, western-northwestern and northeastern).

The southern formations are the following:

- Collingham;

- Vischkuil;
- Laingsburg;
- Ripon;
- Fort Brown; and
- Waterford.
- The western - northwestern formations are as follows:
- Teiberg;
- Skoorsteenberg;
- Kookfontein; and
- Waterford.

The northeastern formations are composed of:

- Pietermaritzburg;
- Vryheid; and
- Volksrust.

The coal seams of most important economic value occur in the Vryheid formations. The Vryheid formation rests unconformably on the Dwyka formations which are mainly composed of diamictites and varved shales. The facies of Dwyka formations is interpreted as being the result of glacial, fluvio glacial and glacio-lacustrine deposition. The thickness of the Vryheid formations varies from 70 m in the northeastern portion to 300 m in the eastern portion of the basin where the outcrop has been preserved" (Snyman 1998).

2.1 Coalfields

In South Africa, based on variations in sedimentation, origin, formation, distribution and quality of coal seams, up to 19 coalfields are distinguished. All those variations are tributary to specific deposition condition and local tectonic history (magmatic intrusion). The

boundaries between the Witbank and Highveld coalfields are very subjective and are not based on geological differences, but rather on historical and geographical considerations. According to Snyman (1998) both coalfields are separated by a ridge of Rooiberg felsite, also called Smithfield Ridge, trending roughly 60 km east-west.

In both the Witbank and Highveld coalfields 5 coal seams can be recognised. The seams are numbered 1 to 5 from bottom up and each seam belongs to a depositional sequence mainly composed of sandstone, gritstone, interbeds of finer siltstone and mudstone.

2.1.1 Coal Seams in the Witbank Coalfield

No 1 seam is better developed in the Witbank coalfield than in the Highveld coalfield. In the Witbank coalfield the No 1 seam has a thickness ranging between 1.5 and 3 m. The thickness of this seam is mainly controlled by the palaeo floor. The seam tends to be thicker in palaeo valleys and to pinch out against palaeo highs.

No 2 seam is host to about 69 % of coal resources in the Witbank Coalfield, and contains some of the best quality coal. The thickness of No 2 seam is approximately 6 m in the central part of the Witbank coalfield and thins down to 3 m toward the east and the west of the coalfield. No 2 seam is divided into 6 clearly defined zones based on quality of the coal. The basal five zones are of high quality and are mined out to supply the steam coal export market while the top zone of much poorer quality supplies the local Eskom power generation.

No 3 seam is not well developed (<0.5m) within the Witbank coalfield and therefore is not economically profitable in spite of the high quality coal it contains. However, at places where the thickness is in excess of 0.8 m it might become profitable for some open cast operations.

No 4 seam contains almost 26 % of the resource of the Witbank coalfield. The thickness varies from 2.5 m in the central region of the coalfield to 4 m elsewhere with places where it reaches 6 m around the Delmas area. No 4 seam is subdivided into No 4 Lower, No 4 Upper and No 4 seam. The quality of No 4 Upper seam is deemed too poor.

No 5 seam has been extensively eroded. However, in places it attains a thickness of 1.8 m. The seam consists of a blend of bright, banded coal with thin clastic partings in a few localities. The seam contains high quality low phosphorous coal suitable to serve as blend coking coal.

2.1.2 Coal seams in the Highveld Coalfield

Unlike in the Witbank coalfield, the Highveld coalfield No 2 and No 1 seams are poorly developed and cannot be profitably mined. However, No 4 is by far the most profitable coal seam of the coalfield and contains a dull and dull lustrous coal which is used for local electricity generation and Sasol feedstock. At places such as Twistdraai operation, No 4 seam produces a coal of quality suitable for the export market after beneficiation. No 5 seam is present in the Highveld Coalfield and consists of two bright coal zones separated by a shale parting, but is often not profitable.

2.2 Structural geology

The southern African region has undergone several magmatic intrusion and rifting events. Some intrusions have transgressed the coal bearing Vryheid formation in the Witbank and Highveld coalfields, and therefore are of paramount importance in understanding the in-situ stress regime within the coalfields (du Plessis 2008).

The intrusions are mainly Dolerite dykes or sills. The very basic principle is that dykes have intruded when at some points in time the earth's crust was in tension, whereas sills intruded preferably when the ground was in compression. In the vicinity of a dyke the direction of the major horizontal stress is expected to be perpendicular to the strike of the dyke (du Plessis 2008).

Table 2-1 summarizes trends and the associated structures in the Witbank and Highveld coalfields on a regional scale.

Table 2-1 Summary of the regional scale trend relationships relating dykes, sills or lineaments in the Witbank Coalfield (du Plessis 2008)

TREND	REGIONAL SCALE STRUCTURAL ASSOCIATION
NE	Karoo-age dolerite dykes.
	Sabi monocline-3rd arm of a plume generated Karoo-age triple junction
	Ventersdorp Fabric (2.7 Ga rifting - extensional event) - strong aeromagnetic signature, Pre-Karoo diabase trend.
NS	Regional joints sets preferably favoured by the B8 dolerite sill in the Secunda Coalfield
	Lebombo monocline - part of Karoo age triple junction
	Karoo-age dolerite dykes.
	Ventersdorp-age intrusives in the Evander Goldfield
NW	Regional joints sets preferably favoured by the B8 dolerite sill in the Secunda Coalfield
	Pongola fabric-aeromagnetically quiet
EW	Regional joints sets preferably favoured by the B8 dolerite sill in the Secunda Coalfield
	Karoo-age Ogies Dyke
	Pre-Karoo diabase
	Long axis of the Bushveld Complex
NNW	Karoo-age dolerite dykes.
	Predominant lineament trend from Landsat MSS image
WNW	Okavango Dyke Swarm (failed arm of a Karoo-age triple junction)
ENE	Tuli-Soutpansberg troughs - syn-Karoo graben resulting from reactivated Archaen structures
	Retreat of Drackensberg Escarpement
NNE	Extensional structures of a Karoo-age triple junction of the East Coast
	Olifants River Dyke Swarm - important feeder to Karoo-age sills
	Axis of the main Karoo basin

A very comprehensive report on spatial position and orientation of dolerite intrusion in the Witbank and Highveld coalfields was given by du Plessis (2008). The map in Figure 2-4 gives a regional view of positions of dykes as lineaments within the coalfields. The map shows also the position of the Ogies dyke (in green) which strikes E-W, dividing the coalfields into two parts: North and South. It is found that the majority of dykes south of Ogies dyke strike NS and EW while those north of Ogies dyke dominantly strike EW although dykes oriented WNW, ENE and NS are observed as well.

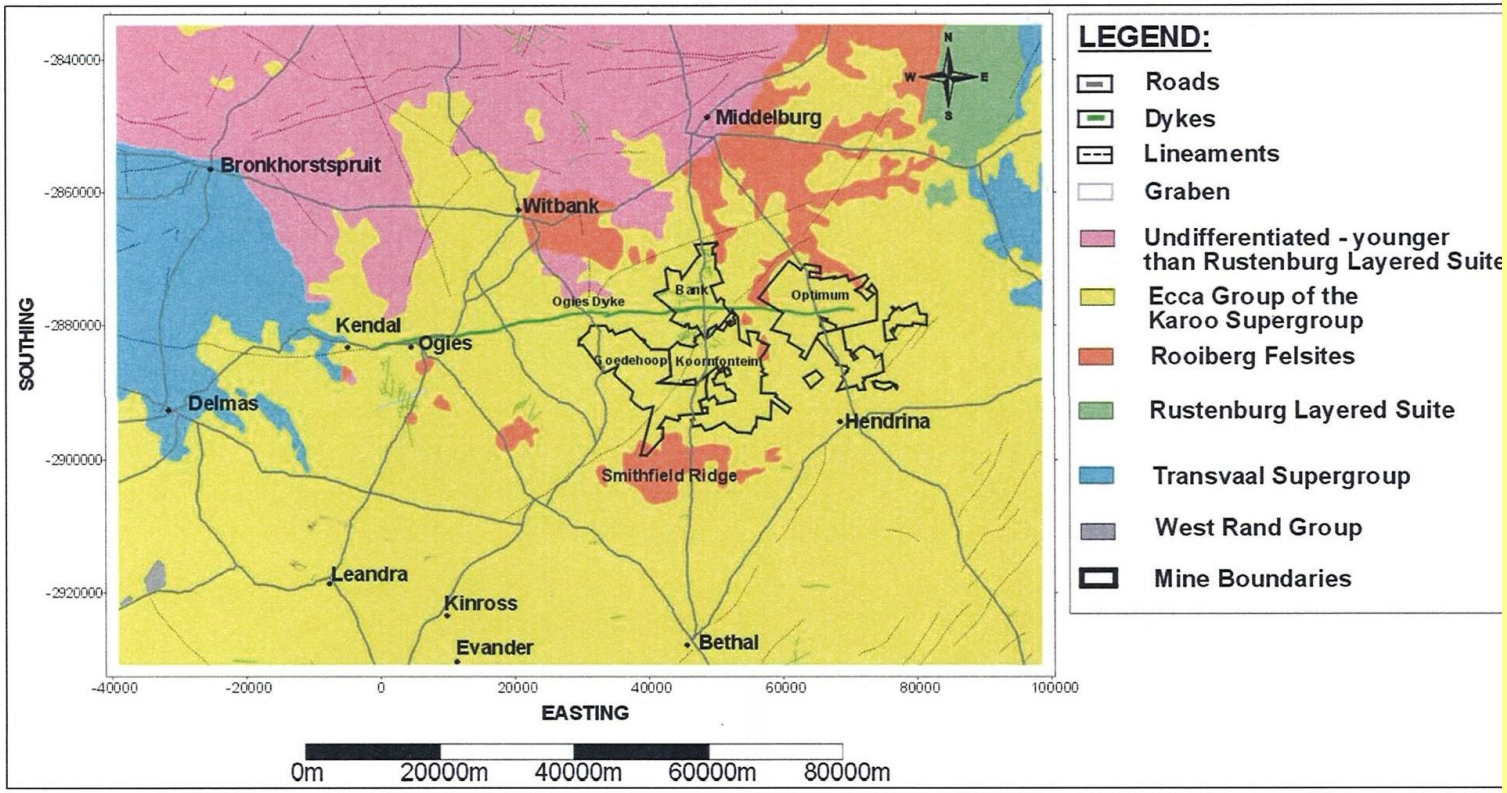


Figure 3.2: Regional scale geological map.

Figure 2-4 Regional scale geological map showing position of dykes (after du Plessis 2008)

By combining geological and basement maps it was found that the NE trend of the dolerite in the lower right corner of the map coincided well with the orientation of the Ventersdorp fabric and that propagation paths of some dolerite within the coalfields were controlled by pre-existing fabric resulting from 2.7 Ga Ventersdorp rifting event (du Plessis 2008).

The EW strike direction of the Ogies dyke seems to correlate well with NW, EW, NE trends observed in the pre-karoo diabase basement. This suggest that the Ogies dyke had probably intruded a pre-existing plane of weakness. The EW pre-karoo diabase trend is similar to the Bushveld Complex axis that is associated with a craton wide EW compression (du Plessis 2008). The EW and NS striking dykes north of the Ogies dyke have probably re-utilised fractures created by contraction of the Ogies dyke during its cooling process. This is supported by the absence of sills north of the Ogies dyke and the difference in geochemical composition.

In addition, in the flank of the basin, features such as compression joints are present and possibly due to the differential compaction of sediments.

CHAPTER 3

Review of stress effects at shallow depth

In this section, a survey of stress effects at shallow depth is made with emphasis placed on the failure mechanisms observed in underground coal mines around the world. The theory pertaining to stress origin and an overview of the geological nature of the Witbank and Highveld Coalfields are also discussed.

3.1 Survey of stress effects at shallow depth

3.1.1 United States of America

Thomas (1948) made the observation that for guttering to take place at the corners of a roadway, the immediate roof should consist of a material more competent than the material above it, otherwise guttering occurs in the centre of the roadway. According to Thomas's observation, the material properties are the key factor defining the location of guttering in the roadway. From these observations, roof instability is associated with two mechanisms:

- A relatively strong thinly laminated roof with strong cementation between laminations
- Or a series of weaker strata that tend to sag and load the more competent roof below them.

Su and Peng (1982) presented mechanisms involved in cutter roof and its causes based on observations in coal mines in West Virgina in the USA. Note that cutter roof is the American term for guttering. According to the authors, cutter roof is a failure that initiates and propagates vertically from one or both corners of an entry. Once fracture has been initiated the cutter roof can eventually extend above the roof bolt anchorage horizon, producing bedding separation, beam bending, formation of secondary cracks and ultimately failure. Subsequently, these researchers carried out numerical modelling, aimed at assessing the effect of the following:

- Horizontal stress magnitude;
- Stiffness of the roof;
- Topographic surface; and
- Beds separation and gas pressure.

From the finite element analysis carried out, the following was found:

- High values of horizontal stresses have less effect when the roof consists of a soft material than a stiff material.
- The differential stress (difference of maximum and minimum horizontal stress) has little influence at the entry corners, but has the most effect at midspan of a stiff roof.
- The magnitude of horizontal stresses is more critical in cases where both horizontal stresses are greater than the vertical.
- When the coal is stronger than the first immediate roof layer under low horizontal stress and thick overlying layers, guttering is more likely to take place at rib–roof contact. However, under an excessive horizontal stress field with high differential stress, the horizontal stress arch occurs deeper into the roof. It was therefore concluded that a stiff roof combined with thick overlying layers is a condition sufficient for guttering to take place.
- The effect of a sloping topographic surface and an excessive horizontal stress field such as found at some depths, resulted in cutter roof being likely to occur in one corner of the excavations than in both.
- It was also speculated that gas entering the opening between separated beds can decrease the factor of safety at midspan, but not as much at the corners.

Murali and Peng (2005) studied weak roof guttering at a coal mine in Illinois where abundant guttering took place using a Finite Difference Code (FLAC 3D). Strain Softening constitutive model was used to simulate the behaviour of the roof. The model was calibrated based on observations on the mine and results of a laboratory testing programme. Murali and Peng (2005) believed that the limitations of the actual continuum code used in the analysis can be overcome by making use of the right constitutive model. The choice of FLAC 3D was justified by the robustness of an explicit code, as opposed to implicit code, in handling convergence issues since it was anticipated that removal of failed elements was needed in the solution process, which normally leads to convergence issues. In the analysis the development layout was mined out in a 13 cut sequence. The in situ stress regime was given by previous in situ stress measurements at the mine.

From their analysis, the following controlling factors were found:

- The magnitude and direction of in situ stresses;
- Strength of the roof;

- Cutting sequence;
- The position of the face with respect to the closest intersection;
- The direction in which crosscuts are developed with respect to the direction of in situ horizontal stresses; and
- Pillar size and the number of entries.

The study also validated mapping as a means of deriving horizontal stress orientation (Figure 3-1).

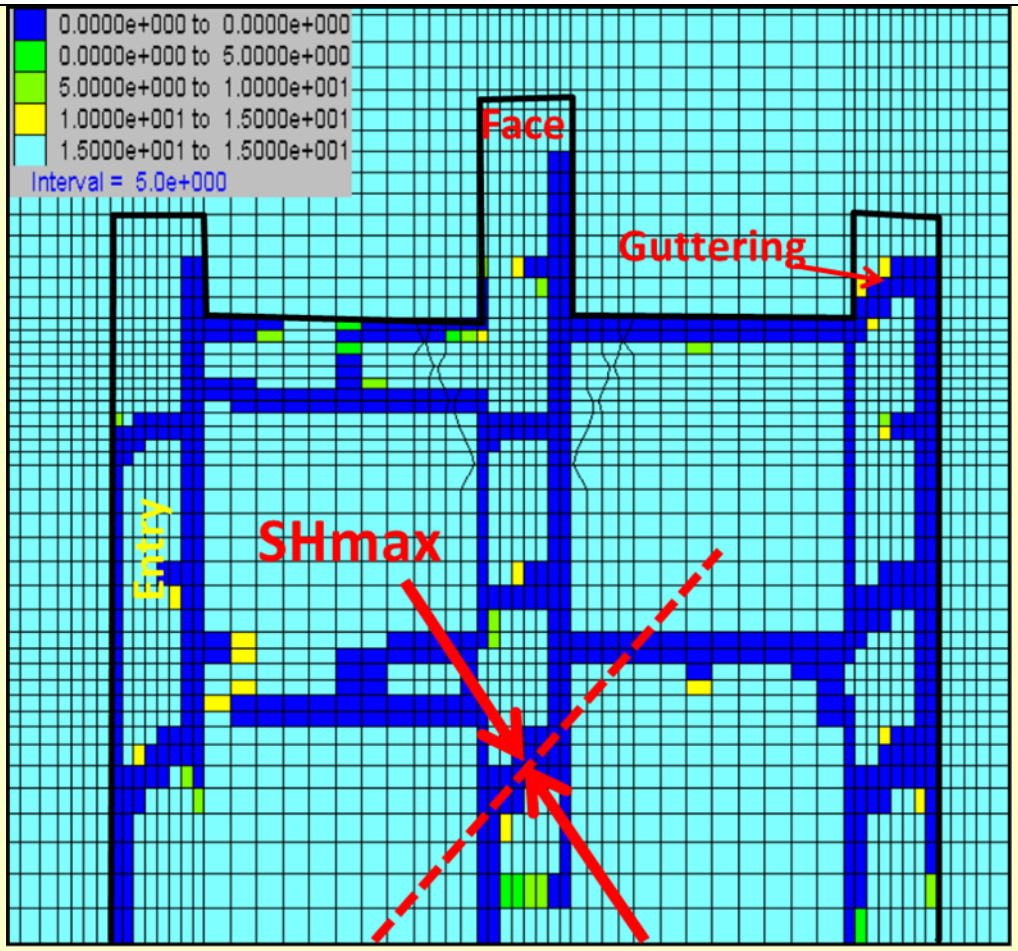


Figure 3-1 FLAC 3D results showing the spatial distribution of gutters in a simulated development layout. The Figure also indicates that direction of gutters (in dark blue) varies with the position where they occur within the Layout but that there is a general trend oriented perpendicular to the direction of the major horizontal Stress (SHmax) (Estherhuizen et al, 2008)

Esterhuizen et al (2008) investigated horizontal stress effects on roof stability in US Limestone mines. From their observations, roof damage in limestone mines can manifest in one of the following manners:

- Roof guttering which is process similar to the cutter roof (Figure 3-2).
- Beam instability, whereby each layer behaves separately from others. Buckling and shear fracturing have been identified as the dominant mode of failure here (Figure 3-3).
- Oval shaped falls where shear/buckling fracture propagates upward in the roof due to the deflection of beds between pillars (Figure 3-4).
- Failure propagation; where an oval shaped fall of roof propagates across a relatively large area within the panel due to stress concentration at the ends of the oval cavity.

In addition to this, a 3 dimensional numerical analysis was conducted using FLAC 3D. In this analysis, a two stage brittle/shearing failure criterion was used; the extensional strain criterion was used to locate where failure initiates and the Mohr Coulomb strain softening criterion was used to study how failure propagates. The numerical modelling, results obtained correlated with guttering occurrences on site.



Figure 3-2 Roof guttering at a roof-pillar contact (Esterhuizen et al, 2008)

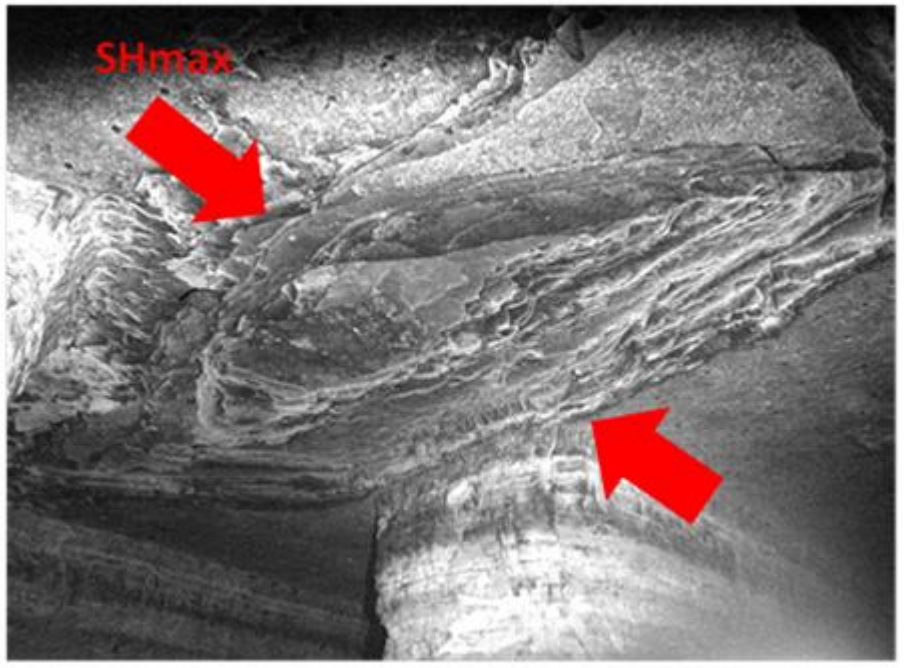


Figure 3-3 Horizontal stress induced failure between two pillars, arrows indicate the orientation of maximum horizontal stress (Esterhuizen et, 2008)



Figure 3-4 Large oval-shaped fall into the weaker overlying strata in a limestone mine (Esterhuizen et al, 2008)

3.1.2 Australia

Adams (2002) gathered monitoring data from different coal mines in Australia and identified two major typical roof behaviours that are referred to as:

- Static Roof

- Buckling Roof

A static roof is formed when the level of stress acting within the roof is insufficient to create bedding separation or bedding failure either in tension or in shear. The roof preserves its integrity and does not break down into thin layers which can later buckle. Essentially, the roof thickness is such that all the stress changes caused by the roadway creation are quickly absorbed without any significant change of state except for elastic movements. As one would expect, the likelihood of formation of a static roof increases with the bedding thickness, and the tensile and shear strengths of the bedding planes. Whilst the former property is nature given and therefore unlikely to change over time, the strength of the material is time dependent. External influences such as weathering can therefore weaken the roof over a period of time.

Highly stressed roadways (up to 30 MPa horizontal stress) at some Southern Coalfield mines are reportedly standing stably where high stress occurs combined with thickly bedded rocks. Conversely, cases of roof buckling in comparably low horizontal stress situations were reported, especially when thinly bedded rocks were present in the roof. Figure 3-5 shows the relationship between the roof displacement and time (Adams, 2002). It is important to note that in typical static roof conditions, the roof undergoes vertical displacement < 5 mm. The measurements were collected at a distance at least 0.5 m from the roof skin so as to avoid influencing results. The monitoring point was chosen far enough from the face to avoid any influence of the mining face.

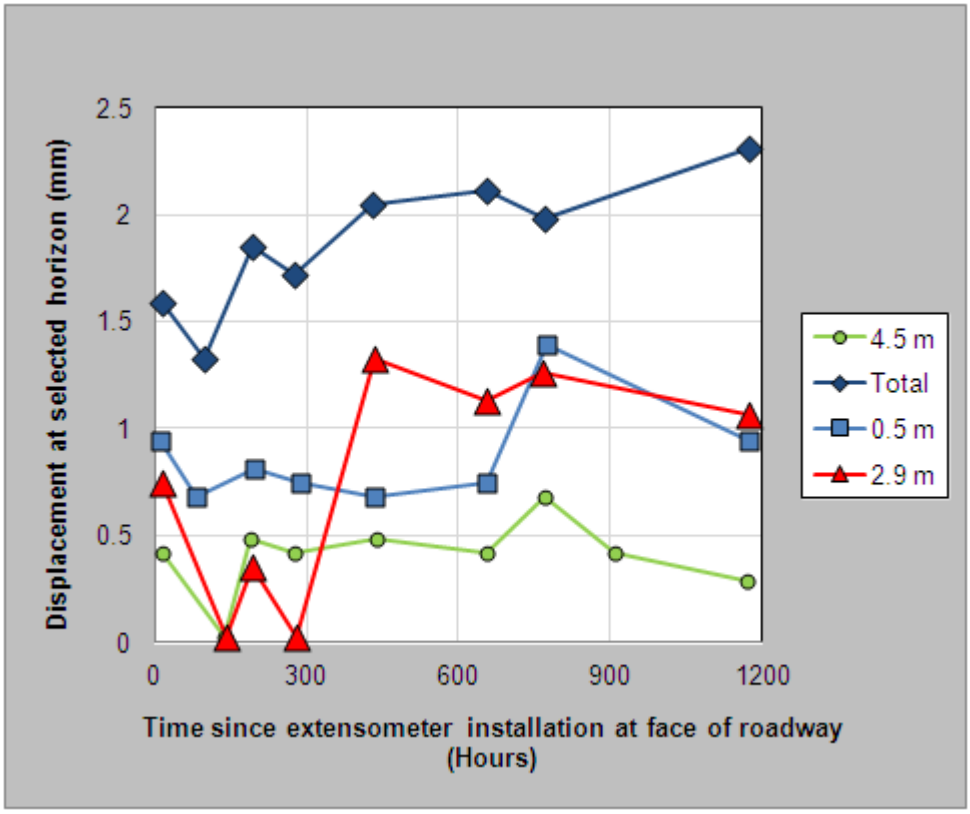


Figure 3-5 Chart showing the time dependent behaviour of a static roof (Adams, 2002)

According to Adams (2002), buckling roof occurs due to a shear or tensile failure on the bedding planes. As a result, thin layers are formed which behave as discrete units that can easily buckle under the action of horizonal stress. Furthermore, Adams (2002) points out that the onset of buckling should not be viewed as ultimate failure of the roof, because in many instances the roof can still develop full equilibrium afterwards.

Figure 3-6 illustrates the buckling of the roof in a coal mine. The picture also shows clearly the presence of a low angled shear crack running through the roof.



Figure 3-6 Picture showing a buckling roof at Kenako shaft in South Africa

The buckling of the roof in coal mines can be explained by the Euler beam theory. Under the influence of the horizontal stress, the roof deflects and gradually mobilises the internal reaction until equilibrium is reached. The relation between the loading bearing capacity and lateral displacement in an Euler beam is given by the following equation:

$$P = E\,I\left[\cos^{-1}\left[\left(\frac{e}{u+e}\right)\times\frac{2}{L}\right]\right]^2$$

where:

P: End-load

e: eccentricity (distance from the neutral axis to the axis of loading of the beam)

I: Moment of Inertia (m^4)

E: Young's Modulus

u: lateral displacement

L: Length of the beam

By applying the formula of the Euler beam using an elastic modulus E of 5 GPa and a beam length of 10 m, the load bearing capacity-vertical deflection graph in Figure 3-8 was obtained for various beam thicknesses. It is important to note that the thickness of the beam has a great influence on its load bearing capacity. Whilst a 0.4 m beam can only withstand a load of about 5 MPa maximum, a 1 m thick beam can accommodate up to 90 MPa load for the same amount of vertical displacements.

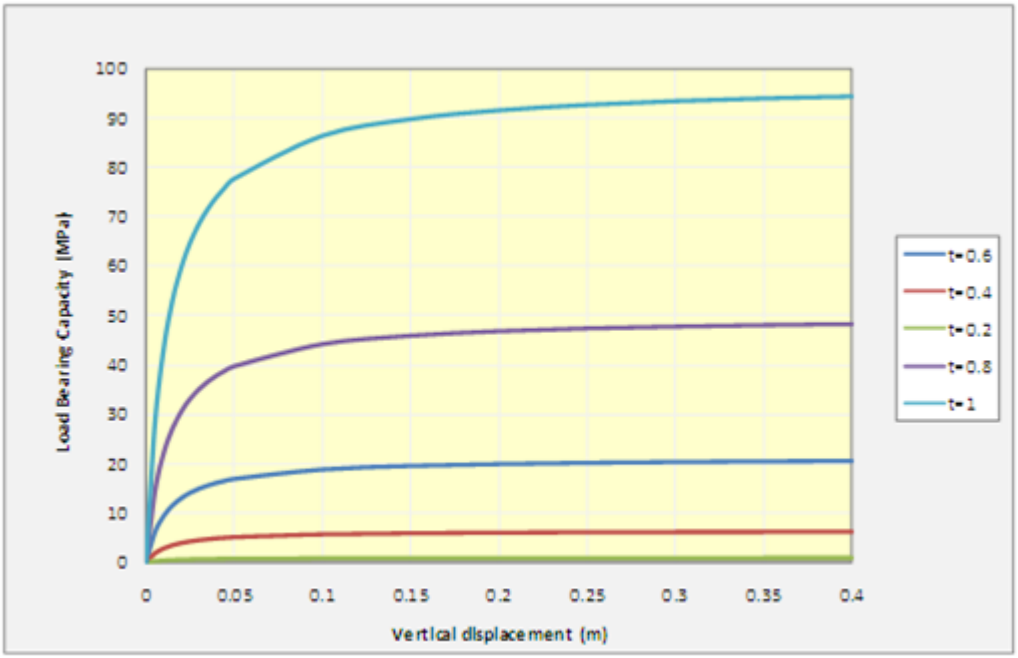


Figure 3-7 Chart showing variation of Load bearing capacity of an Euler beam versus vertical displacements for different beam thicknesses

In addition, Figure 3-8 illustrates how the load bearing capacity of a 0.8 m thick buckling beam varies with change of eccentricity. It can be seen that the lower the eccentricity the higher the horizontal load the beam can carry.

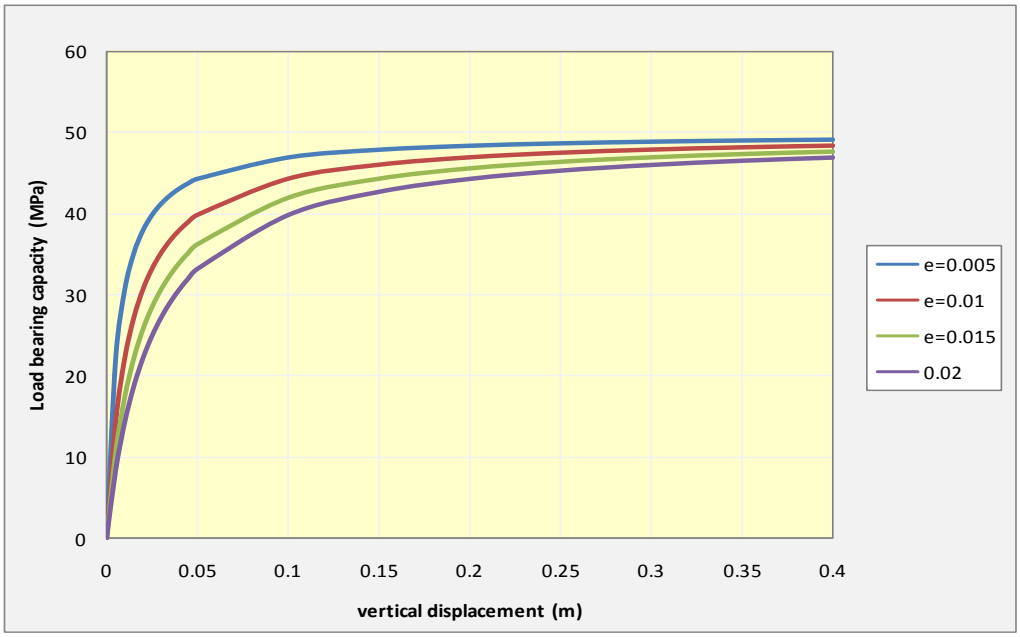


Figure 3-8 Chart illustrating the variation of Load bearing capacity with vertical displacement at different values of eccentricities

According to Adams (2002), two scales of falls of ground should be distinguished, a skin and a full width scale. It is reported that the falls of ground at both scales have similar causes, but require different ground control solutions. A complete strata control solution will therefore be required to address issues on both scales. Adams seems to recognize that high horizontal stresses have a roof stabilizing effect in discontinuous roofs and ground control measures should focus on ways to preserve that inherent stabilizing effect. Three driving mechanisms for falls of ground were identified, namely:

- Horizontal shortening of the Roof under the influence of horizontal stress
- Low Stress " Plug" Falls; and
- Mid-Angled Discontinuities.

3.1.3 Horizontal shortening of the Roof under the influence of horizontal stress

Under the influence of high horizontal stress and buckling, the roof naturally shortens. These on-going displacements will lead to a continuing lowering of horizontal stress. In this process of horizontal stress relief, a potentially unstable block forms. The amount of displacement required for this block to form largely depends on the geotechnical environment and the performance of support installed. As illustrated in Figure 3-9 and Figure 3-10, such instability is often associated with a low angle shearing across individual beds of the buckled, but unfailed roof.

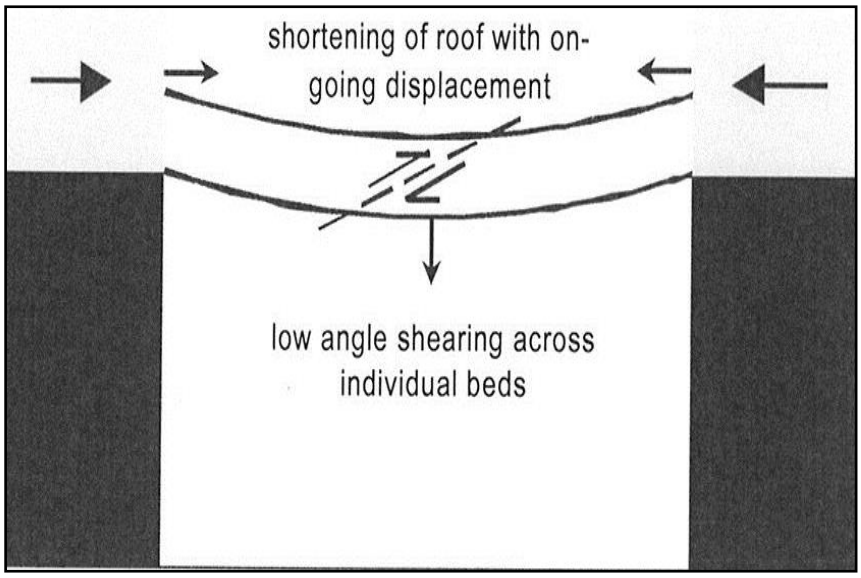


Figure 3-9 Figure illustrating shortening of the roof with on-going displacement and low angle shearing across individual beds (Adams, 2002)

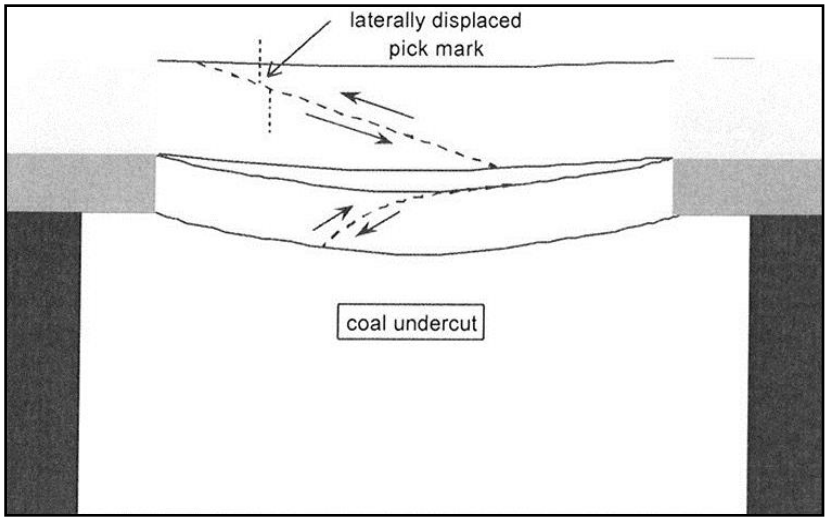


Figure 3-10 Sketch illustrating the formation of a low angled shear crack as the roof buckles (Adams, 2002)

3.1.4 Low Stress "Plug" Falls

The low stress plug fall is a failure mechanism associated with shallow depths where horizontal stresses are low. In this case there is plug-type of fall that takes place along the pre-existing vertical planes of weakness when a bedding separation occurs above the support horizon. According to Adams (2002), this form of instability is rare provided that the cohesion and friction along bedding plane is high enough to prevent them from occurring.

3.1.5 Mid-Angled Discontinuities

The presence of a discontinuity oriented unfavourably in the roof can also contribute in lowering the horizontal stress in the roof and thereby the stabilizing effect. In essence, as slip takes place along the discontinuity the continuity of horizontal stress is disrupted and the likelihood of formation of unstable block increases (Figure 3-11).

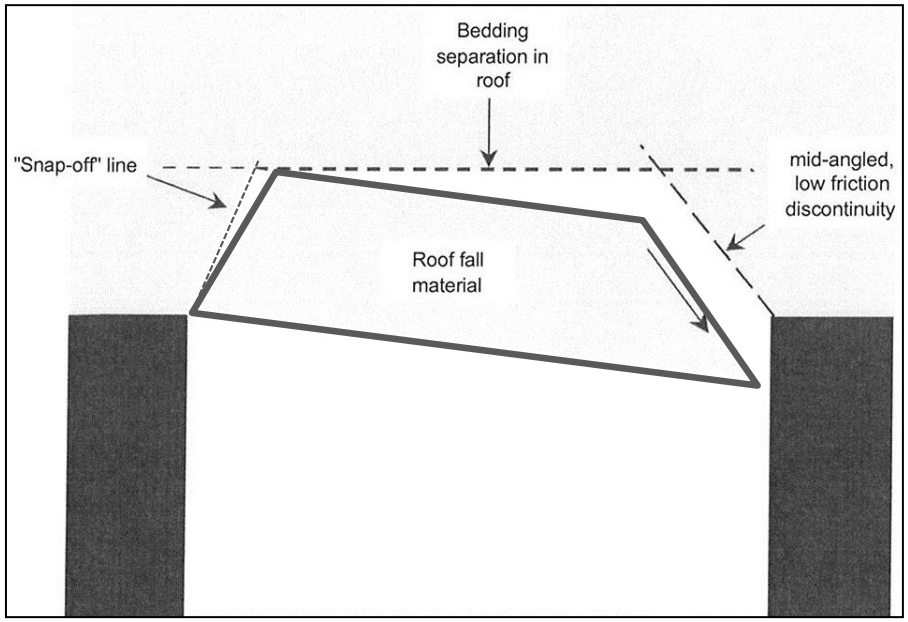


Figure 3-11 Sketch illustrating Mid-Angled Discontinuities mechanism (Adams, 2002)

In the present report, this failure mechanism was further investigated to assess the likelihood of occurrence in South African coal mines.

In this analysis the mid-angled, low friction discontinuity (Figure 3-11) was assumed to be 45 degrees and the snap-off line 90 degrees. It was anticipated that the cohesion times the thickness of the beam will generate a stabilising resisting moment which increases, whereas the driving moment is generated by the weight of the falling block times the span of the roadway. The unit weight of the material was taken as 25 KN/m3. The stability was assessed based on a Factor of safety which is the ratio of the resisting to the driving moment. The result of this analysis is presented in Figure 3-12. It can be seen that for an 8 m wide roadway, this mechanism of failure is likely to take place if the cohesion is less than 100 KPa.

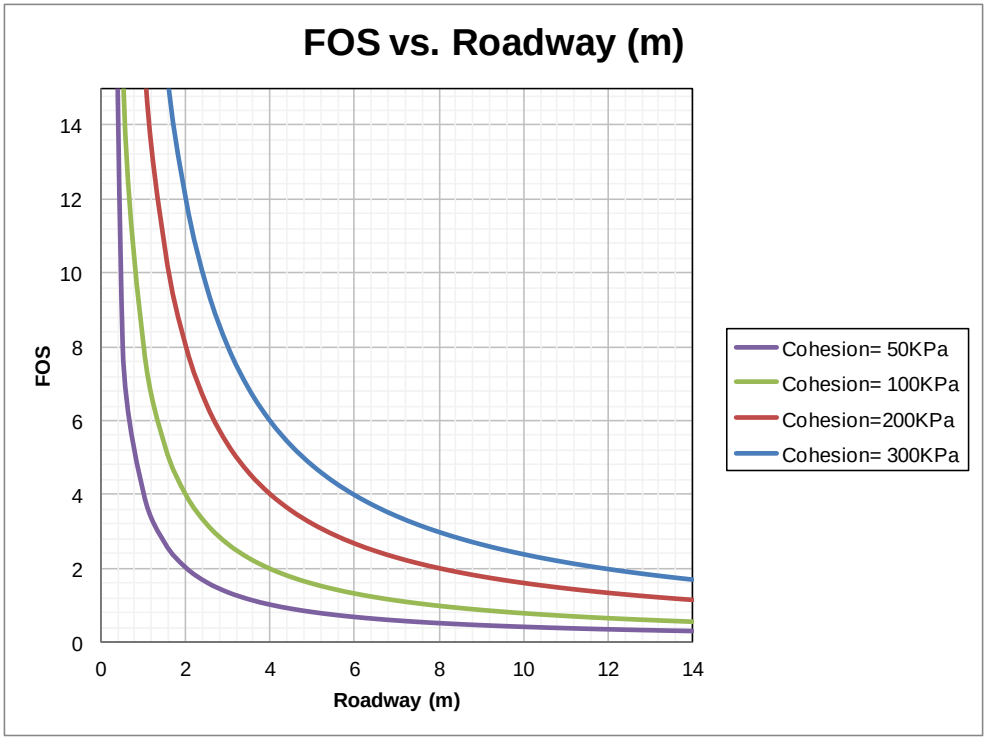


Figure 3-12 Graph of FOS vs. Roadway width

To combat the above mentioned roof instabilities, Adams (2002) suggested solutions such as limiting displacements of the buckling roof and local stabilization of discontinuities along which slip is likely to take place.

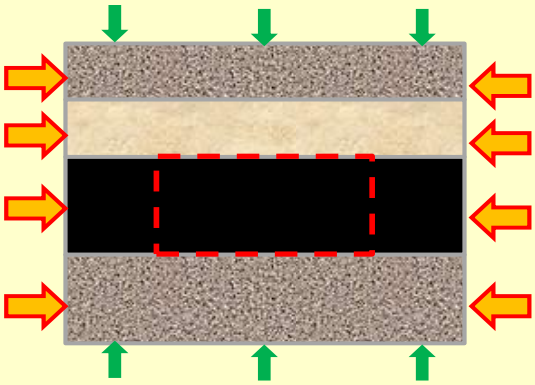
3.1.6 South Africa

Alan and John (2003) have documented stress related falls of ground at Goedehoop in the Witbank Coalfield in South Africa. The authors have identified two different mechanisms by which failure was occurring:

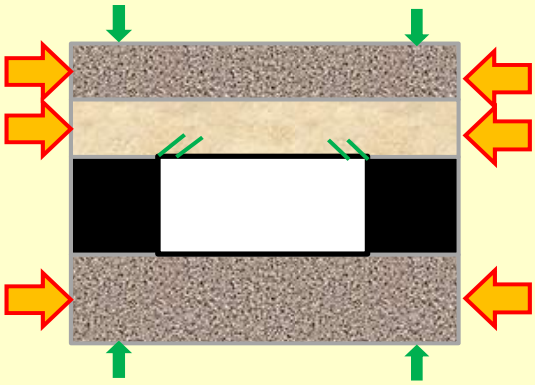
- Failure with slip
- Failure without slip

Figure 3-13 illustrates the mechanisms involved in a failure without slip. Initially, there is a concentration of the horizontal stress in the floor and the roof which in turn leads to the onset of a shear failure around corners of the roadway. Following the shear failure initiation, a stress concentration occurs around the failed zone leading to propagation of fractures

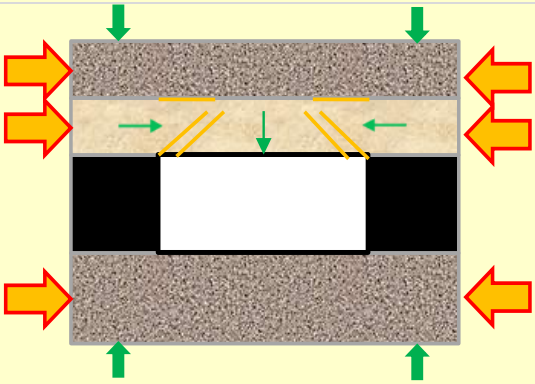
upwards in the rock until a bedding plane is encountered resulting in the fall of the unstable block under gravity.



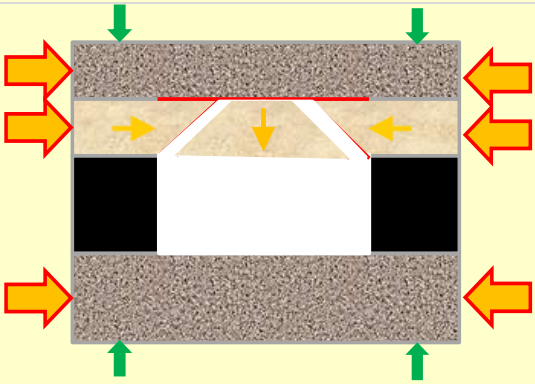
(a): before excavation of the roadway



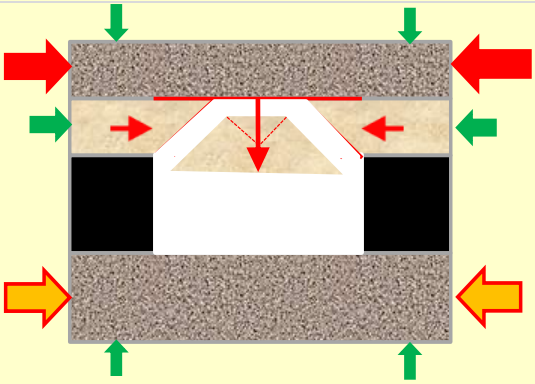
(b): Onset of failure



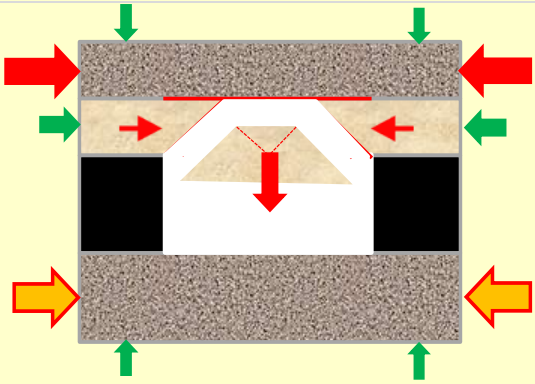
(c): Failure propagation



(d): Formation of the unstable block



(e): detaching of the unstable block



(f): Ultimate failure

Figure 3-13 Diagram showing mechanism of roof failure due to shear, the colours and the size of the arrows denote the magnitude of horizontal stress and displacements (Alan et al 2003)

It can be seen in Figure 3-13 that a tension crack (secondary crack) formed right after the unstable block has formed.

Failure with slip was observed where a slip was running parallel to the roadway over a distance of about 10 m. This failure is associated with a crack running through the intact rock and along the bedding planes on the other side of the slip. As shown in Figure 3-14, failure initiates by a slip along the joint under the influence of high horizontal stress, the slip creates a moment on the other side of the roadway where a crack progressively develops. When the forming crack has fully developed, a fall of ground takes place.

According to van der Merwe (2000), the roof mechanism in a roadway is similar to a clamped beam whose stresses and deflection are given by the following equation:

$$\sigma_{bc} = \frac{f\gamma L^3}{2t_b}$$

where:

σ_{bc} : Magnitude of maximum stress (occurring at the ends of the beam)

γ : Unit weight of the rock, usually 0.025 MN/m3

L: Length of the beam (width of the roadway)

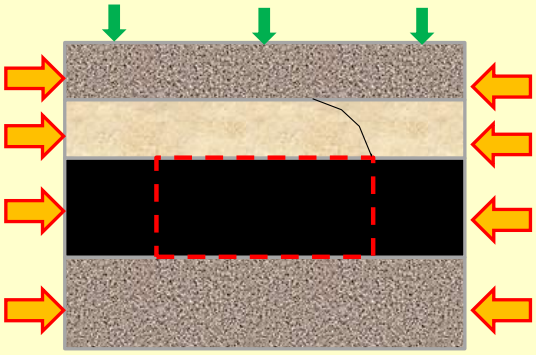
$f = \frac{t_T}{2t_b}$

t_b : thickness of the beam

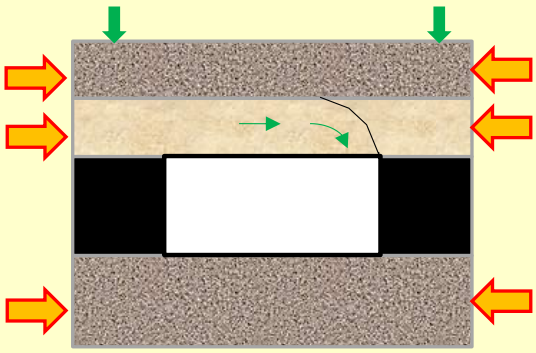
t_T : total thickness of beam and softer material resting on top of beam, or suspended from beam by bolting.

When a slip is present at the rib side, a cantilever is formed and the magnitude of stress at the opposite corner increases six fold.

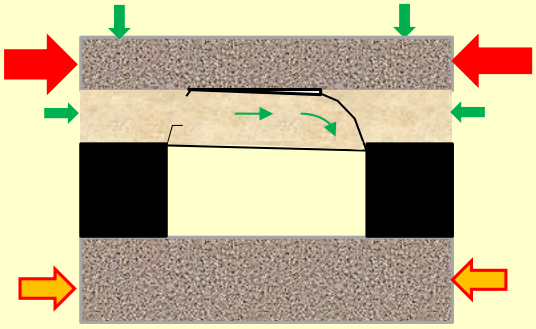
The deflection of the roof and the existing horizontal stress in the ground generates a moment which, in turn, generates an additional horizontal stress component.



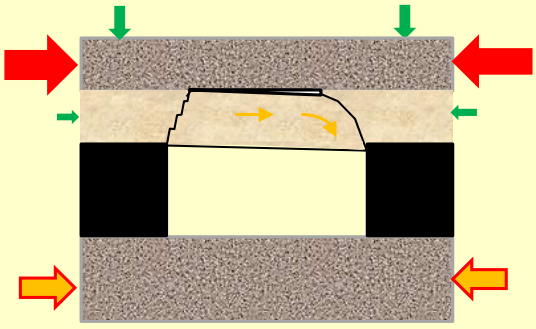
(a): Before excavation



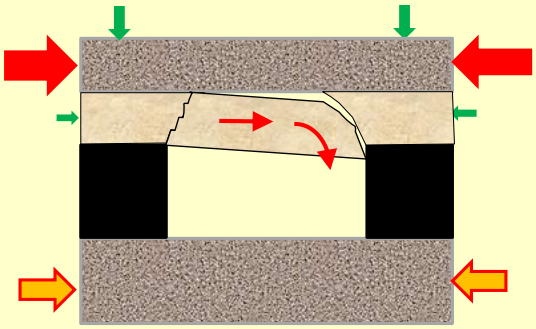
(b): Onset of slip after excavation



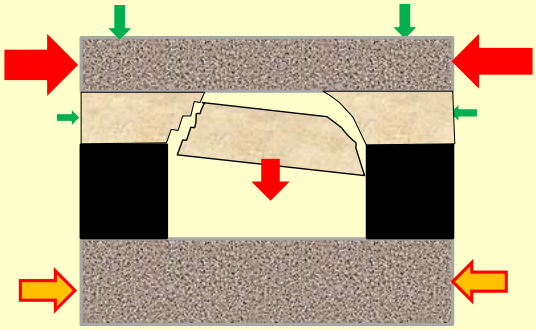
(c): Bending of the roof and crack initiation, Reduction of stress



(d): Full formation of the crack, further bending of the roof



(e): acceleration of roof movement



(f): Ultimate failure

Figure 3-14 Diagram showing failure mechanism when high horizontal stress is combined with a slip (Alan et al 2003)

Van der Merwe (2000) has documented cases where rock falls reportedly caused by horizontal stress were found later to be due to other reasons. The first case refers to a mine in South Africa where gutters were forming in the roof when an air head had to be blasted in particularly bad areas. The problem was seemingly resolved by narrowing the width of the roadways which points to a beam mechanism rather than an issue of horizontal stress.

In the second case where mining was carried out at a depth of about 45 m, major rock falls were taking place in the back area and progressed diagonally across the section. Since the roof falls were oriented at 90 degrees to the line of maximum horizontal stress, a high horizontal stress was postulated and, for confirmation purposes, an in situ stress measurement was carried out. The test results revealed a magnitude of 6.4 MPa for the major horizontal stress and a k-ratio in excess of 5.7. Although the stress was relatively high for a depth of 45 m, Van der Merwe argued that 6.4 MPa is equivalent to the stress prevailing at a depth of 134 m in normal conditions and that roof falls were quite unusual at these depths. Subsequently, the Coal Mine Roof Rating of the roof was found to be 23, which is considered as weak. The problem was rather a result of the weak roof than a high horizontal stress.

In the third case study, van der Merwe (2002) described an area of a colliery affected by major falls of ground. Prior to the falls of ground, the roof bolts installed in the roof snapped in spite of the fact that pull-out resistance tests performed on them indicated that their resistance was significantly greater than the standard required (150KN compared with 30KN).Investigations indicated that the high value of horizontal stress was the cause of the falls of ground. However, a close look at the broken roof bolts revealed that the problem lay elsewhere. The roof bolts were equipped with a shear pin to enable proper mixing of the resin. Upon initial spinning before pre-tension of the bolts, because of the presence of the groove, a misalignment of threads occurred. This misalignment resulted in the shear pin staying mangled in the thread. As a result, damage to the roof bolts was due to the excessive torque at the position where the threads ended, hence the failures of the bolts.

Ndlovu and Stacey (2007) embarked on a study aiming at understanding guttering occurring at Nooitgedacht (now called Kenako), a coal Mine in Mpumalanga province in South Africa. They concluded that guttering was a major threat to safety and productivity. The falls of ground observed at Nooitgedacht were sudden and violent, and unlike most cases of guttering, they were occurring in the centre of the roadway. The study focused on trying to understand the mechanism involved through numerical modelling by making use of a three-

dimensional Finite Difference Code (FLAC 3D). Elastic, transversely anisotropic elastic and inelastic models were investigated and the stress distribution around a roadway analysed.

Different failure criteria such as Mohr- Coulomb, Mohr-Coulomb Strain Softening and Extension Strain were used in turn to predict the extent of failure. It was found that neither the elastic nor transversely anisotropic models predicted abnormally high stress at the middle of the roadway to justify onset of failure in this location as observed at the mine. In the inelastic models, neither the Mohr-Coulomb nor the Mohr Coulomb strain softening models predicted the depth or the width of the guttering adequately. However, the extension strain criterion was found to be more successful. The extension strain is a failure criterion which was designed to predict failure of brittle rock under relatively low stress. This failure criterion predicted the onset of failure at the corners of the roadways and in the centre of the roadways ahead of the face. Therefore, it was postulated that fracture initiation was taking place ahead of the face and that there was an opening up of fractures occurring on blasting. This conclusion agreed well with observations made at the mine where sudden failures were occurring directly after blasting the face.

3.2 Review of theory related to stress origin

A sound understanding of the origin of ground stress allows the prediction of their magnitude and orientation on a regional scale. There are various theories which make an attempt to explain origin of virgin in situ stress (the undisturbed stress regime) and the high horizontal stresses observed at shallow depth. In this section the most common theories related to ground stress origin have been reviewed and analytical and numerical models have been used to illustrate some of these theories and investigate the influence of factors such as weathering, erosion, sedimentation and topography on in situ stress.

Stephansson and Amadei (1997), have presented the most popular theories of ground stress origin which are:

- Poisson's effect;
- Tectonic stress;
- Residual stress; and
- Dyke intrusion;

Each theory has its own limitation and there is no single theory applicable in every case.

3.2.1 Poisson's effect Theory

The Poisson's effect theory postulates that rock under a vertical stress tends to expand laterally and that horizontal stress builds up as a result of restriction of this lateral deformation. For an isotropic, homogeneous and elastic material, the horizontal stress component is given by the following expression:

$$\sigma_h = \sigma_v \nu/(1-\nu)$$

Where:

σ_v: Vertical stress component

σ_h: Horizontal stress component

ν: Poisson's ratio (< 0.5)

From this equation, for an hydrostatic condition (Horizontal stress =Vertical stress), the Poisson's ratio is equal to 0.5. Therefore, this theory does not explain horizontal stresses higher than the vertical stress.

3.2.2 Tectonic Stress Theory

The tectonic stress theory is widely accepted in the USA and Australia. According to this theory, high horizontal stresses result from the thrust generated by continental plates pushing one against others. In addition, the continuing movement of the earth's crust over the molten magma is the driving force which causes faulting and uplifting.

3.3 Origin of in-situ stress in Southern Africa

The Earth map in Figure 3-15 is a summary of the configuration of the tectonic plates and the position of the Africa plate (AF), the Somalia plate (SO) and the East Africa rift.

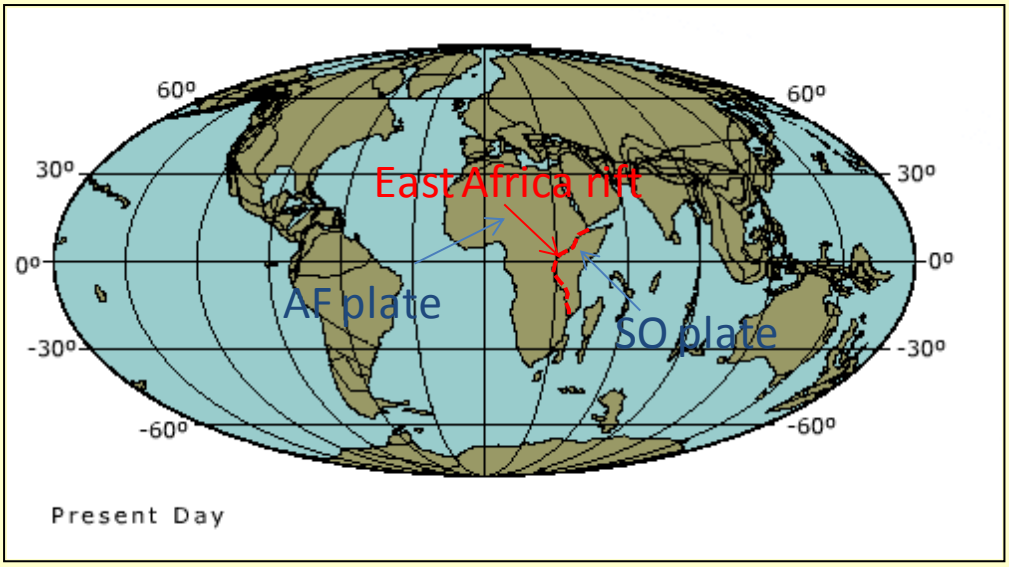


Figure 3-15 map showing the configuration of tectonic plates as is today and the East Africa rift (Unkown 2010)

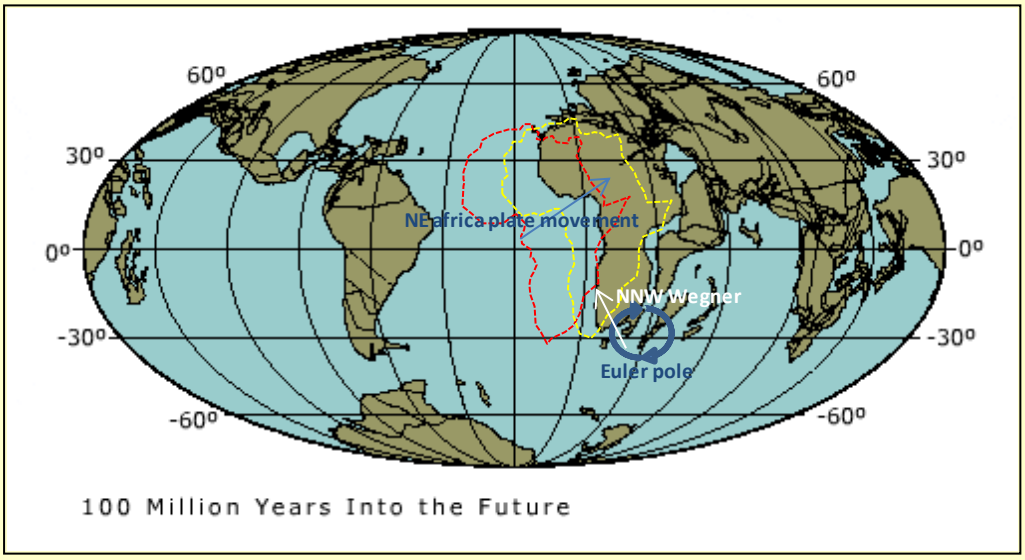


Figure 3-16 Map illustrating the anticipated configuration of tectonic plates 100 Ma into the future, NE movement of the Africa plate, The Euler pole and the NNW direction of the Wegner stress (Unknown 2010)

The map in Figure 3-16 is a projected position of continental plates 100 Ma in the future and emphasizes the main tectonic activities in southern Africa. The movement northward of the Africa plate creates the Mediterranean Sea and the Alps. The position of the Euler pole, which is the centre of rotation of the Somalia plate relative to the Africa plate as estimated by Chu and Gordon (1999) is also identified in the figure.

Although the East Africa rift is recognised to propagate southward and the Africa plate northeast, the south-western African region is broadly dominated by an in situ stress regime orientated NW-SE to NNW-SSE also referred to as Wegener anomaly (Bird, et al. 2006).

The Wegner anomaly was studied in detail by Bird, et al. (2006) who collected information on stress "regime" described by the associated Andersonian fault types (Figure 3-17) and use a thin shell finite element analysis with realistic rheology to test three hypothesis of stress origin:

- Lateral variations in density momentum
- Resistance of unbroken lithosphere to relative plate rotation, and
- Stress concentration ahead of a crack tip.

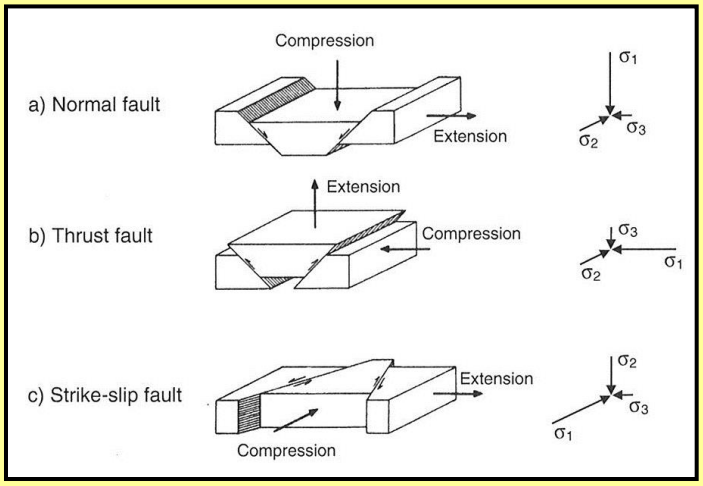


Figure 3-17 Anderson theory for determining orientation of rock stress

Further to this analysis it was found that the model with lateral variations in density momentum was unsuccessful in reproducing the stress regime and the azimuth of in-situ stress (59-73% incorrect regimes; 32-40° azimuth errors). A model, in which Africa-Somalia spreading has been regulated at a realistic level by remote boundary conditions, yields more accurate results (18-41% incorrect regimes; 25-35° azimuth errors) (Bird, et al. 2006).

It was also found that by assuming a frictionless East Africa rift, the accuracy obtained previously decreased. Therefore, it was concluded that the Wegener anomaly was most likely the result of the resistance to the relative rotation of the Somalia and Africa plates and that the large strains occuring at the rift would have weakened the rock significantly(Bird, et al. 2006).

The origin of the Wegener anomaly as a result of resistance of the tectonic plates to the southward motion of the East Africa rift has been contested by Andreoli, et al. (2007) following a tectonic study around Cape Town. The study confirmed evidence of the Wegner anomaly in rocks which predates the initiation of the East Africa rift by more than 60 Ma which is in contradiction with the result that the East Africa rift is the driving force behind the Wegner anomaly. As far as the author is aware no plausible theory can explain the origin of the Wegener anomaly since the Cretaceous age and it is important to recognise that there is not yet any universally accepted theory pertaining to the origin of in situ stress in Southern Africa.

3.3.1 Residual Stress Theory

According to the residual stress theory, millions of years ago the earth's crust was covered by thousands of metres of materials such as lava and ice. On erosion of that material, the vertical stress relaxed while the horizontal stress remains locked in.

To illustrate this theory a numerical model using the Finite element program Phase2 by Rocscience was set up as shown in Figure 3-18. The model is made of 9 layers which are gradually mined out to simulate an erosion process. A query is placed at 700 m below the free surface of the model. A gravitational field stress was used as virgin in situ stress with a unit weight of 0.025 MN/m3. The parameters used in the numerical and analytical model are summarized in Table 3-1.

The initial k-ratio was set up as 1. The resulting k-ratio function of the height of erosion is illustrated in Figure 3-19.

Table 3-1 Summary of the parameters used in the erosion model

Elastic Modulus (Gpa)	20.7
Shear Modulus (GPa)	8.28
Poisson's ratio	0.35
Unit weight (MN/m3)	0.027
Initial stress ratio	1

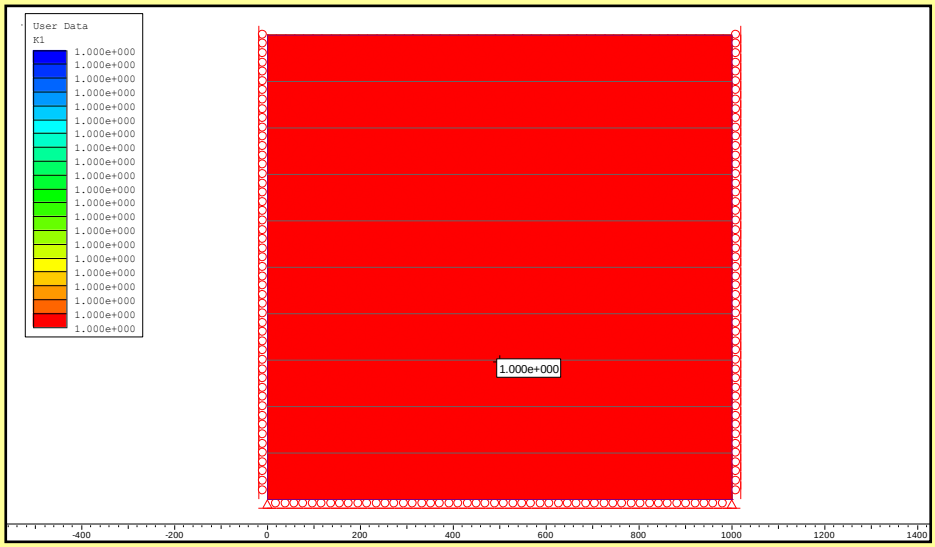


Figure 3-18 Phase 2 model used to investigate the influence of erosion on the k-ratio

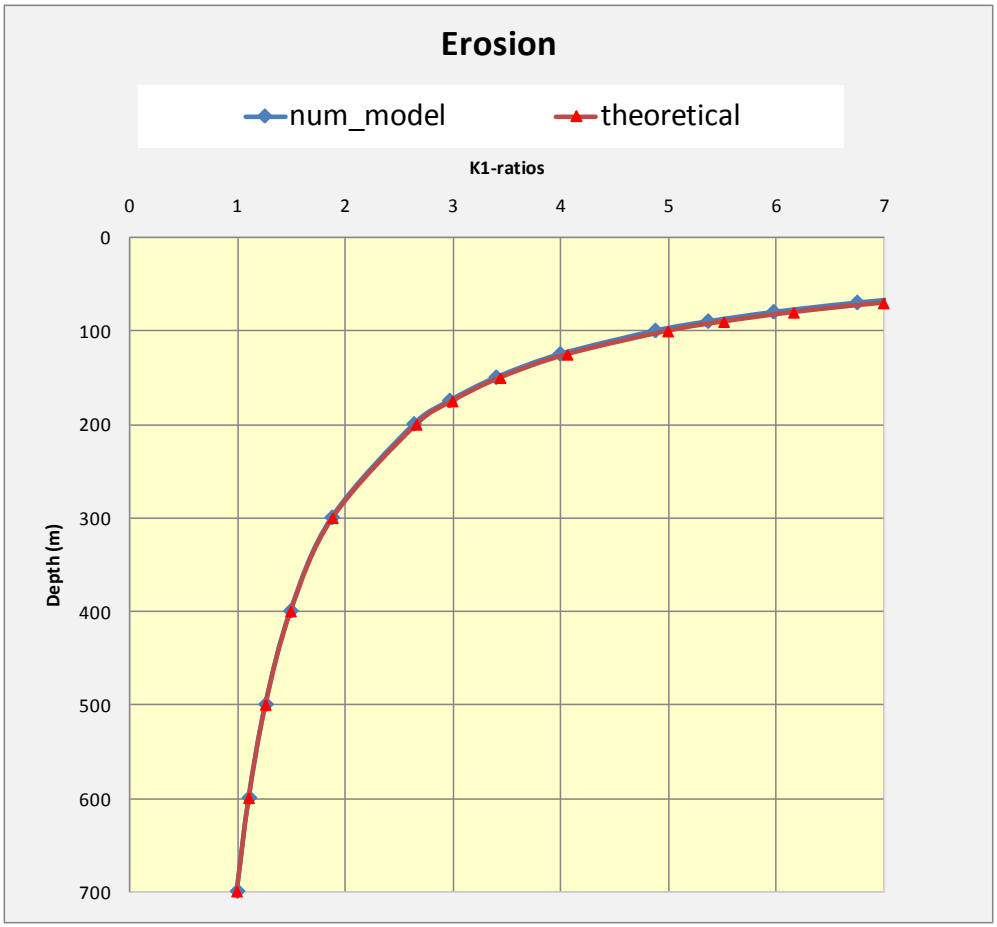


Figure 3-19 Graph illustrating how the k-ratio varies with depth on erosion

To support the results obtained by finite element analysis, an analytical approach was used. In this regard the following formula proposed by Baek et al (2006) was used:

$$K = K_0 + \left[\left(K_o - \frac{\nu}{1-\nu}\right)\Delta Z\right]\frac{1}{Z}$$

where:

K_o: initial k-ratio

ν: Poisson's ratio

ΔZ: depth of erosion

Z: depth at which the measurement is taken

The results of the analytical approach are also plotted in Figure 3-19 allowing comparison with the results from the numerical model.

The variation of k-ratio on sedimentation was investigated using a very similar model. The input parameters were the same. However, in this analysis, layers are added on top of others so as to simulate a sedimentation process. The results obtained following the analysis are given in Figure 3-20.

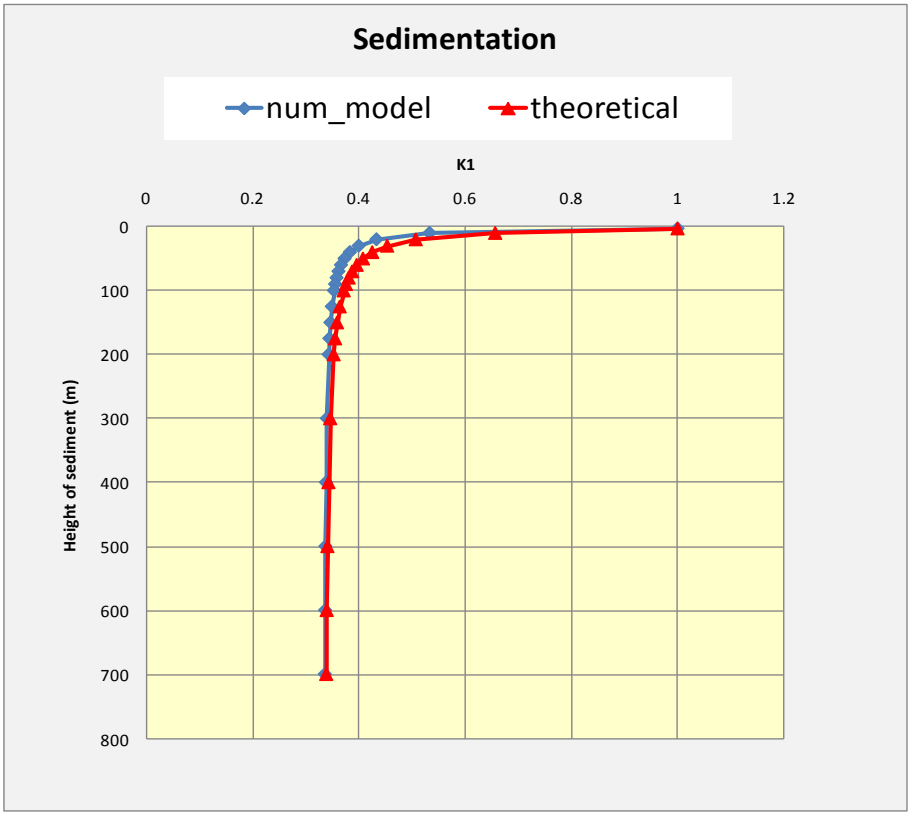


Figure 3-20 Graph showing variation of k-ratio on sedimentation

As for the erosion case, validation of results obtained by numerical analysis was conducted analytically using the following formula proposed by Baek et al (2006):

$$K = K_0 - \left[\left(K_o - \frac{\nu}{1-\nu}\right)\Delta Z\right]\frac{1}{Z}$$

The parameters in the equation are as defined above. It can be seen in Figure 3-20 that results for both approaches correlate well.

In Figure 3-19 the variation of k-ratio with erosion is small at the beginning of the erosion process and intensifies as the erosion process proceeds. In Figure 3-20, the k-ratio decreases rapidly to a residual value of about 0.35 and stays approximately constant for the remainder of the sedimentation process. In both analyses the initial k-ratio of 1 indicates that all stresses (vertical and horizontal) have fully relaxed to equilibrium as per Heim's rule which stipulates that for weak rocks unable to withstand large deviatoric stress difference, lateral and vertical stresses tend to equalize over geological time (Tani 1997).

The results of the erosion model show clearly that the vertical stress relaxes at a higher rate than the horizontal stress. The results also show that the horizontal stress stays locked in. This is demonstrated by the increase in k-ratio as the erosion process proceeds.

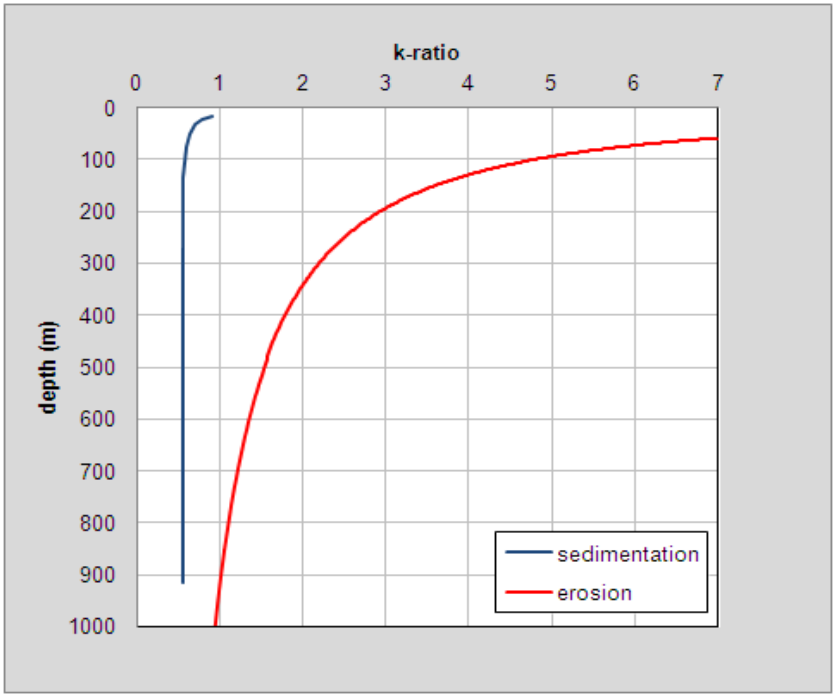


Figure 3-21 Graph illustrating k-ratio versus depth for both sedimentation and erosion

The sedimentation and erosion curves are shown together in Figure 3-21. In reality, the formation of a basin involved both stages of sedimentation and erosion combined. Therefore in situ stress measurements can be expected to give values falling somewhere between the two curves. Furthermore, the difference between the curves at a particular depth is a measure of the variability of the k-ratio. Note that this variability is small at deeper levels and very high at shallow depths. From the graph it has to be noted that, at the same depth below

surface, district formed by erosion will exhibit higher k-ratio (high horizontal stress) than those formed by sedimentation.

The inherent variability in k-ratio also explains why accuracy of stress measurements at shallow levels is much lower than at deep levels.

3.3.2 Horizontal stress generated by magmatic intrusion

According to this theory, high horizontal stress is the result of high thrust developed during the igneous intrusion of dykes. This theory holds when high horizontal stresses are associated with structural features such as dykes, but is questionable in the absence of such features.

3.4 Influence of weathering

It is often perceived that high concentration of horizontal stress occurs underneath weathered material. Mines in South Africa have reported experiencing ground control issues when mining under rivers and weathered material. In order to investigate and verify these reported cases, analytical and numerical models have been conducted and the outcomes of these analyses are presented in this section.

3.4.1 Theoretical model

The theoretical model of weathering follows the work of Baek, et al (2006). The model is subdivided into two regions; intact rock at the bottom and weathered rock at the top. The weathered rock is subdivided into 5 m thick layers. In this weathered region of the model the model material properties (cohesion and friction) are gradually reduced from the bottom up. It is assumed that the weathered material has zero cohesion and that its strength is purely frictional. The effect of confinement and the corresponding increase of frictional strength with depth are addressed by linearly increasing the friction angle of layers in the weathered region with depth. The k-ratio in this region is computed using the following formula:

$$k = (1 - sin\emptyset)/(1 + sin\emptyset)$$

Where:

Ø: friction angle of the layer (degree).

For the intact rock, the k-ratio is computed using the formula:

$$k = 1 + \frac{C}{\gamma H}$$

Where:

C: lateral Pressure (MPa)

γ: Unit Weight of the material (MN/m3)

H: depth (m)

The material properties used in this analysis are summarized in Table 3-2.

Table 3-2 Summary of parameters used in the numerical and theoretical analysis

Material type	Layer 1	Layer 2	Layer 3	Layer 4	Layer 5	Layer 6	Layer 7	Layer 8	Layer 9
Initial element loading	field stress & body force								
Unit weight	0.027 MN/m3	0.003125 MN/m3	0.00625 MN/m3	0.009375 MN/m3	0.0125 MN/m3	0.015625 MN/m3	0.01875 MN/m3	0.021875 MN/m3	0.027 MN/m3
Elastic type	isotropic	isotropic	isotropic	isotropic	isotropic	isotropic	isotropic	isotropic	isotropic
Young's modulus	20 MPa	78.75 MPa	157.5 MPa	236.25 MPa	315 MPa	393.75 MPa	472.5 MPa	551.25 MPa	630 MPa
Poisson's ratio	0.29	0.29	0.29	0.29	0.29	0.29	0.29	0.29	0.29
Failure criterion	Mohr-Coulomb								
Tensile strength	0 MPa	0 MPa	0 MPa	0 MPa	0 MPa	0 MPa	0 MPa	0 MPa	
Peak friction angle	2 degrees	3.75 degrees	7.5 degrees	11.25 degrees	15 degrees	18.75 degrees	22.5 degrees	26.25 degrees	
Peak cohesion	0.01 MPa	0.01 MPa	0.01 MPa	0.01 MPa	0.01 MPa	0.01 MPa	0.01 MPa	0.01 MPa	
Material type	Plastic	Plastic	Plastic	Plastic	Plastic	Plastic	Plastic	Plastic	0 MPa
Dilation Angle	0 degrees	0 degrees	0 degrees	0 degrees	0 degrees	0 degrees	0 degrees	0 degrees	30 degrees
Residual Friction Angle	2 degrees	3.75 degrees	7.5 degrees	11.25 degrees	15 degrees	18.75 degrees	22.5 degrees	26.25 degrees	0.1 MPa
Residual Cohesion	0.01 MPa	0.01 MPa	0.01 MPa	0.01 MPa	0.01 MPa	0.01 MPa	0.01 MPa	0.01 MPa	Elastic
Piezo to use	None	None	None	None	None	None	None	None	None
Ru value	0	0	0	0	0	0	0	0	0

Figure 3-22 illustrates the trend of k-ratio with depth in both the weathered (plastic) region and in the intact (elastic) region at a depth of weathering of 40 m and a lateral pressure (horizontal stress) of 2 MPa.

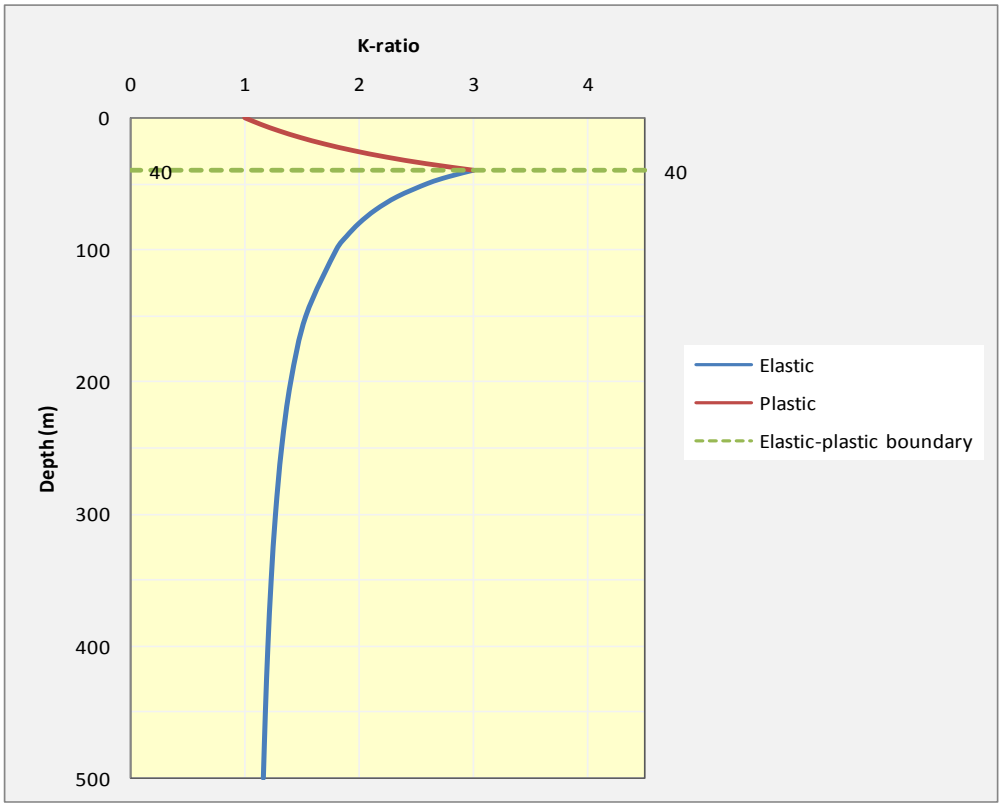


Figure 3-22 Elasto-plastic curves of k-ratio as a function of depth at a lateral pressure of 2 MN/m^2 and at a corresponding weathering depth of 40 m

Figure 3-23 shows the effect on the k-ratio of increasing the depth of weathering from 40 m to 80 m and increasing the lateral pressure. The dashed curve in the figure is that of the k-ratio as a function of depth in the intact rock for a 2 MPa lateral pressure. It can be seen that this curve crosses that of k-ratios in the weathered material at a depth which is less than 80 m. For both curves (k-ratios in the intact and the weathered material) to cross each other at the set up weathering depth of 80 m the lateral pressure has to be increased from 2 MPa to 4 MPa. This indicates that when everything else remains constant, an increase in the weathered depth implies a proportional increase in the lateral pressure (horizontal stress).

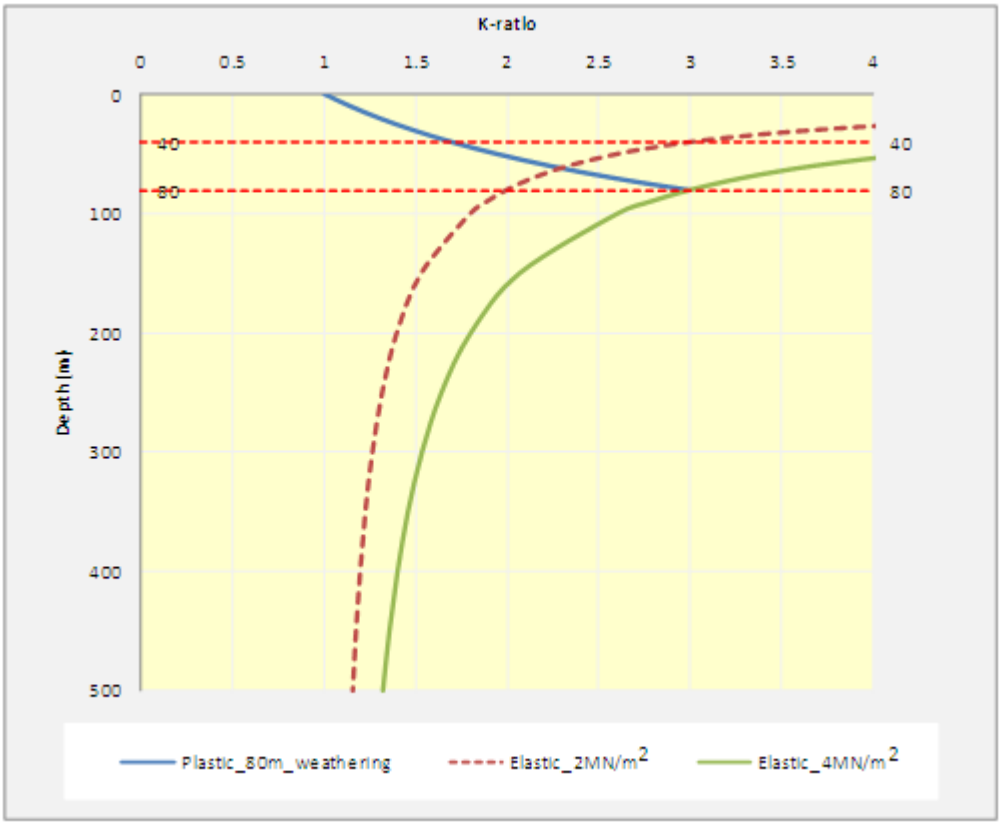


Figure 3-23 Graph showing that increasing the depth of weathering implies an increase of lateral pressure

Similarly, Figure 3-24 illustrates how increasing weathering depth implies an increase of lateral pressure. In the figure weathering depths used are 40 m, 80 m and 120 m; the lateral pressure was found as 2 MPa, 4 MPa and 6 MPa. It is important to note that in the figure the maximum k-ratio does not change and in this case, is equal to 3. The reason is because the maximum k-ratio is function of the strength of the intact rock alone. Therefore at the same weathering depth, a higher k-ratio (higher horizontal stress) is expected when the underlying intact rock is competent (stiff) as opposed to a soft rock (Figure 3-25). The relationship between the maximum k-ratio and the frictional strength of the intact rock is given by the following equation:

$$K = \frac{(1+\sin\Phi')}{(1-\sin\Phi')}$$

Figure 3-26 illustrates the relationship between the maximum k-ratio and the frictional strength of the underlying intact rock. Figure 3-27 compares elasto-plastic curves obtained

from the theoretical model and from a numerical model using the finite element program Phase2. The input data for the numerical analysis are the same as for the theoretical model and are summarized in previous Table 3-2. The lateral pressure in the model was assigned using the "locked-in pressure" option available in Phase2. The locked in pressure is a constant additional pressure assigned to the whole model on top of the normal horizontal stress generated by Poisson's effect. This option is useful since it helps take account of stress concentration in particular layers for instance (stiff material). Results of the numerical analysis are slightly different from those obtained by the theoretical model with a maximum k-ratio of 4 instead of 3. However the trend of k-ratio with depth remains very much the same.

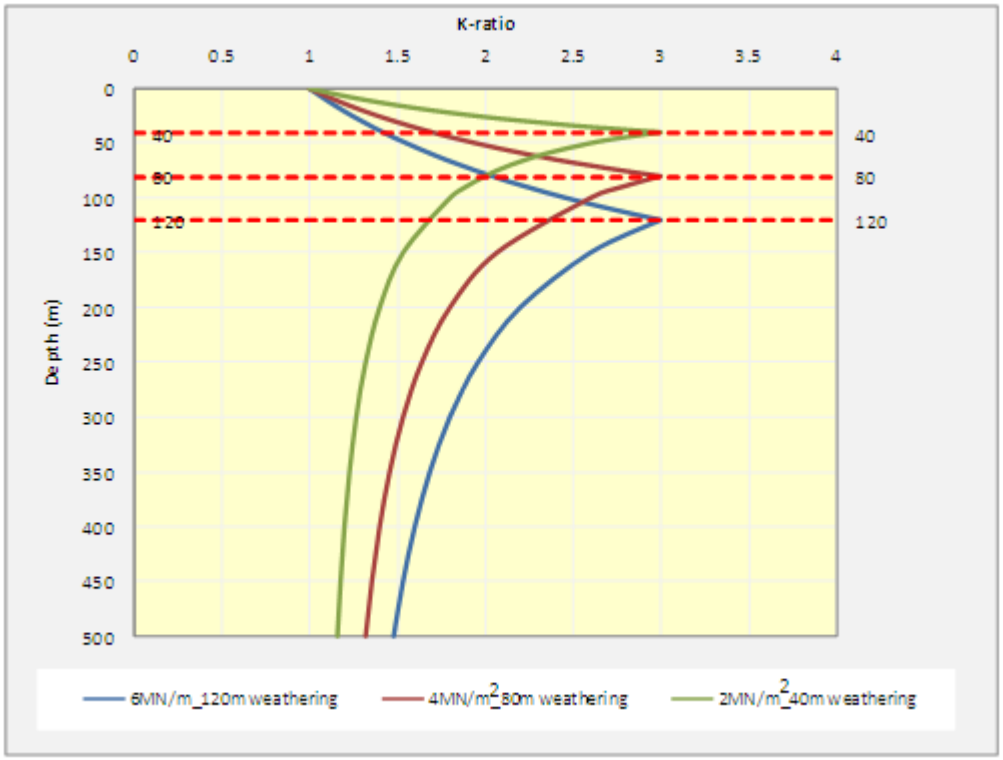


Figure 3-24 Graph showing how increase of lateral pressure leads to a corresponding increase of the weathering depth while keeping the maximum value of the stress-ratio unchanged

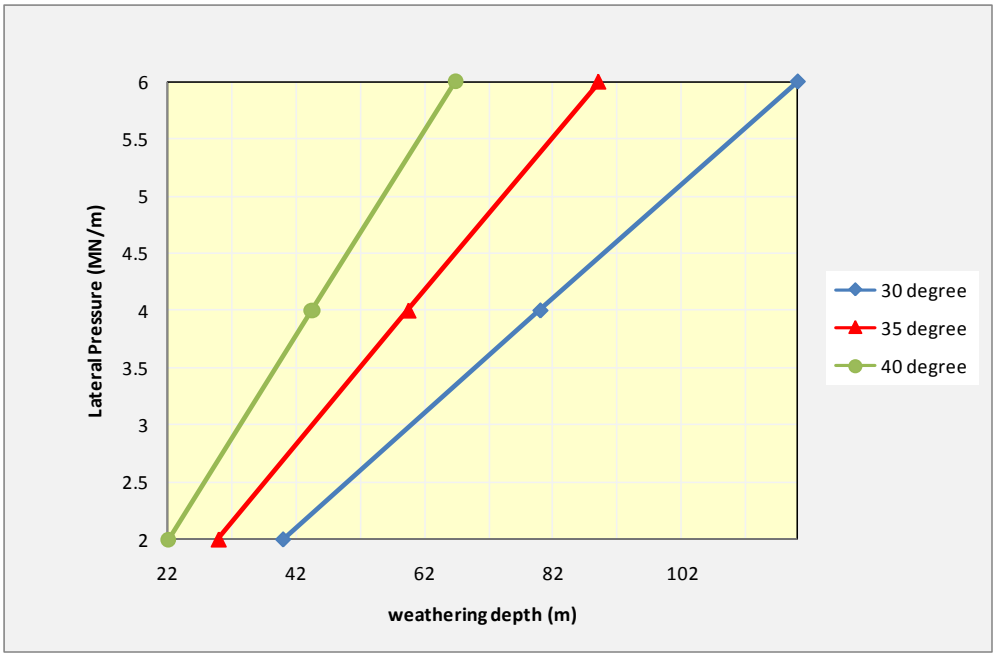


Figure 3-25 Figure illustrating the relationship between the depth of weathering and the Lateral Pressure for different values of friction angle of intact rock

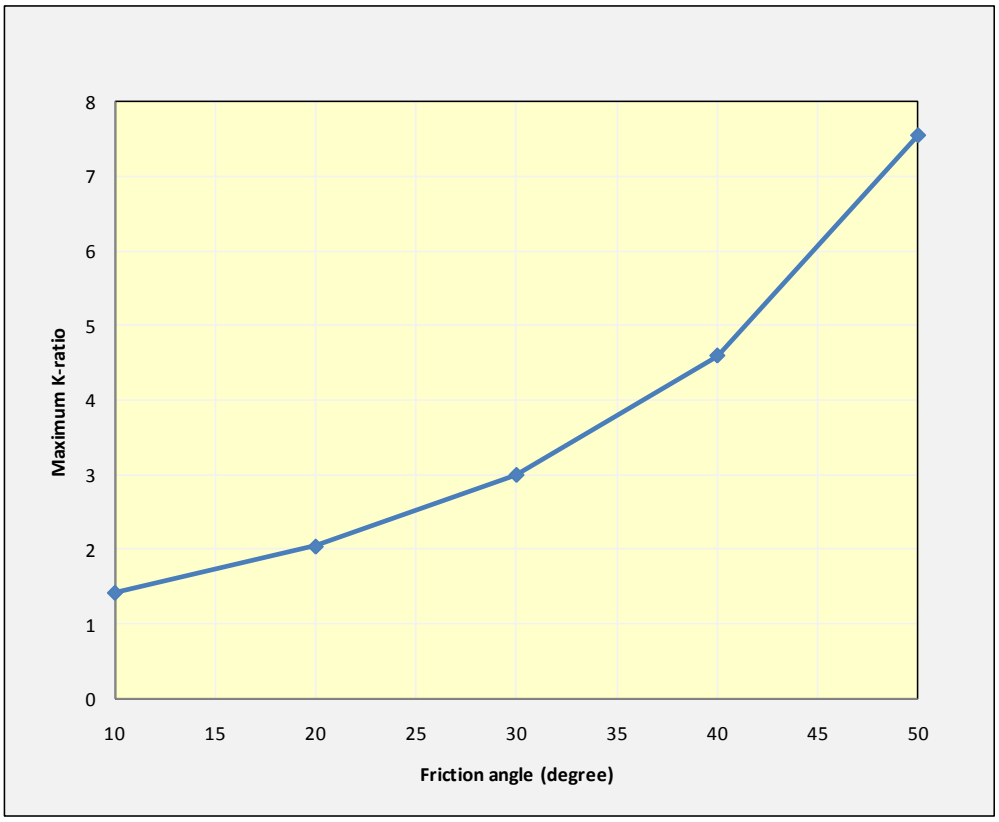


Figure 3-26 Graph showing trend of K-ratios with the strength (friction) of the intact rock

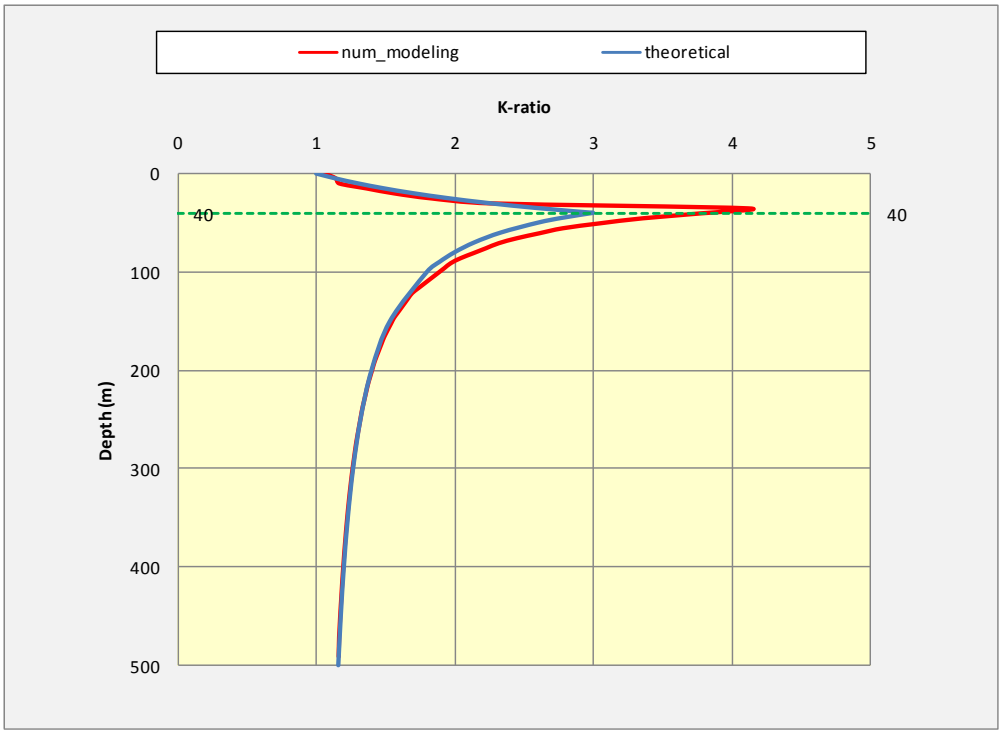


Figure 3-27 Figure illustrating the elasto-plastic curves obtained by numerical modeling and analytically for a weathering depth of 40 m and a lateral pressure of 2MPa

3.4.2 Evidence of impact of weathering on Horizontal stress

Evidence of high horizontal stress underneath a thick weathered layer was observed in the box cut of Nooitgedacht colliery, in the Witbank Coalfield where buckling was developing in a weak horizon (Shale) below a thick layer weathered material (Minney 2011). These peculiar features were some times associated with fracturing of the rock. In addition, it was observed that the adjacent competent sandstone layer remained horizontal.

A very similar phenomenon was observed in a cut slope on the National road 17 to Bethal where undulated features were observed in the shale layer underneath a soil layer while the competent sandstone below showed no sign of buckling (Figure 3-28).

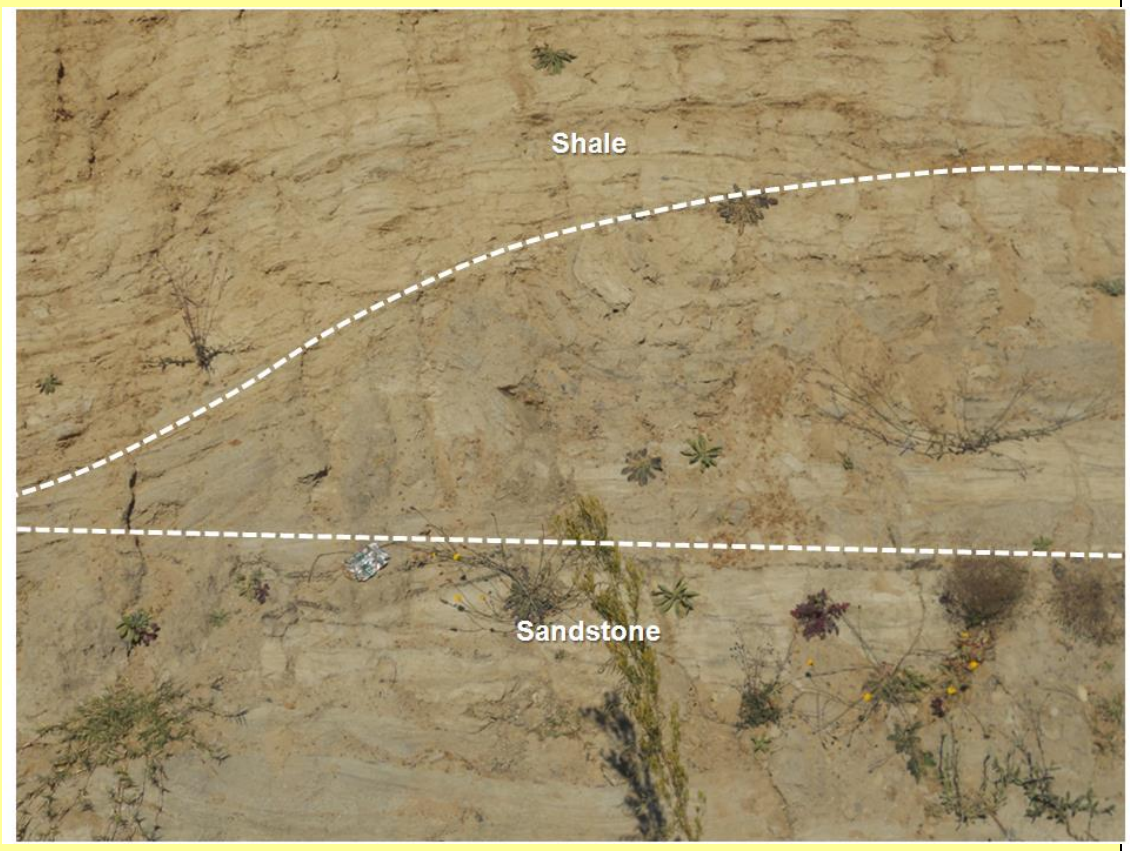


Figure 3-28 Picture showing the site on the road to Bethal where a stress induced buckling in a shale layer was observed

In order to ascertain the origin of these features, wherever possible, the dip direction was measured using a compass as shown in Figure 3-29. It was anticipated that if these features resulted from stress relief, the dip direction would correlate with the NNW-SSE direction of the major horizontal stress in the region.



Figure 3-29 Pictures illustrating measurement of dip direction with a compass

Table 3-3 and Figure 3-30 summarize the measurements of dip direction taken on site. The distribution of the dip direction was generated knowing that the dip direction generally follows a normal distribution. Following this exercise, it was found that the average dip direction was in the same range as the known NNW-SSE direction of the major compressive horizontal stress in the Highveld and Witbank coalfields. Therefore, it was concluded that this buckling in the shale is most likely stress driven and could be proof of the increase of horizontal stress due to weathering.

Table 3-3 Summary of dip direction measurements

measurement	Dip direction
1	340
2	345
3	338
4	320
Mean	335.75
Stdev	9.44
CV	2.81%

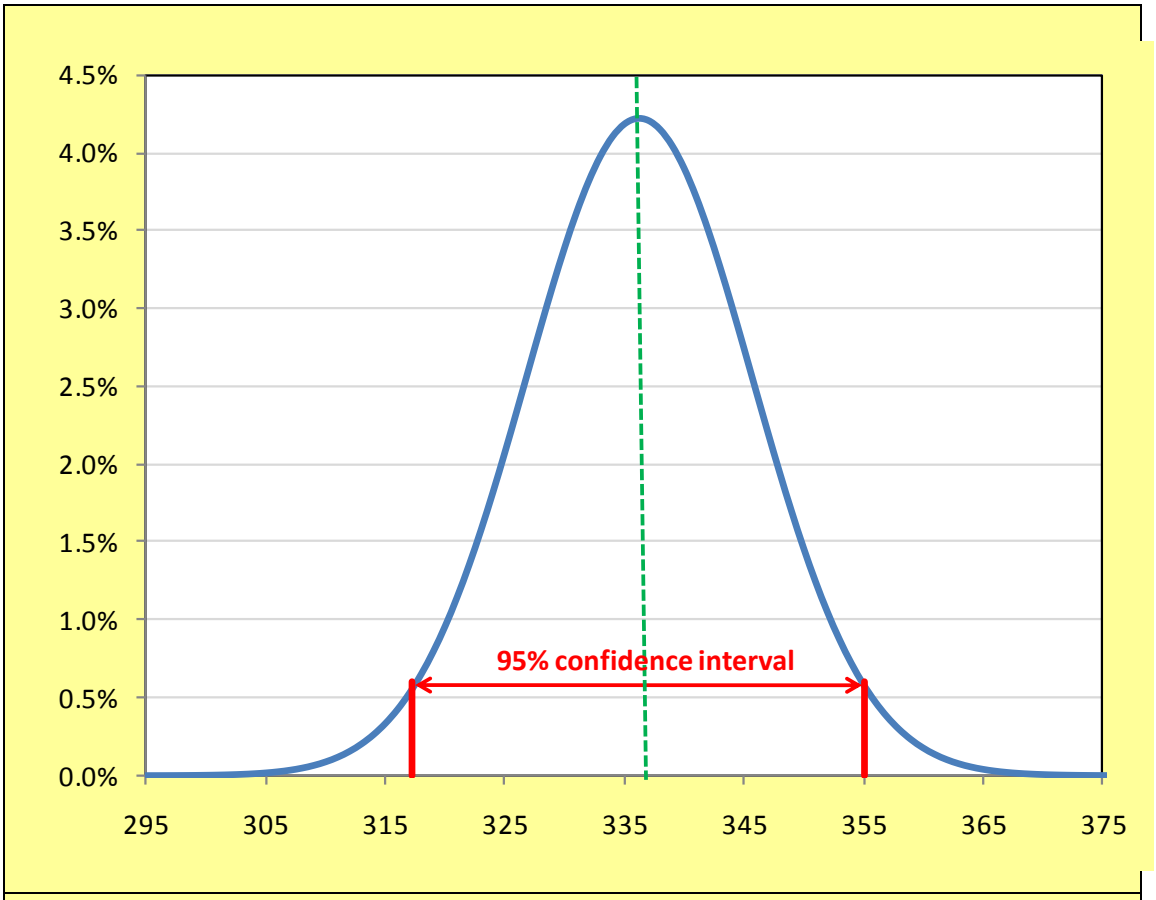


Figure 3-30 Probability density function of dip direction showing the extent of 95% confidence interval

3.5 Influence of topography

Topography has a significant influence on the orientation and magnitude of horizontal stress at shallow depth. In many shallow depth cases (less than 200 m), the influence of topography on orientation of principal stresses is as important as that of tectonic movements (Guangyu, Bai and Jiguang 1986).

In high mountains or valley regions, it was proven by observation and modeling that topography is a dominant factor influencing in situ stress whose maximum principal component coincides with the line between the measuring point and hill-top. However, in smooth terrains the orientation of principal stress is chiefly defined by the orientation of tectonic movements (Guangyu, Bai and Jiguang 1986).

In this section the influence of topography such as hilly districts and basins formed by erosion and sedimentation are examined in detail using numerical analysis. Particular attention has been given to the influence of edges of a basin on in situ stress.

3.5.1 Hilly district formed by erosion

Initially, the model of a hilly district formed by erosion was set up in Phase 2 and boundary conditions and the geometry assigned to the model are as presented in Figure 3-31. The erosion process was simulated by running the model in two stages with stage 1 shown in Figure 3-32 and stage 2 shown in Figure 3-33. The element mesh density was deliberately finer around the hilly district, which is the area of interest. The material properties used for the analysis are summarized in Table 3-4.

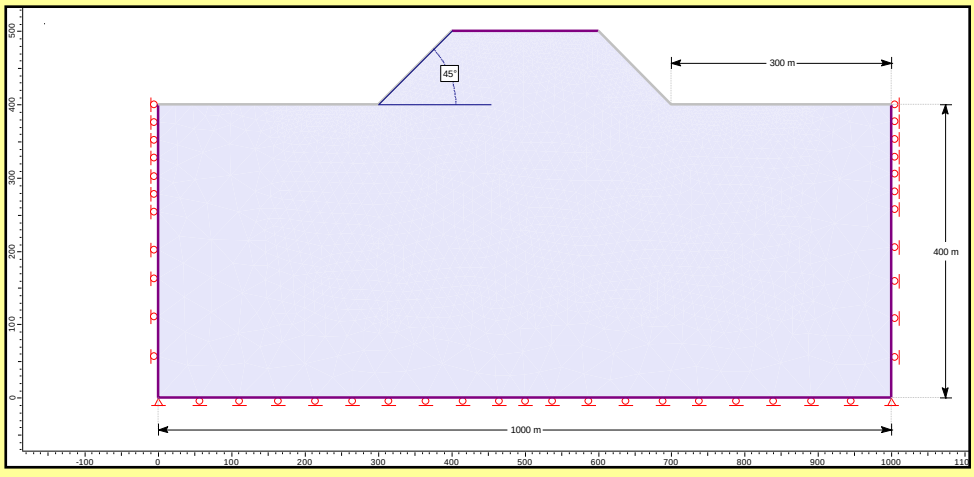


Figure 3-31 Model geometry of the hilly district model (100 m high hill)

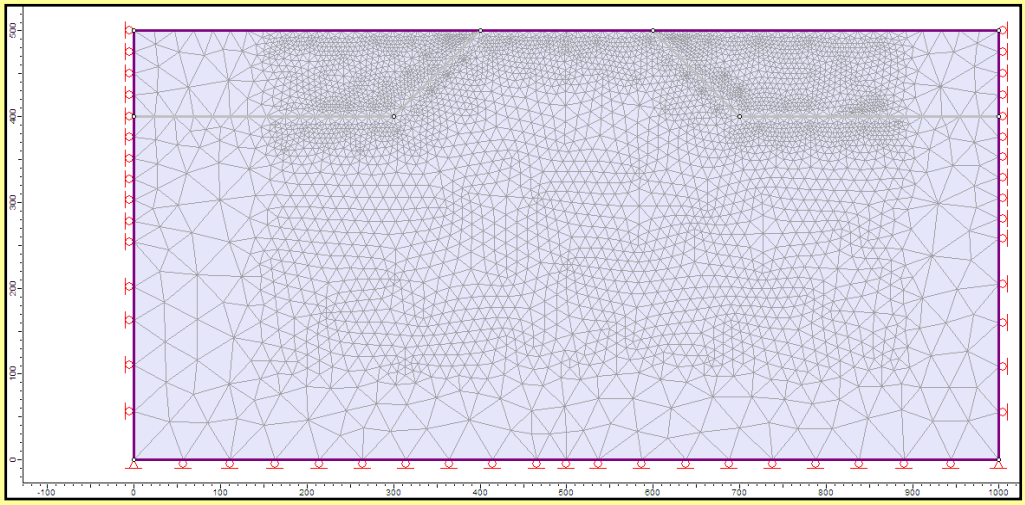


Figure 3-32 Stage 1 of the Hilly district Phase 2 model showing the mesh element density and boundary conditions

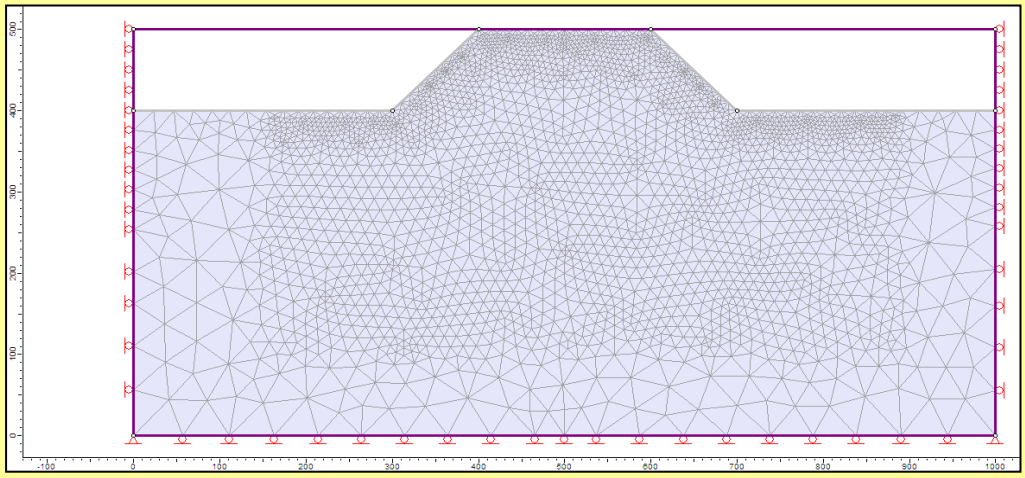


Figure 3-33 Stage 2 of the hilly district Phase 2 model

Table 3-4 Summary of parameters used in the analysis

Elastic Modulus (Gpa)	20.7
Shear Modulus (GPa)	8.28
Poisson's ratio	0.35
Unit weight (MN/m3)	0.027
Initial stress ratio	1

Figure 3-34 presents contours of k-ratio obtained during the analysis. It is important to note that on top and on both sides of the hilly district the k-ratio is in excess of 3. On top of the hilly district the k-ratio decreases rapidly with depth to its initial value of 1 whereas on the sides the k-ratio reverts slowly to its initial value. Expectedly, in the middle of the hilly

district, there is formation of a zone with k-ratio < 1 which persists at depth several times the height of the hill and is due to gravitational spreading (Swolfs and Savage 1986).

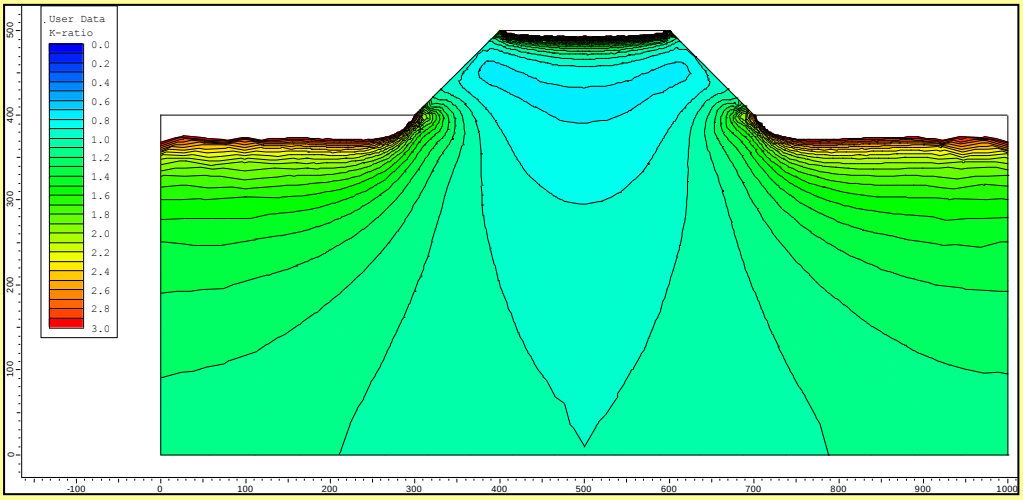


Figure 3-34 Contours of k-ratio after formation of the hilly district by erosion (100 m hill)

3.5.2 Hilly district formed by sedimentation

Similarly, another model was set up to simulate, a hilly district formed by sedimentation. In the program Phase2 the sedimentation was simulated by dumping the hilly district in the second stage. Figure 3-35 presents the contours of k-ratio obtained during the finite element analysis. The same material parameters as used in the erosion case have been used in this analysis.

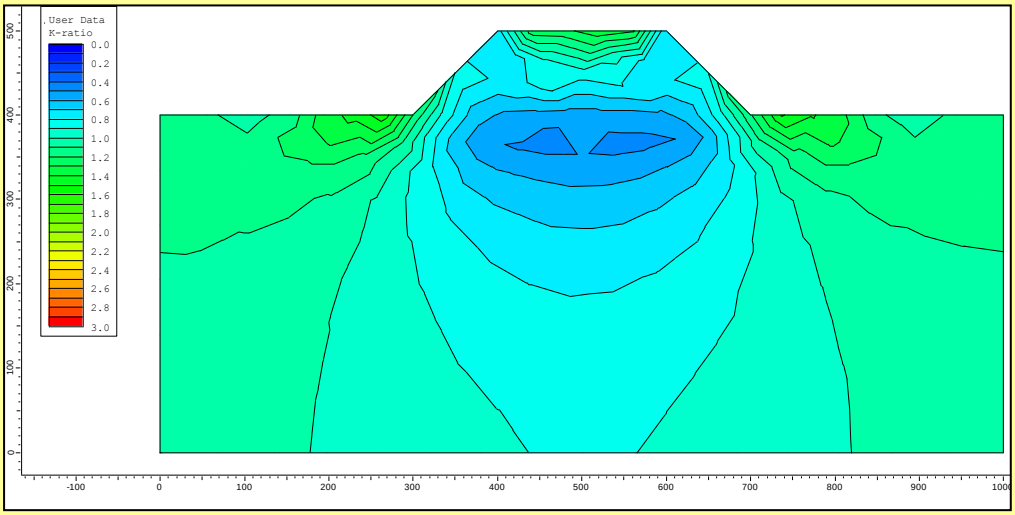


Figure 3-35 Contours of k-ratio after formation of the hilly district by sedimentation (100 m hill)

As observed in the erosion case, there is an increase of k-ratio on top and on both sides of the hilly district. However, unlike the erosion case, this increase is less dramatic. In addition to this, there is formation of a much wider zone where k-ratios are less than 1.

3.5.3 Basin formed by erosion

The influence of a basin formed by erosion on in situ stress was analysed using the program Phase2. In this case, a 100 m wide and 50 m deep basin was gradually widened in100 m steps, to simulate the erosion process taking place. The profile of k-ratio was queried at 10 m below the bottom of the basin rather than on the bottom because results right on the bottom were very erratic. Figure 3-36 to Figure 3-39 present k-ratio contours obtained following the analysis for different widths of the basin and give the profiles of k-ratio 10 m below surface of the basin.

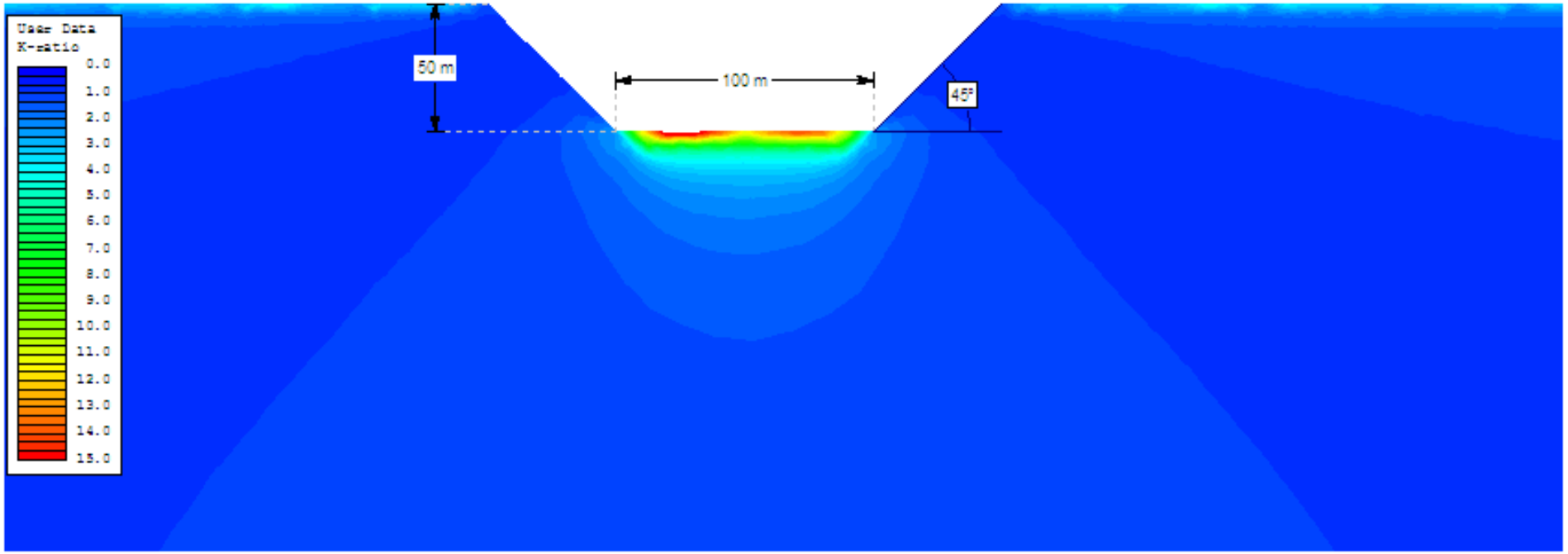


Figure 3-36 Contours of K-ratio for a basin width equal to 100 m

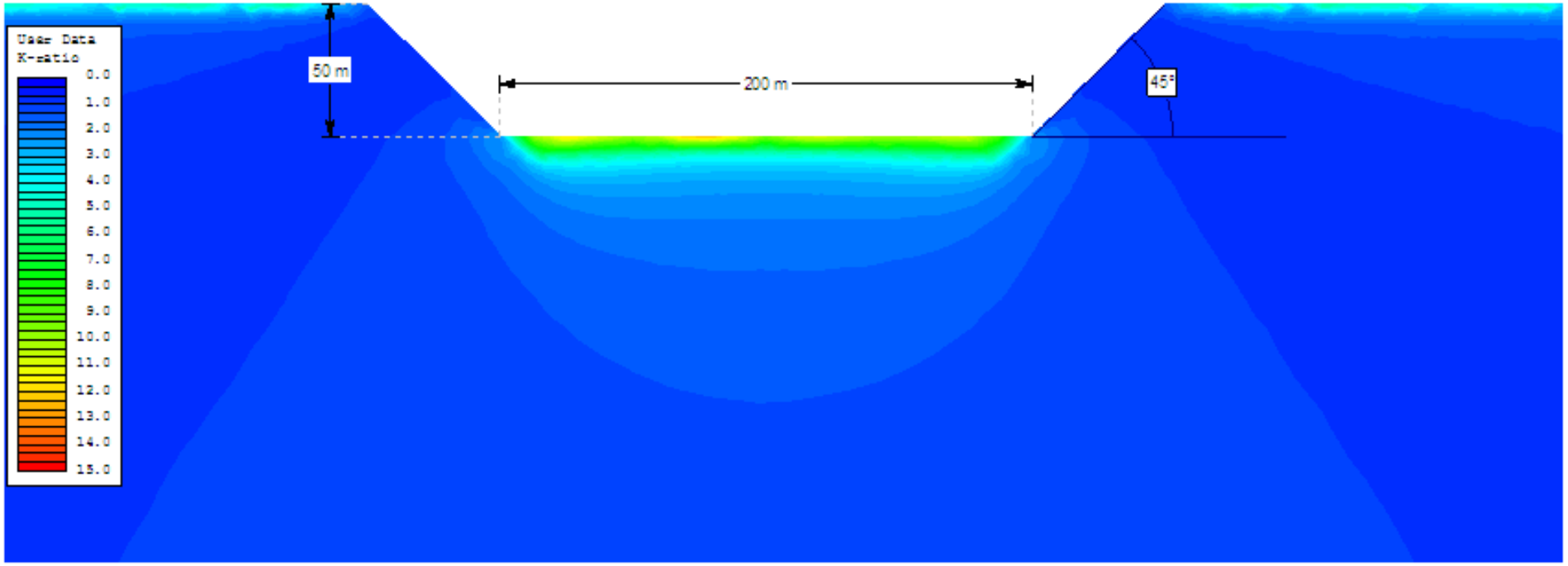


Figure 3-37 Contours of K-ratio for a basin width equal to 200 m

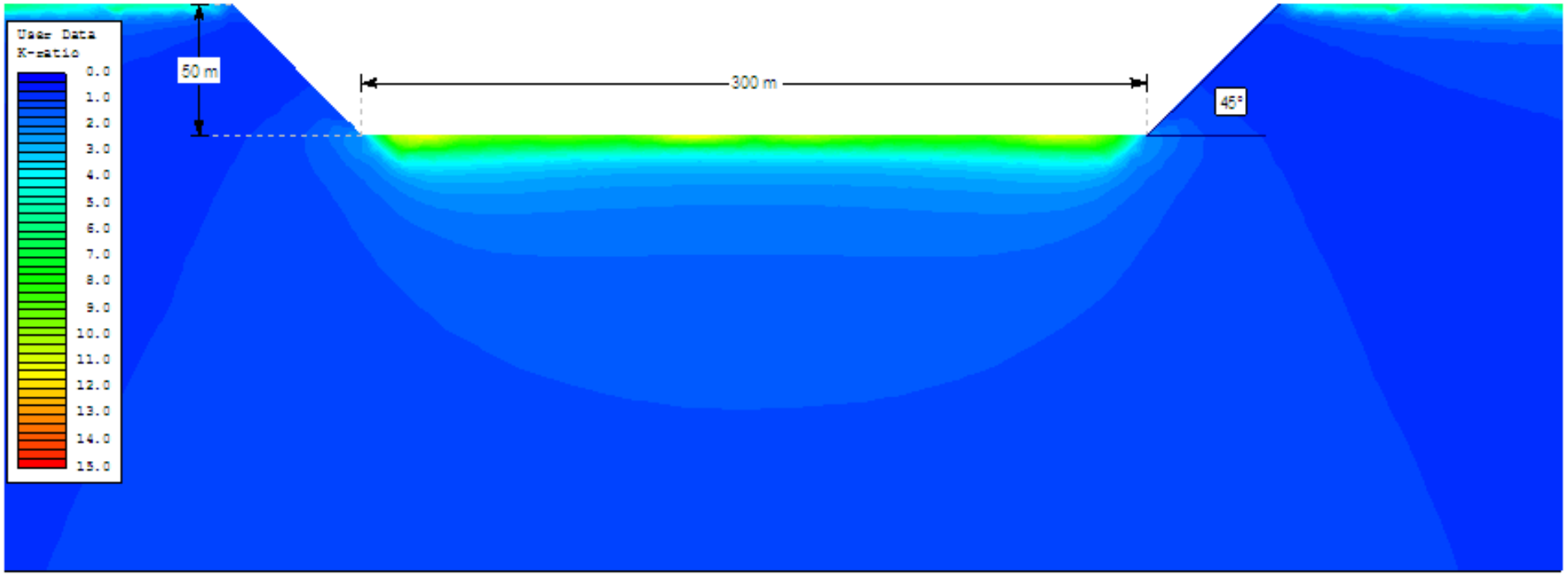


Figure 3-38 Contours of K-ratio for a basin width equal to 300 m

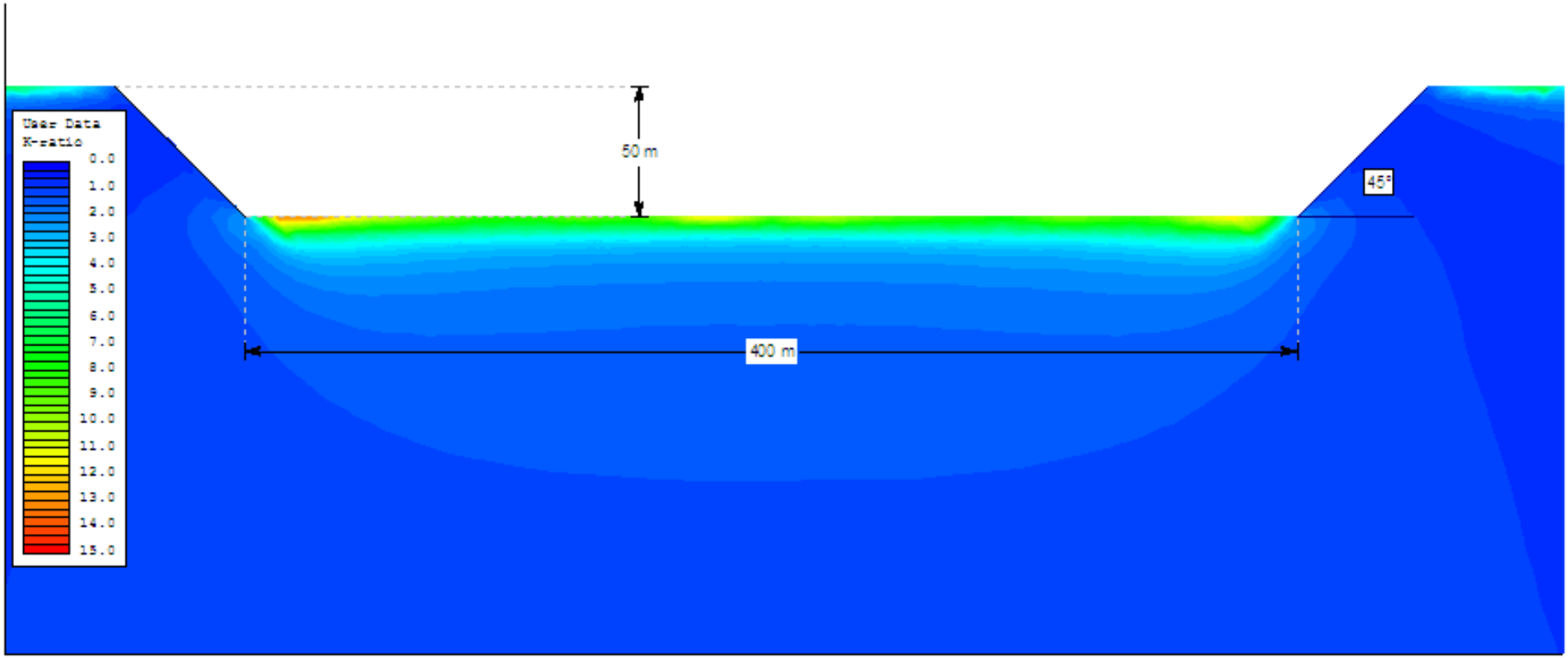
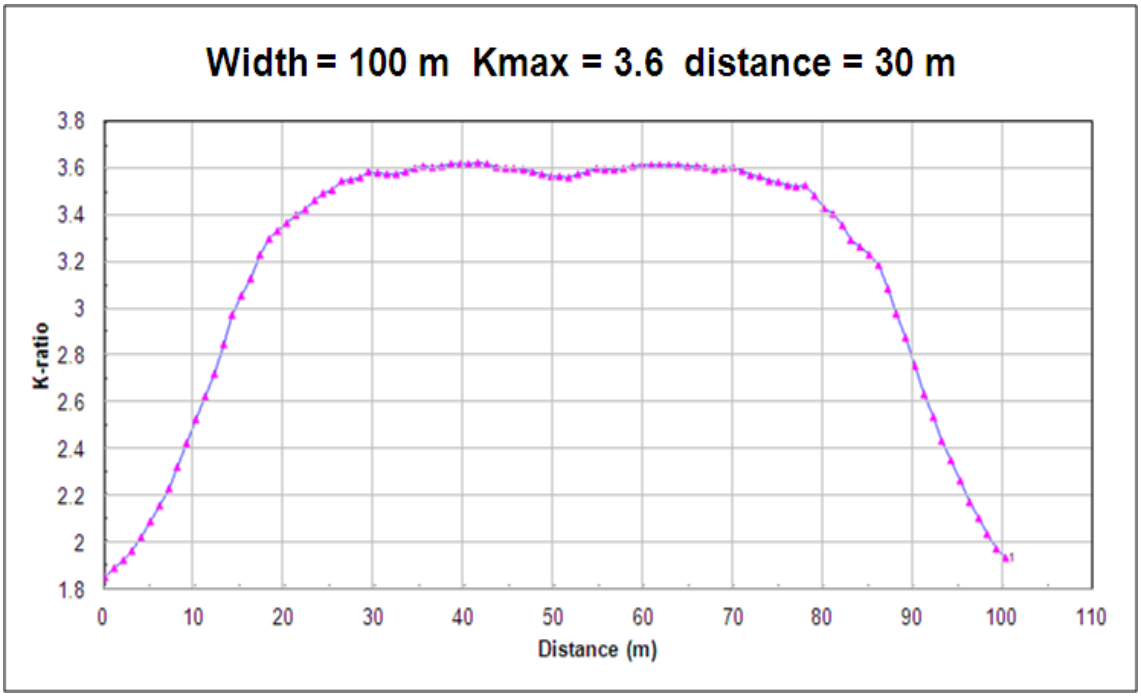
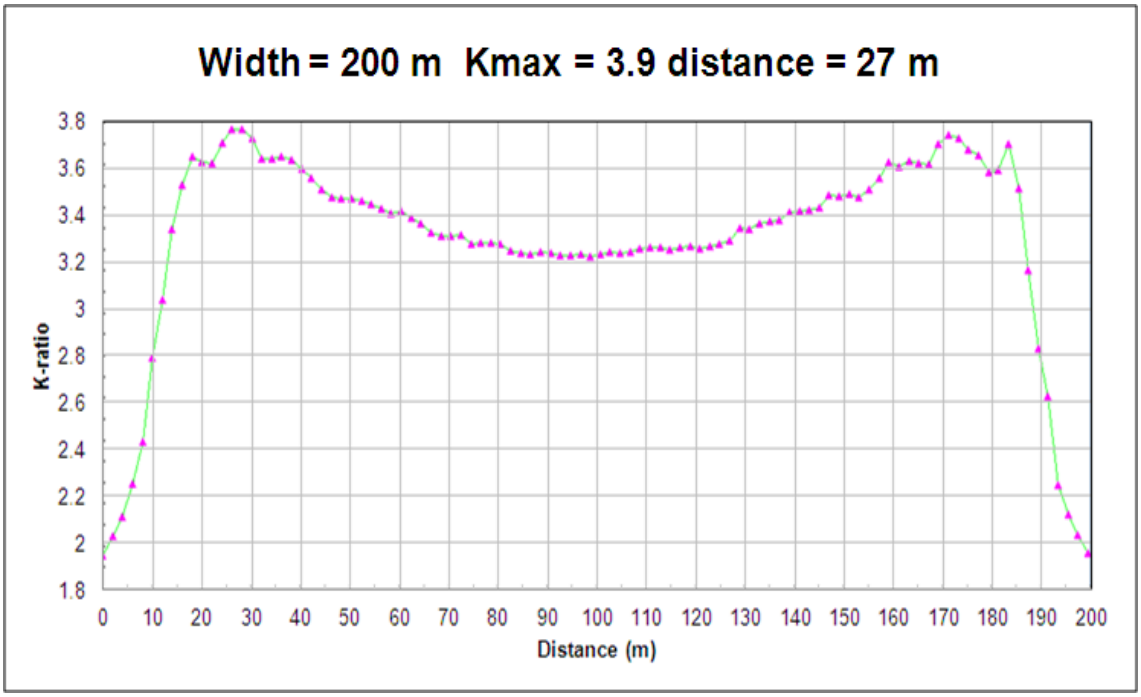
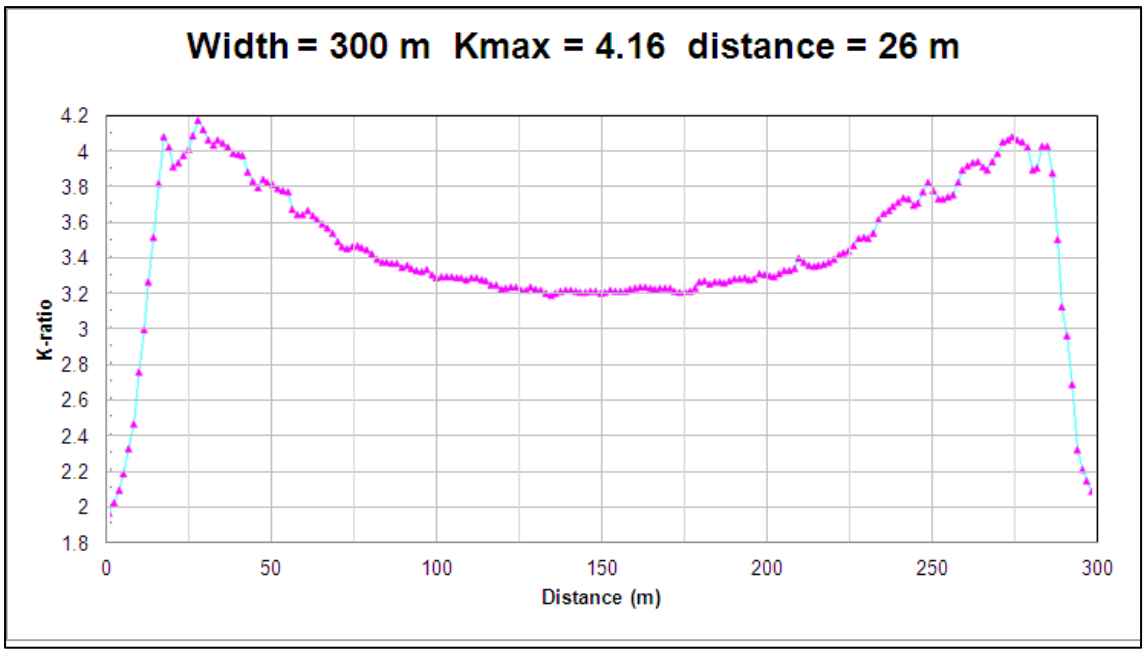


Figure 3-39 Contours of K-ratio for a basin width equal to 400 m


Width = 100 m Kmax = 3.6 distance = 30 m
K-ratio
Distance (m)
3.8
3.6
3.4
3.2
3
2.8
2.6
2.4
2.2
2
1.8
0
10
20
30
40
50
60
70
80
90
100
110


Width = 200 m Kmax = 3.9 distance = 27 m
K-ratio
Distance (m)
3.8
3.6
3.4
3.2
3
2.8
2.6
2.4
2.2
2
1.8
0
10
20
30
40
50
60
70
80
90
100
110
120
130
140
150
160
170
180
190
200



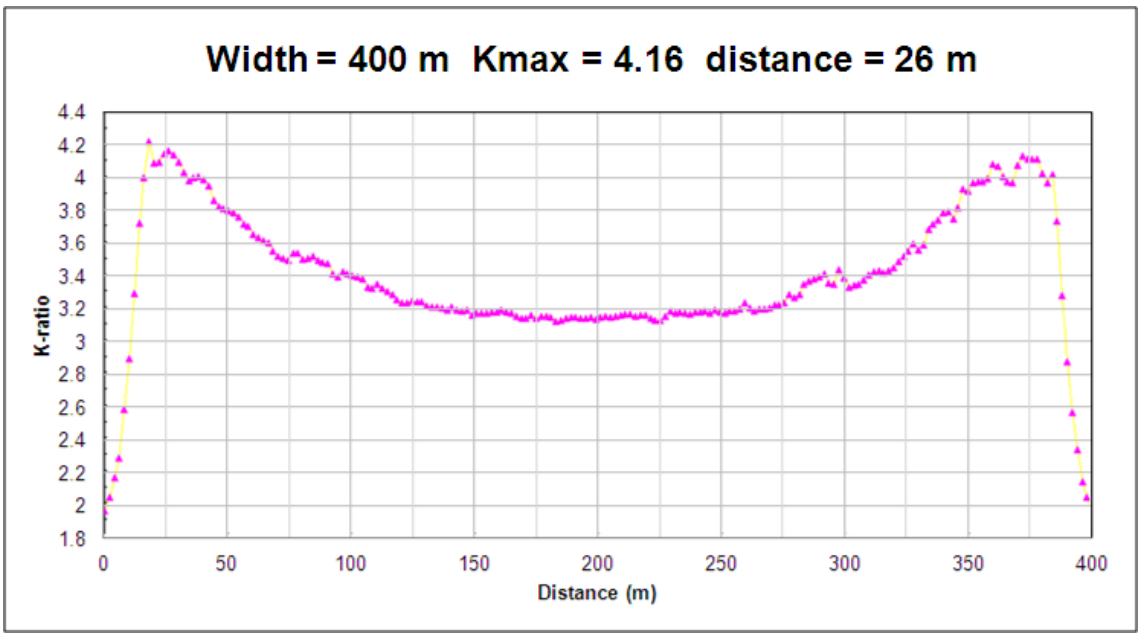


Figure 3-40 Profiles of k-ratio along the bottom of the basin 10 m below surface

The analysis has shown that the k-ratio along the bottom of the basin varies and attains a maximum value at about 26 m from the edges of the basin and a minimum value at midspan. It can also been seen that the maximum values of the k-ratio increase as the erosion proceeds but remain steady beyond 300 m. Conversely, minimum values at the middle of the basin decrease as the erosion process evolves, as illustrated on Figure 3-41.

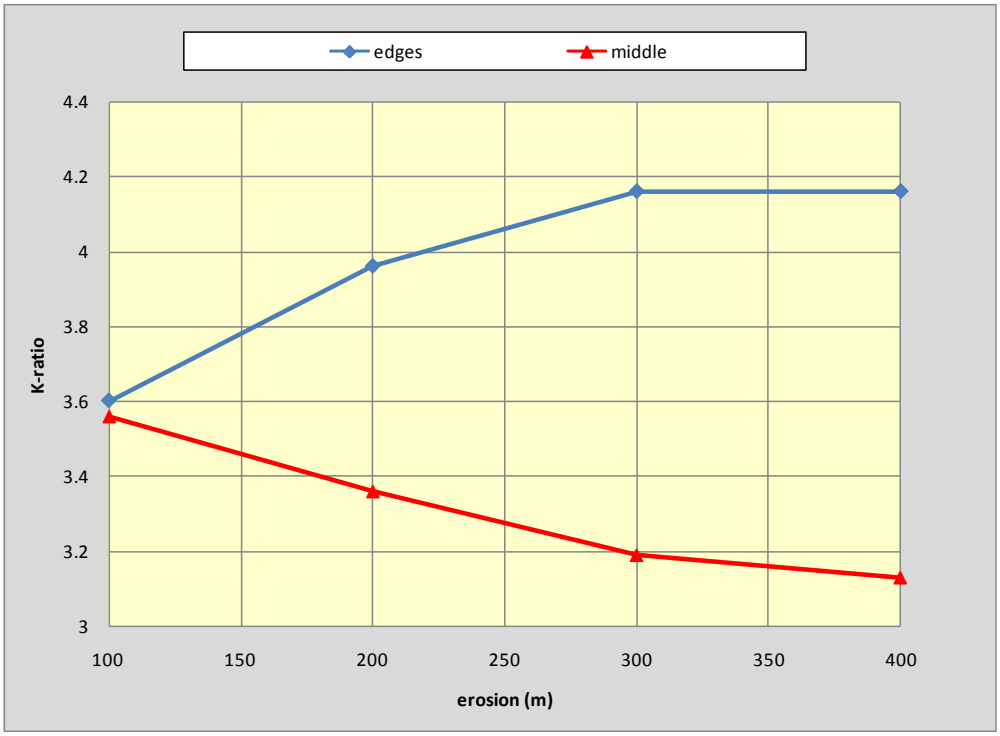


Figure 3-41 Figure illustrating the maximum k-ration as a function of width of erosion

3.5.4 Basin filled by sedimentation

In this case a basin initially formed by erosion has been gradually filled in by sediments by gradually reducing its widths. The analysis therefore simulates a case of sedimentation that follows erosion. As in the erosion case, the finite element code Phase2 was used to conduct the analysis. The k-ratio contours obtained following the analysis are given in Figure 3-42 along with profiles of k-ratio 10 m below the bottom of the basin (Figure 3-43).

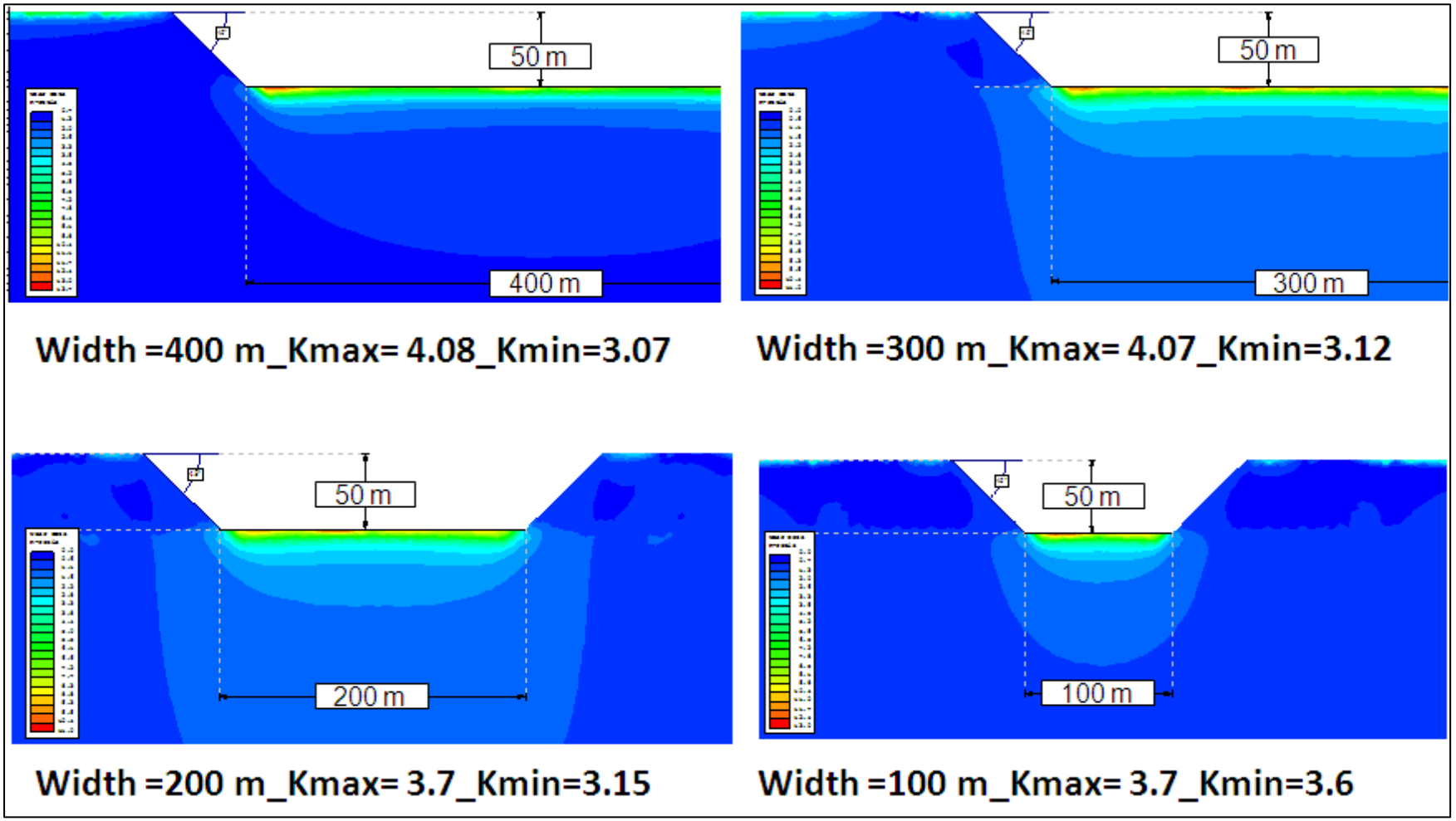
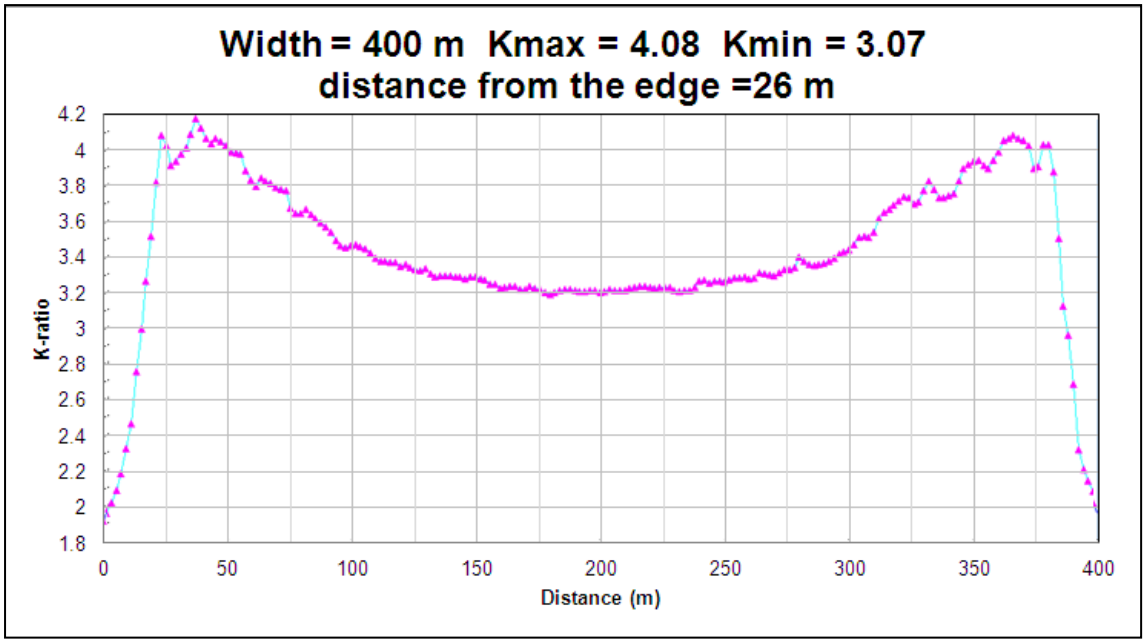
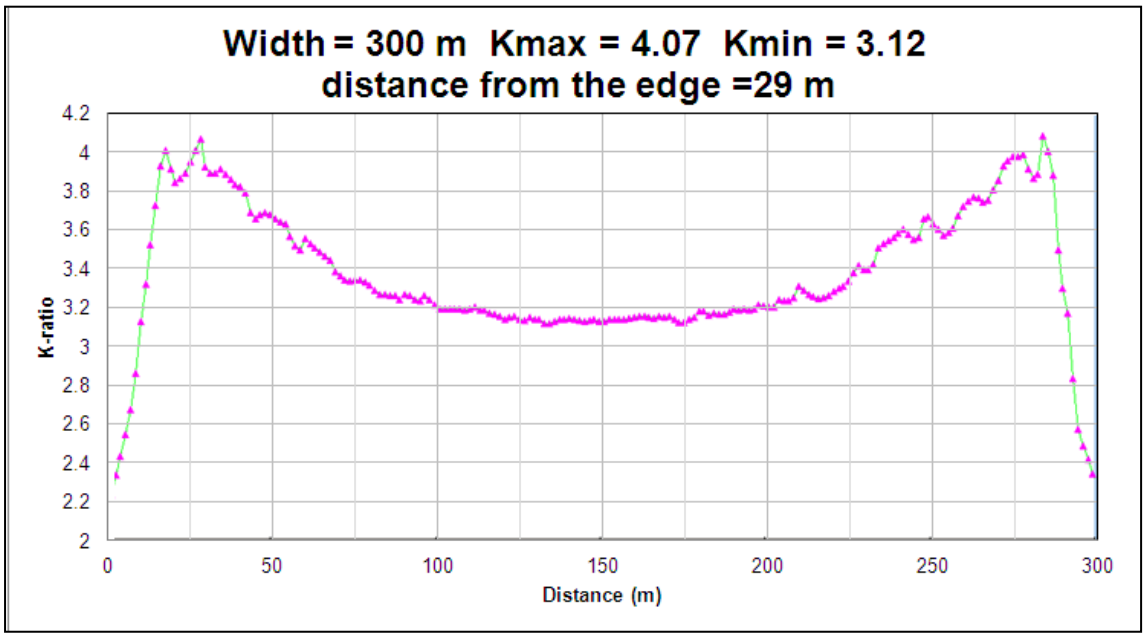


Figure 3-42 Figure illustrating k-ratio contours around a basin filled by sediments


Width = 400 m Kmax = 4.08 Kmin = 3.07
distance from the edge =26 m
K-ratio
Distance (m)
4.2
4
3.8
3.6
3.4
3.2
3
2.8
2.6
2.4
2.2
2
1.8
0
50
100
150
200
250
300
350
400


Width = 300 m Kmax = 4.07 Kmin = 3.12
distance from the edge =29 m
K-ratio
Distance (m)
4.2
4
3.8
3.6
3.4
3.2
3
2.8
2.6
2.4
2.2
2
0
50
100
150
200
250
300

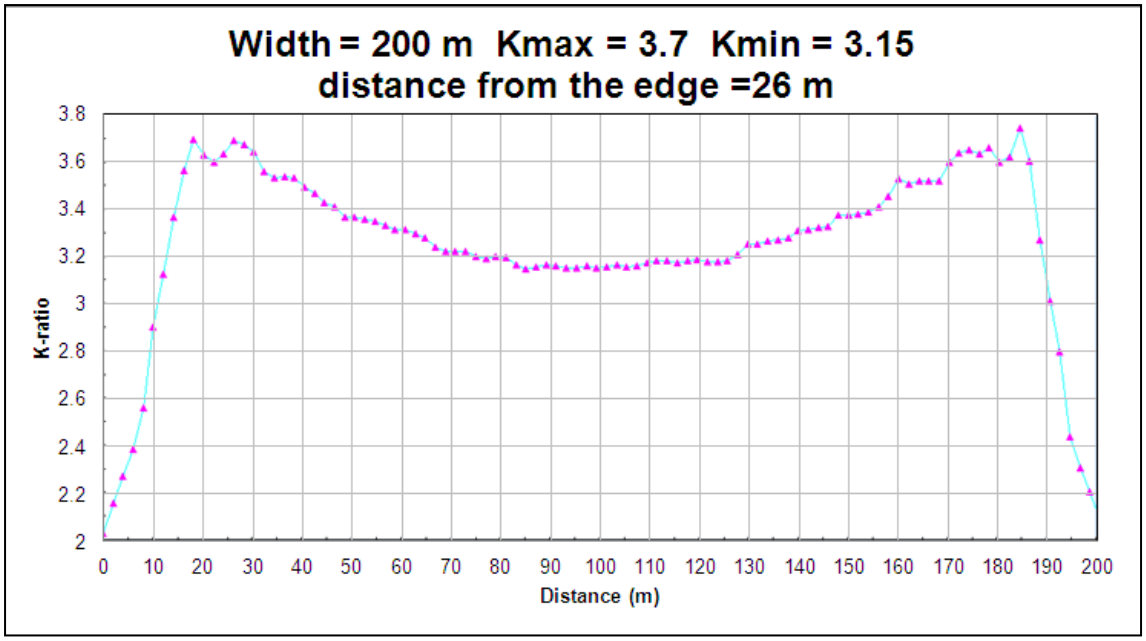


Figure 3-43 Profiles of k-ratio along the bottom of the basin 10 m below surface (sedimentation)

Figure 3-43 illustrates profiles of k-ratios 10 m underneath the basin. It is important to note that maximum values are occurring at about 26 m to 30 m from the edge of the basin. Maximum values and minimum values of k-ratio with sedimentation follow the trend given in Figure 3-44.

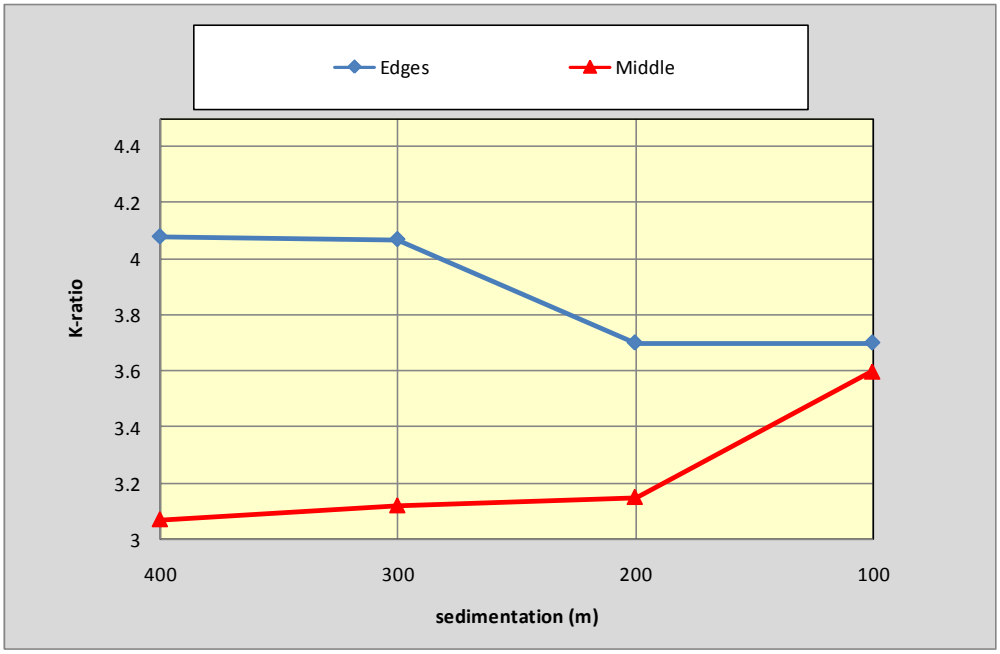


Figure 3-44 Figure illustrating the maximum k-ratio as a function of width of sedimentation

3.6 Induced stress around Mine excavations

Prior to an excavation, stresses in the rock mass are in equilibrium. Once an excavation is made this equilibrium is destroyed and stress redistribution takes place. Some zones in the near field of the excavation being made will experience stresses higher than the initial field stress, whereas others might experience lower stresses. However, both high and low stress zones are of concern because of their implication on stability. In essence, high stress can induce failure through the intact rock and low stress can induce fall of rock blocks because of lack of confinement.

From numerical modelling the stresses around excavations are generally determined assuming that the response of the rock mass to the opening is purely elastic and linear. This simplification is supported by the fact that this response is similar to an unloading process that laboratory tests have proven to be linear and elastic. Mathematically, the zero support introduced by the excavation being made is catered for by superimposing a field stress equal to the initial field stress but with opposite sign around the periphery of the excavation. This leads to a redistribution of stress around the opening.

There are two ways to compute induced stress; an analytical approach and a numerical approach (Brady and Brown 2006). The analytical approach is often used to produce closed form solutions and in this respect Poulos and Davis (1974) have presented a comprehensive collection for most tractable problems in rock engineering. On the other hand, the numerical route offers advantage in cases of complex shapes.

To illustrate the numerical approach of determination of stress around simple openings, a series of analyses were performed. Square, circular and horse shoe shaped openings were used, and results have been computed with respect to principal stresses. Emphasis has been placed on the concentration of horizontal and vertical stresses into the roof and the floor.

The numerical analysis was conducted using the software program Examine 2D of Rocscience. Examine 2D is a very fast two-dimensional indirect boundary element program for calculating stresses and displacements around underground and surface excavations in rock. Unlike the Finite Element and Finite Difference methods, the boundary element method only requires meshing around the excavation boundaries, eliminating the need for complex volume mesh generation.

In Examine 2D, the stress and strain are computed based on the plane strain assumption which implies that the out-of-plane dimension of the model is infinite and that the deformations (strains) along that dimension are zero. For situations where this assumption is not respected, results obtained with such a program thereof (strain and stress) will be exaggerated, but still useful, since they can be considered as conservative.

In addition, Examine 2D, as in most boundary element codes made the assumption that the material is elastic, linear, homogeneous and isotropic. Failure criteria are not used during the analysis but can optionally be used to compute a Strength Factor.

3.6.1 Model set up

The following excavation shapes were investigated:

- Square
- Square with rounded corners (Square R)
- Horse shoe
- Circular

Dimensions of the different excavations are given in Table 3-5:

Table 3-5 Summary of excavation dimensions

Excavation	Dimension	Comment
Square	2m x 2m	side
Circular	4m	radius
Horse shoe	4m	Hydraulic radius

In all models the number of boundary elements was set up as 200 because it was observed that more than this number of elements had no effect on the results.

3.6.2 In situ stress

The analysis was conducted assuming that excavations were made at 100 m below surface. Under those conditions the vertical in situ stress was computed as 2.7 MPa assuming a Unit weight of 0.027 MN/m^3. The k-ratio, which is the ratio of horizontal stress to vertical stress was gradually increased from 1 to 4.

3.6.3 Material Properties

The material properties used for the analysis are those of a rock with a Young's modulus (E) of 10000 MPa and a Poisson's ratio of 0.25. It can also be noted that results of elastic analyses are only sensitive to these two parameters.

3.6.4 Results

Figure 3-46 to Figure 3-48 illustrate contours of the major principal stress σ_1 (Horizontal stress) around simple excavations for 3 values of k-ratio (1, 2, 4). The very fundamental principle is that stress cannot be transmitted in the void. Therefore all stresses perpendicular to the skin of the excavation are zero. Therefore horizontal stress will concentrate in the roof and the floor of the excavation. The concentration of horizontal stress in the immediate roof was further investigated for circular, horse shoe, square excavations and square excavations with rounded corners. As illustrated in Figure 3-50 and the concentration of horizontal stress is the highest in the crown of the horse shoe excavation and the lowest for square excavations. This is probably due to the sharp corners of the square excavation since it was found that for the square excavation with rounded corners horizontal stress in the roof was slightly higher.

Figure 3-45 shows also concentration of horizontal stress in the roof. However here stress concentration was expressed as a ratio of absolute values of stress to the field stress.

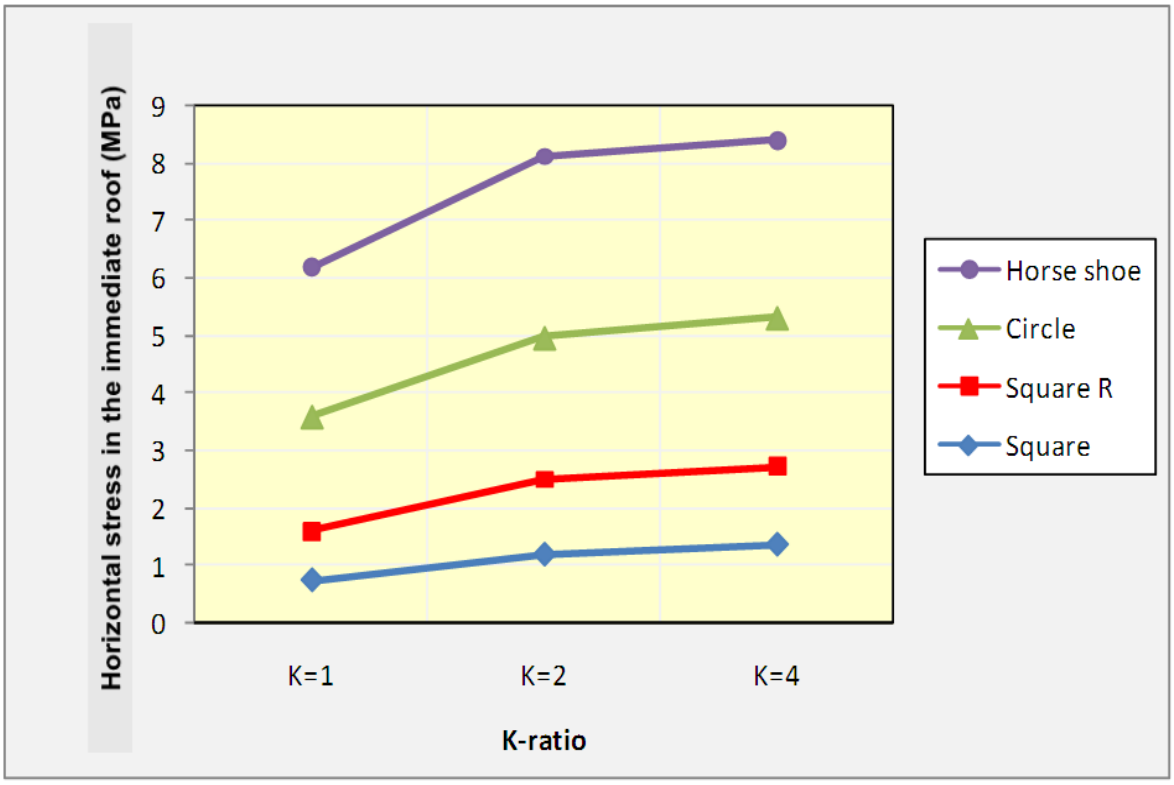


Figure 3-45 Concentration of horizontal stress in the immediate roof

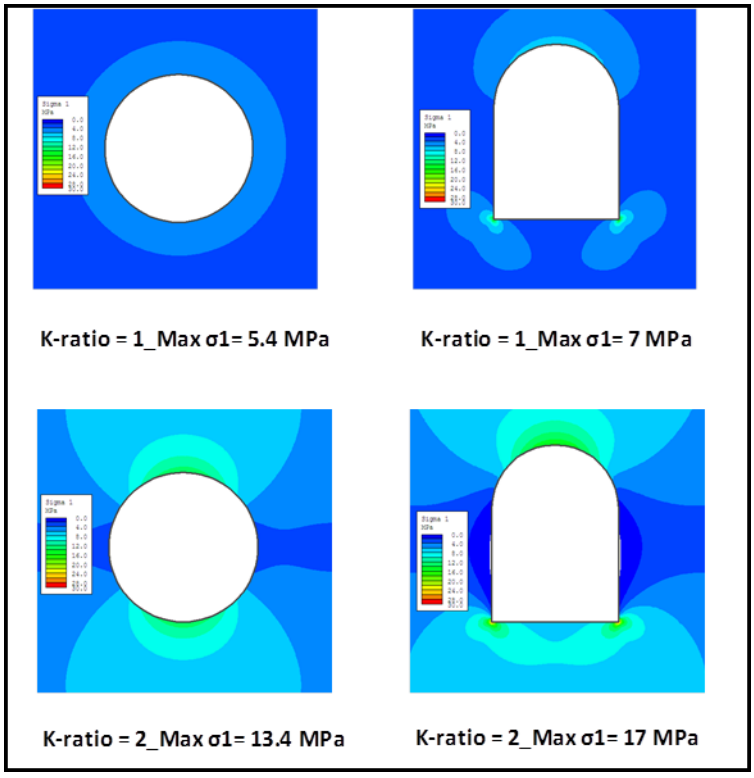


Figure 3-46 contours of σ1 around circular and horse shoe excavations for k-ratio of one and two

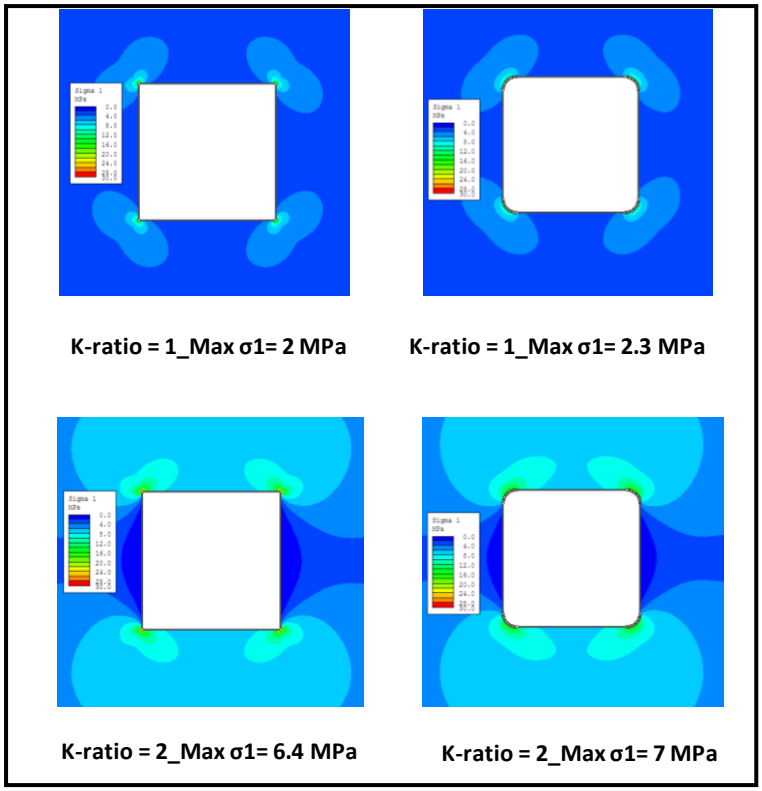


Figure 3-47 contours of σ1 around square and square with rounded corners excavations for k-ratio of one and two

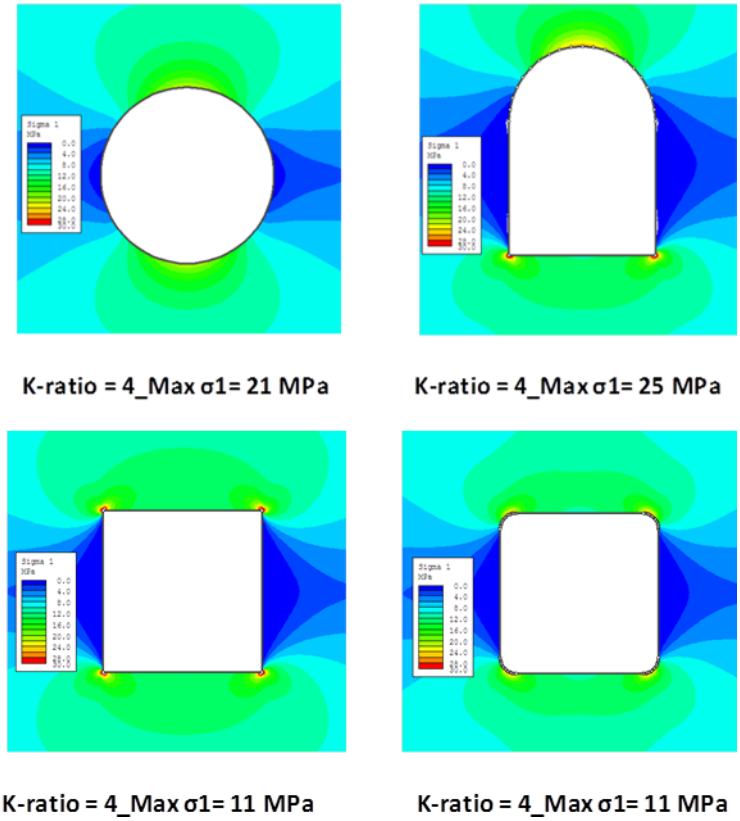


Figure 3-48 contours of σ1 around circular, horse shoe, square and square with rounded corners excavations for k-ratio of four

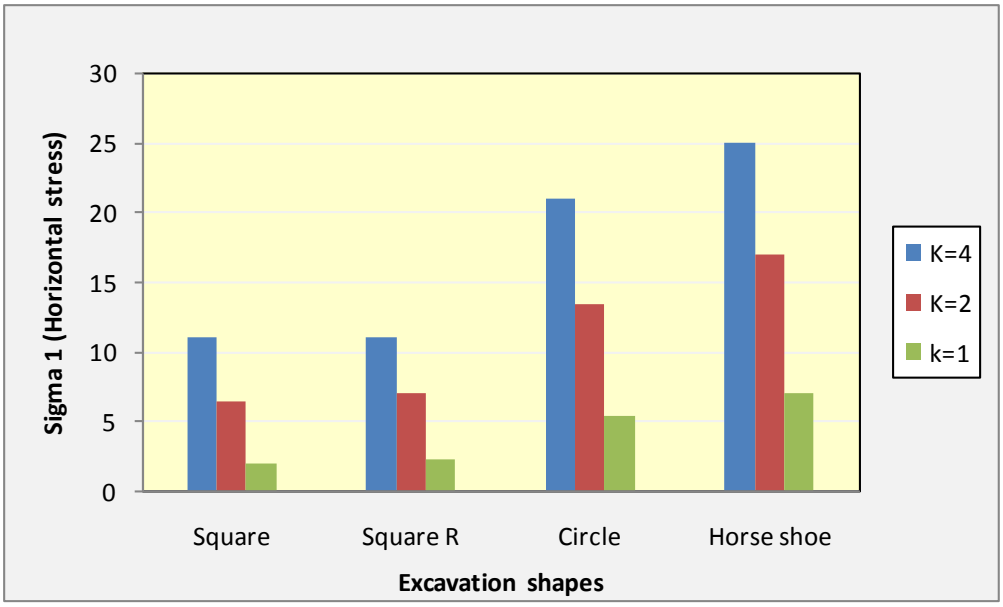


Figure 3-49 Graph of horizontal stress in the immediate roof for different excavation shapes and k-ratio

Figure 3-50 shows how vertical stress concentrates in the sidewalls for excavations of different shape.

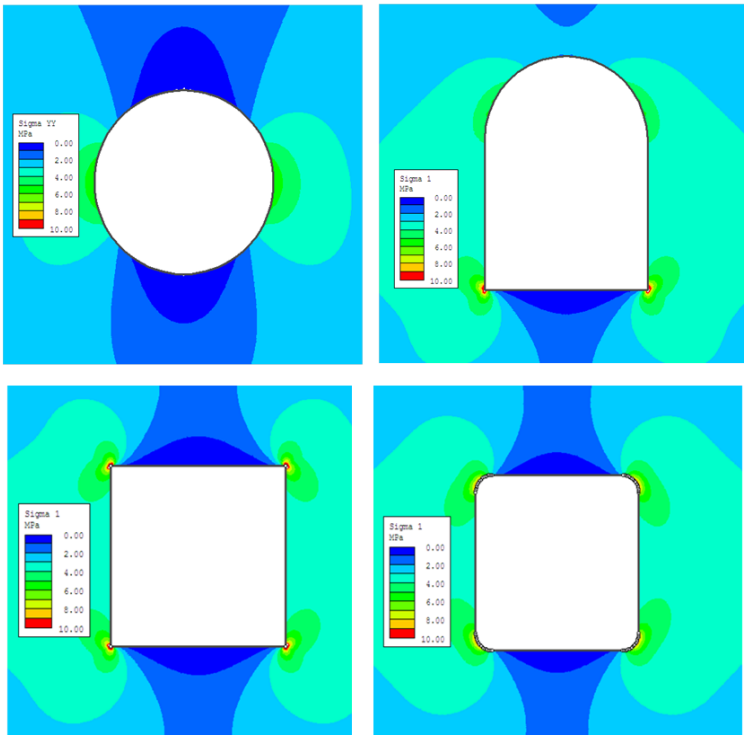


Figure 3-50 Contours of vertical stress and its concentration in sidewalls

3.7 Conclusion

Research in coal mines around the world has indicated that horizontal stress can manifest in form of guttering or buckling. Sometimes, the failure is associated with the presence of structural features such as slips and joints.

Numerical modelling has shown that the effect of horizontal stress depends largely on:

- the geological contrast of the roof (contrast in stiffness);
- the difference in magnitude between horizontal and vertical stresses; and
- Strength of coal compared to the strength of roof.

Sometimes, horizontal stresses have a stabilising effect. In this case, failure occurs where the clamping forces are due to high horizontal stress.

High horizontal stress can have various origins such as:

- Poisson's effect, where horizontal stresses build up as a result of restricted lateral deformation in the ground.
- Tectonic effect, where horizontal stress is considered to be generated as the result of moving tectonic plates which push against each other.
- Residual effect, where an unusual k-ratio observed at shallow depth is the result of thousands of metres of ice and magma covering some parts of the earth which were eroded during geological time. As a result, the vertical stress was relaxed, whereas the horizontal stress remained locked in.
- Magmatic intrusion effect, where localised increase of horizontal stress can be the result of the intrusion of a magmatic body such as a dyke.

As part of this research, numerical analysis was conducted to illustrate how the erosion of the large thickness of sediments associated with the formation of the coal has resulted in high k-ratios observed at shallow depth. The effect of weathering on horizontal stress was also investigated through elasto-plastic analytical and numerical modelling. It was shown that both depth of weathering and the contrast in stiffness between the weathered horizon and the competent rock beneath it are major contributors to high horizontal stress. Indications of high horizontal stress associated with weathering was observed in the Highveld coalfield on the road national N17.

Finite element analysis was also used to illustrate stress distribution around topographic features such as hilly districts and basins. This analysis has shown that for hilly districts formed either by erosion or filled by sedimentation, higher k-ratios form on top and in the valleys on both sides of the hill, while a zone of relatively low k-ratio forms at the core of the hill. However, this effect is more significant when the hilly district is formed by erosion than by sedimentation.

Finite element analysis has also shown that for a basin formed by erosion, the magnitude of horizontal stress around the edges of the basin is higher than in the centre. The magnitude of the maximum horizontal stress is a function of the basin width. The distance at which the maximum stress occurs was found to be the same for various basin widths. The same observation was made for basins with sediments.

Boundary element analysis was carried out to analyse stress distributions around simple excavations. As one would expect, the horizontal stress component concentrated in the roof and floor, whereas the vertical component concentrated in the side walls. However, the level of concentration depends on the shape of the excavation. Four different shapes of excavation were considered in this study even though openings in South African coal mines are almost always rectangular.

CHAPTER 4

Coal Mining methods and their influence on stress

In this section, classifications of mining methods used in coal extraction are reviewed with emphasis placed on their impact on the field stress. This also includes a review of multi seam mining which is sometimes encountered in the Witbank coalfield.

4.1 Generalities on Mining Methods

Underground mining aims for the maximum economic recovery of minerals (Atlas Copco 2008). The orebody consists of the amount of recoverable ore having taken into consideration losses of incurred by dilution and reserves sterilised in pillars left underground. The amount of losses will largely depend on the mining method used.

- Mining methods depend mainly on the following parameters:
- Shape of the mineralisation,
- Dimensions of the mineralisation, and
- Strength of the orebody and the host rock,
- Number of economic seams (in coal mining for instance).

To carry out underground coal mining, generally development is needed such as transport infrastructure of material and personnel, production, power supply, ventilation, drainage and pumping and workshop for maintenance of equipment (Figure 4-1).

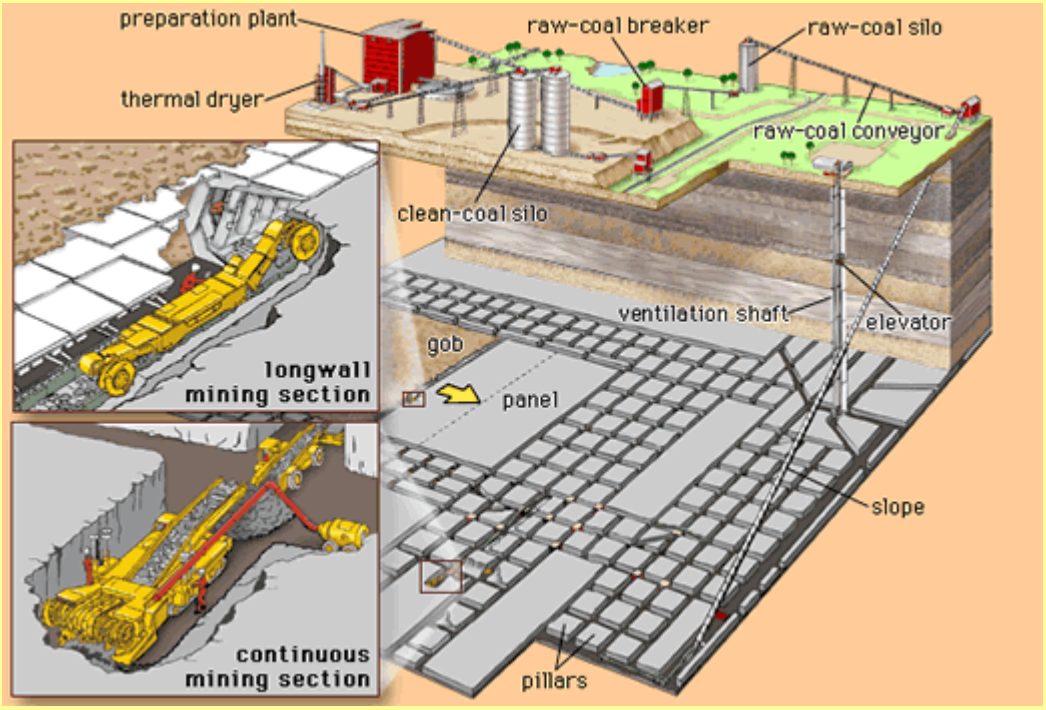


Figure 4-1 Infrastructures of a typical underground mine (Coal Mine.Art 2011)

4.2 Mining method classification

The aim of classification is mainly to facilitate the determination of a mining method that will best suit a particular deposit.

Mining methods are often classified with respect to support of the roof strata. This classification takes into account three forms of support – natural (pillars), artificial (fill), and none (caving) (Dougall 2009). This classification, although useful, did not find broad application since it does not include details such as properties of the deposit (seam), properties of the country rock and their relation to the method of working, which are essential to sustain the method (Brady and Brown, 2006).

In order to overcome the limitations of the classification, the system has been modified and improved several times. Figure 4-2 illustrates one modification of the system which includes Thick seam mining. This modified scheme as presented in Figure 4-2 does not include all the underground coal mining methods; however, the missing methods can easily be added.

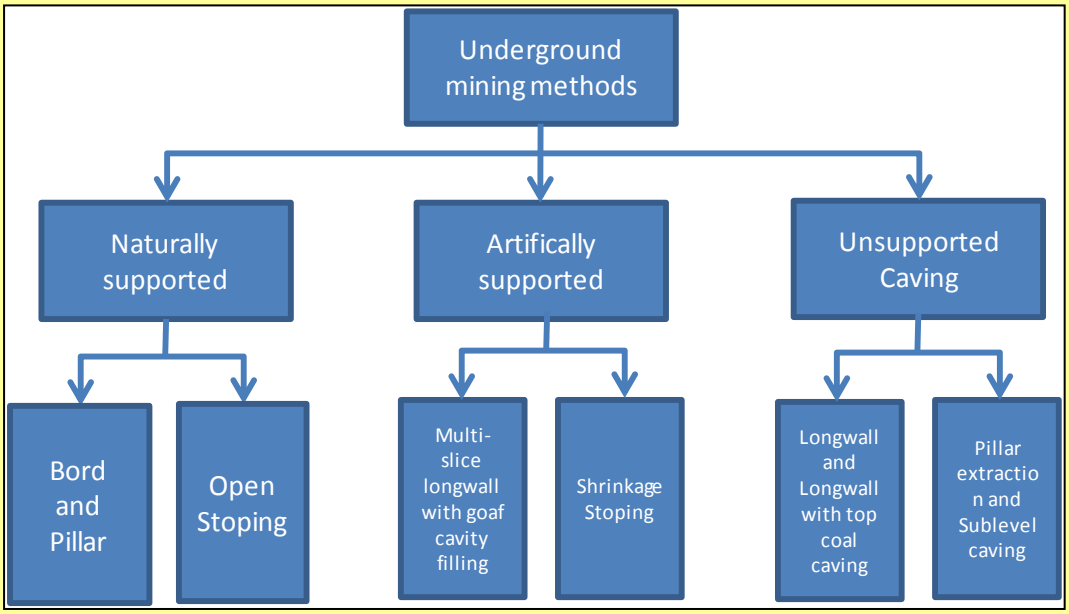


Figure 4-2 Modified Scheme of coal mining method classification (after Galvin 1981)

4.3 Impact of mining method on stress

The footprint of a given mining method on the in situ stress regime is directly related to the disturbance caused by this mining method. On mining, there is a redistribution of stress that takes place: some areas in the disturbed rock will experience increases in some stress components and others will experience a relief of stress. From a rock engineering perspective, increase or decrease in stress is important since they can influence falls of ground.

A very basic principle is that in naturally supported methods such as bord and pillar, displacements in the near field are restrained. This restriction of displacements is obtained at the expense of an increase of stress in the pillars. Therefore a sound procedure of pillar design which is a tradeoff between safety and economy has to be adhered to. In addition to this, it is important to distinguish between orebody near field and the stope peripheral zone. While the near field behaviour is mainly controlled by pillar design, the stability of stope peripheral zones is achieved by various forms of articial support such as roof bolts (Brady and Brown 2006).

At the other end of the spectrum, in unsupported caving methods, large displacements in the near field are induced and roof strata are allowed to cave. It is therefore conceivable that the effect of such a mining method on the stress regime will be greater than in the former case. In the proximity of a goaf (caving), two types of areas can be distinguished with respect to stress, namely; abutment stress and shadow stress. Abutments are places where lines of stress concentrate and shadows are places where the density (concentration) of lines of stress decreases. In the abutment stress, damage in the intact rock can occur, whereas in the shadow stress, failure along planes of weakness is far more likely.

4.4 Mining methods used in the Witbank and Highveld

The mining methods commonly used across the Witbank and Highveld coalfields are the following:

- Bord and Pillar mining,
- Longwall mining,
- Pillar extraction, and
- Multiseam mining
    - Bord and Pillar-Bord and Pillar
    - Bord and Pillar-Pillar extraction
    - Pillar extraction-Pillar extraction

The contribution of each mining method to the total underground production in South Africa is presented in Figure 4-3. It can be seen that about 90% of coal from underground mining is from Bord and Pillar operations whereas the remaining 10% is split equally between Pillar extraction and Longwall mining.

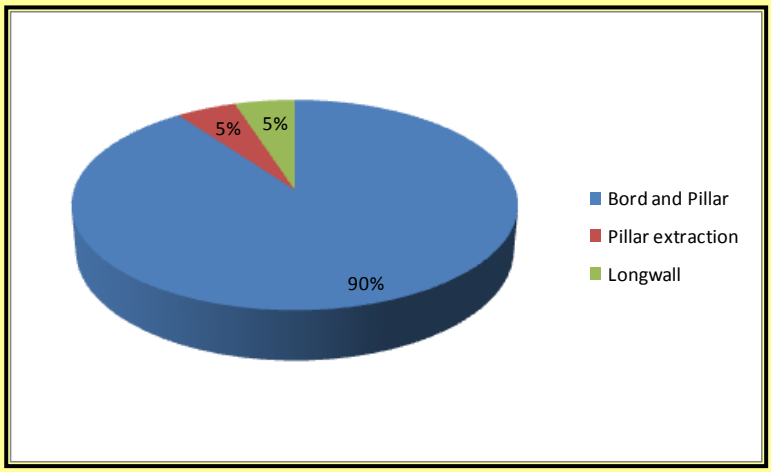


Figure 4-3 Contribution of the different underground mining method to the total South African underground coal production (after Dougall 2009)

4.4.1 Bord and Pillar mining

The bord and pillar mining method was designed for flat, bedded deposits of comparatively limited thickness (Atlas Copco 2008). The method consists in mining the orebody and leaving behind some ore as pillars to support the roof. The pillars left underground are either temporary or permanent and should be viewed as a loss of fully proven and developed mining reserves. Ideally, the amount of ore committed to pillar support should be kept to the minimum possible (Brady and Brown 2006).

In bord and pillar mining, equipment has been developed and for mining heights in the range of 1.2 to 4.5 m (Buchan et al, 1981). In South Africa, 40% of coal reserves occur in seams of thickness between 4.5 and 6 m and a great deal of research has been devoted to address issues pertaining to mining at such heights (Dougall 2009). In spite of the developments in this regard, management at collieries still promote a cutoff height of 4.5 m by giving preference to the 12HM31 Continuous Miner (CM), mainly because of its versatility.

Another crucial aspect concerning bord and pillar mining is the design of the pillar. The procedure used has evolved over the years. In the past, pillars were designed through trial and error, which of course resulted in fatalities and enormous production losses through pillar failures. In the begin of the twentieth century, a worldwide awareness of the problem led to the initiation of laboratory testing programmes on coal specimens so as to determine the strength of coal pillars. From these testing programmes, trends such as the increase in strength with pillar width and the decrease in strength with pillar height were established.

However, due to the wide scatter in the results, extrapolation of strength to a full pillar scale was difficult. In the late 1930s, underground pillar testing was initiated in the United State of America. These full size tests gave insight into the strain-stress behaviour of pillars, but the tests were very time consuming and expensive (van der Merwe and Madden 2010).

In South Africa the issue of pillar design gained momentum as a result of the 1960 Coalbrook incident which claimed the lives of 437 miners. Hoek (1966) investigated the potential for underground testing at Wolvekrans, Witbank colliery, in No. 4 seam. This study opened the way to an intensive underground testing conducted by the CSIR, whose results have been summarised by Bieniawski and Van Heerden (1967). Having conducted tests on specimens up to 5 ft cubed (0.14 m^3), Bieniawski and Mulligan (1967) concluded that the strength of coal varies little beyond this size. A parallel testing programme was conducted by Cook et al. (1971). Following this programme it was found that because of confinement, the centre part of a pillar could withstand stresses much greater than the known strength of the pillar, depending on the Width to Height ratio. In addition to this, the results of this programme showed that, unlike the elastic modulus which is property of the coal, the post-peak modulus is rather a structural property and is mainly a function of the width to height ratio.

A totally different approach to pillar design was initiated by Salamon and Munro (1967). The method involved a probabilistic analysis conducted on a database composed of 98 intact cases and 27 failed cases to determine the parameters of pillar strength. Salamon and Munro's analysis resulted in a pillar strength formula of the following form: $S = Kw^{\alpha}h^{\beta}$. The analysis gave a value of 0.46 for α, 0.66 for β and an intact strength of coal (K) of 7200 kPa.

As for the Load on the pillars, Salamon and Munro (1967) used the Tributary Area Theory. A theory that the weight to be supported by a square coal pillar should equal the weight of the rock strata above it plus the weight of rock equal in area to one-half the size of the opening adjacent to all four sides of the pillar.

This theory works well when the pillar width is equal to or greater than the mining depth and also assumed that pillars are square pillars of the same size. Salamon and Munro argued that these conditions are often met in the South African context. Oravecz (1973) investigated pillar loading using field measurements, analytical models and an electrical resistance analogue. Following this study it was found that in the South African bord and pillar

workings, characterised by relatively low stress and small displacements, the theory of elasticity applies.

Since the development of the Salamon and Munro formula, new occurences of pillar failures have taken place and other researchers (Madden 1991) have included them in the database to refine the initial Salamon and Munro formula. Van der Merwe (2003) expanded the database, and used a different statistical approach. Following this analysis, a linear formula was obtained. In spite of all the development in this regard, the initial Salamon and Munro strength pillar formula is still widely used across the Witbank and Highveld coalfields because it results in the most conservative FOS.

The Salamon and Munro formula has been modified to account for the conservative results obtained for pillars of width to height ratio exceeding 5 to 6. The modified formula tends to cater for the observation that pillars of width to height ratio in excess of 10 were virtually indestructible. This modification is referred to as the Squat Pillar formula (Salamon and Oravecz 1976).

Salamon and Canbulat (2006) improved the Salamon and Munro (1967) coal pillar strength formula by including new instances of collapsed and uncollapsed pillars. The new database was composed of 77 collapsed cases and 245 uncollapsed cases. The Maximum Likelihood method was the statistical approach used. This method has the advantage of being an unbiased and minimum variance estimator. Unbiased means that for a large size of observations, the average of the estimations is exactly equal to the population value, whereas minimum variance simply means that amongst all the estimators, it is the estimator which provides the smallest variance. The Likelihood function was formulated based on three assumed probability density functions of Factor of Safety of collapsed and uncollapsed cases:

- Lognormal distribution (conventional),
- Gamma distribution, and
- Weibull distribution.

The Factor of Safety (FOS) was computed for different combinations of parameters using three different approaches:

- Power formula,

- Linear formula, and
- Non-linear formula.

The combination of parameters which maximised the Likelihood function were recommended as optimum factors for pillar design. In addition, it was observed that by including all the data from the database in the analysis, the resulting maximum likelihood function was comparatively low, which suggested that it was not possible to have a single formula pertaining to the all coalfields in South Africa. The study went on to divide the database into subsets in order to generate formulae specific to various coalfields. One of the major advantages of the modified approach is that collapsed and uncollapsed cases have all been included in the analysis.

4.4.2 Longwall Mining

In longwall mining the coal is won while the stope face is advanced by ploughing or shearing the coal by an ongoing translation of the cutting device along the stope face. The won coal is simultaneously loaded onto an armoured conveyor to be transported to a roadway lying parallel to the direction of advance of the stope face (Brady and Brown 2006). The mined out area behind the face is allowed to collapse while the face area is supported by a set of props or other type of support (shields in the South African context).

Figure 4-4 illustrates a typical Longwall mining operation as practiced in South Africa. Three roadways are mined as maingate and three others as tailgate. The reason for having three roadways instead of one or two is mainly to take into consideration the fact that two roadways are normally lost into the goaf. A chain pillar is left in between the roadways as presented in Figure 4-4. In practice, at first the tailgate and maingate are developed up to the end of the panel and the coal is won on retreat. The maingate of the panel being mined will serve as tailgate to the next panel.

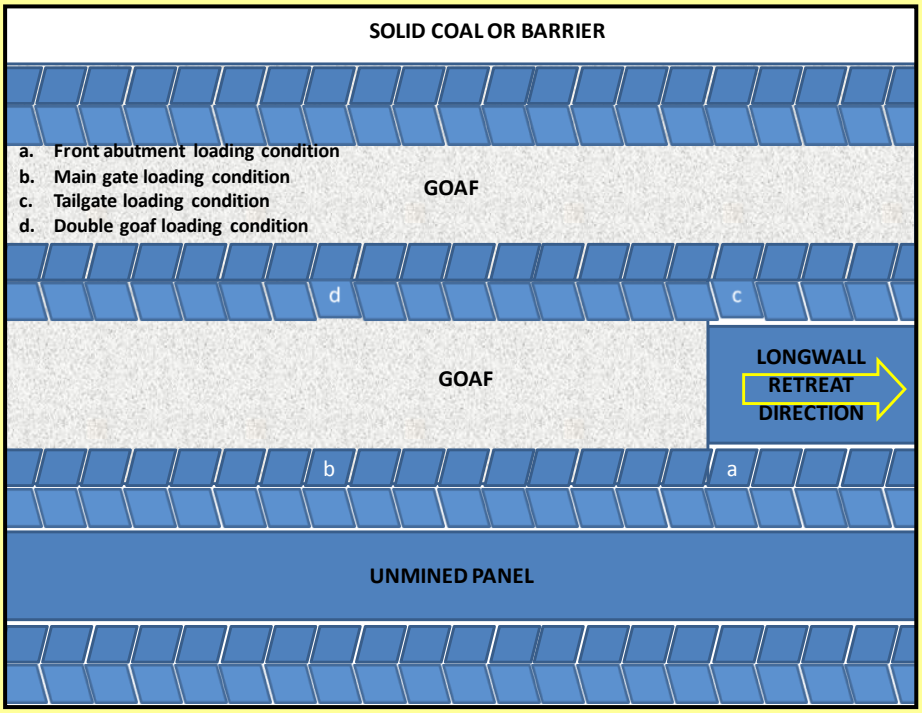


Figure 4-4 Typical multiple roadways longwall mining illustrating the chain pillar loading cycle (after Colwell et al 1999)

The chain pillars are designed for various function such as to limit the displacements in the roadways to a value compatible with the function the roadways are intended to play (transport…) over the life span of the panel (from days to several months). In addition to this function, the pillars are intended to compartmentalize the section in case of fire, flood and major collapse. As illustrated in Figure 4-4, chain pillars will undergo various loading condition throughout their life and therefore it is important that the design cater for this aspect as well.

The stress distributions around coal longwall panels have been investigated by various researchers. For many years, the model widely accepted was that after Whittaker (1974). The model suggests a vertical stress of zero at the face of the longwall panel and at the rib sides, and a rapid increase of stress in the yielded unmined coal with a peak value reached at a distance from the face and the rib side which depends on the in situ stress and the mechanical properties of the rock (Figure 4-5).

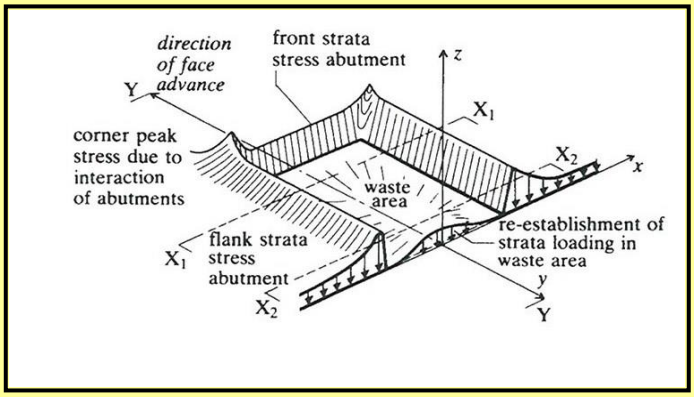


Figure 4-5 three dimensional representation of stress distribution around a longwall panel (after Whittaker 1974)

Similarly, in the mined out zone, stress build up gradually from zero, at the face or rib side, to the insitu stress where full closure has occured. This analysis was based on a stress balance approach which assumes that the vertical force over a reasonably large area remains constant. A shortcoming of this model is that it assumes a hydrostatic in situ stress regime as often encountered in the United Kingdom.

Minney (2011) made the observation that there should not be peak stress at the corners as suggested by the Whittaker model. Minney's argument is that at the corners there is 75% of abutment as opposed to 50% at the walls (flanks). Threrefore, this should reflect in a decrease of stress at the corners rather than a peak. In order to confirm this, a MINSIM model was prepared. MINSIM is a boundary element program which operates on the discontinuity displacement (DD) element logic. Figure 4-6 shows the longwall model set up in MINSIM. Table 4-1 summarises the material properties and other parameters used in this run.

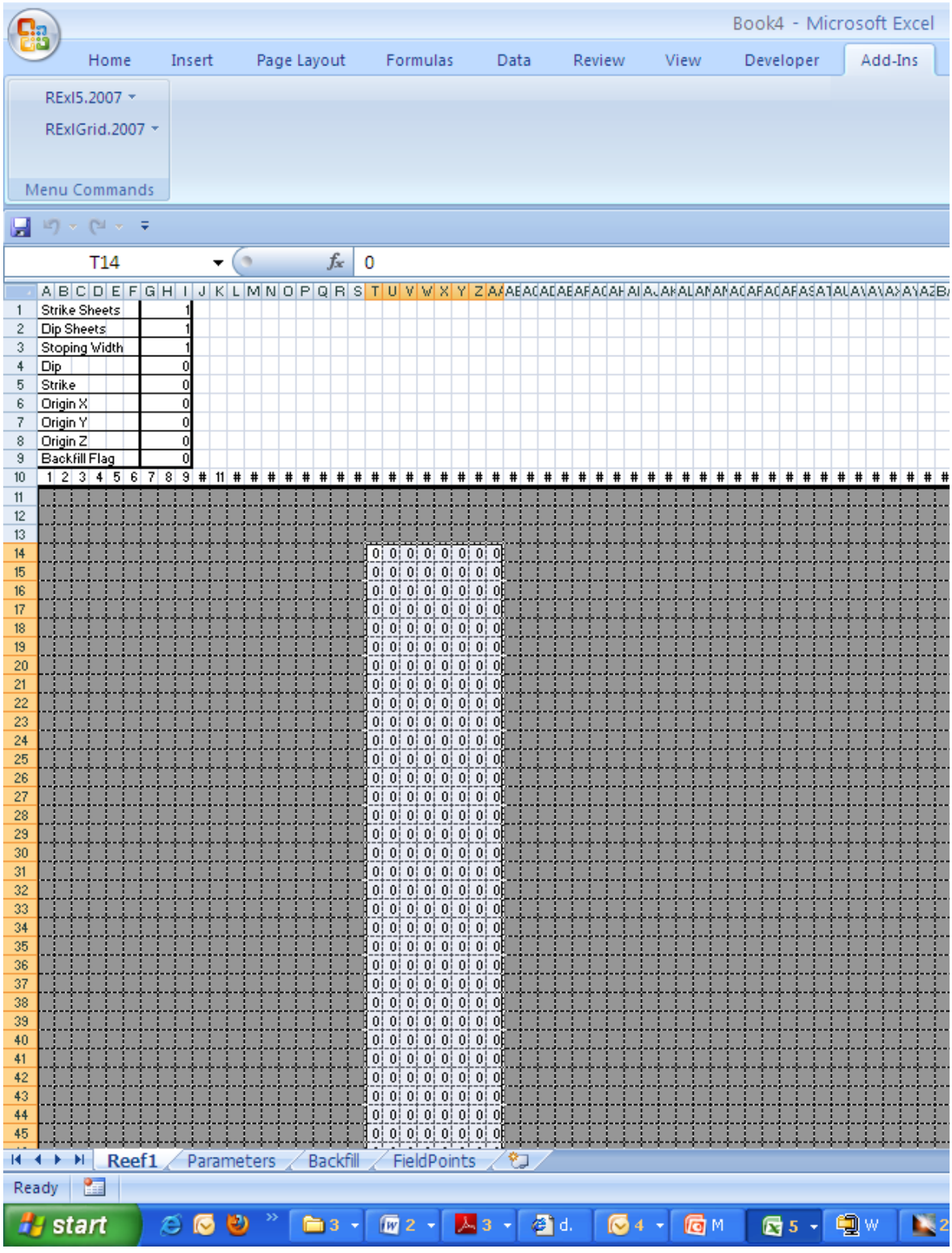


Figure 4-6 MINSIM model used to analyse the stress distribution around a longwall panel

Table 4-1 Summary of parameters and material properties used in the longwall stress analysis

Job Name	longwall.PPC
Date	20/06/2011
Working Folder	C:\Minsim_test
Number of Mining Steps	0
Current Mining Step	0
Number of Active Fill Materials	0
Current Backfill Character	A
Sheet Iterations	50
SOR	1.5
Stress Tolerance	0.01
Global Iterations	1000
Element Size	1.00
Free Surface Elevation	100.00
Poisson's Ratio	0.20
Young's Modulus	70000.00
Depth Option	I
TXX Gradient	-0.027000
TYY Gradient	-0.027000
TZZ Gradient	-0.027000
TXY Gradient	0.000000
TXZ Gradient	0.000000
TYZ Gradient	0.000000
TXX Fixed	0.000000
TYY Fixed	0.000000
TZZ Fixed	0.000000
TXY Fixed	0.000000
TXZ Fixed	0.000000
TYZ Fixed	0.000000
Current Terrain Height	1.00

Results of the MINSIM analysis are presented in Figure 4-7 as 2D and 3D stress plots. Based on these results, it was found that, as suggested by Minney (2011), the stress at the corners of a longwall panel under hydrostatic in-situ stress conditions is significantly lower than the stress at the face and the walls.

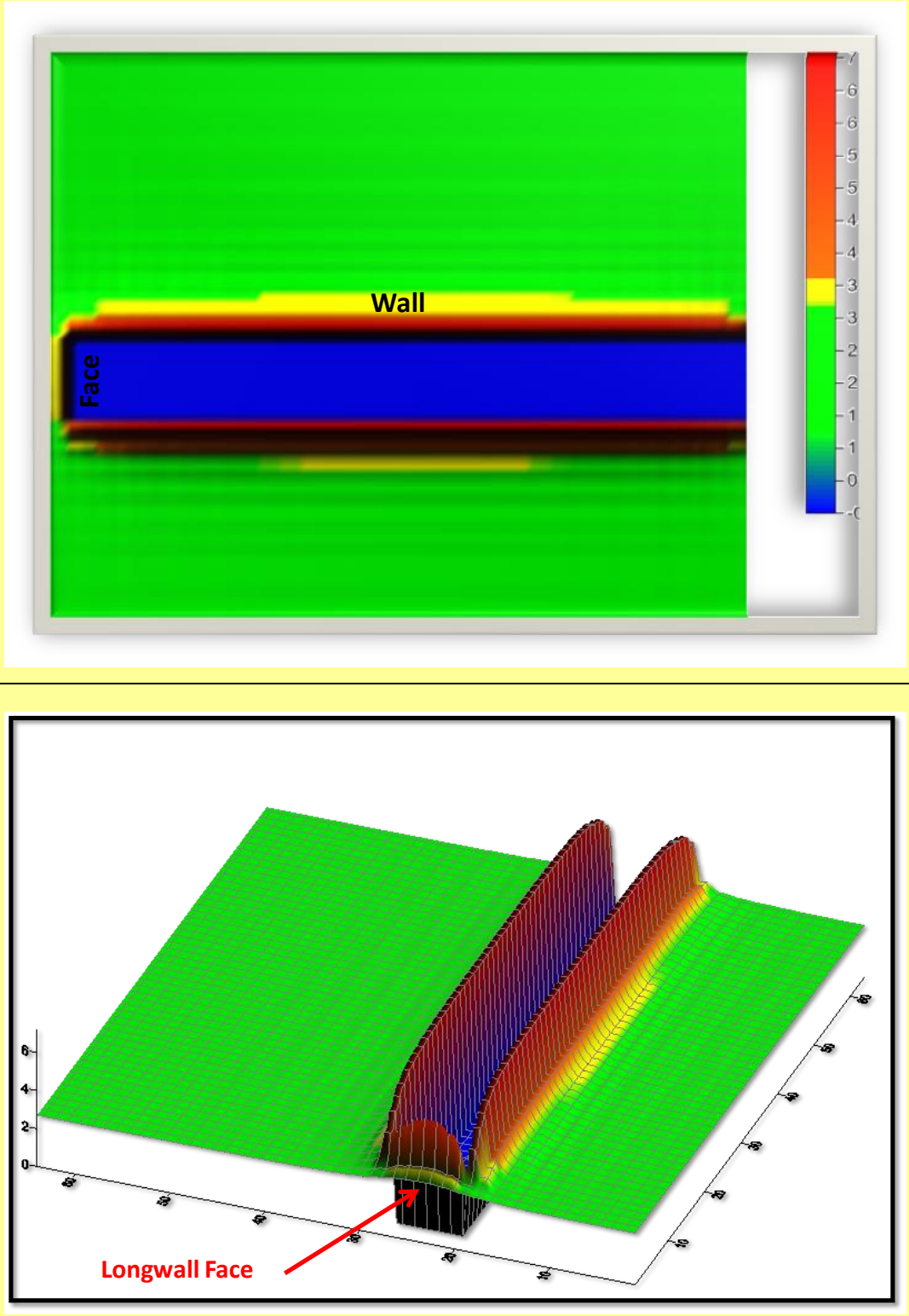


Figure 4-7 Two and three dimensional plots showing the vertical stress in the hanging wall of a longwall panel as obtained following a MINSIM analysis

However, it is important to note that in South Africa and other countries such as Australia, the major principal stress happens to be horizontal. Gale and Blackwood (1987) investigated

this issue for collieries of the Southern Coalfield, New South Wales, in Australia. A three dimensional boundary element stress analysis was used whereby the direction of the roadway was changed with respect to the stress. In the model, the major, intermediate and minor stresses were horizontal, vertical and horizonal respectively; as is the case in Australia. The material properties used were those known for the coalfield investigated and principal stresses of 25, 16 and 15 MPa were used as field stresses. The information obtained from the analyses was used to define a level of "good roof condition". Results of this analysis are illustrated in Figure 4-8.

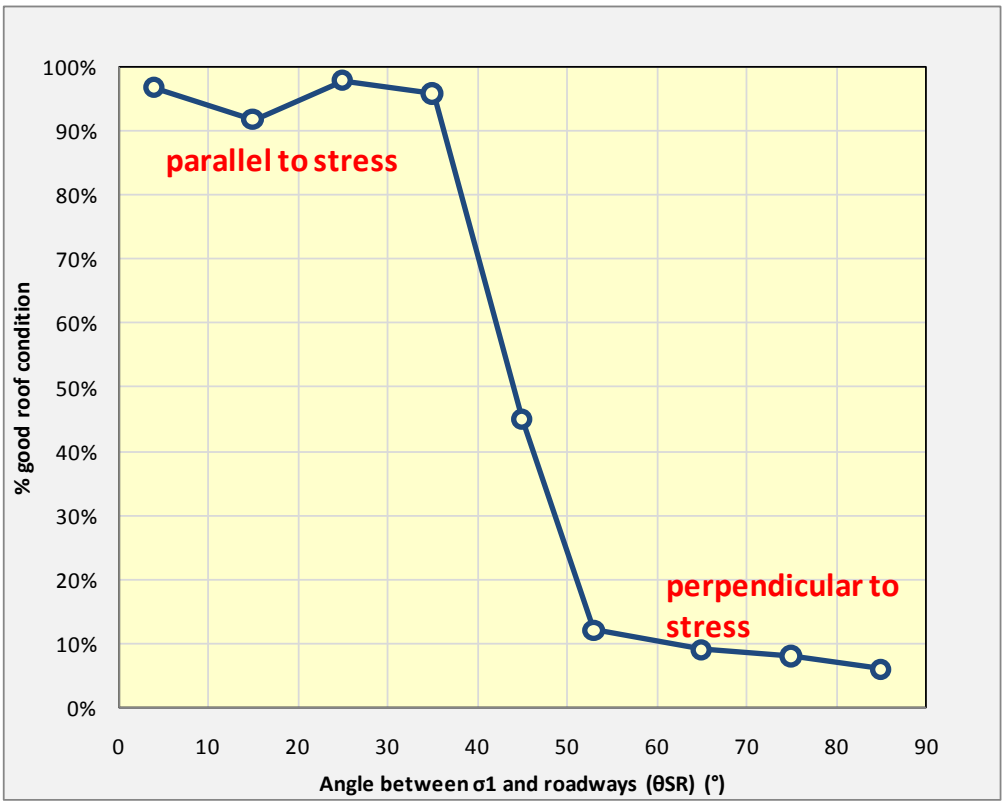


Figure 4-8 Graph illustrating angle between the major principal stress and roadway direction (after Gale and Blackwood 1987)

These results emphasized the importance of mining longwall panels almost parallel to the direction of the major horizontal stress.

In longwall mining, the issue of stress is directly related to the issue of caving. When caving occurs, a stress relief takes place as a result of this. On the contrary, when the roof hangs up there is stress concentration occurring at the longwall face which can lead to failure of the face. In the recent years, a great deal of understanding of the caving process has been gained through a major industrially sponsored research program in Australia (Kelly et al, 2002). An

integrated approach to the issue of caving was used which includes geological, geomechanical characterization of rock mass, micro-seismic monitoring, two dimensional and three dimensional numerical stress-displacement modeling and a range of underground monitoring methods and three dimensional visualization techniques. The major findings further to this study are the following:

- Micro-seismic event locations showed that rock fracture and shear failure occurred generally about 50-30 m, on occasion up to 80 m, ahead of the longwall face,
- Similarly, micro-seismic event locations showed that rock fracture occur up to 100 m above and below the longwall level even though this figure is very sensitive to the presence of previously mined out seams,
- In addition to this, micro-seismic event revealed the potential of activation of a geological discontinuity at the distance as far as 212 m from the face in the solid side of the longwall panel,
- Water content and pore pressure exert an influence on the rock failure mechanism,
- Longwall caving mechanics is complex being influenced by the local geology and previous mining. Presence of thick sandstone layers was found to have a defining impact on initiation and propagation of caving.

However, the South African context is somehow different from the Australian, and therefore the reproducibility of the above-mentioned results is highly unlikely.

A different approach to longwall mining and very specific to the South African context was once presented by van der Merwe and Madden (2010). According to van der Merwe and Madden, longwalls in South Africa are characterised by a width of about 300 m and a mining depth not greater than 200 m. Another critical aspect which typifies longwalls in South Africa is the mining height, which reached up to 6 m at places such as Matla colliery (Dougall 2009). Mining at such a height in one pass is very challenging with several face breaks reported from Matla colliery. In addition to this, the presence of a dolerite sill in the overburden is very typical of South African Coalfields and plays a paramount role in the caving mechanisms. It is important to note that most longwall mining operations in South Africa use shields as face support.

Figure 4-9 illustrates the concept of stress history as a function of face advance. In essence, when the longwall face advances, two scenarios have been observed. Either the roof collapses at a typical distance of between 150 m and 200 m with a corresponding decrease of the stress ahead of the face or the roof does not collapse and the stress ahead of the face keeps on increasing and eventually stabilises for an advance of the face of about one and a half times the panel width (van der Merwe and Madden 2010). The hikes on the Figure 4-9 represent sporadic stress increase due to the goaf hang ups.

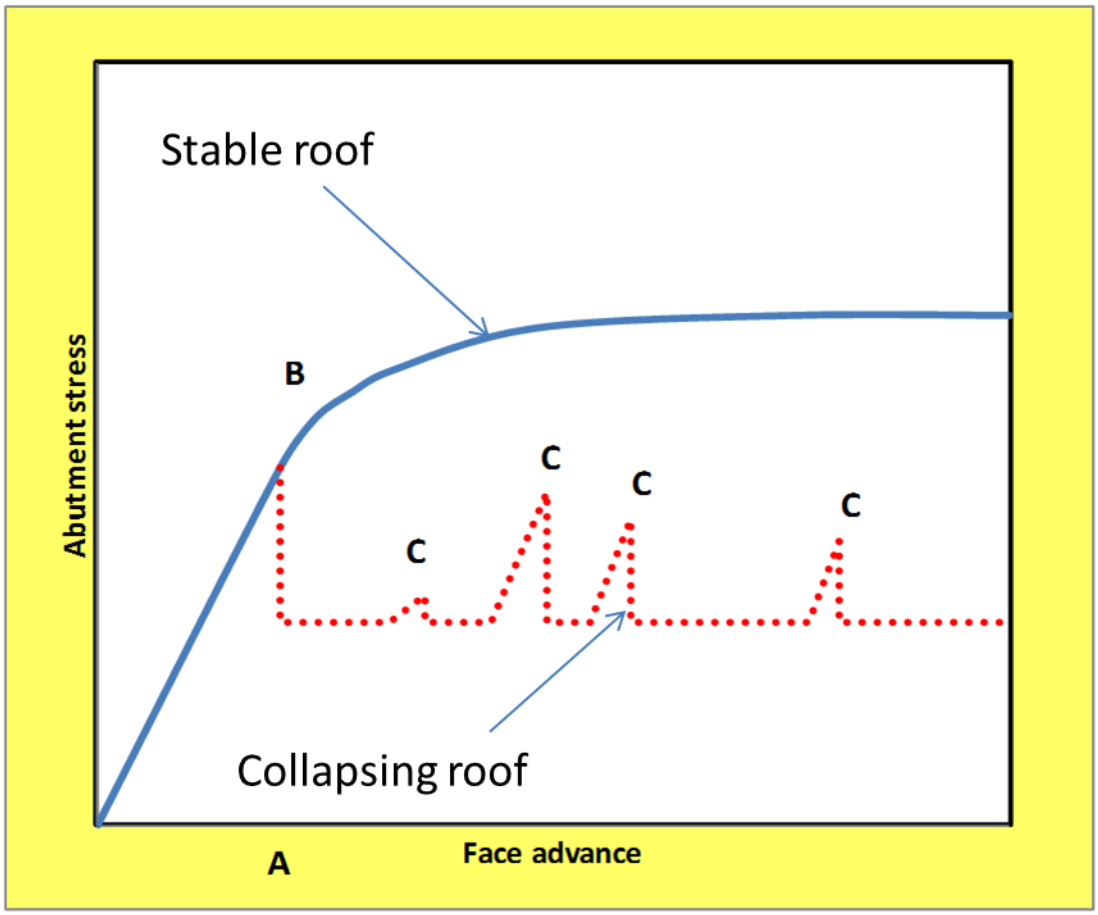


Figure 4-9 Conceptual curves of stress as a function of face advance (after van der Merwe and Madden 2010)

One of the major design decisions in longwall mining is whether to allow the roof to collapse or to leave it intact. This decision is in fact a tradeoff between the stress relief as a result of the goaf and other technical issues such as mine subsidence or ground water ingress. In some instances it is not sound to allow a massive quantity of water to invade the mine workings especially when mining is conducted downhill with water accumulating at the face.

Another important aspect in the goaf mechanism has to do with the presence of dolerite sills in the overburden. In practice the goaf will rather develop up to the dolerite sill horizon but will not extend any further unless the panel is made much wider. This is due to the strength properties of dolerite sills which are relatively high. As a result of this, in instances where a dolerite sill is present in the roof, stress in the inter panel pillars will be higher and much wider pillars might be needed as a response to this increase in stress.

The optimum orientation of longwall panels is a consensus between the shape of the mine properties and other considerations such as geological structures and orientation of in situ stress. When conditions allow, the best orientation will be slightly off the orientation of the major horizontal stress so as to limit stress related damage in the roadways and in meantime to avoid a configuration whereby joints run parallel to the roadways (van der Merwe and Madden 2010).

Another operational problem often encountered in longwall mining is a face break. This is a situation whereby the face breaks ahead of the shield, temporarily rendering the coal winning operation impossible. The most significant impact of a face break is mainly the downtime that it brings, rather than the fear of burial of equipment (van der Merwe and Madden 2010). This argument is based on the fact that longwall mining is capital intensive and is profitable only when the level of production is kept relatively high. Many face breaks have reportedly occurred after prolonged production break downs which sometimes are due to human factors. The mechanism involved in a face break can be explained by the fact that the high level of stress which occurs ahead of the longwall face is given enough time to induce failure of the rock. It is important to bear in mind the time dependent characteristic of rock failure.

The magnitude of stress ahead of a longwall face is an operational parameter that one can define by changing the geometry of the face, taking into account the geomechanic characterstics of the overburden and the coal. In some instances, high stress ahead of the face will aid production since it breaks the rock, whereas in others it can be detrimental to the production through face breaks.

4.5 Pillar extraction (stooping)

Full pillar extraction has always involved a basic contradiction. On the one hand, the ground needs to cave to minimize the loads on the active pillar line. But on the other, the caving must

not occur until after the miners have safely left the area (Mark and Zelanko, 2001). This statement highlights the very basic principle at the heart of any stooping operation.

In essence the wide span of a panel being stooped will more likely result in collapse of the roof. The collapse of the roof is often attributed to the large tension zone which develops above the panel being stooped. It has been proven that the extent of this tension zone is a function of the span of the stope, the properties of the rock mass and most importantly the depth of mining (Wagner and Schumann 1996).

As for longwall mining, when stooping is contemplated in a particular panel, it is up to management to decide whether the roof should be kept in place or allowed to collapse. The decision will mainly be based on the advantage that the goaf offers with respect to stress relief on the pillars and the detrimental effects of the goaf which range from purely economic to environmental (disturbance of water table, ground water ingress or subsidence on surface). It is important to note that the span of the panel is the controllable parameter available to achieve this goal. In the case of incompetent strata, the critical panel span, which allows the collapse of the overburden, is given by the expression:

$Lc = 2H*\tan\varphi$

Where :

Lc = the critical mining span,

H = depth of mining below surface, and

Φ = goaf angle; 15° off the vertical in absence of more exact data (van der Merwe and Madden 2010)

In the highveld coalfield occurrences of massive dolerite sills is very common. In those instances, the high strength properties of the dolerite sill can arrest the expansion of the goaf unless the panel is made wider. Van der Merwe (1995) has proposed a formula to derive the critical panel width needed to induce failure of the dolerite sill:

$$L_c = 2T\sqrt{K_s + \frac{\beta}{D}} + 2(H - D)tan\varphi$$

With:

$$\beta = \frac{1.53}{\gamma_m} - 0.8$$

$$\gamma_m = 0.025\frac{D - T}{D} + 0.03\frac{T}{D}$$

Where:

$K_s = ratio\ of\ horizontal\ to\ vertical\ virgin\ stress$

H= mining depth

D = depth of dolerite base

T = thickness of dolerite

Φ = goaf angle (measured off the vertical)

Although in a pillar extraction panel the roof is deliberately allowed to collapse, ideally, the roof should collapse in a gradual manner. Where violent failures of goaf have occurred they have been associated with enormous effects on personnel and equipment especially due to the direct effect of the failure and the wind blast caused by such a violent collapse. The rate of failure is defined by the stiffness of the overburden and the pillar being extracted (Salamon and Oravecz 1976). A violent failure is the result of the energy supplied by the loading system exceeding that required by the pillar to continue to deform. According to Van der Merwe and Madden (2010), in the South African context, characterised by shallow depth and a stiff overburden, the deformation of the overburden will not lead to failure of the pillar

unless the stiff sandstone fails first. In this scenario, the stiffness of the overburden system drops to zero and, as a result of this, a violent failure of the pillar can take place. The following parameters are to be borne in mind when designing for rate of failure:

- When a pillar is split, the resulting stress on the fenders is higher, which increases the likelihood of a violent failure,
- The stiffness of the fenders is less because of the w/h ratio, which is less than for a pillar prior to the split, which increases the probability of a violent failure,
- The stiffness of the loading system is a function of the width of the panel. The wider the panel the softer the system, and
- Natural discontinuities in the rock mass such as the faults, joints and dykes adversely affect the stiffness of the system.

Amongst all the above mentioned parameters, only the width of the panel and the w/h ratio of pillars can be controlled to some extent. It is also important to bear in mind that the stiffness of the pillar referred to here is the post-peak modulus which is a system property unlike the pre-peak one which is a material property. It means that this stiffness can change with parameters of the system, mainly with the w/h ratio of the pillar. By using the Van der Merwe (1998) formula to compute the post-peak stiffness of pillars based on the data of Van Heerden (1975), a w/h ratio of 4.08 yields a post peak stiffness of zero which is the needed stiffness to avoid violent failure when the overburden system stiffness dropped to zero.

Even though the very essence of conducting pillar extraction is to achieve a total recovery of proven reserves, in practice such a goal is just too hazardous to be attained. Therefore, some of the reserves have to be sacrificed in the form of snooks (stumps) in order to give the active intersection enough stand up time to allow the personnel and the equipment (CM) to safely leave the area. The basic principle behind the design of snooks is to make them stand just during the time required by the retreat of the equipment and the personnel and to allow them to fail after this. The failure of snooks is a very important aspect of a stooping operation because if they do not fail they cause the goaf to hangup, which results in an increase of load on the next line of pillars. Various approaches to the design of snooks have been proposed since, because of the irregular shape of snooks, the conventional pillar strength formulae no longer apply.

Mark and Zelanko (2001) once presented an approach to the determination of the load bearing capacity of snooks (stumps) based on a "method of slices". This method makes the following assumption:

The strength of each pillar element is a function of its distance to the nearest pillar rib, and

The strength function is known, for instance by the Mark-Bieniawski formula:

$$\sigma_v = S_l[0.64 + 2.16\,(x/h)]$$

Where:

σ_v : stress function,

S_l : in situ coal strength,

x : distance from the nearest rib, and

h : pillar height.

The load bearing capacity of the pillar is obtained by adding up the strength of each element over the section of the pillar.

The load on the snooks was derived from reports on pillar extraction fatalities recorded from 1983 to 1998 and was found to be about 4000 tons. This approach yields a load much lower than the initial load on the pillar computed by the tributary area theory. In fact, it was postulated that once the extraction of the pillar has started most of its initial load is redistributed onto the surrounding pillars. From the load and the capacity, a safety factor can be computed and based on the limited amount of fatalities data available at the time it was found that a safety factor of 2.5 is preferable.

Van der Merwe and Olivier (1992) proposed an alternative approach to the design of crush pillars in coal pillar extraction operations (the word crush pillar being loosely used in this context). The approach takes cognisance of the time dependency of rock failure. For instance it was observed that most pillars with a safety factor of about 1 take days to fail when loaded at their full capacity whereas most pillars of a safety factor of 0.8 take hours to fail and most of those designed to a safety factor of 0.4 will fail almost immediately. The load on the pillar is determined using a pseudo three dimensional boundary element code. The suggestion made

was to leave snooks of relatively high safety factor close to the solid so as give to the continuous miner enough time to tram out of the split. In doing so, a higher safety factor is assigned to snooks close to where the personnel and equipment spend more time.

The numerous hazards associated with pillar extraction often detract from the high extraction benefit this method actually offers. Lind (2005) attempted to put a figure to the risk associated with pillar extraction in the Witbank and Highveld coalfields based on a set of physical, risk and economic factors. The method involves a rating system and quantifies the potential risk associated with secondary extraction. This method is a valuable tool at the disposal of mine planners who are confronted with the decision of whether and how to conduct stooping in an old bord and pillar panel. Special attention is given to the time dependent deterioration of the panel.

An alternative method of assessing the potential of stooping for old bord and pillar developments was presented by van der Merwe and Madden (2010). This method takes cognisance of the scaling of pillar over time in the computation of the Extraction Safety Factor (ESF). The Extraction Safety Factor (ESF) as opposed to the conventional safety factor, takes into consideration the variation of the load on pillars as pillar extraction proceeds.

The state of the art of pillar extraction as applied in South Africa has been documented in detail by Beukes (1990). It is apparent from this report that little improvement in technology has been made recently in the way of conducting pillar extraction if not for the NEVID method (Lind 2005). The NEVID method, named after Neels Joubert and David Postma who used to work at Sasol at the time, is a mining sequence ordered in such a way that the personnel and equipment are kept away from the area most likely to collapse all the time.

From an in situ stress persective, it is obvious that methods such as longwall mining and pillar extraction, which cause more damage to the surrounding rock, will have a much higher foot print than a conventional bord and pillar development. However, most of the problems are likely to occur while mining in the abutment (concentration of stress lines) of a goaf than in the shadow (dispersion of stress lines) of the goaf.

4.6 Multiple seam mining

The deposition of coal in South Africa was such that a series of 5 seams were deposited one on top of the other. Therefore, instances where two mineable seams are present in the same lease are a common reality, especially in the Witbank Coalfield. Multiple seam occurrences have been identified in the Springs – Witbank coalfield extending from Brakpan and Springs to the West to Belfast to the East (Hill 1994).

Providing that the two seams are likely to interact with each other, it is very important that this interaction is fully understood so as to guarantee the maximum recovery of reserves. In some instances, one of the seams could have been mined out in the past with very little if no information on its layout (position of workings and pillars in the mined out seam). Some of the workings could even be subsided, partially damaged or flooded and the long time effect of these conditions on the next seam can be difficult to anticipate.

In South Africa a proper design procedure for multiple seams mining was lacking up until the early 1960s (Hill 1994). It is only around 1967 that the first investigations started at Coalbrook Colliery and observations continued up to 1972 in order to assess the long term effect of double seam bord and pillar mining (Oravecz 1973). Further to this investigation, a set of guidelines pertaining to multiple seams mining emerged (Salamon and Oravecz 1976). The guidelines are based on the thickness of partings between seams (P) in relation to the centre distance (C) and the bord width (b). The guidelines are as follows:

- If P<(0.75C to 1.00C) : panel pillars are to be superimposed;
- If P > 2b : Pillars can be designed to a safety factor of 1.6. If the pillars must be superimposed, a minimum safety factor of 1.7 is recommended;
- If P < (0.3b to 0.5b), mining adjacent seams will only be practical if the parting contains a fair portion of sandstone;
- If P < (1.5b to 2.0b) the possibility of parting failure cannot be excluded. The safety factor of individual workings should be > 1.8; and

The safety factor of hypothetical pillars with a height equal to the combined height of the working should be > 1.5.

4.7 Conclusion

The mining methods commonly used in the Witbank and Highveld coalfields are:

- Bord and Pillar mining;
- Longwall mining;
- Pillar extraction; and
- Multiseam mining.

The impact of each of the mining methods on the stress regime depends mainly on the damage to the rock mass that this method produces and the volume of void left after mining. As a result, total extraction methods (Pillar extraction and longwall) will tend to have greater impact on stress than the conventional bord and pillar mining method.

In the Witbank and Highveld coalfields, over many years, bord and pillar has been the most used mining method. The most popular method of design of bords and pillars have been summarised as part of this research. However, with the increasing depletion of reserves in these two coalfields, pillar extraction is being more and more practised in spite of operational and safety issues associated with the method. Wherever the conditions are suitable, other high extraction mining methods such as longwall mining are also used.

Multiseam mining is a common reality in the Witbank coalfield and requires a different design approach. Sometimes, the two coal seams are mined simultaneously, but sometimes, there is one seam which was mined in the past and the new mining is carried out above or underneath old mine workings.

CHAPTER 5

Review of stress data

Different sources of stress information were used in an attempt to derive in situ stress trends within the Witbank and Highveld Coalfields as explained in section 1.4. These sources of information include pre-existing in situ stress databases, the World Stress Map database, geological structures (faults, dykes orientation), in situ stress measurements (Overcoring and AE) carried out in the coalfields and results from underground mapping exercises.

5.1 Data Collected from Witbank and Highveld Collieries

A major part of the data collection in this project was covered by a series of underground visits across the Witbank and the Highveld coalfields. These visits constituted an opportunity to see roof conditions under high stress and roof conditions under relatively low stress. During these visits, information pertaining to stress was collected. The mines visited were chosen such as to cover the entire Witbank and Highveld coalfields. In addition to this, an effort was made to include into the study as many mines of company members of Coaltech as possible. However, in some instances, the schedules of some of the mines and other factors prevented some mines from being visited.

Six mines were successfully visited, namely:

- In the Witbank Coalfield:
- Arnot (Exxaro);
- Khutala (Ingwe);
- Boschmans Shaft (Xstrata); and
- Kenako Shaft (ex Nooigedacht, AngloCoal);
- In the Highveld Coalfield
- Brandspruit (Sasol);

Other Coalfields:

- Mooiplaats (Ermelo Coalfield, Coal of Africa Ltd);

In the following section, data and information collected from the mines visited are presented along with the analyses conducted. As mentioned above no restriction was imposed on the nature and the format of data collected from the mines so that each mine would feel free to contribute any information that it had regarding the topic of stress. As a result of this, the type of analysis (quality and quantity) might vary from one mine to another. However, wherever available, the following information was collected:

- Geology and stratigraphy;
- Mining layout;
- Plan showing guttering occurrences and photographs;
- Support standard;
- Stress measurement reports.

5.1.1 In situ stress measurements

In situ stress measurement reports were collected from the following mining companies:

- Exxaro;
- AngloCoal;
- BECSA;

The stress measurements at Arnot Colliery (Exxaro) were carried out by Rock Mechanics Technology in 1999. The tests were conducted to quantify the stress regime in the roof of the No.2 seam at D1 South, E5 and Shaft 10. The technique used was the CSIRO Hollow inclusion stress cell which has the advantage of producing the full three dimensional in situ stress regime from one overcoring test. All the tests were conducted at depth averaging 50m. Table 5-1 and Table 5-2 summarize results of in situ stress measurement conducted at Arnot Coal Mine.

Table 5-1 Summary of principal stress components at Arnot Coal Mine

Test	Major			Intermediate			Minor		
	Values (MPa)	Bearing	Dip	Values (MPa)	Bearing	Dip	Values (MPa)	Bearing	Dip
1	5.7	69	0	2.9	159	8	1.2	338	82
2	3.7	231	5	2.6	140	7	1.2	354	81
3	6.4	42	18	3.5	307	15	1.7	180	66

Table 5-2 Summary of Horizontal and vertical stress component at Arnot

Test	Maximum Horizontal Component (MPa)	Bearing of Maximum Horizontal stress (degrees)	Vertical Component (MPa)	K-ratio
1	5.7	69	1.2	4.8
2	3.7	52	1.2	3.1
3	6.4	45	2.2	2.9

In stress measurements were carried out at various AngloCoal collieries by Rock Mechanics Technology. Five in situ stress measurements were conducted at Goedehoop colliery including those conducted at Hope and Vlaklaatge shafts. In addition, two in situ stress measurements were carried out at Nooitgedacht (today Kenako) at Greenside Colliery. The technique used was again the CSIRO Hollow inclusion stress cell. The results of the in situ stress tests are summarized in Table 5-3 to Table 5-8.

Table 5-3 Summary of principal stress components at Goedehoop Colliery

Colliery	Shaft	Site	Major			Intermediate			Minor		
			Magnitude (MPa)	Bearing (°)	dip (°)	Magnitude (MPa)	Bearing (°)	dip (°)	Magnitude (MPa)	Bearing (°)	dip (°)
Goedehoop	**Vlaklaatge**	**Section 2, Panel 1220**	5.69	336	16	1.36	224	53	0.51	77	33
	Hope	**Section 5/6**	5.2	340	10	1.1	223	34	0.7	83	54
	Hope	**Section 5/6**	5.4	334	12	1	232	42	0.5	79	45
		Block 11		338	10						
		Block 12		345	10						

Table 5-4 Summary of principal stress components at Bank Colliery

Colliery	Shaft	Site	Major			Intermediate			Minor		
			Magnitude (MPa)	Bearing (°)	dip (°)	Magnitude (MPa)	Bearing (°)	dip (°)	Magnitude (MPa)	Bearing (°)	dip (°)
Bank	**5 Shaft**		1	156	65	0.7	326	24	0.2	58	4
	5 Shaft		4.3	175	1	3.8	85	3	1.5	278	87

Table 5-5 Summary of principal stress components at Nooitgedacht (today Kenako)

Colliery	Shaft	Site	Major			Intermediate			Minor		
			Magnitude (MPa)	Bearing (°)	dip (°)	Magnitude (MPa)	Bearing (°)	dip (°)	Magnitude (MPa)	Bearing (°)	dip (°)
Greenside	Nooitgedacht	Inclined Shaft	10.96	20	13	8.28	118	30	4.54	270	56
		50/51	7.49	105	2	5.45	196	36	1.56	13	54

Table 5-6 Summary of Horizontal and vertical stress components at Goedehoop Colliery

Colliery	Shaft	Site	Max horizontal Stress (MPa)	Bearing of Max Horizontal Stress	Min Horizontal Stress (Mpa)	Vertical Stress (MPa)	K-ratio
Goedehoop	Vlaklaatge	Section 2, Panel 1220	5.4	338	0.8	1.4	3.9
	Hope	Section 5/6	5	340	1	1.1	4.5
	Hope	Section 5/6	5.1	334	0.8	1.0	5.1
		Block 11		338			
		Block 12		345			

Table 5-7 Summary of Horizontal and vertical stress components at Bank Colliery

Colliery	Shaft	Site	Max horizontal Stress (MPa)	Bearing of Max Horizontal Stress	Min Horizontal Stress (Mpa)	Vertical Stress (MPa)	K-ratio
Bank	5 shaft		0.8	328	0.2	0.9	0.9
	5 shaft		4.3	355	3.8	1.5	2.9

Table 5-8 Summary of Horizontal and vertical stress components at Greenside (Nooitgedacht today Kenako shaft)

Colliery	Shaft	Site	Max horizontal Stress (MPa)	Bearing of Max Horizontal Stress	Min Horizontal Stress (MPa)	Vertical Stress (MPa)	K-ratio
Greenside	Nooitgedacht	Inclined shaft	10.7	20	7.44	5.8	1.8
	Nooitgedacht	50/51	7.5	105	5.4	1.6	4.7

At Sasol an in situ stress measurement was conducted at Bosjesspruit mine. The results of this in- situ stress measurement are summarized in Table 5-9 and Table 5-10. Apart from the results of the in situ stress measurement conducted at Sasol, documents containing observational information were made available to the present study. These documents contained 364 records of guttering and other high horizontal stress. This database, as discussed later on, can be used to generate various probabilities which can be used in a proper risk assessment or can alternatively be used to gain more insight into the guttering process.

The result of the in situ stress measurement conducted at Khutala colliery was provided by BHP Billiton following the visit to the mine. The results of the stress measurement at Khutala are summarized in

Table 5-11 and Table 5-12.

.

Table 5-9 Summary of principal stress component at Bosjesspruit

Colliery	Shaft	Site	Major			Intermediate			Minor		
			magnitude (MPa)	Bearing (°)	dip (°)	magnitude (MPa)	Bearing (°)	dip (°)	magnitude (MPa)	Bearing (°)	dip (°)
Bosjesspruit		Section 56	9.3	156	10	5.5	270	68	4.1	62	20

Table 5-10 Summary of Horizontal and vertical stress components at Bosjesspruit

Colliery	Shaft	Site	Max Horizontal Stress (MPa)	Bearing of Max Horizontal Stress	Min Horizontal Stress(MPa)	Vertical Stress (MPa)	K-ratio
Bosjesspruit		Section 56	9.2	335	4.3	5.4	1.7

Table 5-11 Summary of principal in-situ stress at Khutala Colliery

Colliery	Shaft	Site	Major			Intermediate			Minor		
			magnitude (MPa)	Bearing (°)	dip (°)	magnitude (MPa)	Bearing (°)	dip (°)	magnitude (MPa)	Bearing (°)	dip (°)
Khutala		22/3-4 area_barrier pillar split 33	4.9	174	1	4.4	264	4	1.3	68	176
Khutala		22/3-4 area_barrier pillar split 33	5.7	354	1	4.5	264	6	1.4	96	173
Khutala		22/3-4 area_barrier pillar split 35	4.7	161	9	4.1	69	16	1.3	279	161
Khutala		22/3-4 area_barrier pillar split 10	4.8	186	4	3	282	34	1.3	282	146

Table 5-12 Summary of principal horizontal stress at khutala Colliery

Colliery	Shaft	Site	Max Horizontal Stress (MPa)	Bearing of Max Horizontal Stress	Min Horizontal Stress(MPa)	Vertical Stress (MPa)	K-ratio
Khutala		22/3-4 area_barrier pillar split 33	4.9	353	4.4	1.3	3.8
Khutala		22/3-4 area_barrier pillar split 33	5.7	355	4.5	1.5	3.8
Khutala		22/3-4 area_barrier pillar split 35	4.6	350	3.9	1.6	2.9
Khutala		22/3-4 area_barrier pillar split 10	4.8	353	2.5	1.9	2.5

5.1.2 Stress Observation at Arnot Coal (Exxaro)

Location

A site visit was undertaken to Arnot Coal which is located between the towns of Middleburg, Carolina and Hendrina in the Mpumalanga Province in South Africa (Arnot Coal 2009). Figure 5-1 shows the location of Arnot Colliery.



Figure 5-1 Regional location of Arnot Coal Mine

Stratigraphy

Figure 5-2 presents a typical stratigraphic column through the Arnot lease area. It can be seen that No 2 seam and No 1 seam are the only seams being mined underground whereas No 4 and No 5 are erratically present in topographically elevated areas and are not included in the stratigraphic column. No 4 and No 5 have a too low a thickness to be mined profitably; therefore they are excluded from the reserves. The mining depth of No 2 seam is about 30 m on average (Arnot Coal 2009).

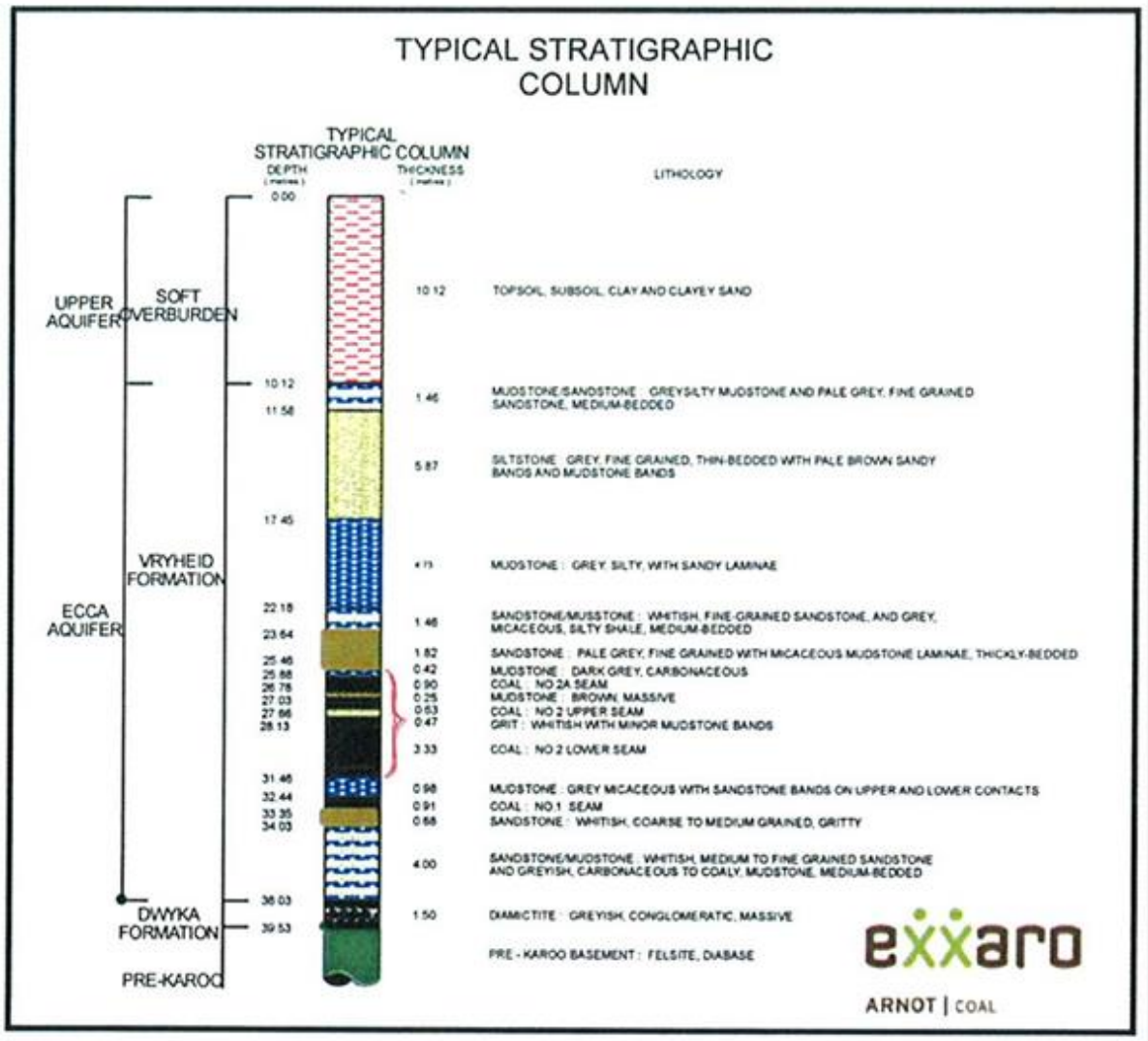


Figure 5-2 Typical stratigraphic Column at Arnot Coal Colliery

Unlike in the rest of the Witbank coalfield, the No 2 seam at Arnot splits into 3 sub-seams, the No 2A seam, No 2 Upper seam, and No 2 Lower seam, all separated by partings.

Mine plans

Mine plans were issued from the mine in DXF format. Mining at Arnot is currently conducted at two shafts (8 shaft and 10 shaft), however, only 8 shaft was visited. Mining is carried out using a Continuous Miner (CM). Figure 5-3 shows the layout of 10 shaft along with the direction of advance of the faces (SSE) at the time of the site visit and the direction of the measured major horizontal stress at Arnot Colliery. It is important to take note of the two longwall sections on the Western side of the shaft. The SW shortwall section is orientated parallel to the direction of the major horizontal stress whereas the NW shortwall

section is orientated at an angle to the major horizontal stress orientation. Figure 5-4 shows the mine plan of 8 shaft along with the direction of advance of faces (NNW, SSE, ENE) and the direction of the major horizontal stress at the mine (NE-SW). The entire shaft is being mined using the bord and pillar mining method. Figure 5-5 illustrates guttering occurrences in a section (Ptn 13) at 8 shaft.

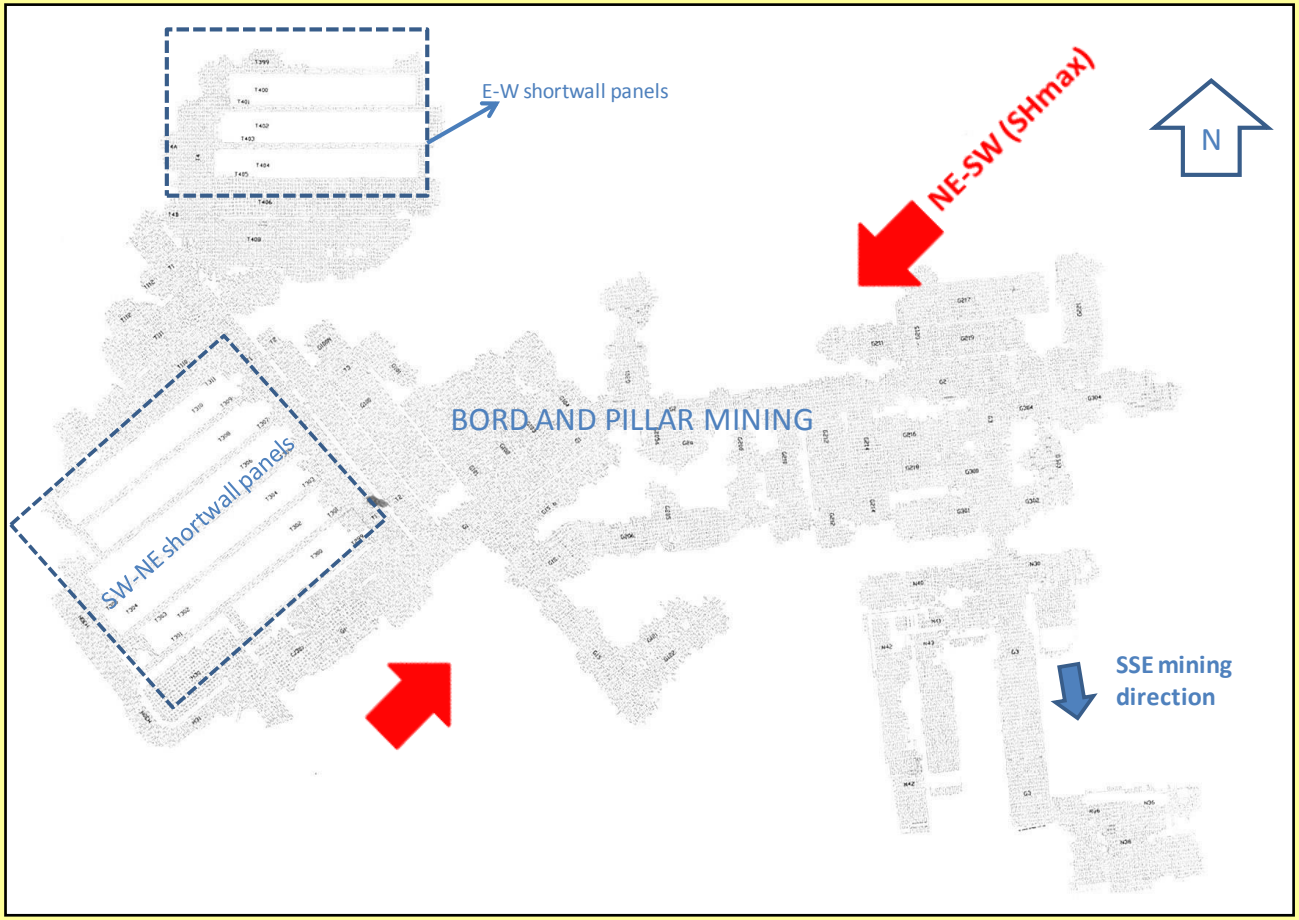


Figure 5-3 Plan showing the layout of 10 shaft at Arnot Colliery, the red arrows show the direction of the major horizontal stress and the blue ones the mining direction

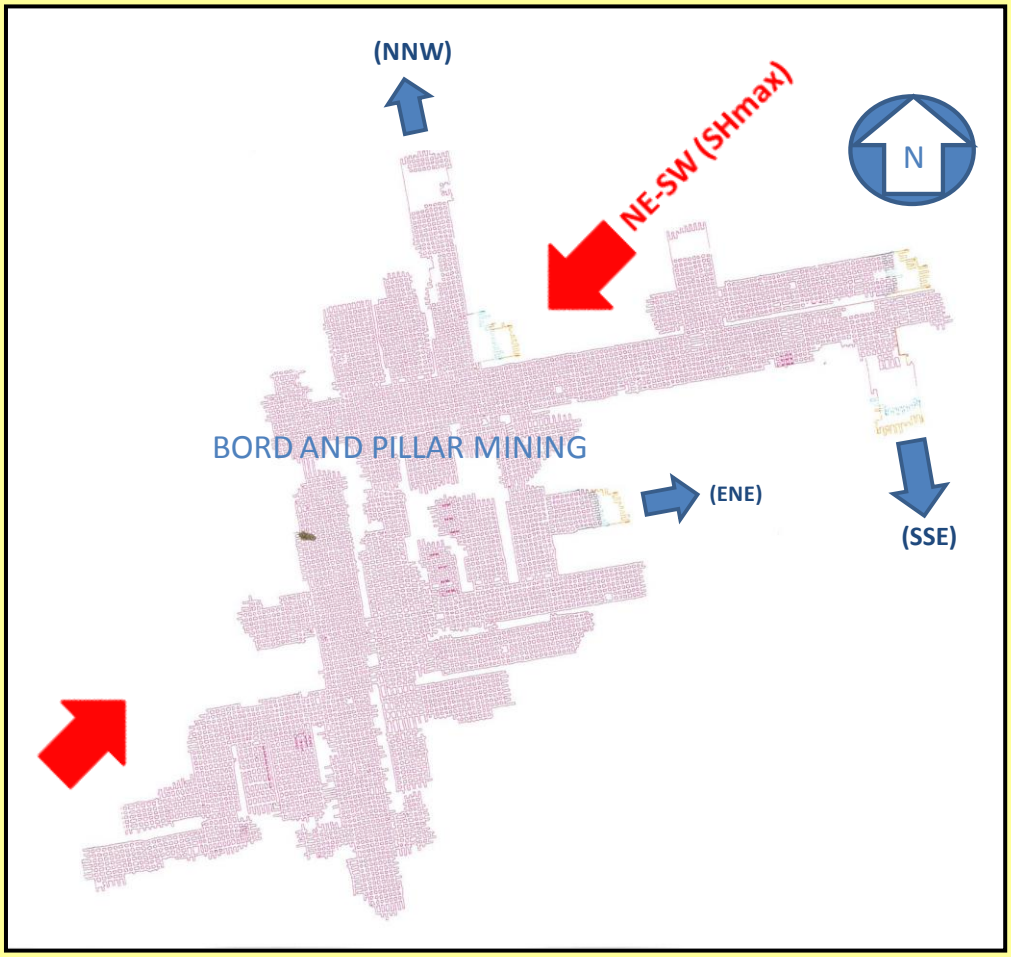


Figure 5-4 Plan showing the layout of 8 Shaft at Arnot Colliery, the red arrows show the direction of the major horizontal stress and the blue ones the current mining direction

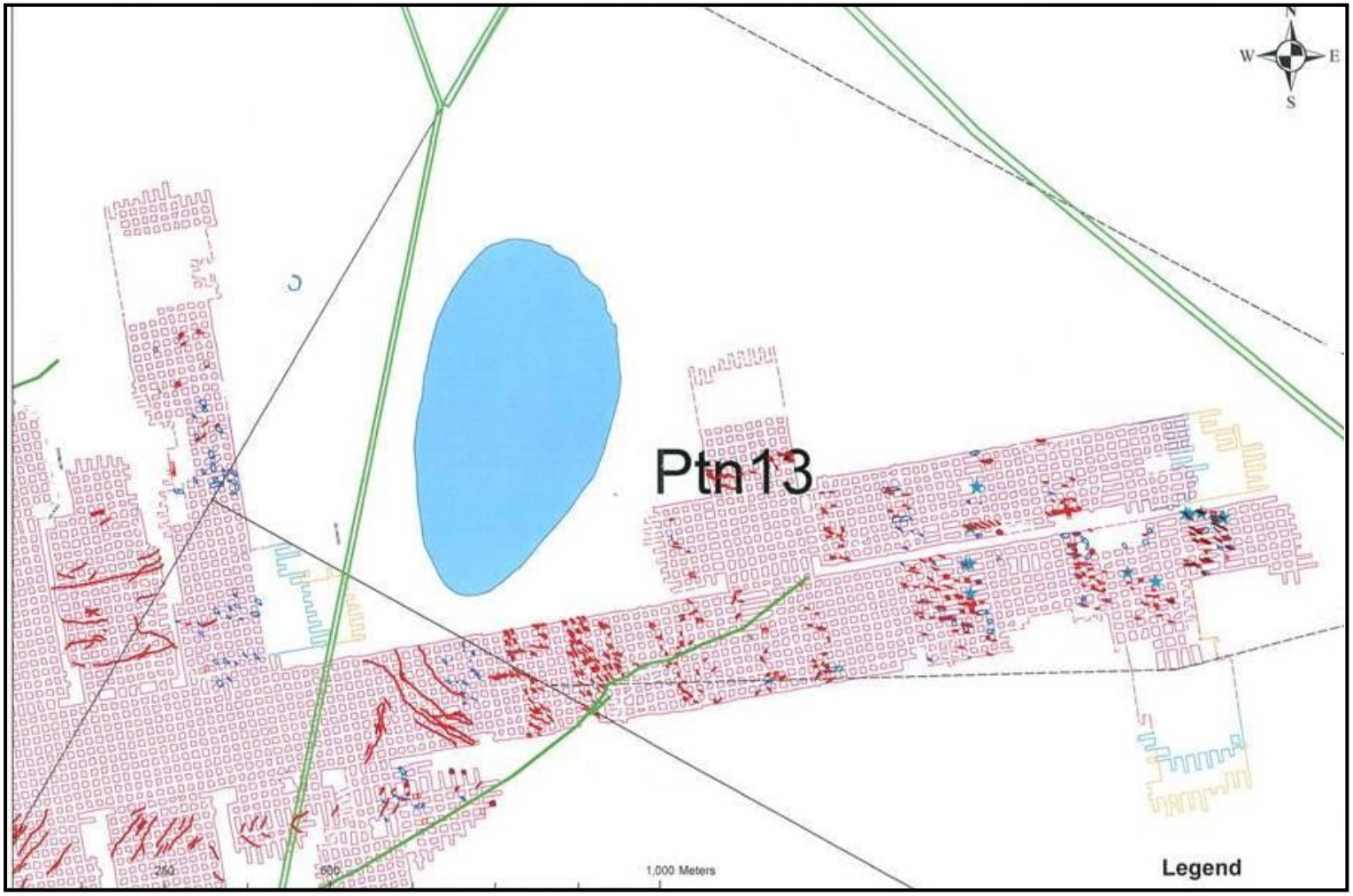


Figure 5-5 Plan showing occurrences of guttering in a section at Arnot, shaft 8

5.1.3 Analysis of data from Arnot Colliery

The guttering data presented in Figure 5-5 were analysed and directions perpendicular to the axis of gutters were measured and plotted on a rosette as shown in Figure 5-6. A similar analysis was conducted using the strike direction of the joints and results of this analysis are presented in Figure 5-7. The most likely orientation of the maximum horizontal stress inferred from both analyses is in very good agreement with the NE-SW direction given by the in situ stress measurement carried out at Arnot Colliery.

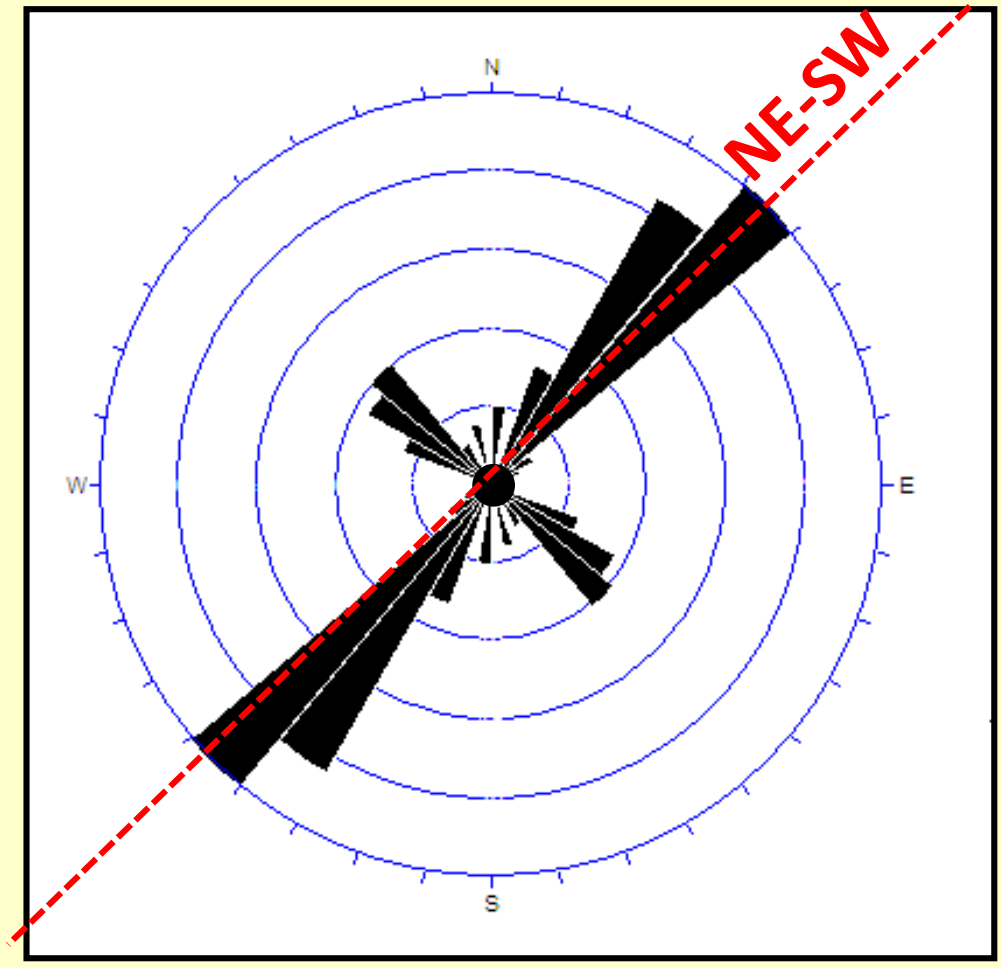


Figure 5-6 Rosette showing the direction of the maximum horizontal stress inferred from the direction of guttering at Arnot

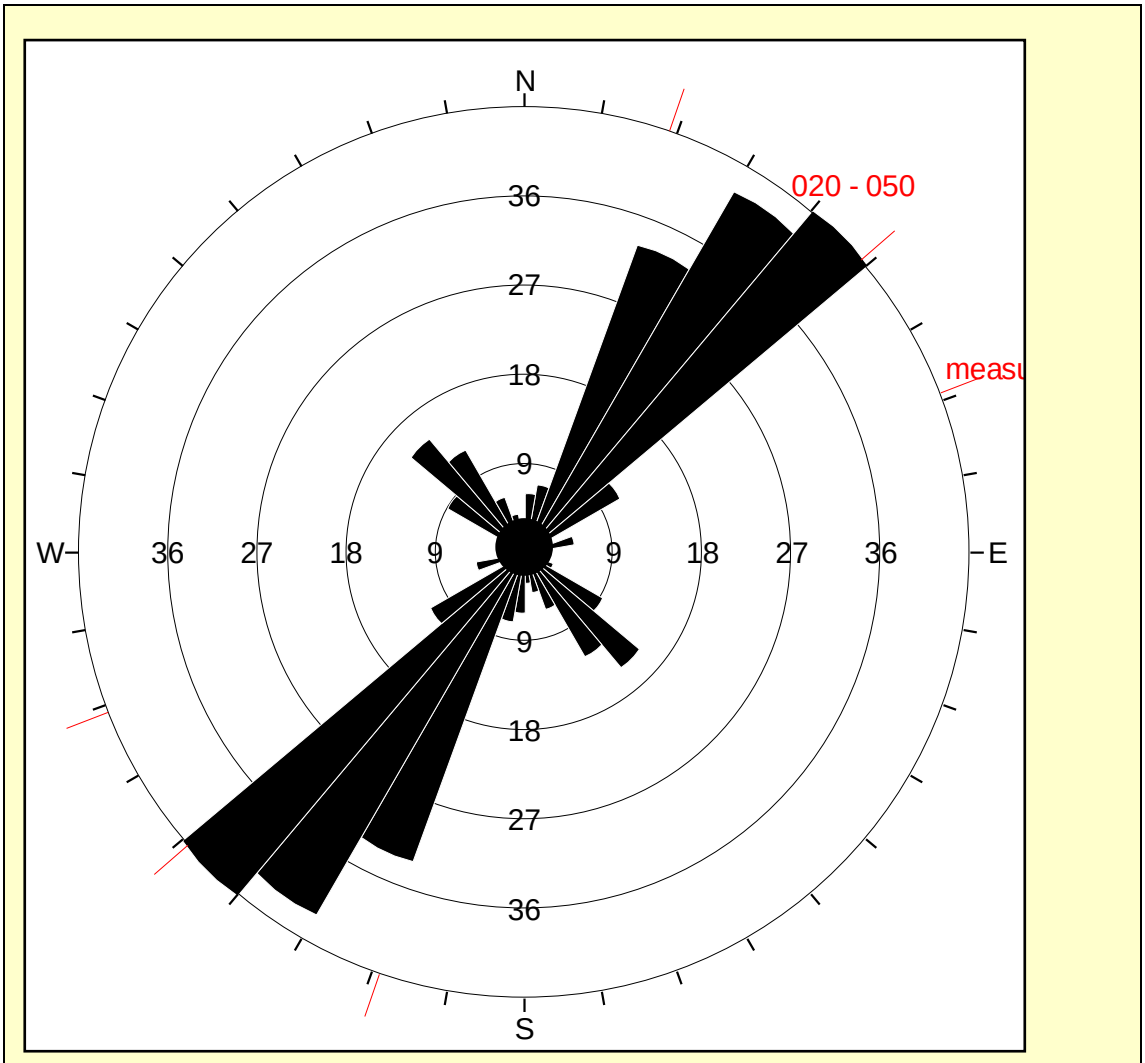


Figure 5-7 Stereonet of strike direction of joints at Ptn 13, Arnot

In addition, the probability distribution function of magnitude of horizontal stress was determined as shown in Figure 5-8.

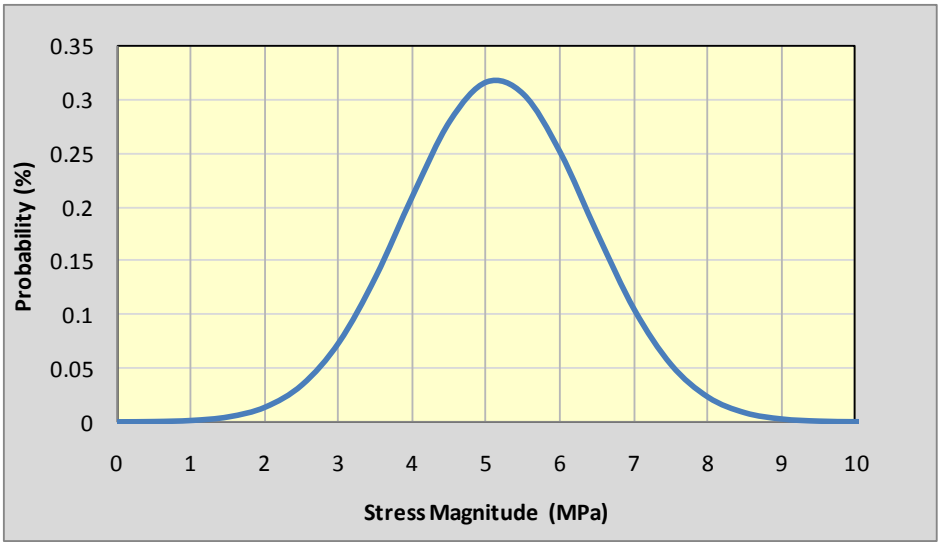


Figure 5-8 Probability distribution of stress Magnitude at Arnot

In these analyses it was assumed that magnitudes are linear random variables coming from a normal distribution function.

Support Standard

The support standard at ARNOT includes 1.5m and 1.8m long 10 ton capacity full column resin grouted bolts as primary support, plus straps as occasional area support. The column of resin is made of a fast and a slow part in order to achieve pre-tensioning of the bolt. The bolts are installed on a 4 by 4 pattern in 6 m wide roadways and a telltale is installed at each intersection. The hole drilled for the installation of the telltale is about 2 m deep.

Ground control techniques applied at Arnot to manage roof instabilities and guttering include the following:

Reduction of cut out distance:

By limiting the cutout distance, the time when the roof is left unsupported is also limited and so is the roof deterioration. In addition to this, it is important to note that the face provides also some form of support to the roof. The closer to the face, the greater the internal support pressure provided by the face.

Reduction of bord width:

This technique consists of reducing the width of the roadway when the condition of the roof is bad. The reduction of bord width has been reportedly used with success at Arnot to prevent guttering from spreading over many road ways.

Straps

Straps are also used at the mine in very bad conditions where guttering and falls between bolts are occurring.

Site Observations

The guttering observed at Arnot has often the shape of an upside down boat with a low angled shear fracture on one side and a tension crack on the other side (Figure 5-9 to Figure 5-11). All the occurrences of guttering observed at the mine were limited to the immediate laminated roof and were mainly taking place between pillars rather than in the intersections of roadways. However, instances of guttering running through multiple intersections were reported on the plans provided by the mine (Figure 5-5).

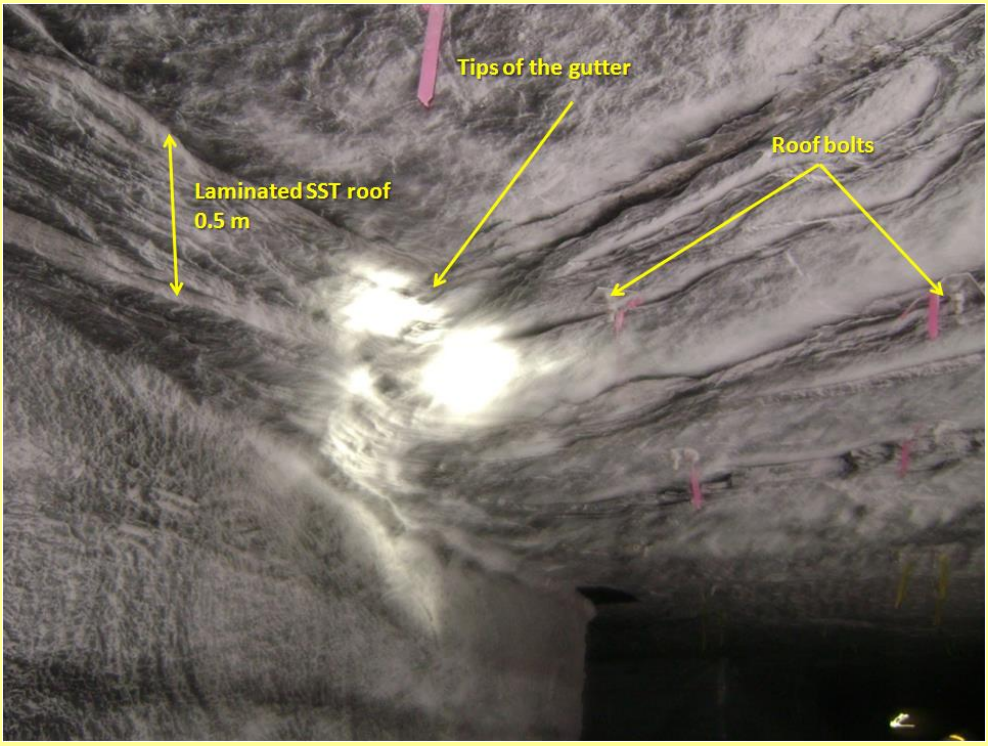


Figure 5-9 Picture showing the tip of a gutter observed at a rib side at Arnot Colliery and how the guttered mudstone roof was re-supported by roof bolts

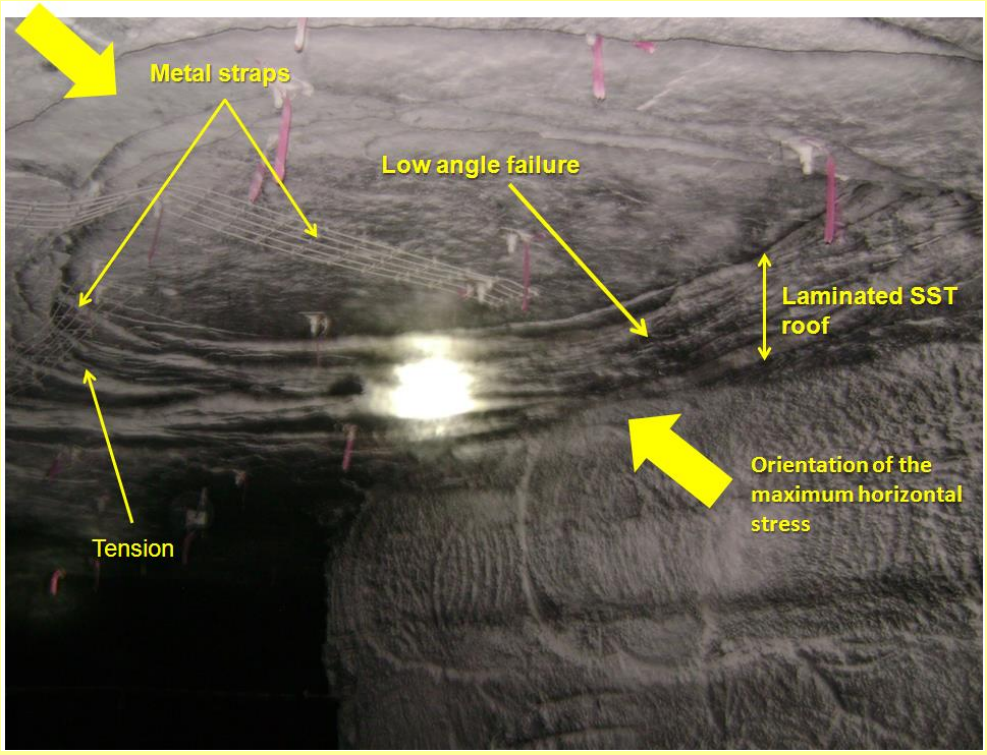


Figure 5-10 Picture showing guttering at Arnot Colliery and how metal straps are used in tandem with roof bolts in order to prevent the guttered roof from peeling off

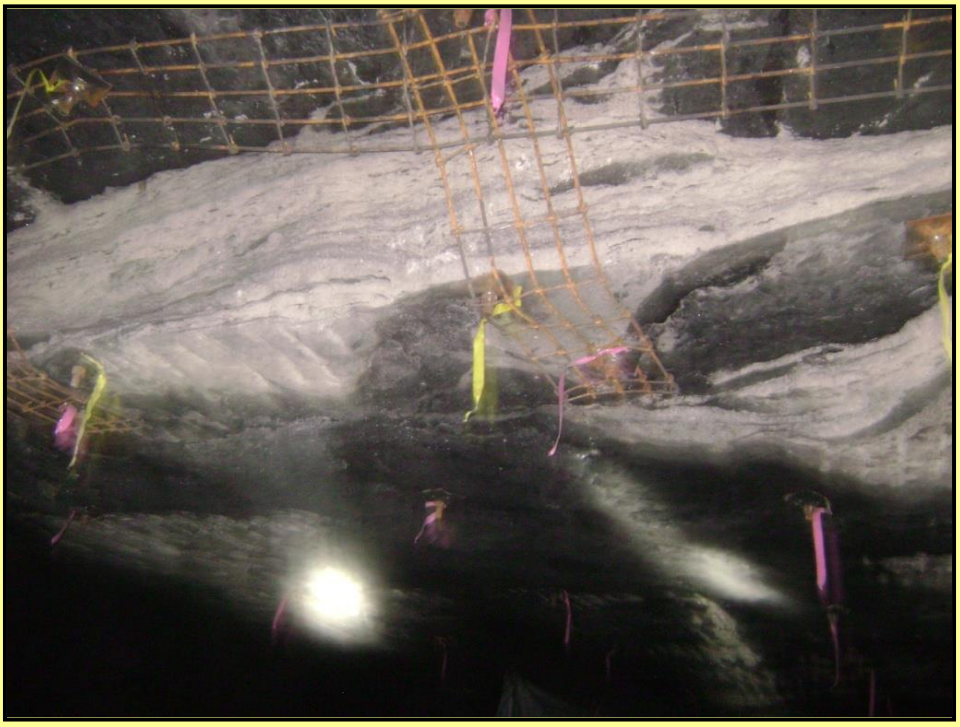


Figure 5-11 Picture showing the tension failure on one side of a guttering in the mudstone roof at Arnot and how it is re-supported by straps and roof bolts after guttering

5.1.4 Stress Observation at Kenako shaft (AngloCoal)

Location

The site visit was undertaken at Kenako shaft (ex Nooitgedacht), at Greenside colliery which is located about 15 Km south east of Witbank, Ogies District, Mpumalanga Province in South Africa (Minney and Munsamy, 2004). Figure 5-12 shows the location of Kenako (ex Nooitgedacht).

The visit was carried out in the back areas of a section where production was abandoned because of major falls of ground associated with high horizontal stress and a weak immediate mudstone roof.

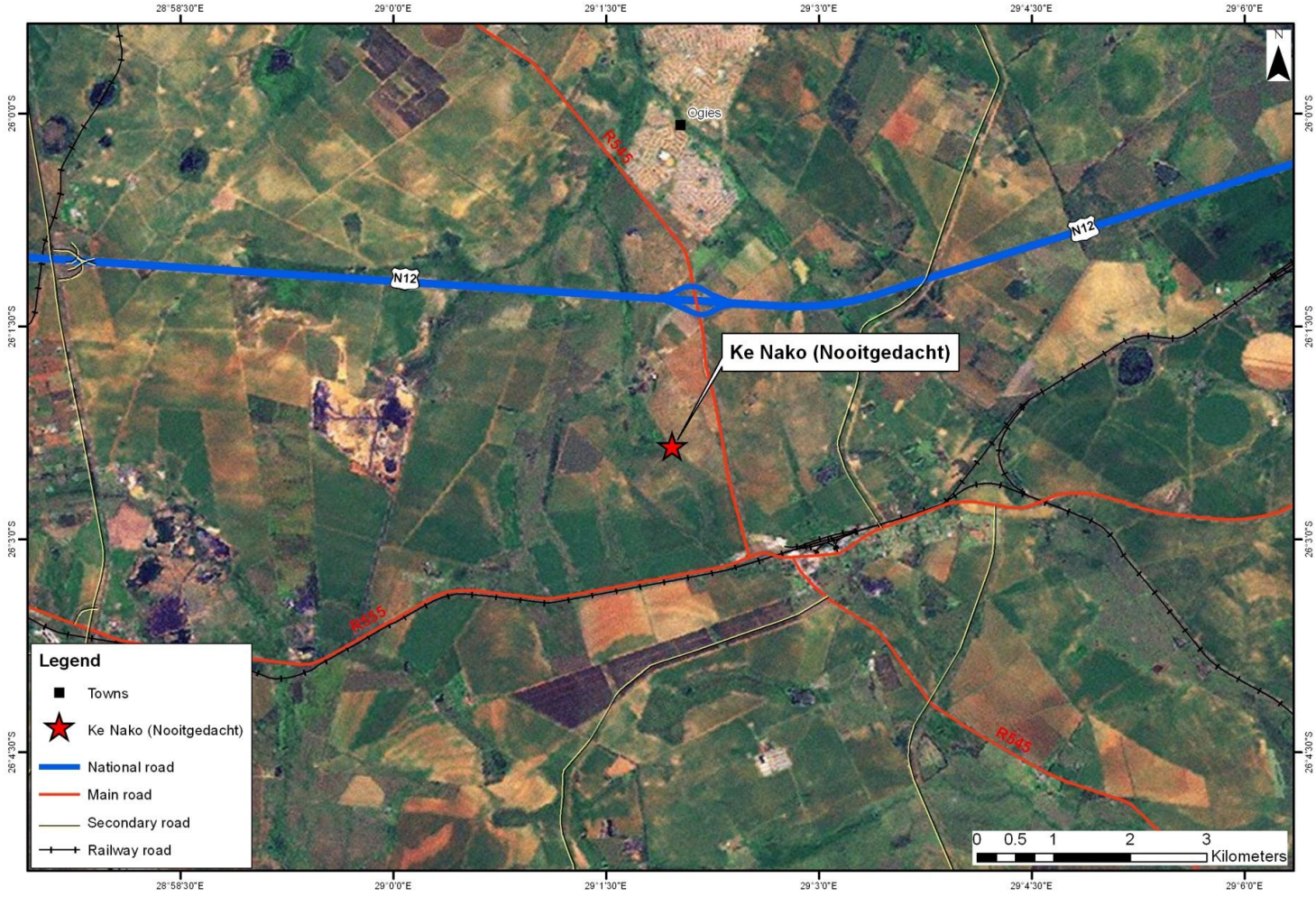


Figure 5-12 Regional location of Kenako shaft

Stratigraphy

Figure 5-13 presents a typical stratigraphic column at Kenako shaft (Greenside Colliery). The coal occurred between 30 m and 60 m below surface and is overlain by mudstone, sandstone and interlaminated shale/sandstone. Kenako Shaft (ex Nooitgedacht) mines the No.5 seam.

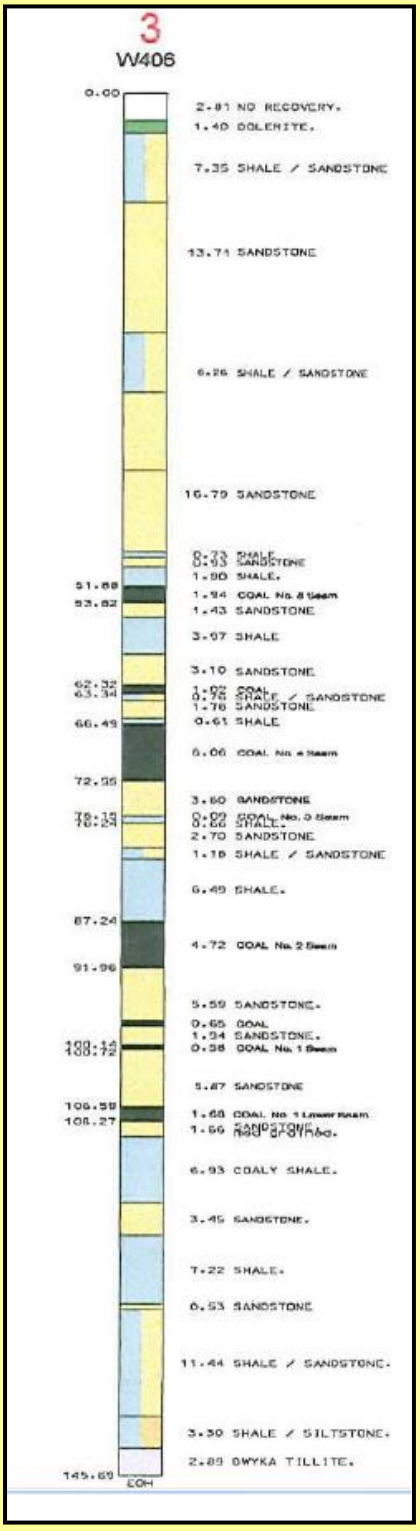


Figure 5-13 Typical stratigraphic Column at Kenako Shaft, AngloCoal

Mine plans

Figure 5-14 shows the layout of Kenako shaft at the time of the visit. It can be seen that virtually all the panels are consistently orientated North-South. In addition to this, the figure shows the orientation of the major horizontal stress as measured in the inclined shaft (N-NE) and in Section 50/51 (E-SE).

It is important to note that mining at Kenako Shaft is conducted using the conventional bord and pillar mining method and unlike most of the mines visited where the coal is won by Continuous Miners, at Kenako shaft, conventional drill, cut and blast is still in use. The uneven floor was pointed out as the major challenge to a Continuous Miner based operation.

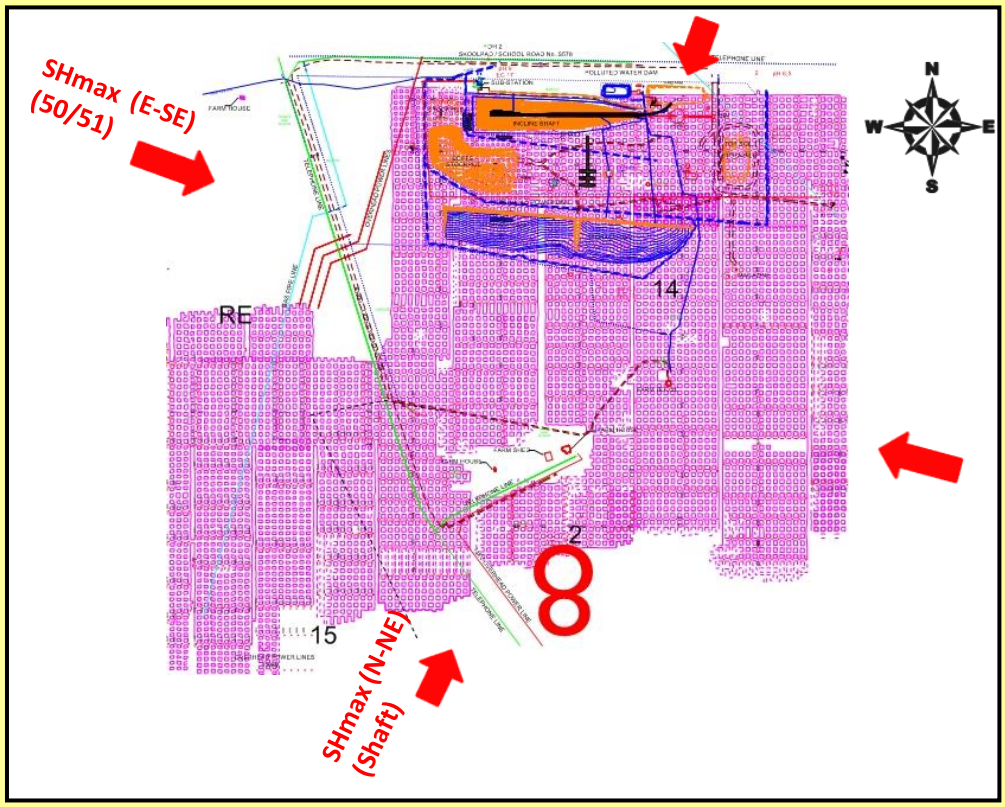


Figure 5-14 Plan showing the layout of Kenako shaft at Greenside Colliery, the red arrows show the direction of the major horizontal stress as measured in the inclined shaft and in section 50/51

Support Standard

The support standard at AngloCoal includes 1.5m long 10 ton capacity full column resin grouted bolts as primary support. The column of resin is made of a fast and a slow part in

order to achieve pre-tensioning of the bolt. The bolts are installed on a 4 by 4 pattern in 6.5 m wide roadways. The spacing between bolts is 1.3 m in the intersection but can occasionally be modified between pillars to a pattern consisting of 1.6 m between bolts and 0.9 m between the ribside and the first line of bolts.

Various ground control techniques have been applied at Kenako to manage roof instabilities and guttering including the sacrificial road technique which was documented by Munsamy and Minney (2004).

Site Observations



Figure 5-15 Picture showing a Multiple splits guttering at Kenako shaft resulting from a progressive slabbing of the laminated roof. Note that the bolts are still in place and do not seem to have been bent

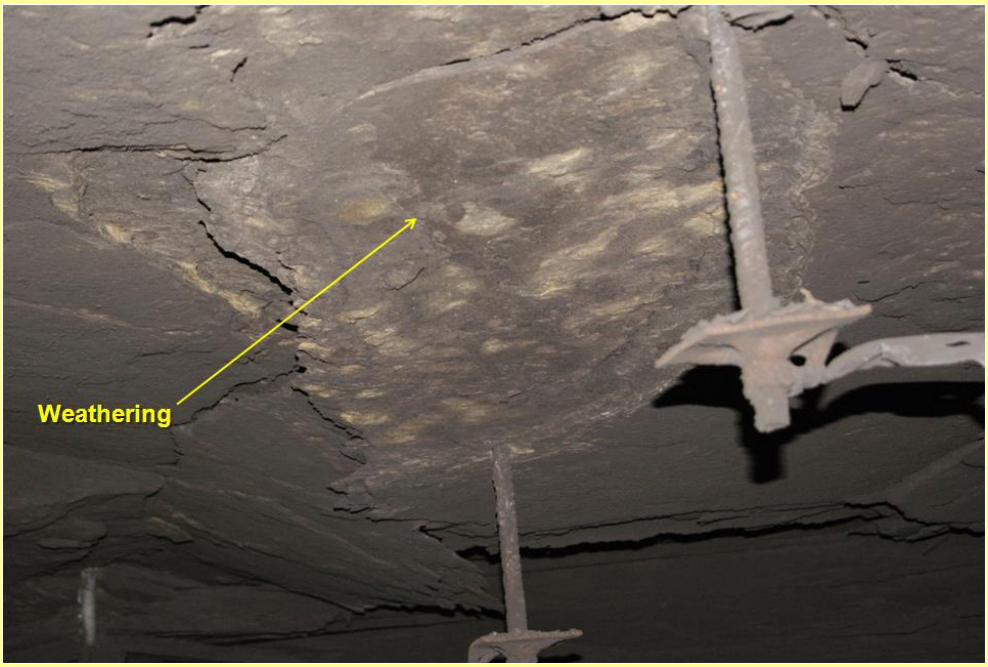


Figure 5-16 Picture illustrating the principal failure mechanism of the roof at kenako, the weathered mudstone roof peels off progressively between the bolts

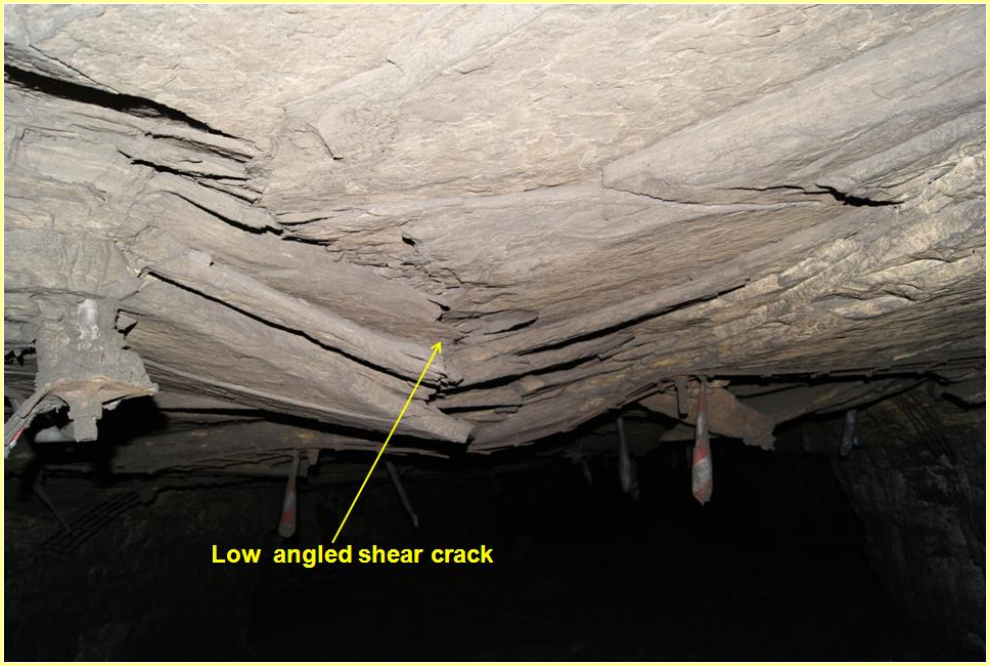


Figure 5-17 Picture showing a typical buckling of the mudstone roof and the low angled shear crack associated with it



Figure 5-18 Picture showing a guttered mudstone roof being re-supported with mine pole, strap and roof bolts

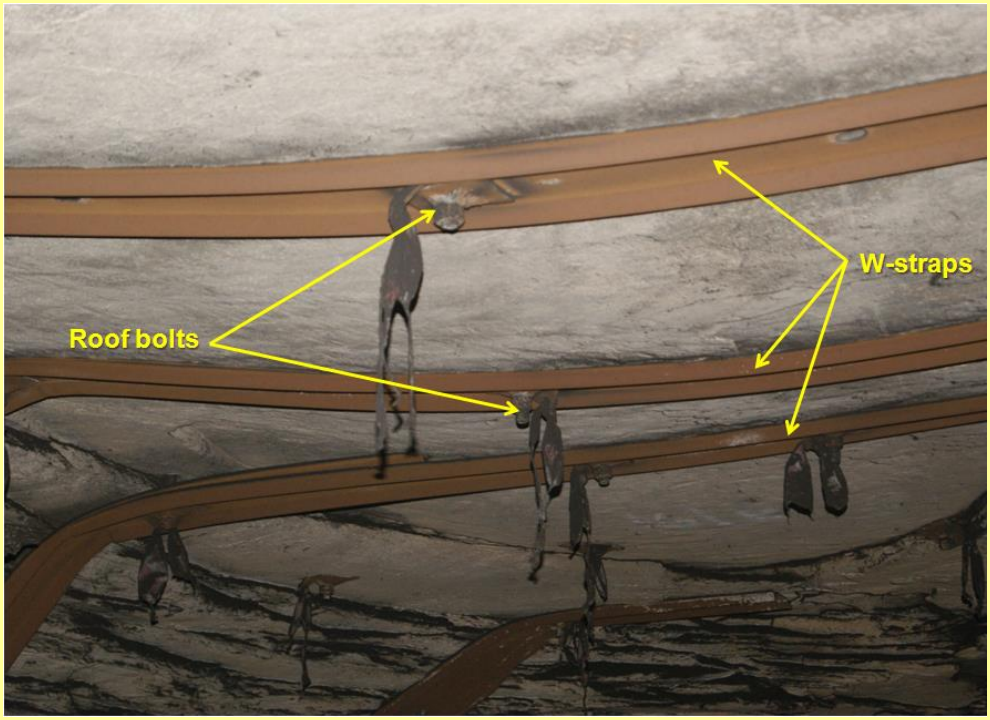


Figure 5-19 Picture showing mudstone roof being supported by w-straps and roof bolts in tandem, the roof seems to be quite stable

During the site visit, instances where massive falls of ground have occurred have also been observed. Figure 5-18 illustrates a case where the tandem w-strap and roof bolts seems to have worked quite successfully in preventing the mudstone from peeling off, whereas, Figure 5-16 illustrates a case where high horizontal stress has caused the roof to buckle, increasing the spalling process. In this latter case, the metal straps and roof bolts were not capable of containing the progressive failure of the roof.

5.1.5 Stress Observation at Brandspruit Colliery (Sasol South Africa)

Location

The site visit was undertaken at Brandspruit shaft near the town of Secunda in the province of Mpumalanga. The regional location of Secunda within the province of Mpumalanga and the location of the mine visited (Brandspruit) are shown in Figure 5-20 and Figure 5-21.



Figure 5-20 Regional location of Secunda and Brandspruit shaft

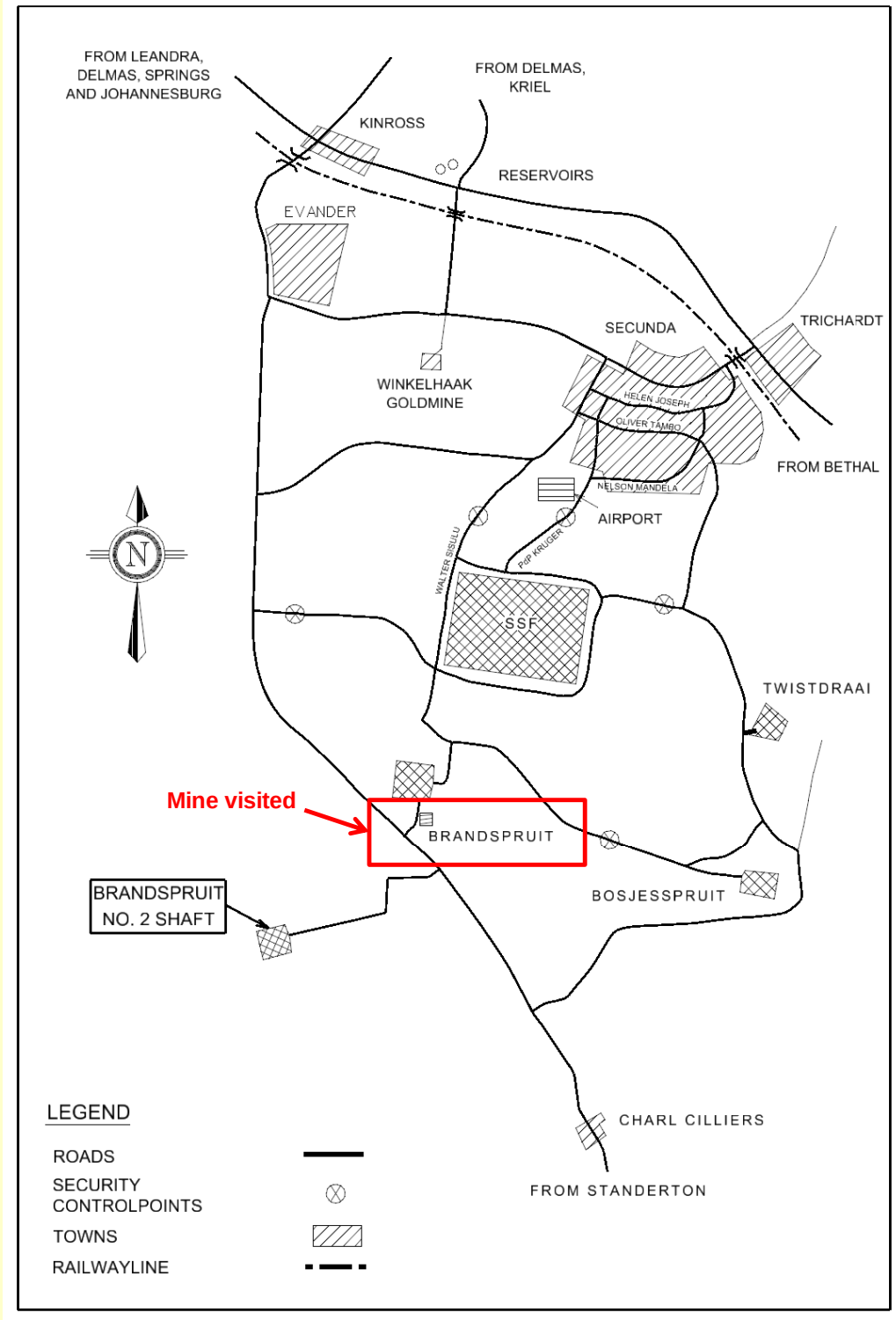


Figure 5-21 Map showing location of Brandspruit in Secunda

Stratigraphy

Figure 5-21 shows a typical stratigraphic column through the Secunda complex in the Highveld coalfield.

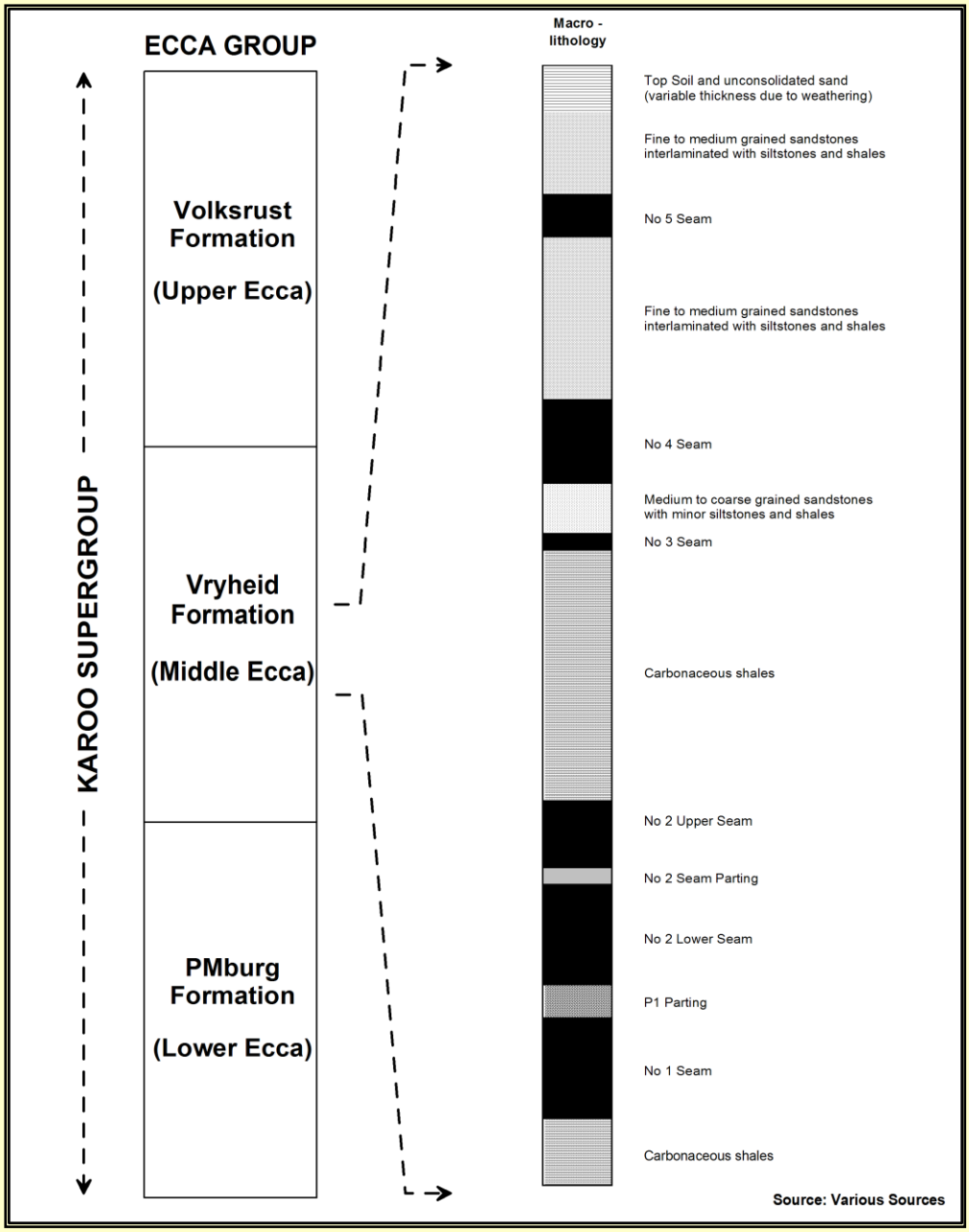


Figure 5-22 Typical stratigraphic Column of the Highveld Coalfield

Ground Support Standard

The ground support standard at Sasol is as follows:

- In competent roof (massive Sandstone), three roof bolts 3 m apart are installed in the roadway. The outermost roof bolts are installed at a distance not exceeding 1.5 m from the sidewall. When approaching an intersection, the distance between the edge of the intersection and the last line of roof bolts should not exceed 1 m. When a corner of the pillar has been broken away, an additional roof bolt is installed at a distance not exceeding 1.5 m from the broken corner. Supports are installed right up to the face.
- When the support system is said onboard, the Continuous Miner (CM) cuts and supports and a staggered roof bolt pattern is used.
- Special provisions are made in the Sasol code of practice for support of first split, temporary support, and support of slips and faults.
- In incompetent roof, four roof bolts 2 m apart are installed in the roadway. The last line of bolts is installed at a distance not exceeding 1.5 m. However, the spacing between bolts in the direction parallel to the roadway remains 3 m as in the competent roof and in case of breakaway of the pillar corner, similar disposition as in the case of competent roofs apply.
- Three lengths of bolt are currently used at the mine, 1.2; 1.5and 1.8 m. Bolts of 0.9 m are considered as illegal and are not in use any more.

Site observation

During the site visit at Brandspruit (Sasol) risks associated with high horizontal stress were observed. A conveyor belt section subjected to severe guttering was visited. Sites subjected to side wall ride and other high horizontal stress indicators such as planar tensile cracks and jagged roof cracks were visited. The side wall ride is characterised by a relative displacement of the roof with respect to the floor, the pillar then being inclined at an angle.

5.1.6 Analysis of data from Sasol

The Sasol complex is one of the South African coalfields experiencing significant stress related problems. The increase of stress observed in this coalfield is often associated with dolerite sill and dyke intrusions. Different methods of recognising risk associated with

horizontal stress have been established over the years at Sasol, and various ways to combat the deleterious effects of stress are recommended in the Sasol Code of Practice (COP).

An Underground visit at Brandspruit Colliery was carried out in order to observe the various hazards associated with high horizontal stress. During the time of the visit, the author benefited from strata control training aimed at showing how risks associated with high horizontal stress can be recognised and managed safely. The Sasol code of practice was provided to the author. Unfortunately, the policy of the company does not allow photographs to be taken underground.

At Sasol, risk associated with high horizontal stress effects is recognised using the following indicators:

- Guttering of the roof,
- Side wall ride,
- Jagged crack in the roof,
- Planar tensile cracks in the roof,
- Layer shift in drainholes, and
- Buckling of roofbolt plates

The presence and the severity of one or more of these indicators are reported in a special document (Sasol document 6). Routinely, the ground assessment is done by a Miner and it is up to him to decide whether the risk at hand can be contained under the current mining parameters or whether a new set of mining parameters is needed, or whether the area has to be barricaded off until further notice. The Shift boss assesses the report (document 6) put together by the miner and in some instances can make amendments. Afterwards, revisions may be made by the mine overseer and the managers and rock engineers (Sasol 1998).

At Sasol, areas close to dyke, goaf, rivers, faults and folding are classified as high risk or stressed areas and are subject to specific supports. While it is plausible that the dykes are synonymous with an increase of horizontal stress, the influence of a river or a goaf in the proximity of a panel being mined is less obvious and therefore has been investigated during

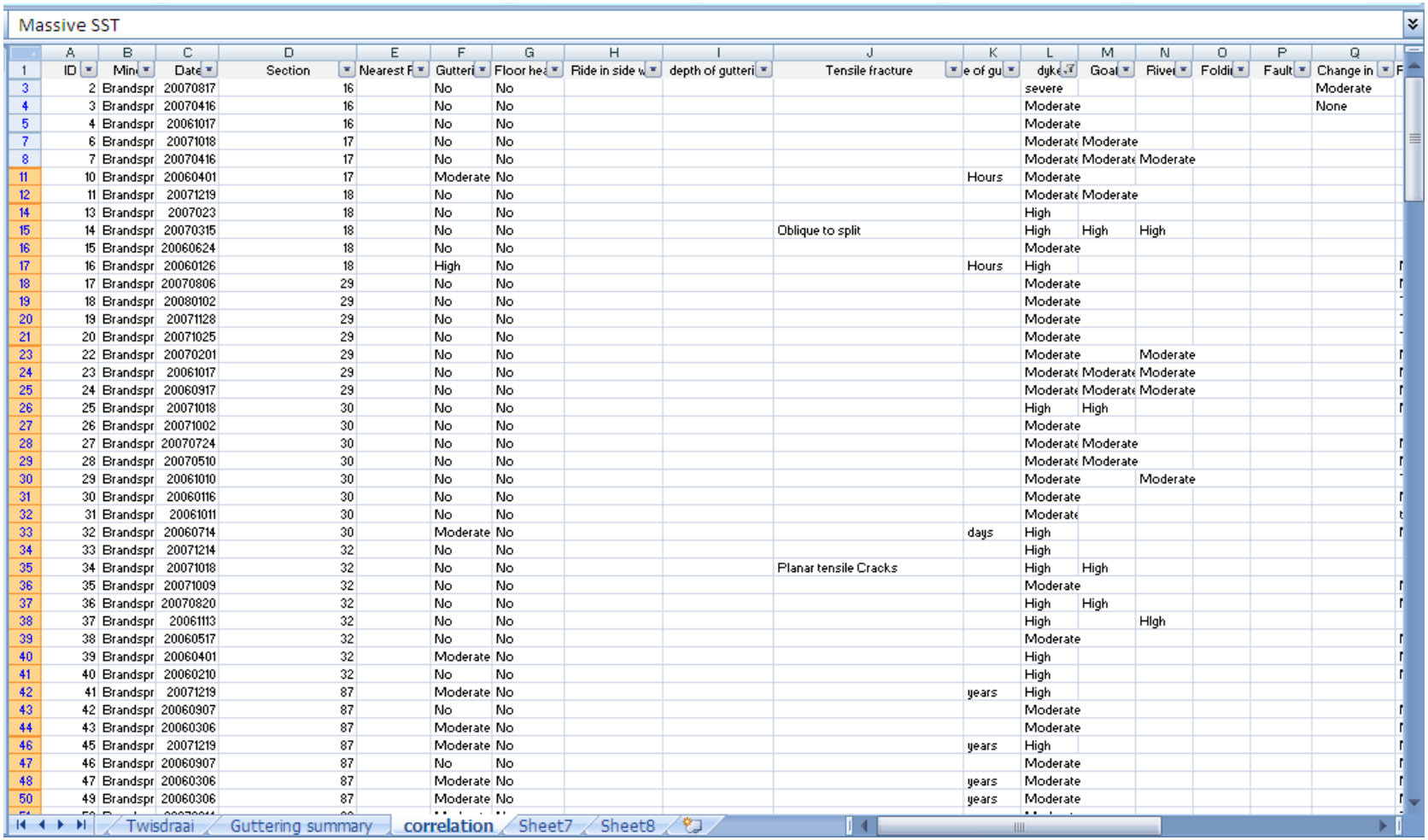
the current study. The time dependent behaviour of guttering within the coalfield is considered briefly.

The aim of such an analysis is to understand better the interaction between factors such as dykes, rivers, rock types, goaf and stress. As a result, more efficient ground control techniques can be implemented based on fact rather than perception.

Over the years, many document 6 reports have been filed at Sasol. Document 6 gives the condition of the ground with respect to dykes, rivers, goaf, faults, and also gives the stress associated effects in a particular section. In order to analyse the effects of these various factors, a spreadsheet database has been developed based on the document 6 reports. Wherever possible, the following fields were recorded:

- ID;
- Mine;
- Date (YYYYMMDD);
- Section;
- Nearest peg;
- Guttering (moderate, high, none);
- Floor heave (moderate, high, none);
- Side wall ride (moderate, high, none);
- Depth of guttering (m);
- Rate of guttering (hours, days, years);
- Tensile fracture (jagged cracks, planar tensile cracks);
- Dyke (multiple, single, none);
- Goaf (multiple, single, none);
- River (high, moderate, none);

- Fold (high, moderate, none);
- Faults (high, moderate, none);
- Roof composition (sandstone, mudstone, shale, mixed); and
- Comment.



Massive SST

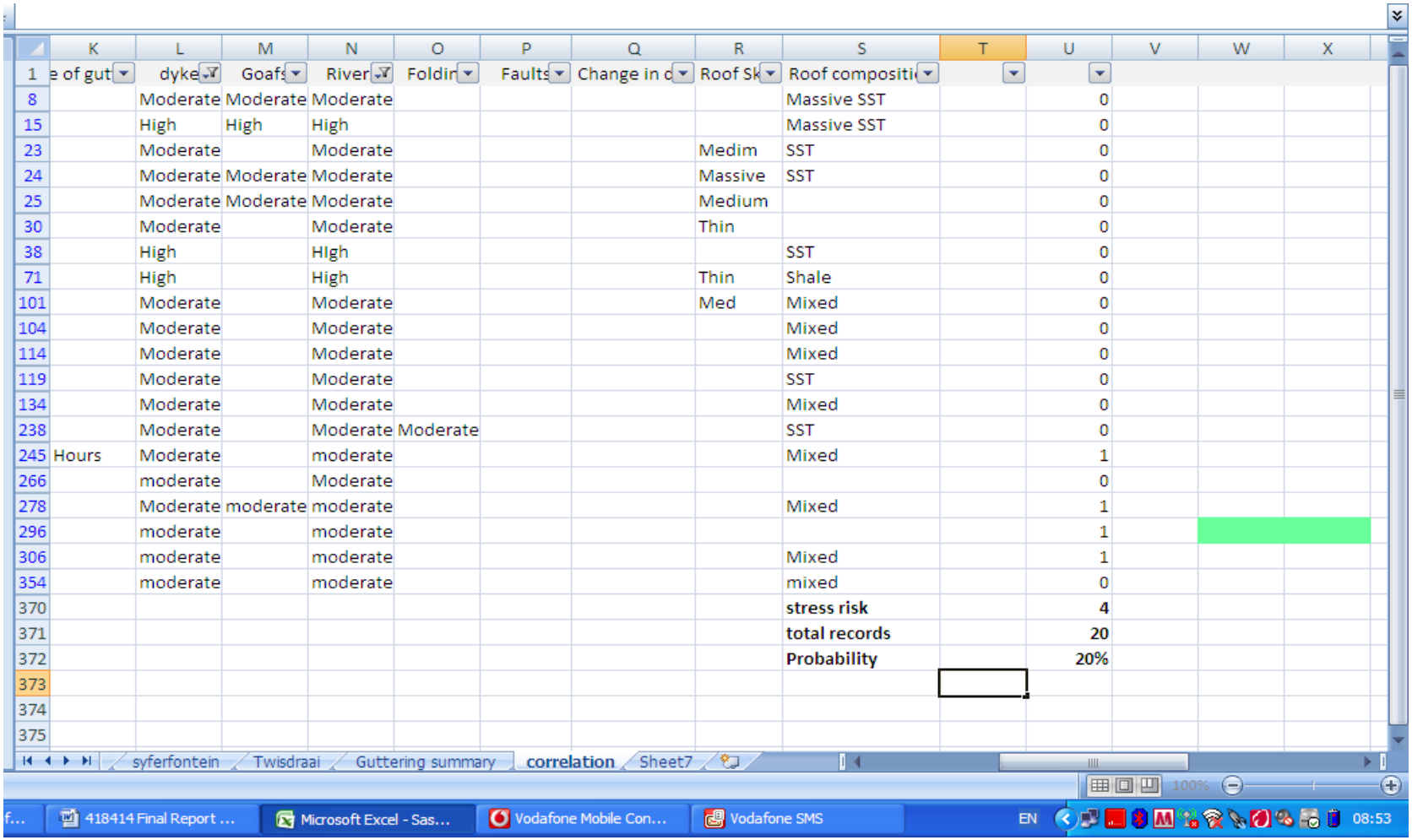
	A	B	C	D	E	F	G	H	I	J	K	L	M	N	O	P	Q
1	ID	Min	Date	Section	Nearest F	Gutteri	Floor hei	Ride in side w	depth of gutteri	Tensile fracture	e of gu	dyke	Goaf	River	Foldi	Fault	Change in
3	2	Brandspr	20070817	16		No	No					severe					Moderate
4	3	Brandspr	20070416	16		No	No					Moderate					None
5	4	Brandspr	20061017	16		No	No					Moderate					
7	6	Brandspr	20071018	17		No	No					Moderate	Moderate				
8	7	Brandspr	20070416	17		No	No					Moderate	Moderate	Moderate			
11	10	Brandspr	20060401	17		Moderate	No				Hours	Moderate					
12	11	Brandspr	20071219	18		No	No					Moderate	Moderate				
14	13	Brandspr	2007023	18		No	No					High					
15	14	Brandspr	20070315	18		No	No			Oblique to split		High	High	High			
16	15	Brandspr	20060624	18		No	No					Moderate					
17	16	Brandspr	20060126	18		High	No				Hours	High					
18	17	Brandspr	20070806	29		No	No					Moderate					
19	18	Brandspr	20080102	29		No	No					Moderate					
20	19	Brandspr	20071128	29		No	No					Moderate					
21	20	Brandspr	20071025	29		No	No					Moderate					
23	22	Brandspr	20070201	29		No	No					Moderate		Moderate			
24	23	Brandspr	20061017	29		No	No					Moderate	Moderate	Moderate			
25	24	Brandspr	20060917	29		No	No					Moderate	Moderate	Moderate			
26	25	Brandspr	20071018	30		No	No					High	High				
27	26	Brandspr	20071002	30		No	No					Moderate					
28	27	Brandspr	20070724	30		No	No					Moderate	Moderate				
29	28	Brandspr	20070510	30		No	No					Moderate	Moderate				
30	29	Brandspr	20061010	30		No	No					Moderate		Moderate			
31	30	Brandspr	20060116	30		No	No					Moderate					
32	31	Brandspr	20061011	30		No	No					Moderate					
33	32	Brandspr	20060714	30		Moderate	No				days	High					
34	33	Brandspr	20071214	32		No	No					High					
35	34	Brandspr	20071018	32		No	No			Planar tensile Cracks		High	High				
36	35	Brandspr	20071009	32		No	No					Moderate					
37	36	Brandspr	20070820	32		No	No					High	High				
38	37	Brandspr	20061113	32		No	No					High		HIgh			
39	38	Brandspr	20060517	32		No	No					Moderate					
40	39	Brandspr	20060401	32		Moderate	No					High					
41	40	Brandspr	20060210	32		No	No					High					
42	41	Brandspr	20071219	87		Moderate	No				years	High					
43	42	Brandspr	20060907	87		No	No					Moderate					
44	43	Brandspr	20060306	87		Moderate	No					Moderate					
46	45	Brandspr	20071219	87		Moderate	No				years	High					
47	46	Brandspr	20060907	87		No	No					Moderate					
48	47	Brandspr	20060306	87		Moderate	No				years	Moderate					
50	49	Brandspr	20060306	87		Moderate	No				years	Moderate					

Twisdraai | Guttering summary | correlation | Sheet7 | Sheet8

Figure 5-23 Microsoft excel database built based on document 6

The database comprises a total of 364 records coming from Brandspruit, Bosjesspruit, Twistdraai, Syferfontein and Middelbult.

Since information in the document 6 reports was provided in form of grades rather than numbers, qualitative analyses were conducted. In many instances, filters were used to produce summary tables, which in turn enabled the determination of various probabilities. Figure 5-24 gives an example of a table which was used to determine the probability of stress effects occurring next to a dyke and a river. The probability is the ratio of the number of occurrences of stress effects (side wall ride, guttering, planar tensile cracks...) to the total number of observations, expressed as percentage.



	K	L	M	N	O	P	Q	R	S	T	U	V	W	X
1	e of gut	dyke	Goafs	River	Foldir	Faults	Change in d	Roof Sk	Roof compositi					
8		Moderate	Moderate	Moderate					Massive SST		0			
15		High	High	High					Massive SST		0			
23		Moderate		Moderate				Medim	SST		0			
24		Moderate	Moderate	Moderate				Massive	SST		0			
25		Moderate	Moderate	Moderate				Medium			0			
30		Moderate		Moderate				Thin			0			
38		High		HIgh					SST		0			
71		High		High				Thin	Shale		0			
101		Moderate		Moderate				Med	Mixed		0			
104		Moderate		Moderate					Mixed		0			
114		Moderate		Moderate					Mixed		0			
119		Moderate		Moderate					SST		0			
134		Moderate		Moderate					Mixed		0			
238		Moderate		Moderate	Moderate				SST		0			
245	Hours	Moderate		moderate					Mixed		1			
266		moderate		Moderate							0			
278		Moderate	moderate	moderate					Mixed		1			
296		moderate		moderate							1			
306		moderate		moderate					Mixed		1			
354		moderate		moderate					mixed		0			
370									**stress risk**		**4**			
371									**total records**		**20**			
372									**Probability**		**20%**			
373														
374														
375														

Figure 5-24 Filtered table constructed in order to determine the probability of stress effects when dyke and river are both present

Further to this analysis, it was found that the combined number of guttering and floor heave occurrences was highest at Brandspruit (24 occurences) and lowest at Bosjesspruit (12 occurences). In addition, it was found that the number of observations from Bosjesspruit and Brandspruit were almost equal (74 and 77 records) whereas the highest number of observations comes from Twistdraai (93 observations). Syferfontein and Middelbult have respectively the first and second lowest number of observations (Figure 5-25). The guttering trend can be partially explained by the observation that the percentage of competent Sandstone in the roof is highest at Bosjesspruit (about 59%) and lowest at Brandspruit (about 39%).

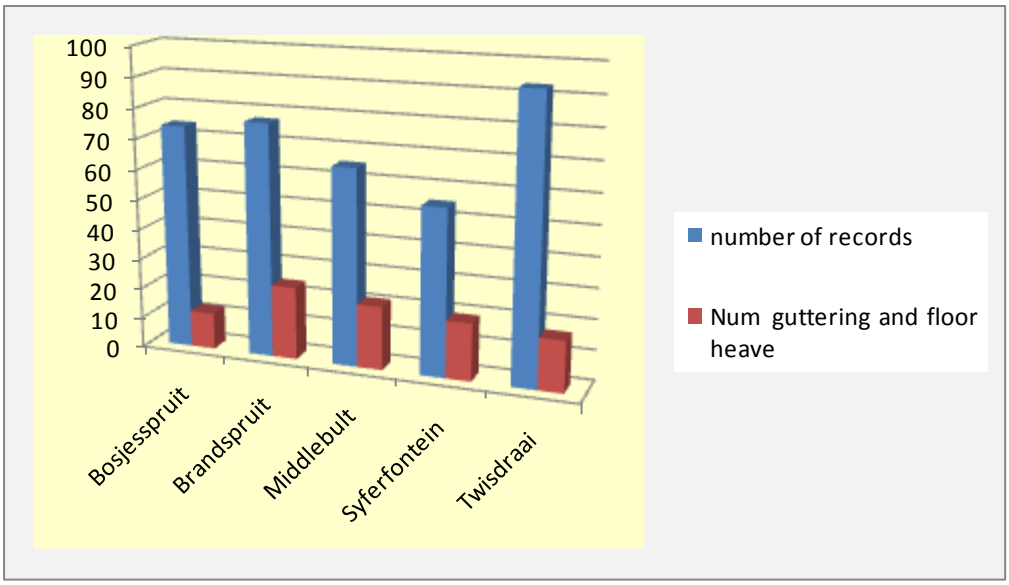


Figure 5-25 number of observations and number of guttering and floor heave per mine

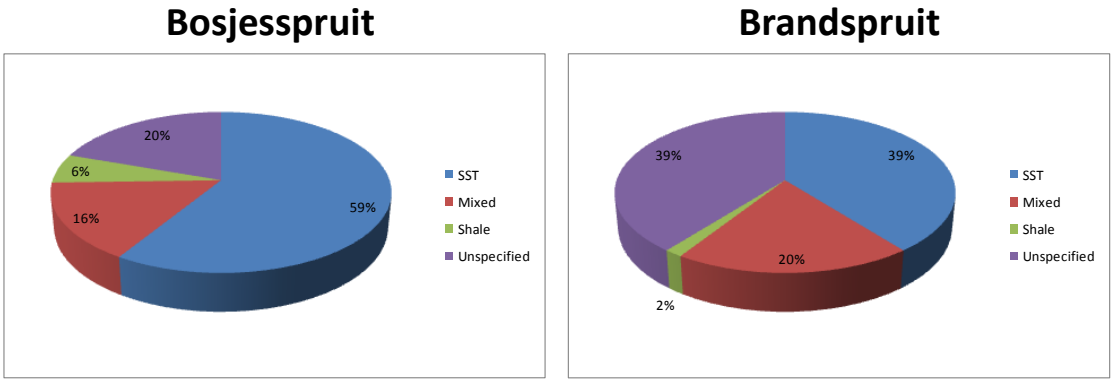


Figure 5-26 Roof composition derived from the database at Bosjesspruit (left) and Brandspruit (right)

The probabilies of occurrence of guttering and floor heave have been calculated and assigned to each mine. This probability is merely the ratio, as a percentage, of the combined numbers of guttering and floor heave to the total number of observations recorded at this particular mine. As summarised in Figure 5-27, Syferfontein, Middelbult and Brandspruit have the highest frequency of guttering and floor heave, but less likely at Bosjesspruit and Twistdraai.

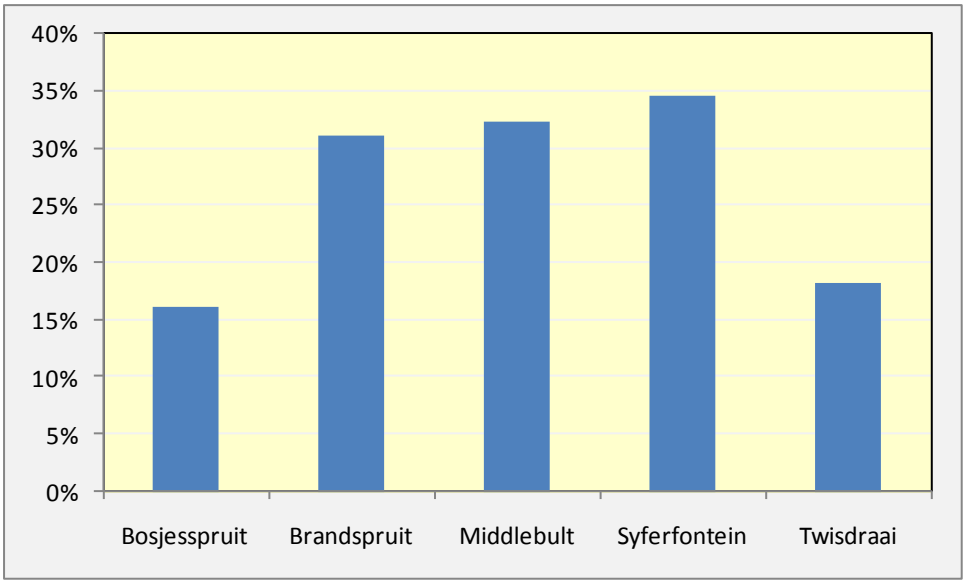


Figure 5-27 Probability of occurrence of guttering and floor heave per mine

By considering all the stress related effects combined (side wall ride, guttering, tension cracks, floor heave), a likelihood of 43% occurrence of these effects was found. An attempt to combine instances with mixed, shale and mudstone roof yielded a likelihood of stress effects of about 40% while a similar analysis, focused on shale and mudstone roof cases, yielded a probability of stress effects of 53%. From this analysis, it is clear that occurrence of stress damage has to do with roof composition; however, more observations are required to determine whether the 10% increase from 43% to 53% is significant noting that the number of observations decreased from 365 to only 17.

Similar analyses have shown that the probability of experiencing one of the stress related problems when mining next to a dyke is about 39% from 274 observations. This probability increase to 40% when the dyke is coupled to a goaf, however, the number of observations decreases to 48. Based on this analysis it cannot be concluded that mining in the vicinity of a goaf necessarily implies an increase of stress problems because one can be mining in the shadow of the goaf as well. Therefore it is recommended that, in the future, document 6

reports include the information as to whether mining is being carried out in the shadow, or abutment stress, of the goaf.

Unexpectedly, the analysis of instances when dyke and a river are both present has shown a significant decrease in the probability to 19% for a total of 21 observations. From this analysis alone it is not clear whether the proximity to a river really induced more stress. However, since the number of occurrences seems low it is recommended that similar analysis be conducted again when more data become available. In addition, it was found that in many instances the distance between the river and the actual panel being assessed was not provided. It is expected that there is a distance limit beyond which this effect is no longer felt.

It was considered important to analyse stress related effects with respect to various roof types (Sandstone, Mixed, shale). As shown in Figure 5-28, and as one could expect, the probability of stress problems increases by about 2% from a Sandstone roof to a mixed roof and further increases by about 18% from a mixed to a shale (mudstone) roof.

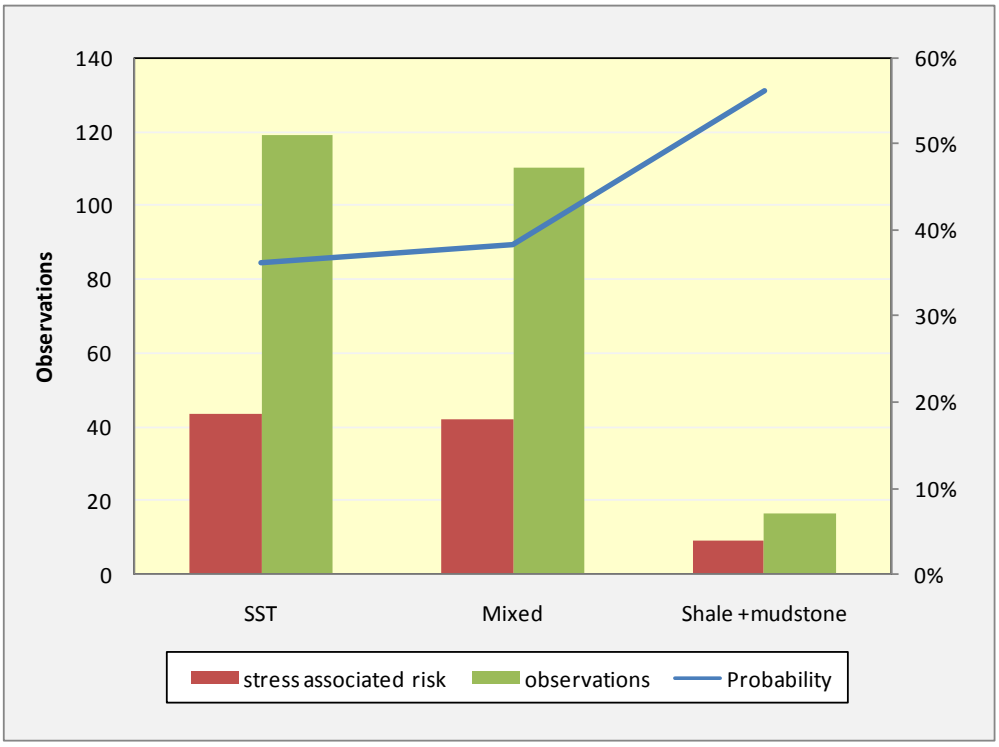


Figure 5-28 graph illustrating number of observations, number of stress related problems and their probability of occurrence per roof type

The actual structure of document 6 reports enables the rate of guttering to be recorded. The rate of guttering is given in hours, days or years. Wherever this information was available, it was recorded in the database. Therefore, it was possible to investigate the time dependent behaviour of guttering in the complex. This analysis was confined to a simple investigation of the time dependent behaviour of guttering as a function of rock type.

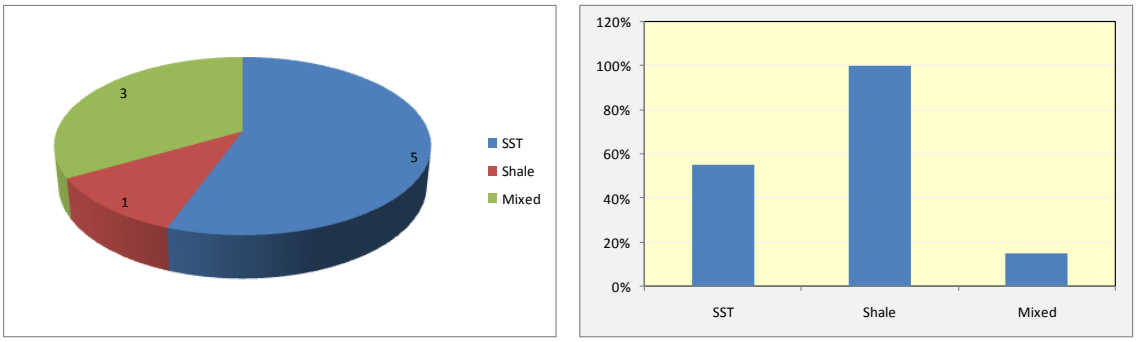


Figure 5-29 Pie chart showing the number of occurrences that have failed within hours per roof type (left) and graph of probability of failure (right)

It can be seen in Figure 5-29 that although more occurrences of guttering that have failed within hours were recorded in a Sandstone roof, the probability of failure is much higher in a shale roof.

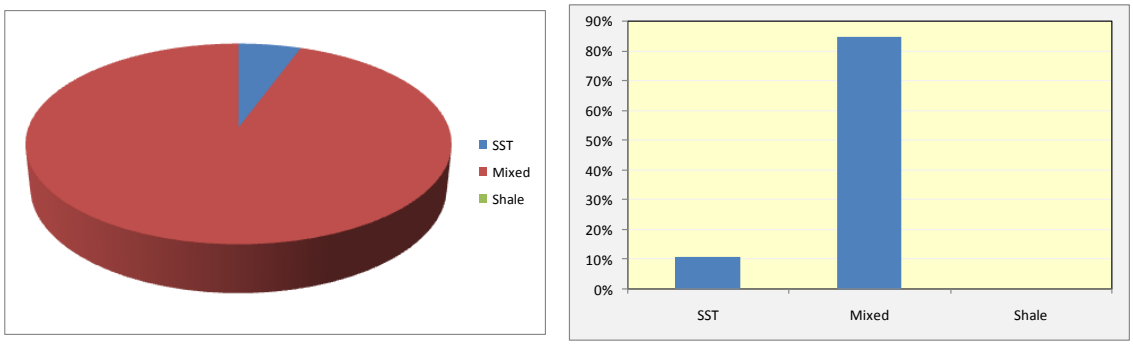


Figure 5-30 Pie chart showing the number of occurrences that have failed within days per roof type (left) and graph of probability of failure (right)

It was observed that the bulk of failure in a mixed roof (competent + weak) occur within days at a probability of more than 85% (Figure 5-30). The probability of failure of shale roof is indicated as zero merely because there was no instance of shale roof in the analysis.

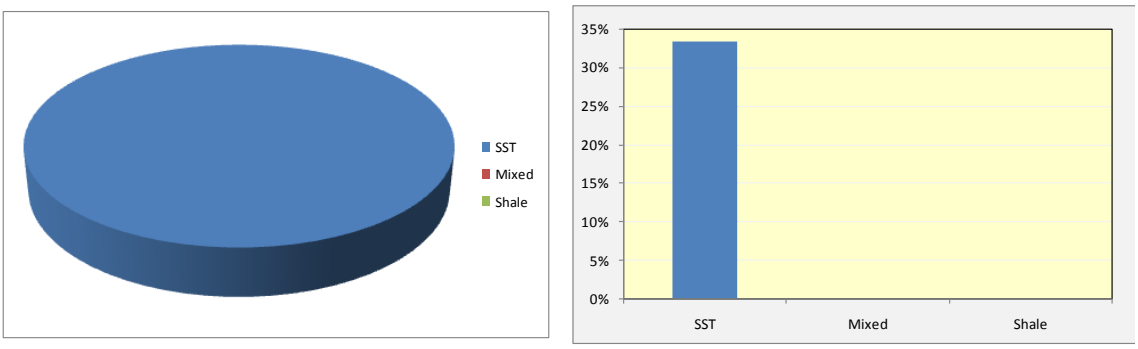


Figure 5-31 Pie chart showing the number of occurrence that have failed within years per roof type (left) and graph of probability of failure (right)

As illustrated in Figure 5-31, all the cases of guttering where failure has occurred within years was found to be in a sandstone roof. Expectedly, these observations are consistent with the strength of the roof: weak roof (shale and mudstone) falls within hours of exposure by mining, mixed roofs (more competent) resist longer and only fail within days, and sandstone roofs (very competent) take years of weathering and time dependent deterioration before failure initiates.

5.1.7 Stress Observation at Coal of Africa (Mooiplaats)

Location

The site visit was undertaken at Mooiplaats located at about 1.7 km from the recently re-commissioned Camden Power Station in the Ermelo Coalfield in the Province of Mpumalanga. Figure 5-32 shows the regional location of the Mooiplaats Colliery.

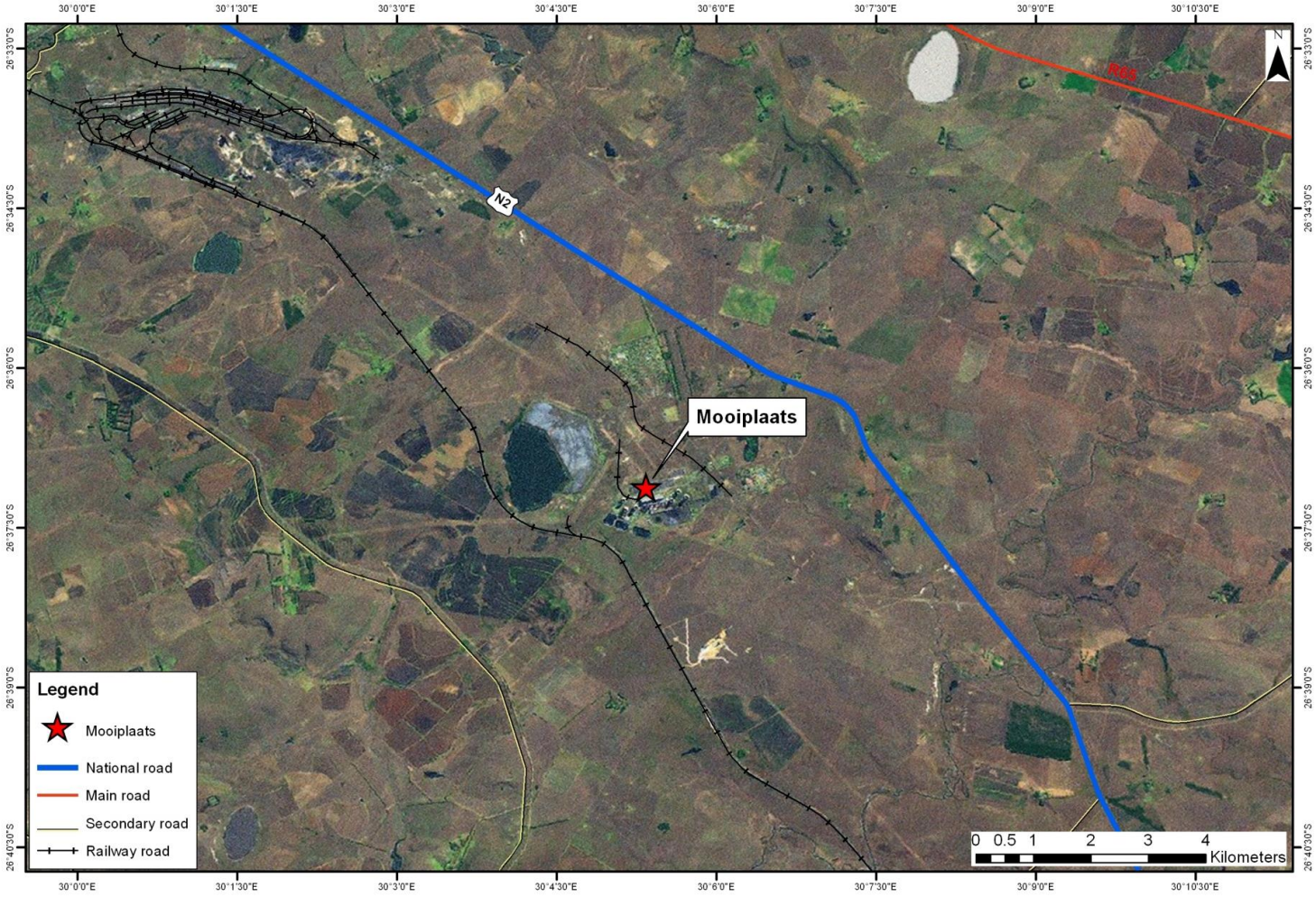


Figure 5-32 Regional location of Mooiplaats Colliery

Stratigraphy

Figure 5-33 shows a typical stratigraphic column of Ermelo coalfield and Mooiplaats Colliery.

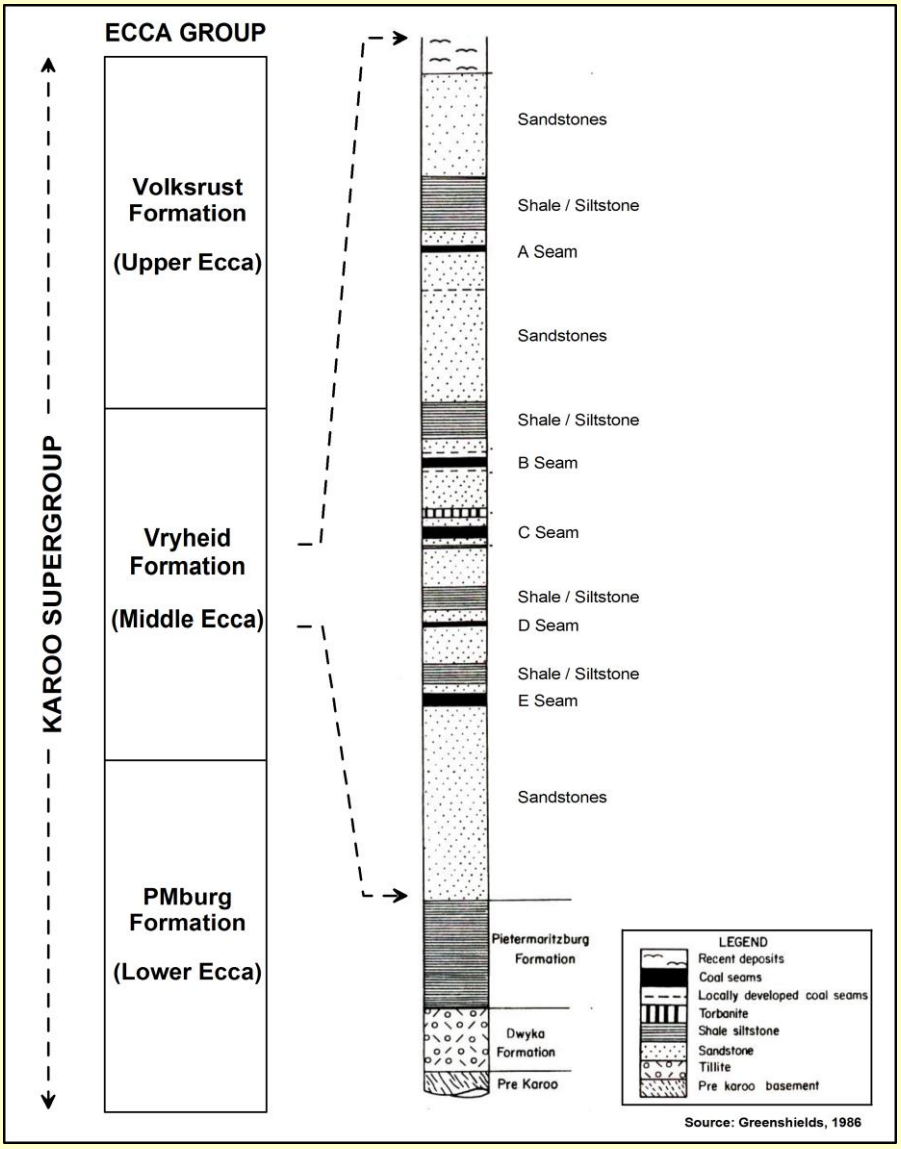


Figure 5-33 Typical stratigraphic Column of Ermelo coalfield and Mooitplaats Colliery (after Greenshields, 1986)

Mine plans

Figure 5-34 shows the layout of Mooiplaats shaft at the time of the visit. It can be seen that three directions of mining prevail, NW-SE, NNE-SSW, NNE-SSW. In addition to this, the

figure shows the NNW presumed orientation of the major horizontal stress as measured in the Witbank and Highveld Coalfields.

It is important to note that mining at this shaft is conducted using the bord and pillar mining while the cutting of the coal is performed by a Continuous Miner (CM).

Figure 5-35 shows the layout of the shaft including occurrences of guttering mapped during the site visit.

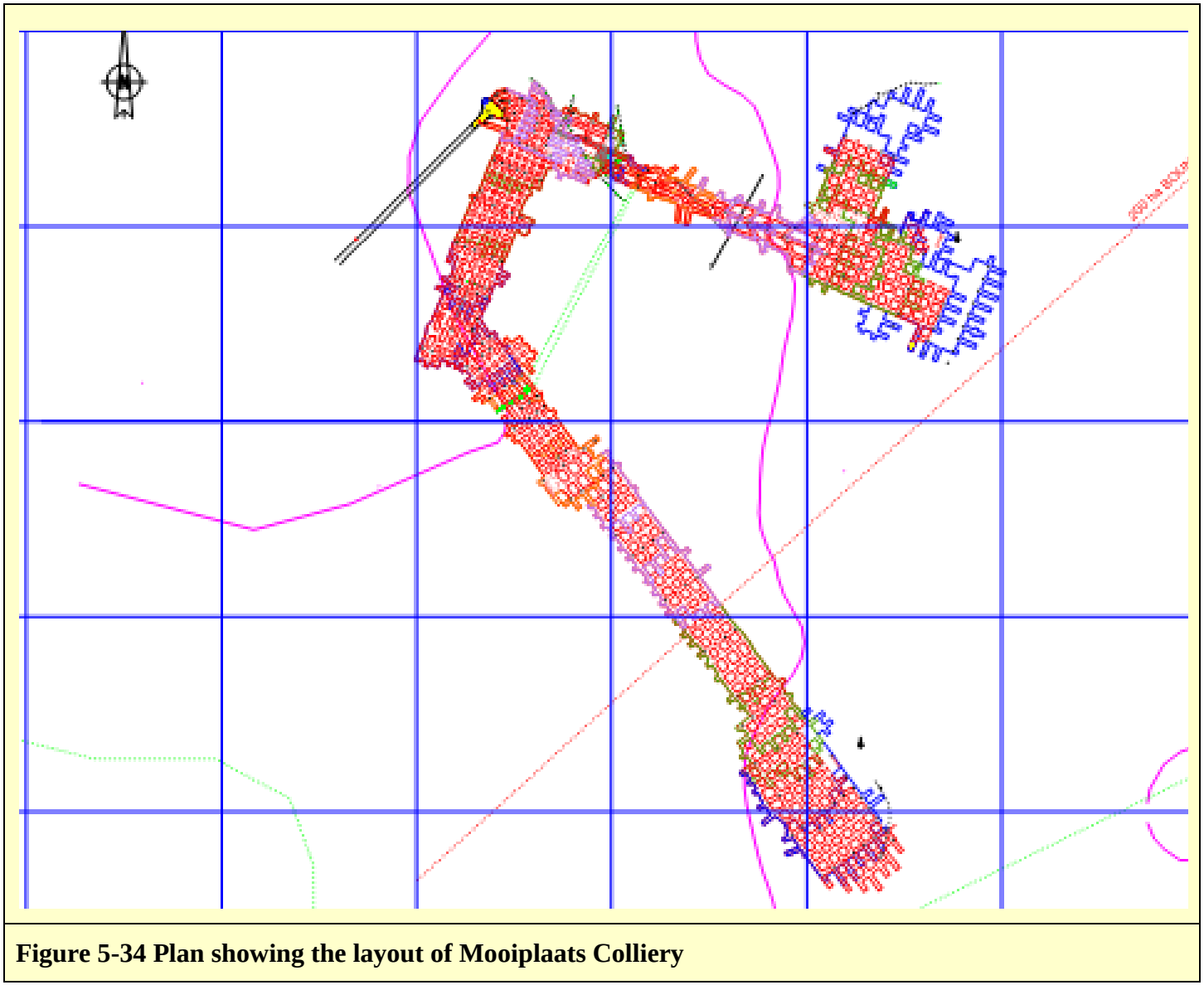


Figure 5-34 Plan showing the layout of Mooiplaats Colliery

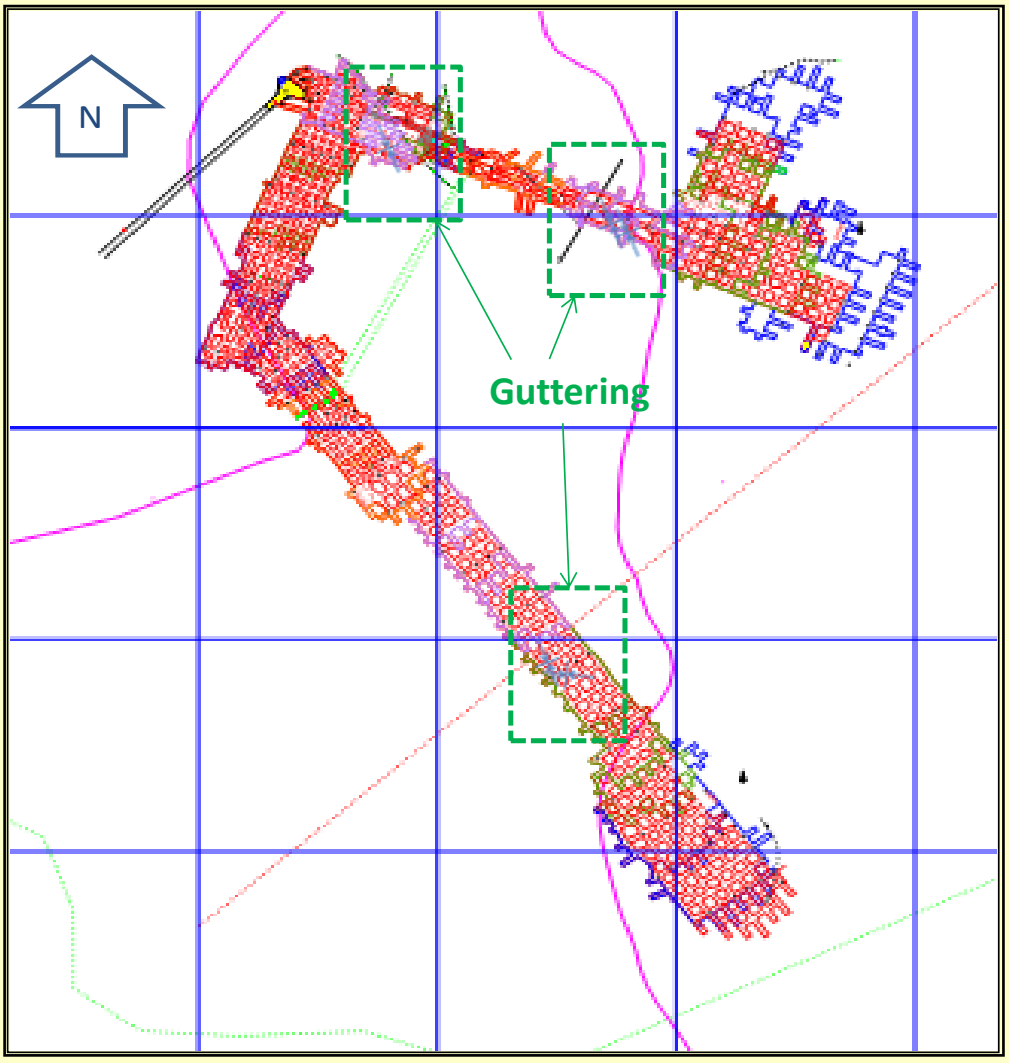


Figure 5-35 Mine Layout of Mooiplaats colliery showing guttering occurrences

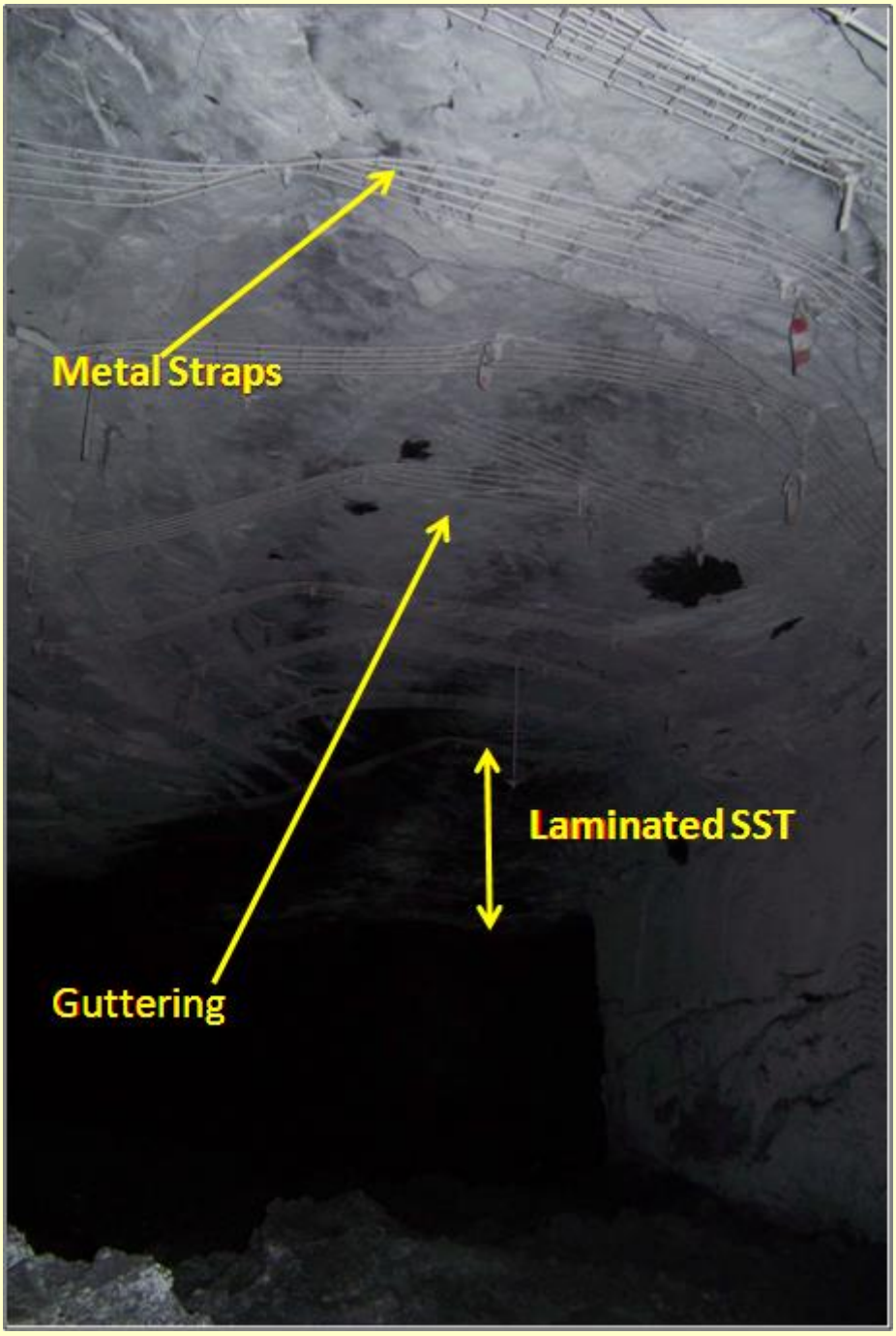


Figure 5-36 Guttering in a laminated Sandstone roof supported by a tandem roof bolt and metal straps at Mooiplaats



Figure 5-37 Picture showing the tip of guttering in a laminated Sandstone roof which is being re-supported by straps and roof bolts



Figure 5-38 Picture illustrating the used of cable anchor in addition to roof bolts and metal straps

During the site visit at Mooitplaats, it was observed that guttering was occurring in a Laminated Sandstone sequence. The support strategy to re-support the damaged roof consists of roof bolts and metal straps (Figure 5-36), and occasional cable anchors (Figure 5-38). It is probable that in this latter case, the roof bolts are used to create a beam whereas the suspension function into the competent roof is fulfilled by the cable anchors.

5.1.8 Stress Observation at Khutala Colliery (BHP Billiton)

Location

The site visit was undertaken at Khutala colliery which is located about 35 Km south east of Witbank, Ogies District, Mpumalanga Province in South Africa. The regional location of Khutala is given in Figure 5-39.

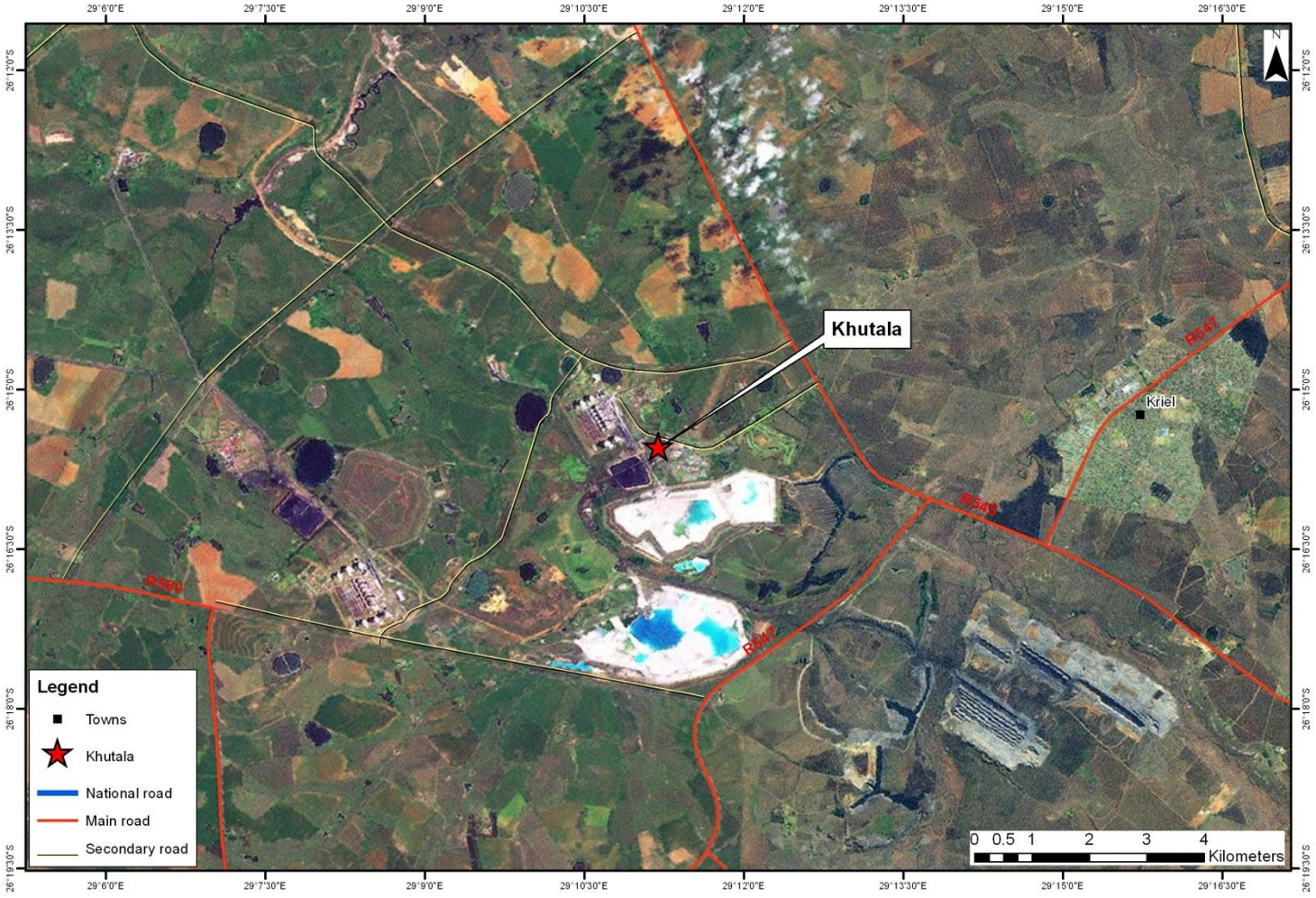


Figure 5-39 Regional location of Khutala colliery

Site Observation

Khutala Colliery is a good example of multiseam mining where No 2 and No 4 seams are simultaneously mined and where the 10 m thick parting requires superimposition of pillars.The site visit was confined to the No 2 seam where the roof was observed to be in relatively good condition, without signs of high horizontal stress, and where structurally controlled failure was the dominant roof failure mechanism. It appeared as if high horizontal stress between the seams was enhancing the shear resistance along discontinuities and hence the stability of the roof. It can be speculated that slip along joints occurs when the horizontal stress relaxes. Besides structurally controlled failure, some forms of instability were recorded in the sidewalls and pillar corners.

5.1.9 Stress Observation at Boschmans Colliery (Xstrata Coal)

Location

Boschmans shaft is located about 30 km southeast of Witbank in the Ogies district, in the province of Mpumalanga, South Africa. The regional location of the shaft is given in Figure 5-40.

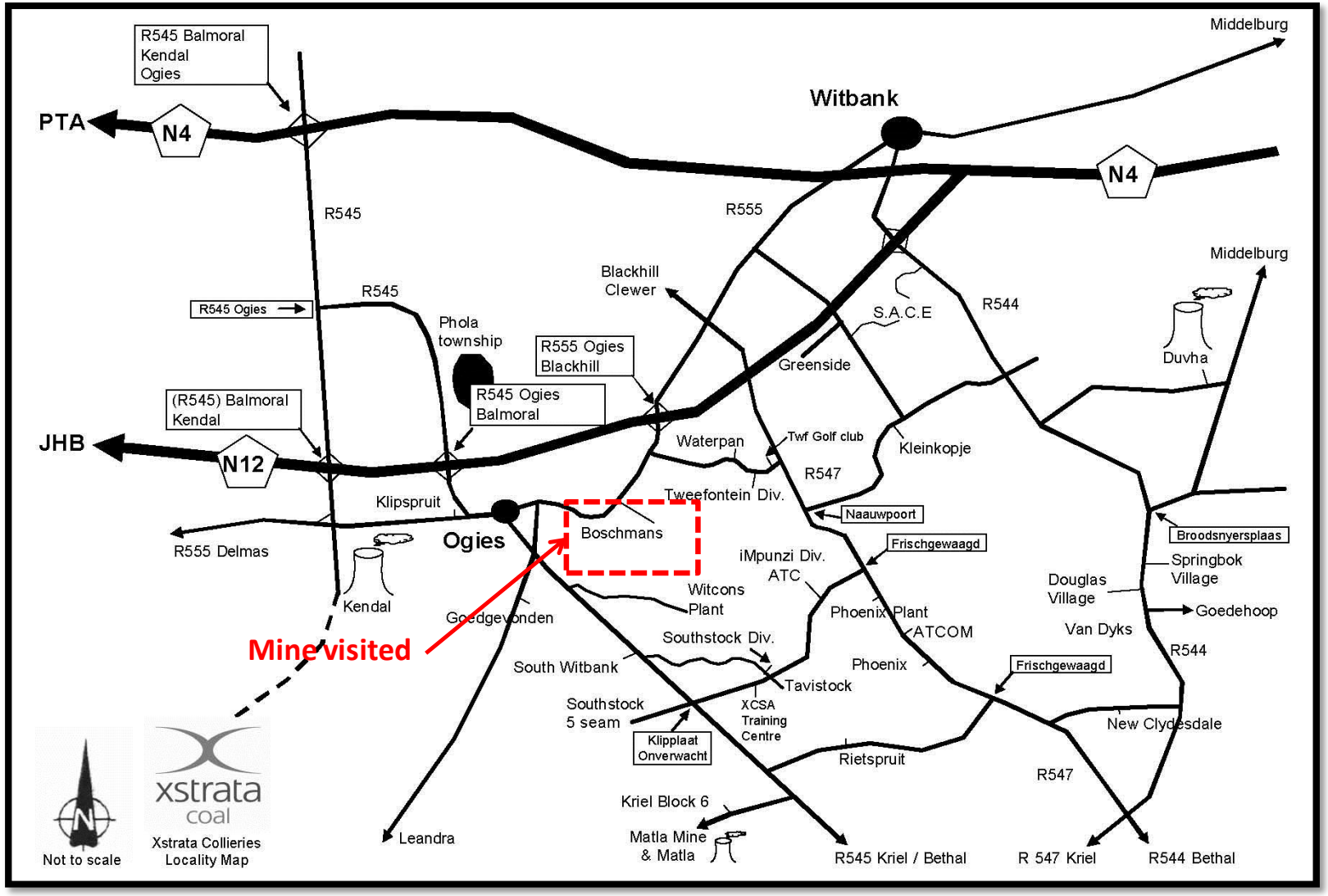


Figure 5-40 Regional location Boschmans Colliery

Site Observation

The area visited was in the vicinity of a dyke. The mine practices undercutting whereby 0.5 m of coal is left in the roof and therefore there was no sign of stress in the roof in spite of the presence of the dyke. Figure 5-41 and Figure 5-42 show the dyke and the way it is being supported by W-straps and roof bolts. The inherent risk associated with the dyke was enhanced by hydrostatic pressure as indicated in Figure 5-43 by presence of dripping water.



Figure 5-41 Picture of a dyke and the way it is being supported by W-straps and roof bolts at Boshmans shaft (X-Strata Coal)



Figure 5-42 Picture of a coal face and the roof in the vicinity of a dyke at Boshmans Shaft (X-strata Coal)



Figure 5-43 Picture showing the dyke visited at Boshmans and the presence of dripping water in the roof (X-Strata Coal)

5.1.10 Stress observation at Forzando (Total SA)

Although a visit to Forzando Colliery (Total SA) was not conducted, the roof conditions were described during personal communication with Lees (2011), a rock engineer at the mine. No significant stress related damage has been observed, providing that the roof is a competent sandstone with a thin false roof of coal.

The ground support standard at the mine consists of a systematic support system composed of three 20 mm roof bolts, 0.9 m long and 2 m apart per roadway. No stress measurement has been conducted at Forzando.

5.2 Review of stress measurement data

5.2.1 Description of stress measurement data

Data from 20 stress measurements carried out in the Witbank and Highveld coalfields were collected:

- Arnot Colliery: 3
- Khutala Colliery: 4
- Bank Colliery: 2
- Nooitgedacht: 2
- Goedoehoop: 5
- Bosjesspruit: 1
- Kriel: 3

Figure 5-44 gives the number of measurements conducted per coal seam. It can be seen that the majority, 55%, of stress measurements were carried out in N° 2 Seam whereas 25% and 20% of tests were conducted in N° 4 and N° 5 Seam respectively.

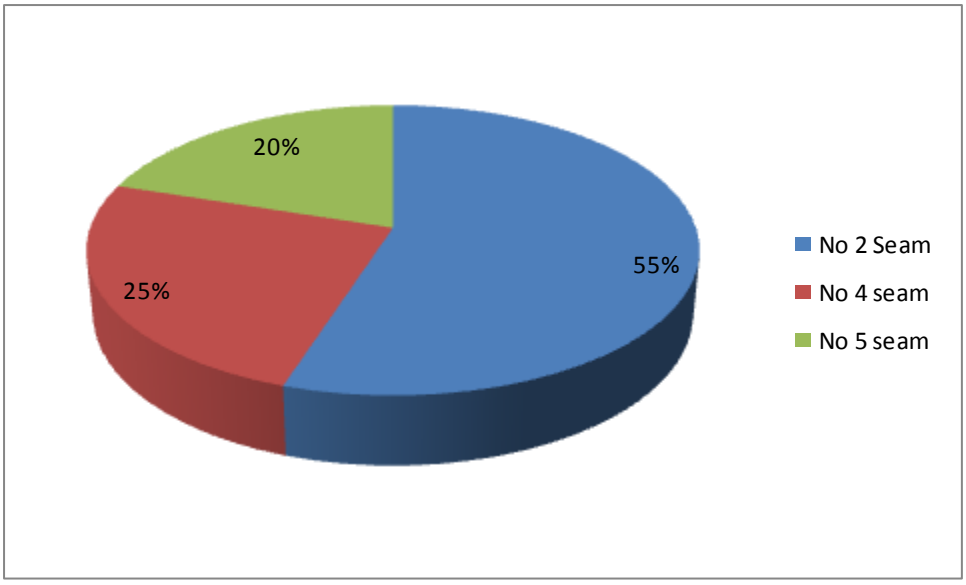


Figure 5-44 Pie showing the repartition of stress measurements by coal seam

Eighteen out of the twenty stress measurements were conducted by Rock Mechanics Technology (Pty) Ltd using the overcoring technique (CSIRO HI cells) and results presented in reports. The Rock Mechanics Technology (RMT) reports include the following:

A brief description of the site including the type of the rock in which the test is conducted along with the coal seam beneath it

A brief description of the test including the date when the pilot hole was drilled and cells were installed, as well as the date when overcoring was carried out, and the results which include the following:

- magnitude and orientation (dip and dip direction) of principal stresses
- magnitude and orientation of major and minor horizontal stress obtained after rotation of the principal stresses onto the horizontal plane
- strain versus time graphs,
- strain versus stress curves obtained from a biaxial compression test, and
- A summary of measured and computed strain for all the gauges as well as their differences

Apart from the Rock Mechanics Technology reports, results of an in situ stress measurement at Nooigedacht colliery was obtained from the literature (Minney and Munsamy, 2004).

In addition to this, underground mapping of guttering was also conducted at Arnot and Mooiplaats in order to infer the direction of horizontal principal stresses. Results of these underground mapping exercises are given along with results of the in situ stress measurements in Figure 5-45. The different colours on the map represent different mining companies within the coalfields. It is important to note the good correlation between measured orientation of horizontal stresses and orientations derived from underground mapping.

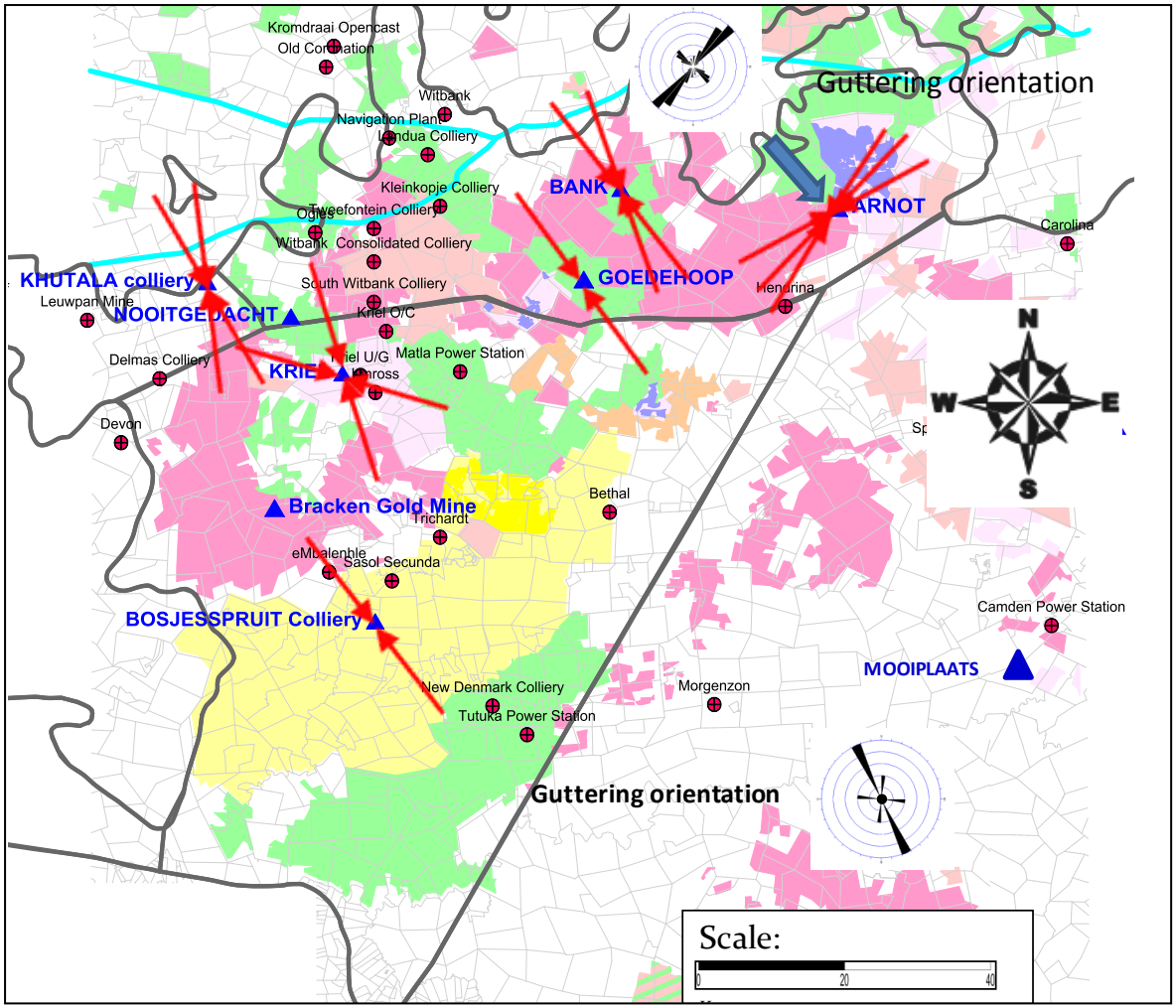


Figure 5-45 Plan showing orientation of major horizontal stress and results of mapping carried out at Arnot and Mooiplaats. Red arrows show the major horizontal stress and the rose diagrams give the results of the underground mapping.

The ratio of major horizontal to vertical stresses was plotted on the plan in Figure 5-46. Only maxima values of these parameters are reported here. It was found that the K-ratios (K1) across the coalfields are almost the same except for those at Khutala and Bank which are much lower. Expectedly, the lowest value of K-ratio was recorded at Bosjesspruit which is the deepest of the collieries where stress measurements were conducted.

The ratio of major to minor horizontal stress is of particular interest for layout design and is given in Figure 5-47. This ratio is a measure of anisotropy of in situ stress on the horizontal plane. As can be seen, this parameter is much more variable across the coalfields with the highest value recorded at Bank and the lowest values at Nooitgedacht (today Kenako) and Bosjesspruit.

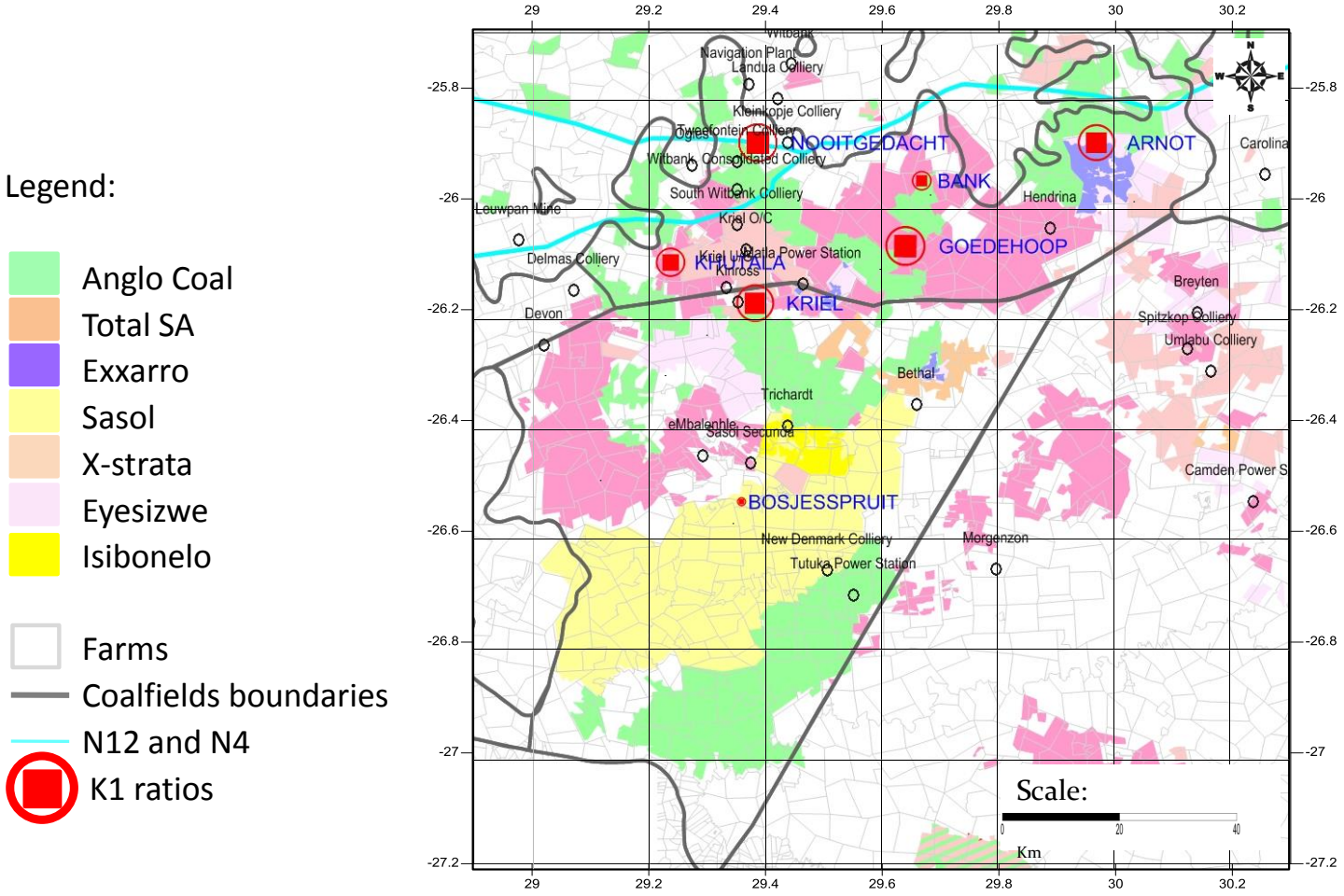


Figure 5-46 Map showing ratios of major horizontal stress to vertical stress (k1)

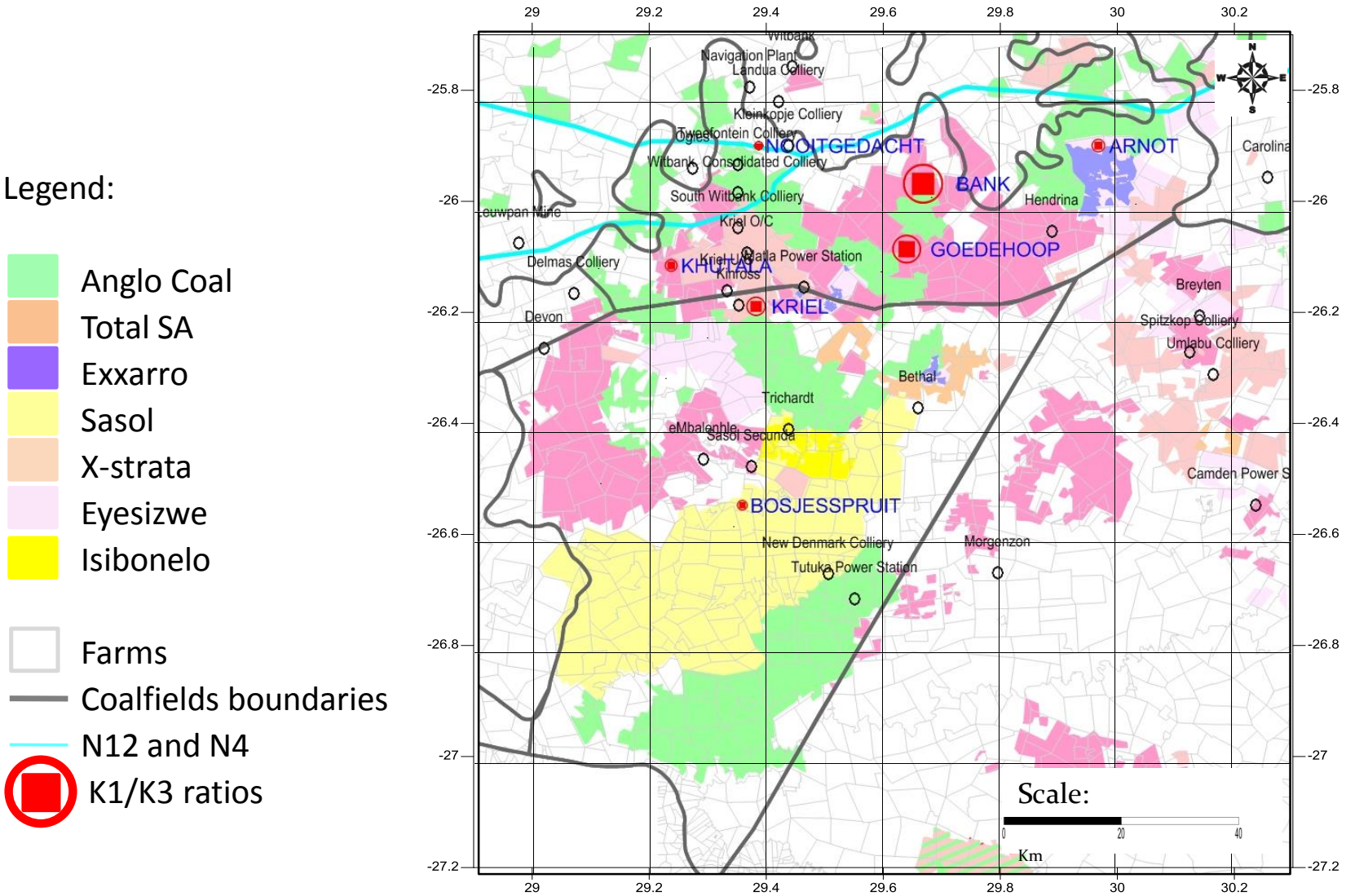


Figure 5-47 Map showing ratios of major to minor horizontal stress (K1/K3)

Table 5-13 summarises the coefficient of variation of k-ratios as a function of the number of tests carried out. The highest variability of k-ratios was recorded at Bank and significant variability has been also recorded at Kriel and Nooitgedacht. A much lower variability was recorded at Khutala and Goedehoop. Figure 5-48 shows the variability of k-ratios as a function of number of tests. Expectedly, a negative correlation between the coefficient of variation of k-ratios and the number of tests was found. Less variability was recorded for collieries (Khutala, Goedehoop) where a relatively high number of measurements was carried out. This relationship can be used to predict the number of in situ tests required to achieve a particular level of confidence.

Table 5-13 Summary of coefficient of variation of k-ratios per colliery

Colliery	CoV	Number of measurements
ARNOT	0.32	3
KHUTALA	0.19	4
BANK	0.77	2
GOEDEHOOP	0.15	5
KRIEL	0.73	3
BOSJESSPRUIT		1
NOOITGEDACHT	0.62	2

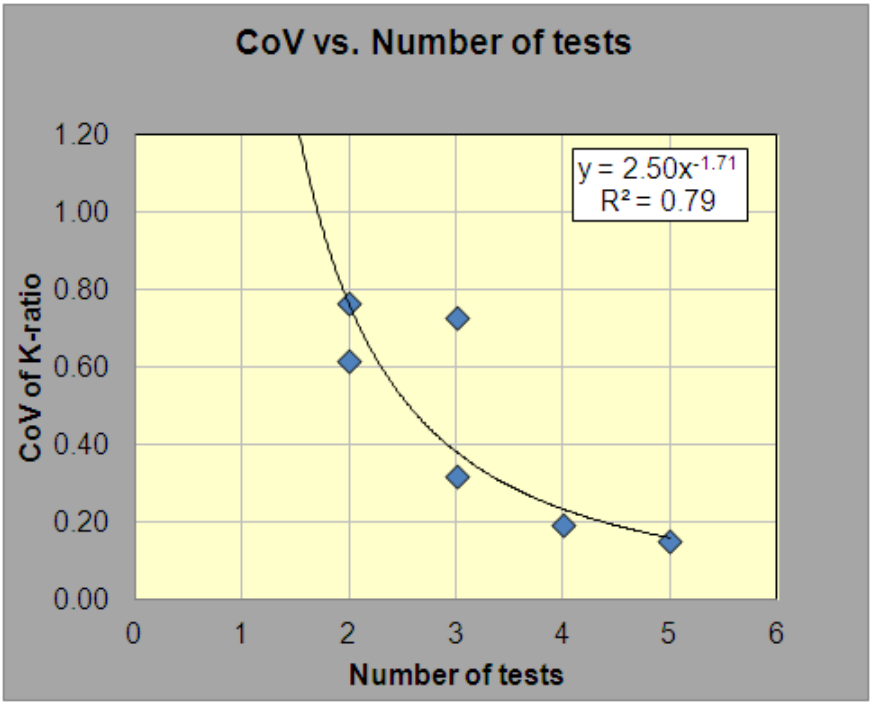
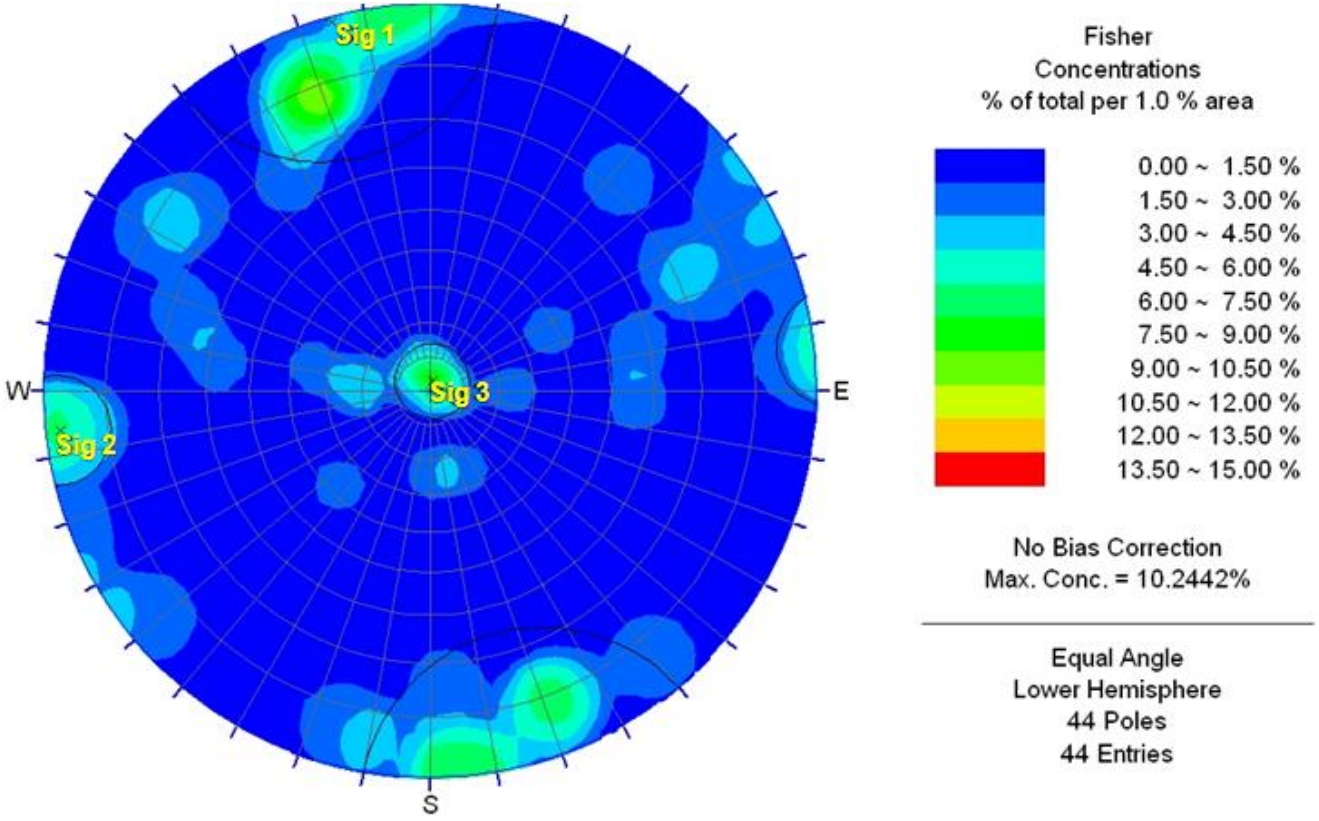


Figure 5-48 Graph illustrating variation of the major horizontal to vertical stresses ratios by collieries where in situ stress measurement were conducted

Figure 5-49 shows a stereonet representation of orientations of stress measurement data. It can be seen that three areas of high concentration (sets) have formed according to the three directions of principal stress. It is important to note that the set corresponding to the major principal stresses (Sig1) is much wider than the other two. The reason is that the database includes records for which only orientations of the major principal stress were known.

A summary of orientations in terms of trend and plunge and variability of the three stress measurement sets is given in the table below the stereonet. Further to this stereonet analysis it was found that one principal stress is orientated sub-vertically whereas the two others are sub-horizontal. The mean of major principal stresses was oriented approximately N17°W. 95.44% of major principal stress data (two times the standard deviation of the population) is within an arc of 25 degrees while 95.44% of minor and intermediate principal stresses are within arcs of 11 and 8 degrees respectively.



Principal stress	Trend	Plunge	Fisher K	Variability	Degree
σ_1	343	3	32	95.44%	25
σ_2	264	2	170	95.44%	8
σ_3	12	86	289	95.44%	11

Figure 5-49 Polar Stereonet illustrating direction of principal stress obtained from stress measurement data

When the number of data is less than 40 or 50, plot boxes are better than histograms to summarize data (Dohm 2010). In Figure 5-50, stress measurement data are summarized as a plot box after determining the median, the first and third quartiles, the maximum and the minimum orientations. Before this, orientations of azimuths less than 180 degrees were transformed by adding 180 degrees to the initial value. This transformation is justified by the fact that an orientation of X degrees is the same as one of X+180 degrees. The Plot box shows that the major horizontal stress directions are skewed toward high values and that 50% of the population is comprised within the arc from 315 to 353 degrees. The expected orientation (median) is about 338 degrees or oriented NNW.

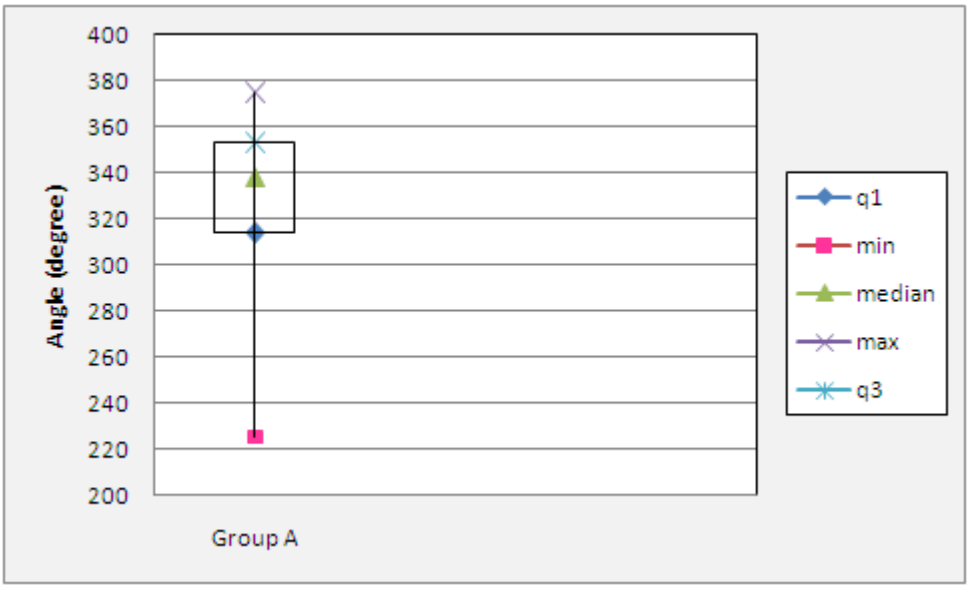
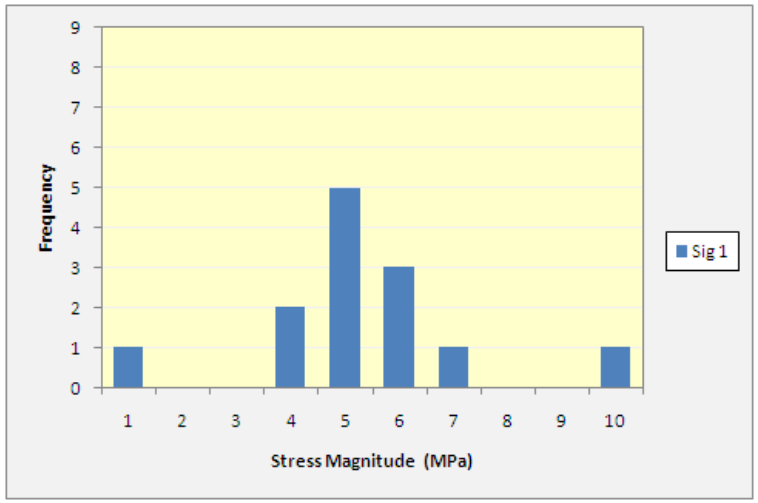
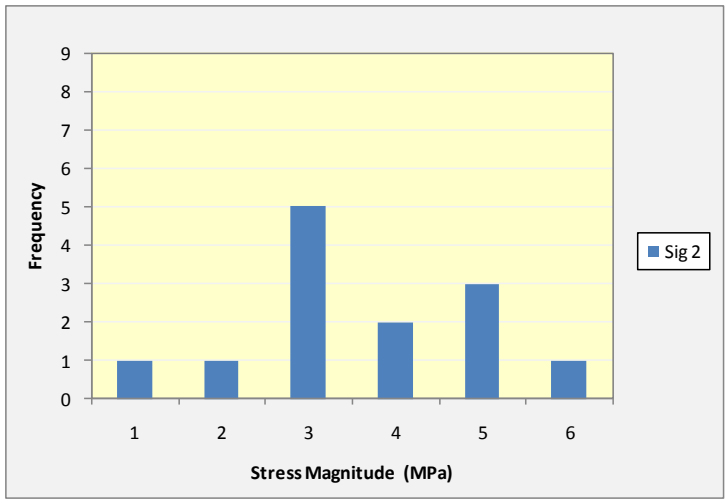
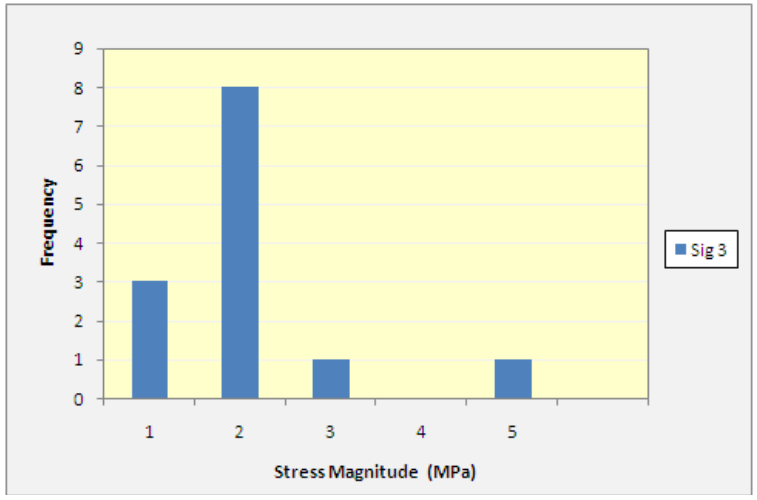


Figure 5-50 Plot box summarizing stress measurement data

Figure 5-51 is a summary of magnitudes of the three principal stresses. It is important to note that the means, medians and modes of the three principal stresses are very close to each other as in a normal distribution.







	σ1	σ2	σ3
Max	9.3	5.5	4.1
Min	1	0.7	0.2
Mean	5.0	3.2	1.4
Std	1.9	1.3	1.0
Median	4.8	3	1.3
Mode	5.7	3	1.3

Figure 5-51 Statistical summary of magnitude of principal stress obtained from stress measurement data

It is important to note that the NNW general orientation of maximum horizontal stress is different from the NE direction of movement of African plate (Andreoli, et al. 2007). However, the stress measurements at Arnot correspond with the NE direction of the movement of African plates. This observation is in line with observations made by other researchers who have examined stress measurements across southern Africa and found that the dataset of stress measurements could be subdivided into two regions, a northeast and a southwest region. In the northeast region maximum horizontal stress are mainly oriented NE, N and ENE such as in northern Botswana, Mozambique, Zambia, Zimbabwe and north-eastern South Africa. In the south western region the maximum horizontal stress axis is mainly oriented toward NW, NNW to WNW as observed in most of South Africa (Andreoli, et al. 1996; Viola, et al. 2005; Bird, et al. 2006). The northeastern region was found to be extensional with predominance of normal faulting, whereas the south western region was found to be compressive with a predominance of strike slip and thrust faults.

In the analyses carried out thus far, little attention has been paid to the depth at which in situ stress tests were conducted. Figure 5-52 illustrates variation of measured vertical stresses with respect to depth and compares this to the theoretical vertical stress calculated assuming an overburden density of 2500 MN/m^3. This analysis gives a way to assess the reliability of in situ stress measurements knowing that in most instances reliable tests will yield vertical stresses close to those generated by the weight of overburden.

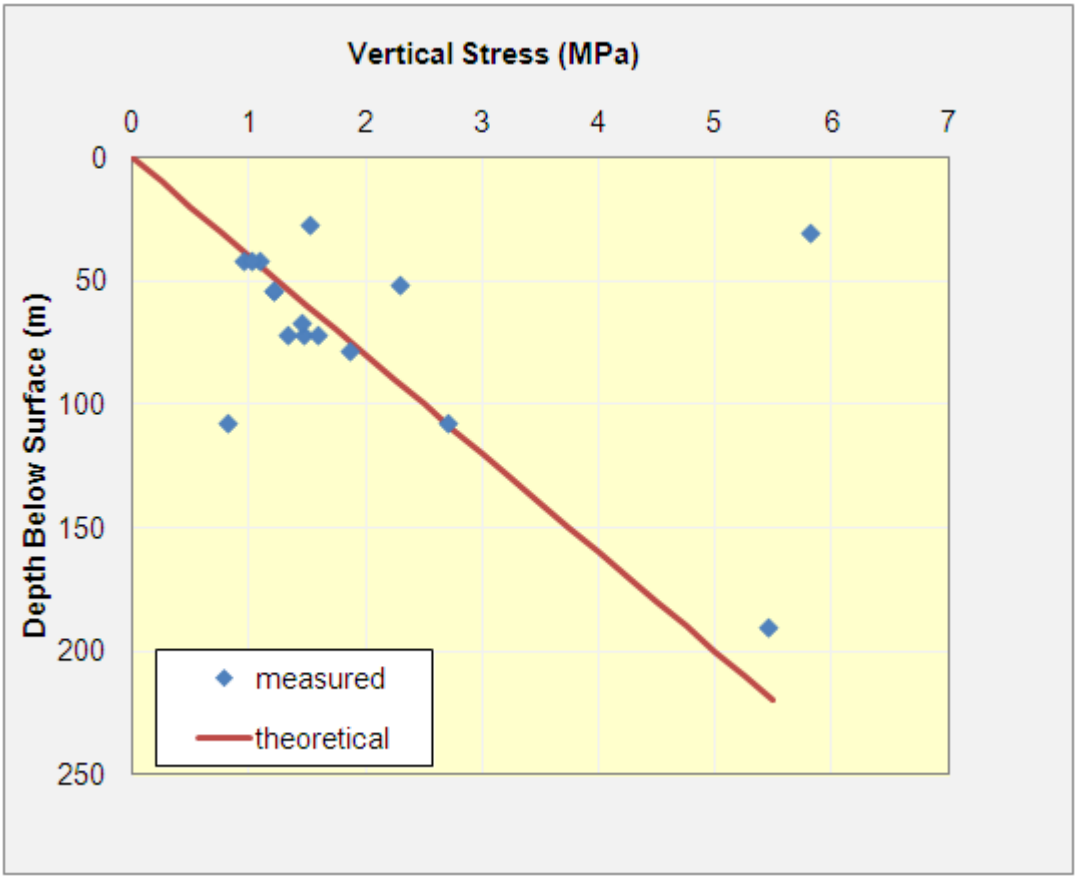


Figure 5-52 Comparison of near vertical stresses calculated from overburden density (2500 MN/m^3) and measured in situ

Amongst all in situ stress data, a measurement at Nooitgedacht was found to be significantly higher than the calculated vertical stress, while on the other hand, at Kriel a measurement was found to be much lower than the anticipated vertical stress.

5.2.2 Validation and subjective quantitative grading of stress measurement data

Data Validation

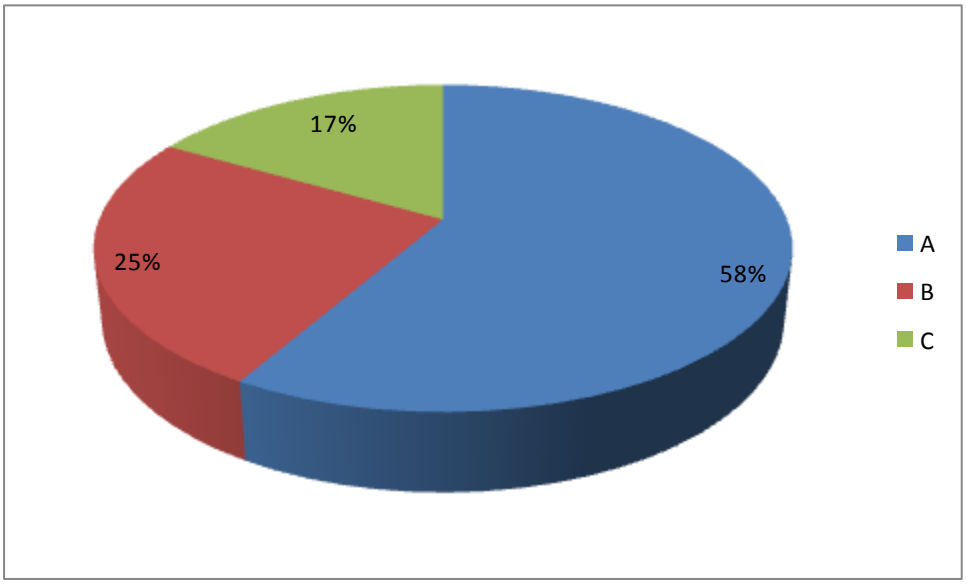
A useful way of validating the in situ stress data consists of plotting the vertical components versus depth and compares the results with the expected vertical stress given by the weight of the overburden. Figure 5-52 shows results of such a procedure applied on the set of in situ stress data of the Witbank and Highveld coalfields. The outliers obtained following this analysis were double checked to confirm whether the measurement could have been influence by the presence of mine workings or geological structures.

Subjective quantitative grading of in-situ stress data

For overcoring stress measurement it is possible to calculate standard deviations of all the components of the stress tensor (Stacey and Wesseloo 1998). For each measurement the maximum standard deviation of all components is used as grading parameter and a grade is assigned according to the grading system given in Table 5-14.

Table 5-14 Grading system for individual stress measurement after Stacey and Wesseloo (1998)

Grade	Grading Parameter
A	<20%
B	20%-30%
C	30%-40%
D	40%-50%
E	>50%



0

Figure 5-53 Repartition of stress measurement included in the data set according to grade

It was only possible to assign a grade to 12 stress measurement data out of twenty. Figure 5-53gives a repartition of the stress data set according to grade. It can be seen that 58% of data have graded A, 25% have graded B and the remainder 17% has graded C.

At collieries where two or more measurements have been conducted, it is possible to assign a group grade. In this regard the group grade is assigned according to the following:

Grade A

Physical measurements, such as overcore, rock slotter, hydrofacture etc, in which measurements were carried out in two or more boreholes beyond excavation influence, and the results of at least 80% of the measurements are in close agreement (normal components (Sx,Sy,Sz) generally within approximately 10% of the average) (Stacey and Wesseloo 1998).

Grade B

Physical measurements, such as overcore, rock slotter, hydrofacture etc, in which measurements were carried out in two or more boreholes beyond excavation influence, and the results of at least 50% of the measurements are in close agreement (normal components (Sx,Sy,Sz) generally within approximately 20% of the average), or where the measurements are of Grade A and have been conducted in a single borehole (Stacey and Wesseloo 1998).

Grade C

Physical measurements, such as overcore, rock slotter, hydrofacture etc, in which measurements were carried out in two or more boreholes beyond excavation influence, and the results of at least 50% of the measurements are in close agreement (normal components (Sx,Sy,Sz) generally within approximately 35% of the average), or where the measurements are of Grade B and have been conducted in a single borehole (Stacey and Wesseloo 1998).

Grade D

Physical measurements, such as overcore, rock slotter, hydrofacture etc, in which measurements were carried out in two or more boreholes beyond excavation influence, and the results indicate a trend in both orientation and magnitude (normal components (Sx,Sy,Sz) generally within approximately 50% of the average), or where the measurements are of Grade C and have been conducted in a single borehole (Stacey and Wesseloo 1998).

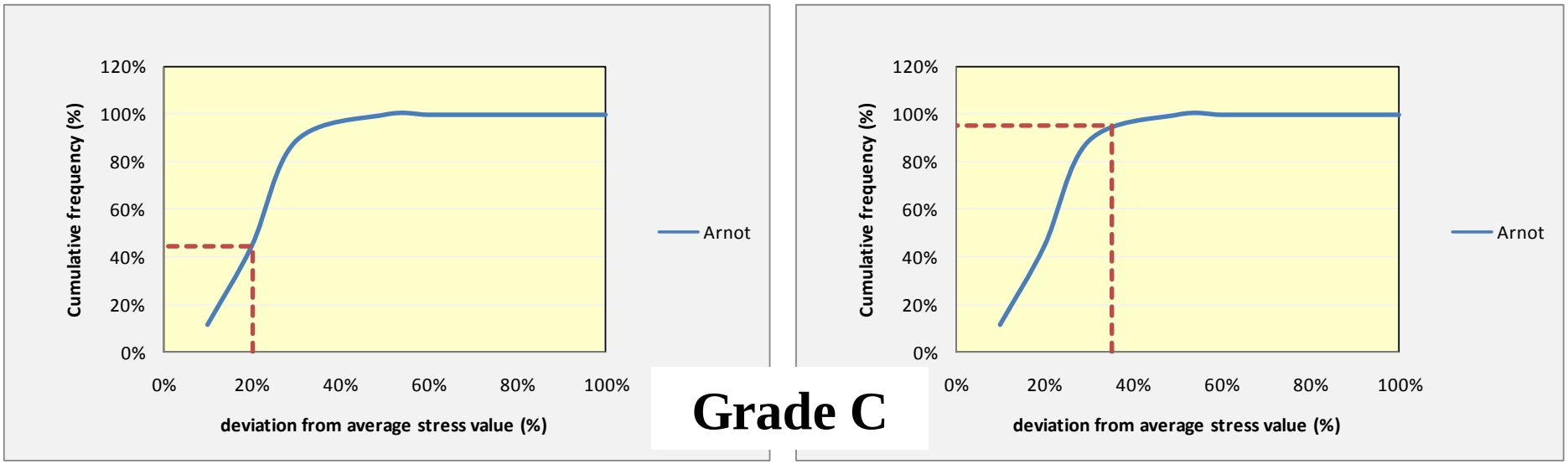
Grade E

Physical measurement, such as overcore, rock slotter, hydrofracture, etc, in which results are too variable to indicate trends in both stress and orientation components (Stacey and Wesseloo 1998).

In order to assign a grade to a group of measurements collected on a given colliery using the above mentioned group grading system, a graphical approach was used. This approach consists of the following:

At first, averages of normal components of stress are calculated for a given group of measurements. Based on averages, differences between averages and stress components are calculated as a percentage.

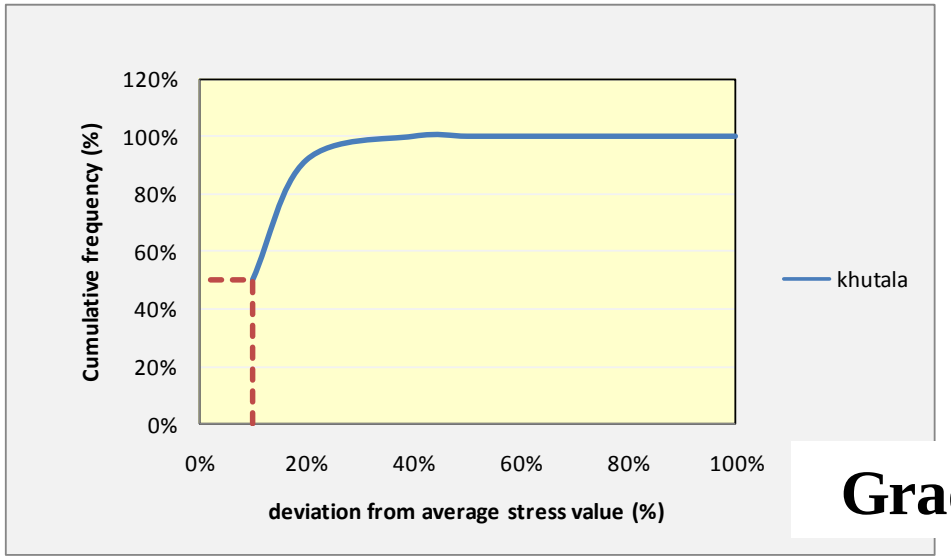
Differences below a certain threshold are counted and expressed as a percentage of the total number of all the differences. Figure 5-59 shows graphs of the cumulative frequency of stress components as a function of the deviation from average stress. The graphs enable the determination of the amount of stress components, as a percentage, which deviate from the average stress for a given percentage.



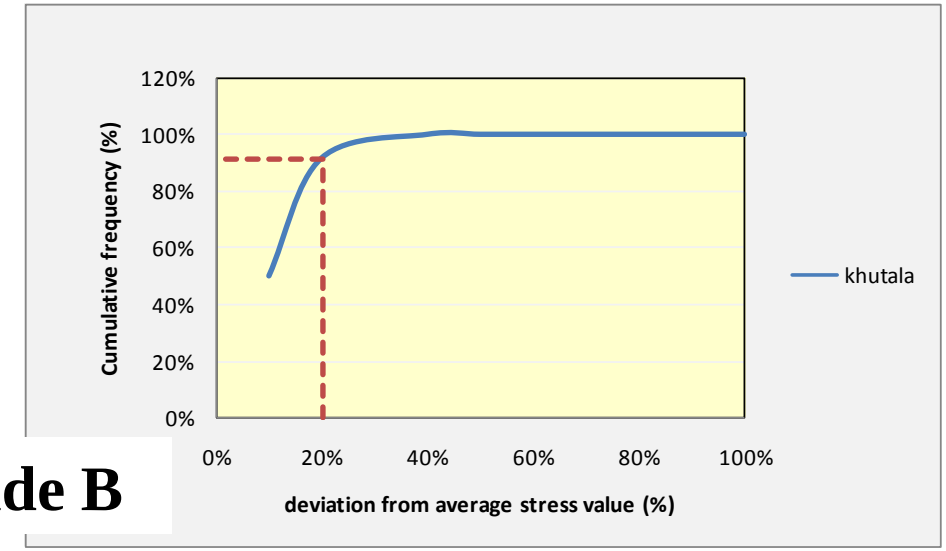
44% of stress components (Sx,Sy,Sz) deviate from average values for less than 20%

95% of stress components (Sx,Sy,Sz) deviate from average values for less than 35%

Figure 5-54 Cumulative frequency curves versus deviation from average stress (Grade C)



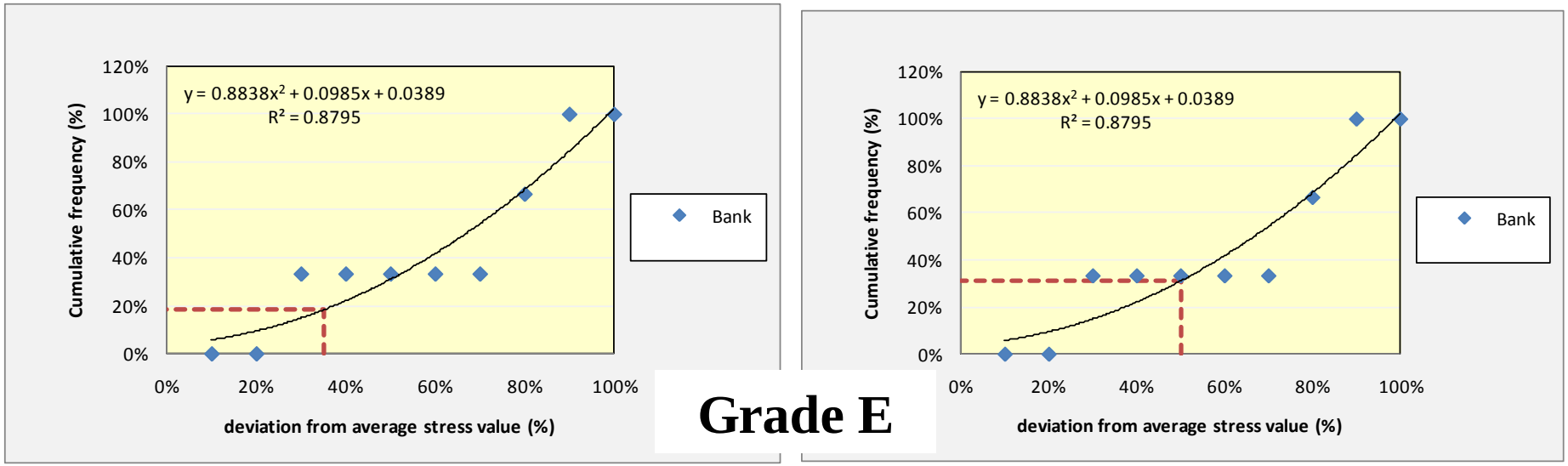
Grade B



50% of stress components (Sx,Sy,Sz) deviate from average values for less than 10%

92% of stress components (Sx,Sy,Sz) deviate from average values for less than 20%

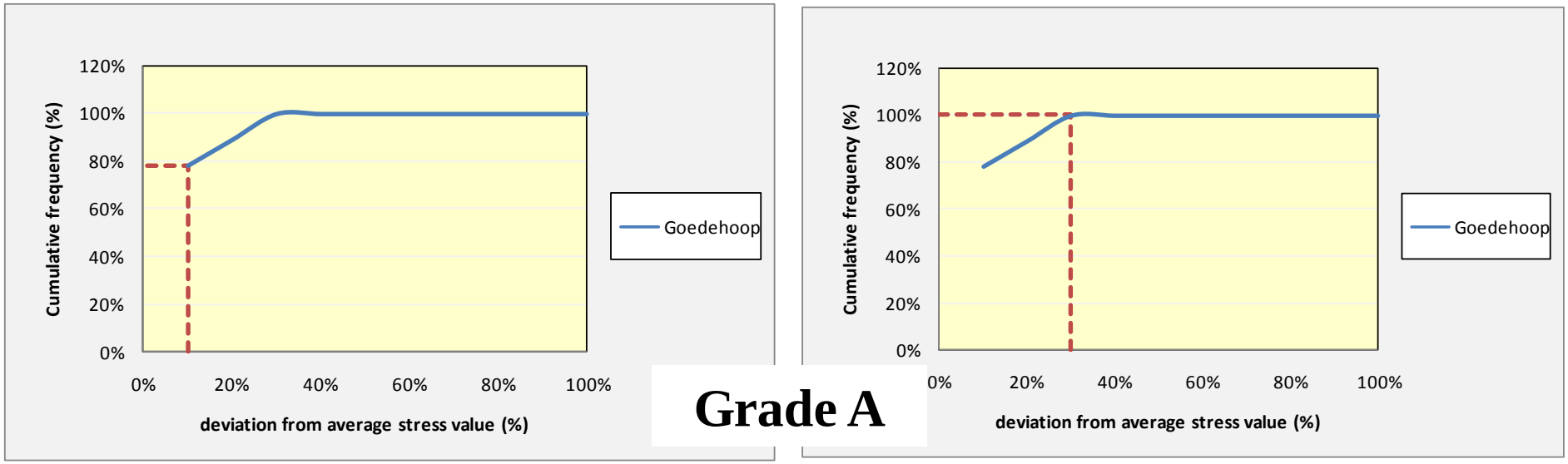
Figure 5-55 Cumulative frequency curves versus deviation from average stress (Grade B)



20% of stress components (Sx,Sy,Sz) deviate from average values for less than 35%

31% of stress components (Sx,Sy,Sz) deviate from average values for less than 50%

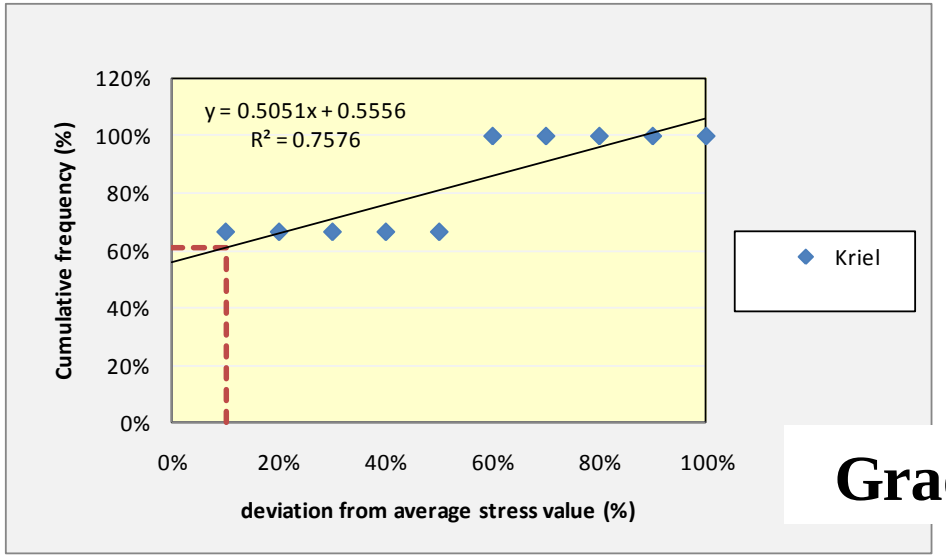
Figure 5-56 Cumulative frequency curves versus deviation from average stress (Grade E)

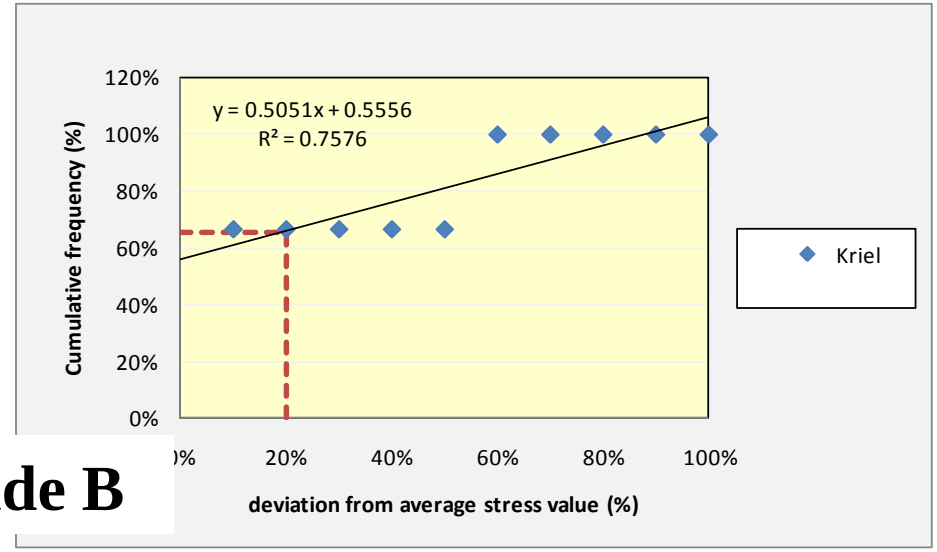


80% of stress components (Sx,Sy,Sz) deviate from average values for less than 10%

100% of stress components (Sx,Sy,Sz) deviate from average values for less than 30%

Figure 5-57: Cumulative frequency curves versus deviation from average stress (Grade A)



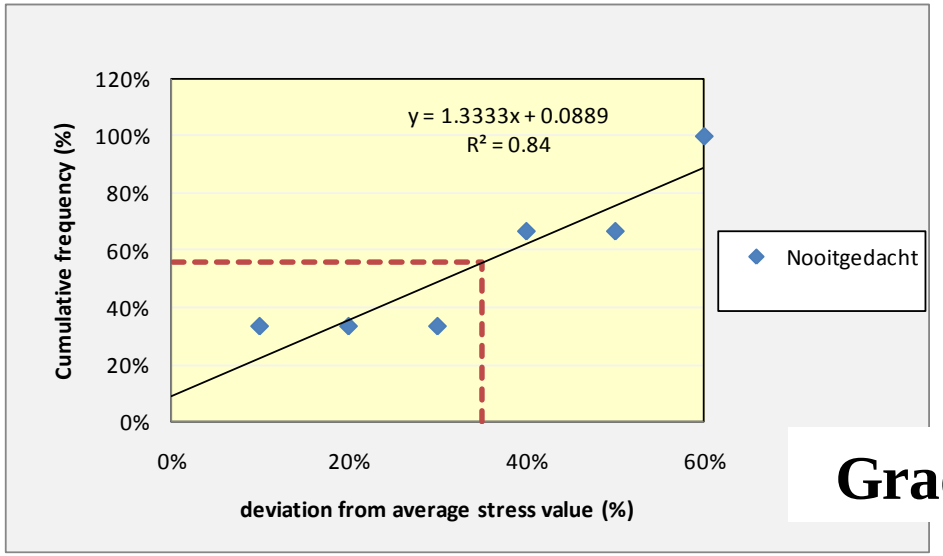


Grade B

61% of stress components (Sx,Sy,Sz) deviate from average values for less than 10%

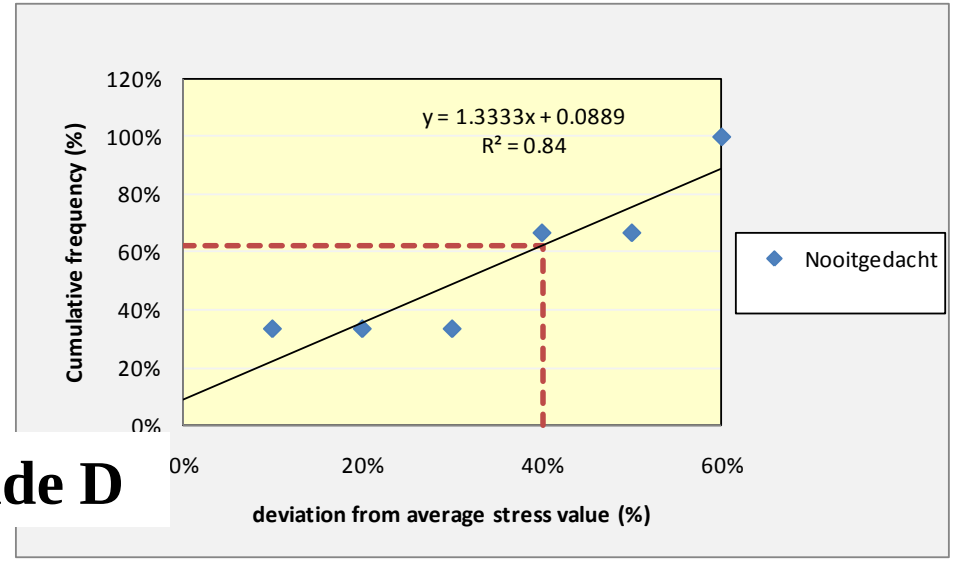
67% of stress components (Sx,Sy,Sz) deviate from average values for less than 20%

Figure 5-58: Cumulative frequency curves versus deviation from average stress (Grade B)



56% of stress components (Sx,Sy,Sz) deviate from average values for less than 35%

Grade D



62% of stress components (Sx,Sy,Sz) deviate from average values for less than 40%

Figure 5-59 Cumulative frequency curves versus deviation from average stress (Grade D)

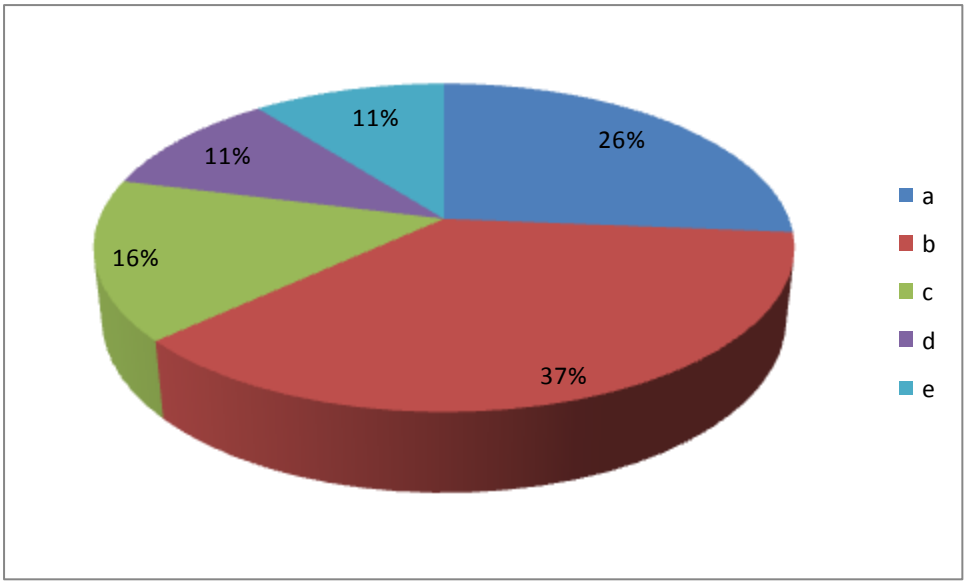


Figure 5-60 Pie Chart showing repartition of group grade within the coal stress database

5.3 Analysis of the stress measurement data

In this section in-situ stress measurements are analysed to determine potential correlation with depth, with the topography of the terrain, the geology, the structural geology and other in-situ stress measurements conducted in other parts of the southern Africa region.

5.3.1 Stress Index

One of the main objectives of this project was to develop a stress map (hazard map) which indicates areas where the most stress issues are likely to occur. In order to develop this map, an attempt was made to use only in-situ stress measurements. However, it was discovered that in some instances, results of in-situ stress measurements on a mine were in disagreement with observations made underground at that mine. Therefore, in order to address this issue, a stress index was computed instead of focusing on the exact magnitudes of major compressive horizontal stresses. The stress index was deemed broader than the magnitude of stress in the sense that it takes cognizance of observations of roof conditions made during the site visits. The stress index was plotted as follows:

- roof conditions were classified as “good”, “mild” and “bad” and a rating was assigned to each category with “good” being given a rating of 2, “mild” a rating of 1 and “bad” a rating of 0.5,

- A rating was assigned to each mine for which the roof conditions were known either through direct observations during site visits or through communication with Rock Engineers working at the mine,
- The in situ stress measurement data were averaged and the mean value was found to be about 5.54 MPa with a standard deviation of about 2.32 MPa. Prior to average magnitude of horizontal stress, the relationship between horizontal stress and depth was analysed to see if there was any correlation. From this analysis, it was found that there is no correlation between depth and magnitude of horizontal stress within the range of depth where stress measurements were taken.
- For mines for which roof conditions were known, the stress index was computed by multiplying the mean value by the corresponding roof condition rating, whereas for those for which no indication of roof condition was given but in situ stress data were available, the stress index was taken to be equal to the result of in situ stress measurement conducted at the mine.
- For mines where only the orientation of stress is known but the magnitude of stress is unknown, and at which no site visit was conducted, the major horizontal stress was assumed to be equal to the average value (the most expected value). For those mines, the conditions are assumed to be mild and hence the stress index was assumed to be equal to the mean value of stresses.

Figure 5-61 shows a conceptual map of stress indices in the Witbank and Highveld coalfields. The green portion is the area of good roof conditions; the yellow is the area of mild conditions and the red spots are areas of relatively bad roof conditions. The arrows on the map give directions of the major compressive horizontal stress either as provided by in situ stress measurement or underground mapping.

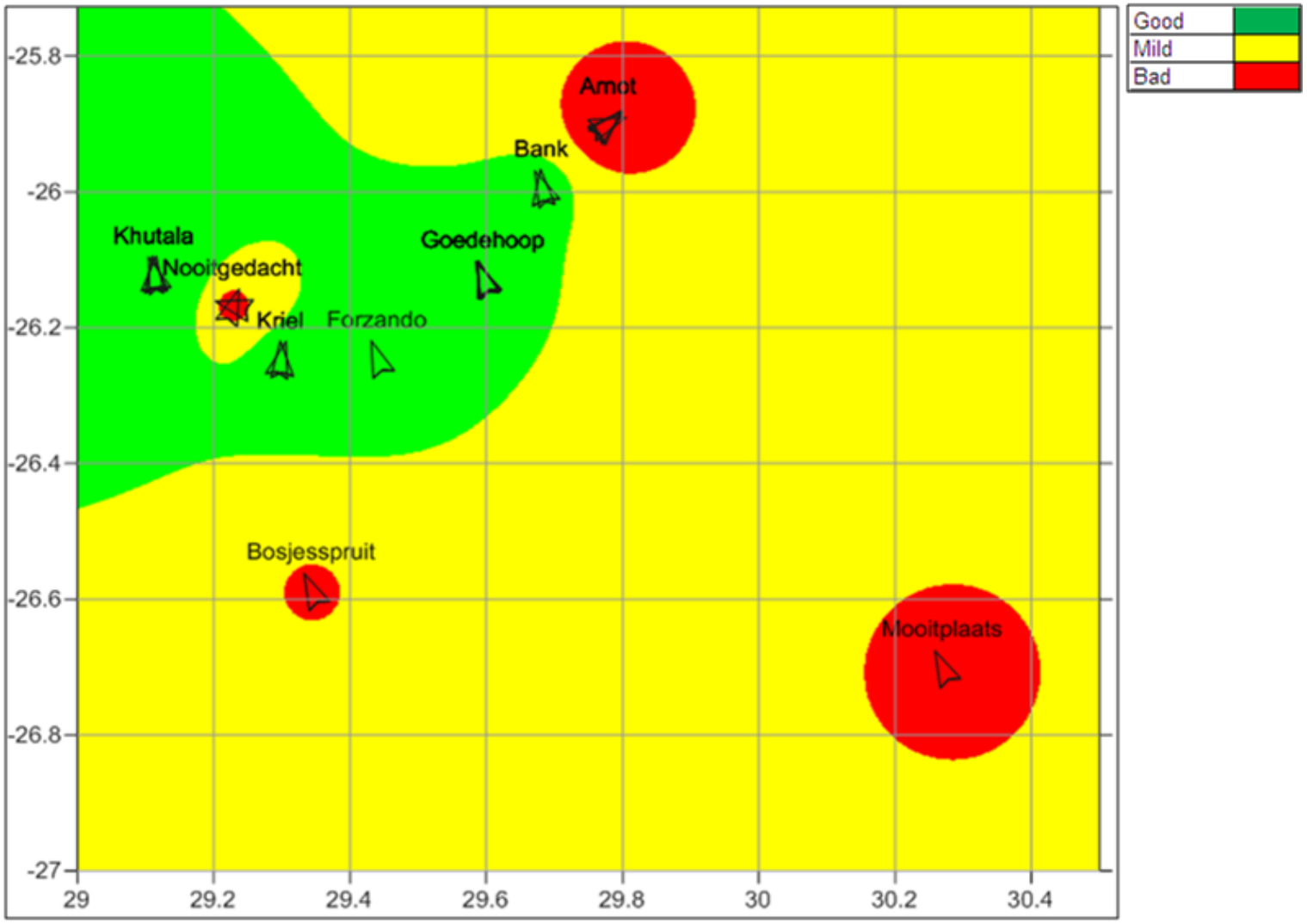


Figure 5-61 Contour map of stress indices in the Witbank and Highveld Coalfields

Figure 5-62 shows a view in three dimensions of the stress index contours and the locations of observations.

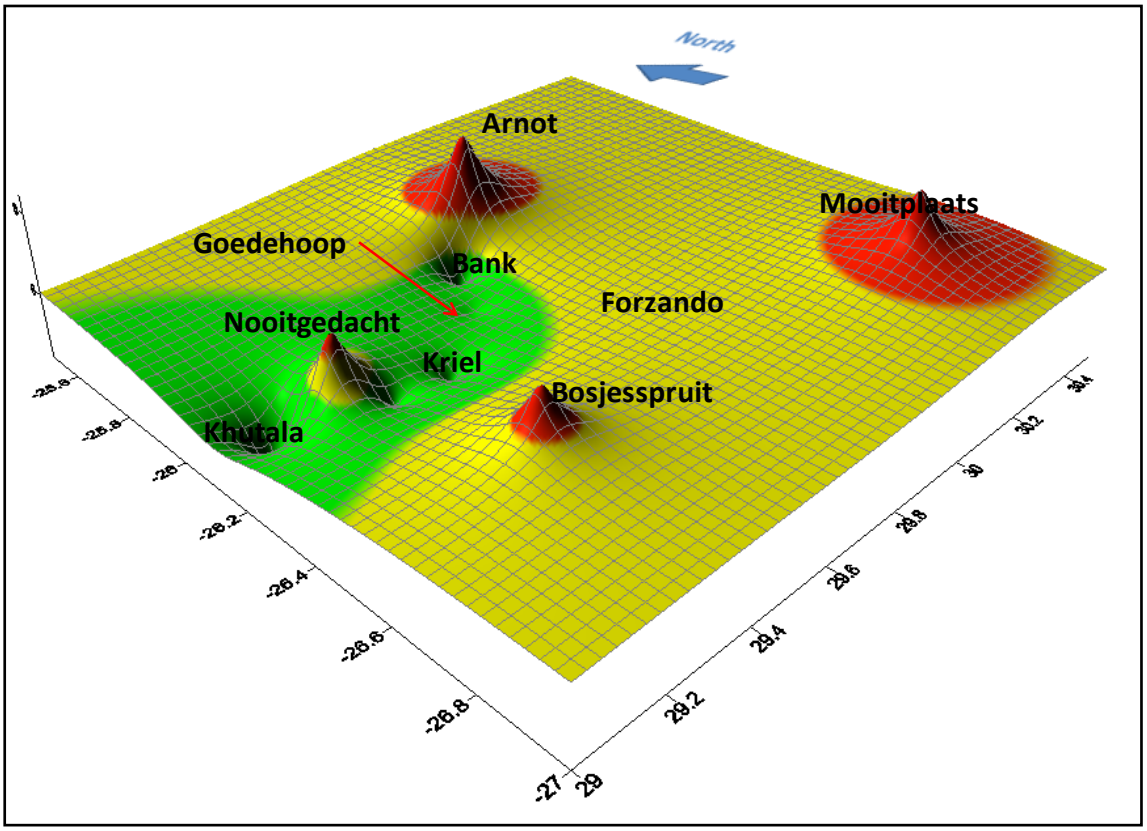


Figure 5-62 3D distribution of the stress index contours

5.3.2 Correlation with depth

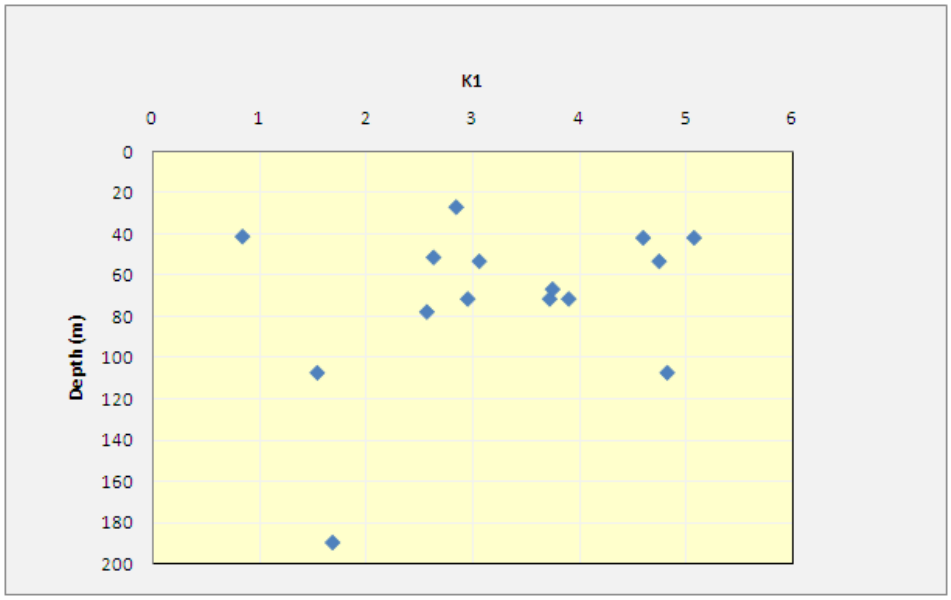
Another way of looking at in situ stress data is to plot the K-ratios against depth, and the plots in Figure 5-63 and Figure 5-64 were obtained for K1 and K3 respectively. Although there is a tendency for K-ratios to decrease with depth, no discernable trend can be derived from the plots.

Figure 5-65 compares the stress measurements with the theoretical models of sedimentation and erosion obtained from numerical modelling in section. Expectedly, all the measurements fall between the two curves. This confirms that if the models are correct the formations of the coalfields involved complex processes of sedimentation and erosion.

However, a discernable trend was obtained upon plotting K-ratio versus measured vertical stress, removing an outlier result (very low horizontal stress obtained at Bank colliery), as

illustrated in Figure 5-66. The trend thereof obtained has the following power equation and coefficient of correlation respectively:

$$Vertical\ stress\ (MPa) = 5.95 \times K1^{-1.142},\ R^2 = 0.7872$$



,

Figure 5-63 Scatter plot of ratios of major horizontal stresses to vertical stress (K1) versus depth

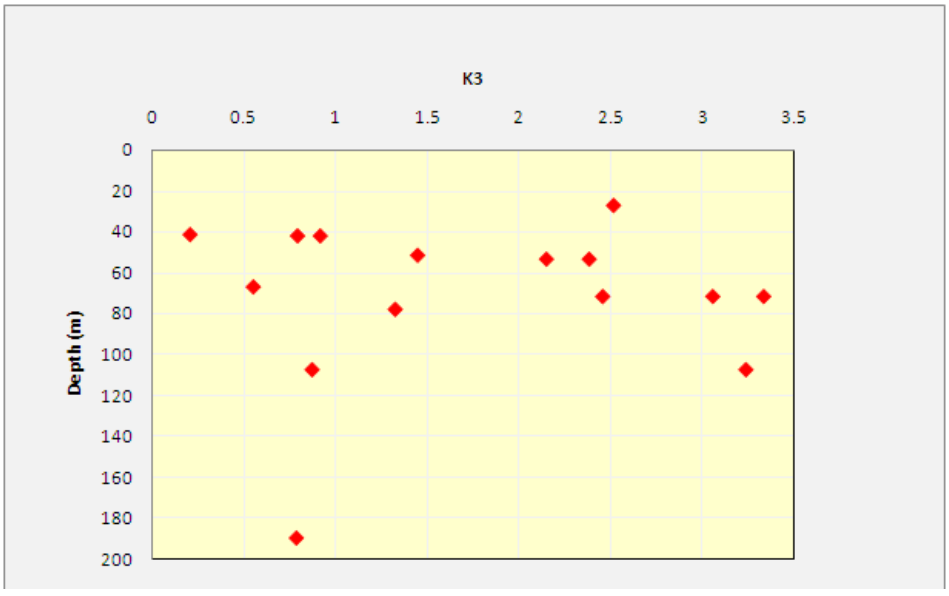


Figure 5-64 Scatter plot of ratios of minor horizontal stresses to vertical stress (K3) versus depth

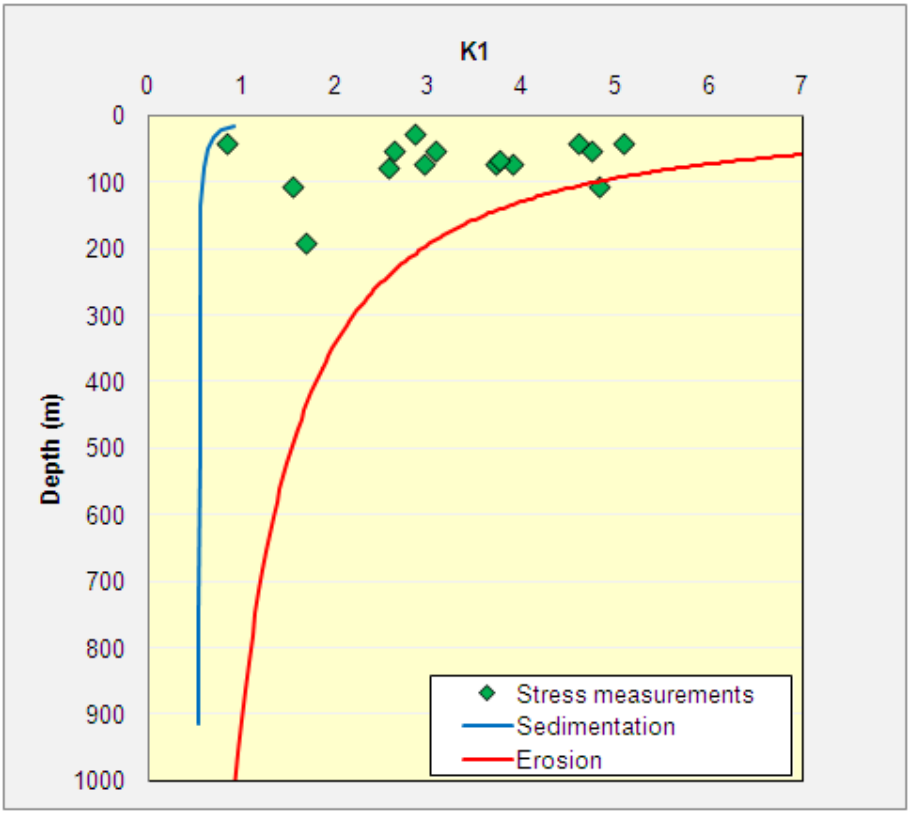


Figure 5-65 k-ratio versus depth graphs comparing the stress measurements with the sedimentation and erosion theoretical models

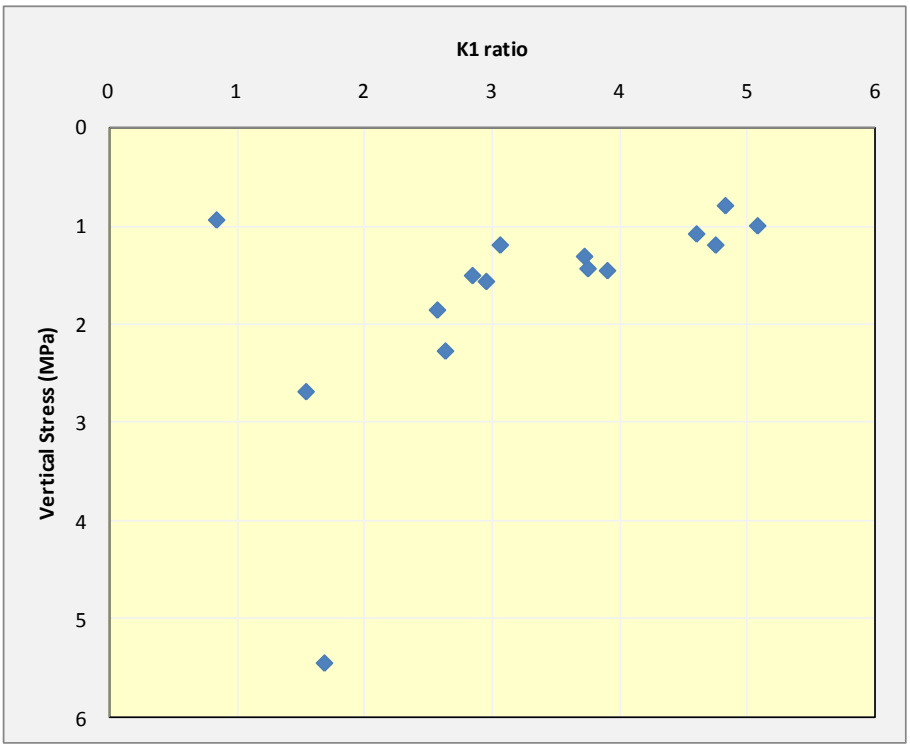


Figure 5-66 Plot of K1 ratios versus Vertical Stress

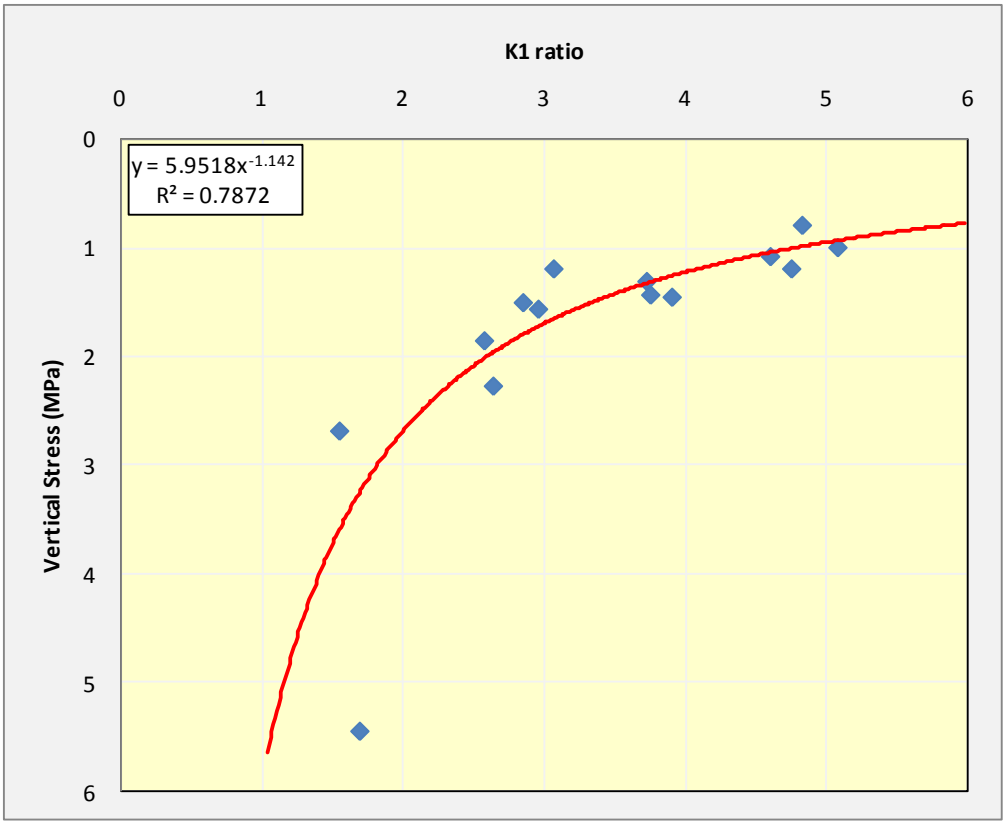


Figure 5-67 Trendline of K1 ratios function of vertical stress after removing an outlier

In practice one is more interested in knowing the K1 ratio prevailing at a given depth. Therefore by transforming the above equation, the following expression is obtained:

$$K1 = 4.7673 \times (vertical\ stress)^{-0.876}$$

In addition, an attempt was made to explain horizontal stress as a function of depth, elastic modulus and Poisson's ratio based on an equation below which was suggested by Cartwright (1997) for coal mines in the United Kingdom.

$$SH_{max} = B_0 + B_1\left(\left(\frac{\nu}{1+\nu}\right) \times Depth\right) + B_2(Modulus\ of\ Elasticity)$$

$Where$:

$B_0 = constant\ in\ MPa$,

B1 = constant in MPa/m

B2 = dimensionless constant commonly referred to as Tectonic Strain Factor (TSF)

A multiple regression at confidence level 95% was conducted on the stress data set using regression facilities in Microsoft Excel so as to determine the optimal values of coefficients B_0, B_1 and B_2. Table 5-15 summarises statistics obtained following the multiple regression process using Cartwright formula. It can be seen that the multiple regression coefficient which is a measure of goodness of fit is as low as 17%. Given such a low multiple R coefficient and given the actual number of stress measurement data, it can be concluded that this formula is not applicable to the Witbank and Highveld coalfields in order to predict horizontal stress. However this conclusion could change as more stress measurements are included in the database.

Table 5-15 Summary of Multiple Regression Statistics using Cartwright formula

Regression Statistics	
Multiple R	0.173217898
R Square	0.03000444
Adjusted R Square	-0.163994672
Standard Error	2.666166181
Observations	13

ANOVA

	df	*SS*	*MS*	*F*	*Significance F*
Regression	2	2.198822691	1.099411346	0.15466277	0.858714372
Residual	10	71.08442107	7.108442107		
Total	12	73.28324376			

	Coefficients	*Standard Error*	*t Stat*	*P-value*	*Lower 95%*	*Upper 95%*	*Lower 95.0%*	*Upper 95.0%*
Intercept	4.139891487	2.96552618	1.396005712	0.19292984	-2.467712583	10.74749556	-2.467712583	10.74749556
X Variable 1	0.061568832	0.115100707	0.534912719	0.604399875	-0.194891524	0.318029188	-0.194891524	0.318029188
X Variable 2	0.048187745	0.151448773	0.318178513	0.756894764	-0.289261149	0.38563664	-0.289261149	0.38563664

An attempt to express horizontal stress based on depths only yielded a multiple regression coefficient of about 0.31 with a R^2 of about 0.1 (Figure 5-68). The low correlation with depth actually indicates that for the range of depth pertaining to coal mines, horizontal stress is constant with variations due to local geology. A similar trial based on elastic modulus alone yielded multiple regression coefficient of 0.047 and a R^2 of about 0.002. Similarly, an analysis based on Poisson's ratios alone yielded corresponding values of 0.03 and 0.0013 respectively. In the light of these results it can be concluded that horizontal stress within the Witbank and Highveld coalfields is better explained in term of depth than elastic moduli or Poisson's ratios.

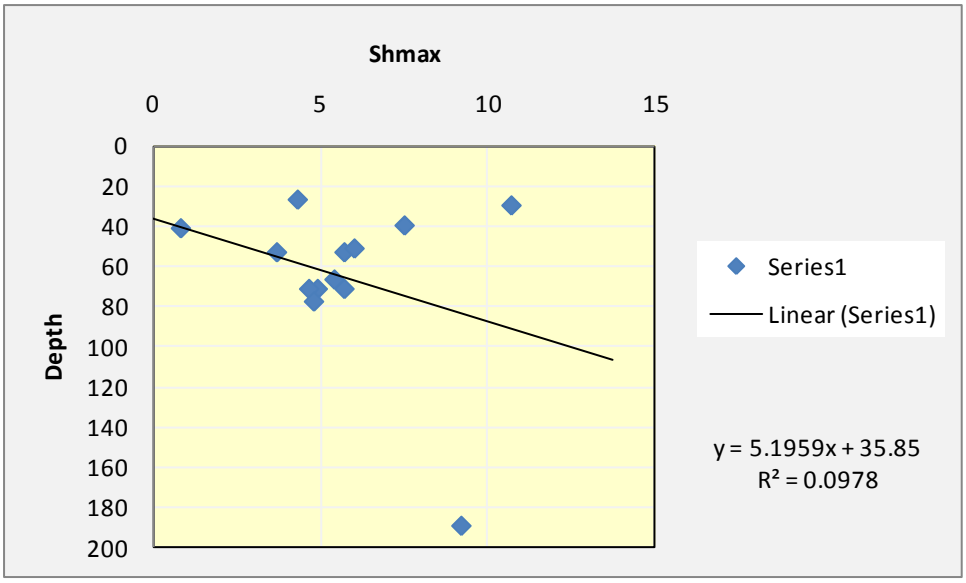


Figure 5-68 Regression line of maximum horizontal stresses versus depth

However, it has been proven that better correlations are achieved when both modulus and depth are combined than when depth alone is used (Cartwright 1997). Therefore in the next step, the effects of modulus and depth were explored simultaneously. The simple regression equation used here is as follows:

$$SH_{max} = B_0 + B_1(Depth) + B_2(Modulus\ of\ Elasticity)$$

In this model the excess stress consists of terms independent of the depth which are the intercept B_0 and B_2 x E. The multiple regression coefficient was in excess of 0.33 and R^2 was about 0.11. This is a slight improvement in both multiple regression coefficient and R^2 upon combining depth and modulus of elasticity. It illustrates that depth and modulus of elasticity do interact in the data set, but that this interaction is minimal.

Similarly, effects of Poisson's ratio and depth simultaneously were explored by using the following equation.

$$SH_{max} = B_0 + B_1(Depth) + B_2(Poisson's\ ratio)$$

Having performed the regression analysis on the stress data set with the above mentioned equation and maintaining the confidence level of 95%, a multiple regression coefficient and R^2 of 0.32 and 0.11 were found respectively. Therefore it can be concluded that the

interaction between Poisson's ratio and depth is even less significant than in the previous case.

5.3.3 Correlation with topography

5.3.4 Topography of the Witbank and Highveld Coalfields

The topography of the landscape plays a defining role in the in situ stress regime. For instance it was shown in Section 3.5 that high horizontal stress is very likely to occur to a certain depth in valleys and in hilly districts.

Various sources of topographical data were investigated and Shuttle Radar Topographical Mission (SRTM) data of NASA is considered to suit perfectly the requirement of the present study (Golden Software 2011). Other alternatives were investigated such as using available topographical information; however, the formats in which this information was provided made the processing in Surfer tedious.

During the SRTM, data were collected at 1 arc second resolution which corresponds to 30 m resolution. However, on the website, data of such a level of resolution can only be downloaded for the US. For the rest of the world, data have a resolution of 90 m (3 arc second). Therefore, in order to improve on the resolution of the topographical map interpolation has to be carried out. It is important to note that areas flooded with water and very high altitude summits could not be surveyed during the shuttle mission and exist in the data base as voids. Techniques and algorithms aiming at interpolating information in the void exist such as Spline interpolation in GRASS GIS. In some instances additional surveys have been conducted to fill in the gap.

The SRTM data, available free on the internet, are structured into tiles covering 1 degree of longitude and 1 degree of latitude. On the website there are two different types of SRTM files, SRTM 1 and SRTM 3. SRTM 1 refers to files covering United State of America while SRTM 3 files are for the rest of the world. For the present study SRTM 3 files were used. The files come with an HGT extension and for them to be read in Surfer they have to be renamed as DEM files. In addition to this, Surfer requires that STX and HDR (Header file) files be created for each HGT file downloaded. In the HDR files, values of ULYMAP and ULXMAP were both set as negative since the area of interest (Witbank and Highveld) falls under the southern and eastern hemisphere.

In Surfer the Grid/mosaic option was used to combine four DEM files (S25E029, S26E029, S25E030 and S26E030) into a single grid. The aim of having four files was to try to cover the whole area of the study. The nearest neighbour method was chosen as the best interpolation technique in this case. The interpolation helps obtain smooth contours in the topographical map from 3" (3 arc second) of resolution files. Figure 5-69 presents the resulting topographical map for the Witbank, Highveld. Areas where stress measurements were carried out are plotted for reference purposes. It can be seen that Arnot Colliery is at an elevation of approximately 1500 to 1700 m while the rest of collieries are at lower elevations of roughly 900 m to 1100 m.

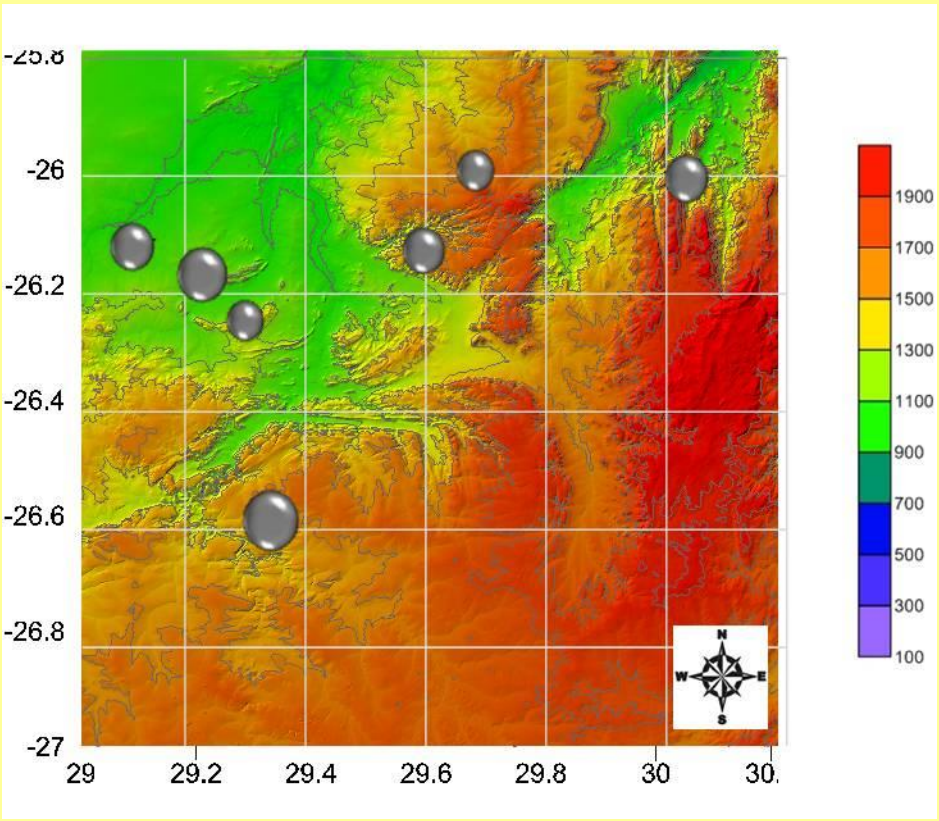


Figure 5-69 Surfer plot of the Topography of Witbank, Highveld and the surrounding regions derived from SRTM data. The size of bubbles on the map indicate magnitude of major horizontal stress

A 3 dimensional topographical Surfer surface was generated so as to enable a view in perspective of the terrain. It can be seen that, Arnot is on a hilly region while the rest of collieries are on more or less flat terrain.

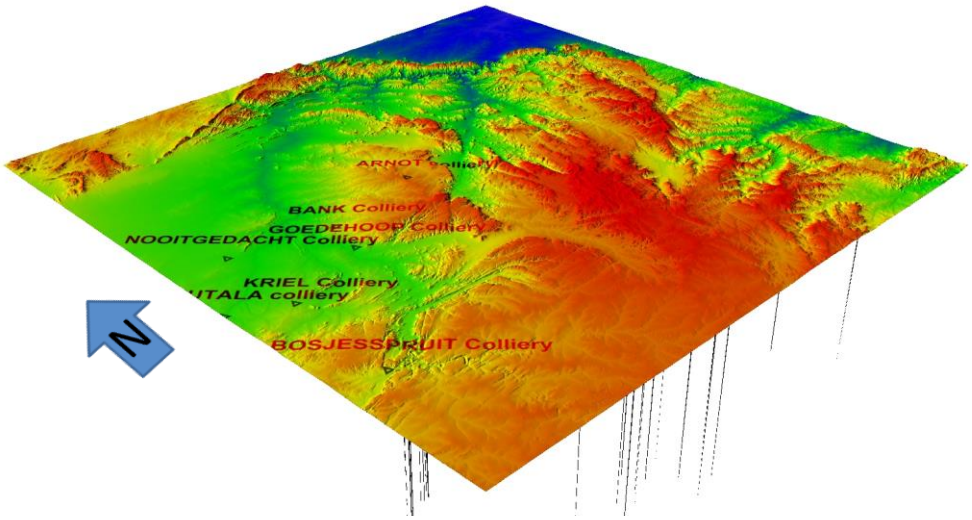


Figure 5-70 Surfer 3-dimensional surface of the topography of Witbank, Highveld and their surroundings

5.3.5 Analysis of the correlation between the stress orientations and the topography surface

Figure 5-71 shows the orientations of measured in-situ stresses overlain on the topographical map of the Witbank and Highveld coalfields.

By scrutinizing the map with respect to the orientation and magnitude of the maximum compressive horizontal stress, no discernable correlation could be found. Therefore, it can be concluded that the topography has little of influence on the orientation of the maximum compressive horizontal stress observed in the Witbank and Highveld coalfields.

.

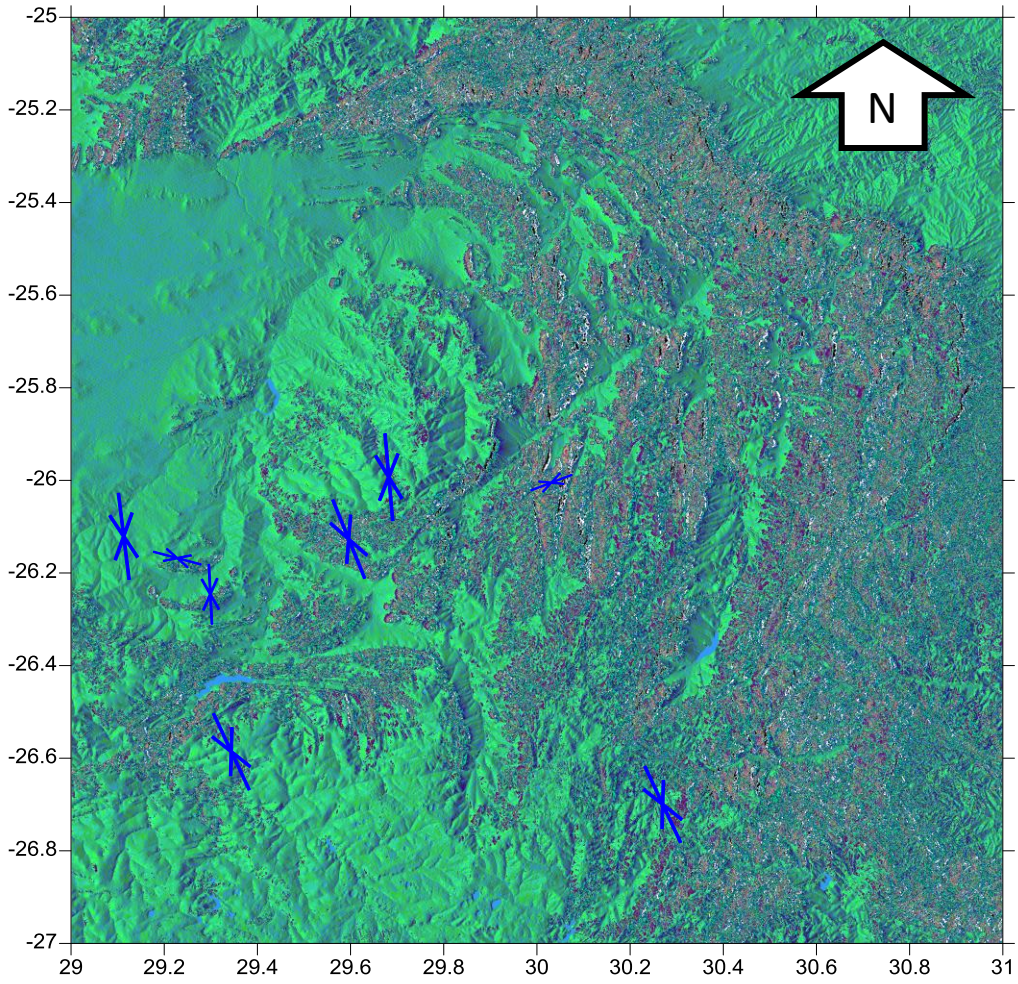


Figure 5-71 Map showing Major Horizontal stress direction and magnitude on the shaded relief map of the Witbank and Highveld

However, after plotting the stress indices versus elevations as shown in Figure 5-72, Figure 5-73 and Figure 5-74 a very discernable trend was obtained. And after removing two outliers from the data set, the equation of stress index as a function of elevation presented in Figure 5-74 was obtained. One of the outliers corresponded to Bosjesspruit, which is in essence the deepest site. It is important to note the surprisingly high correlation between elevation and stress indices (coefficient of correlation of 93%). The equation thereby obtained was inserted into Surfer to generate a map of stress indices based on elevations (see Figure 5-73). The map obtained was then combined with that in Figure 5-62 to produce the "final" map which is presented in Figure 5-75.

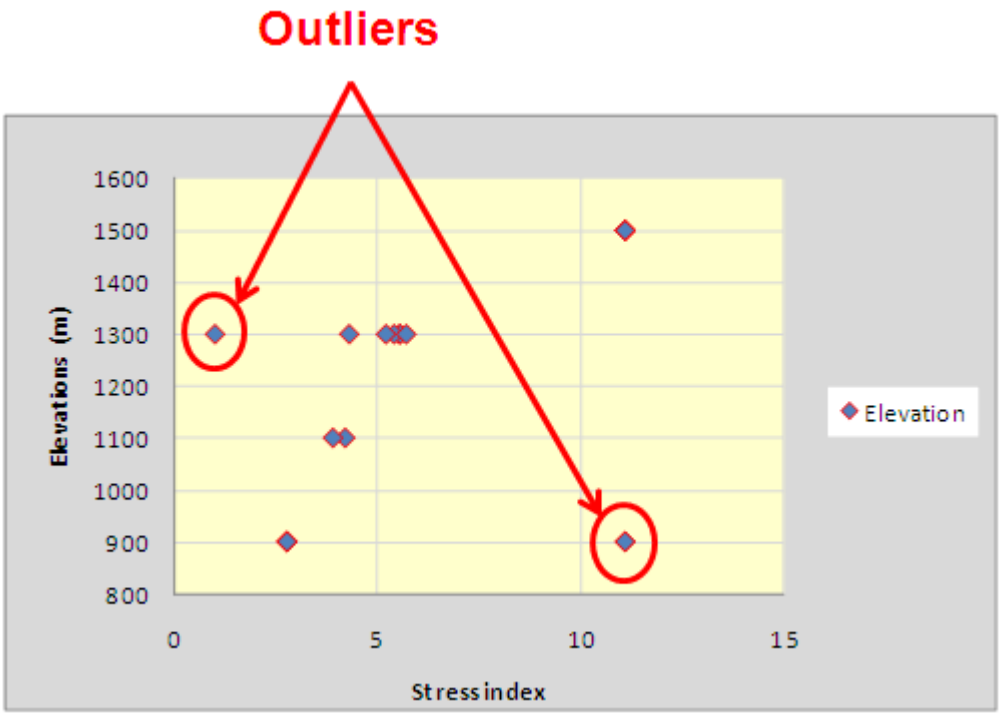


Figure 5-72 Elevations versus Stress Index

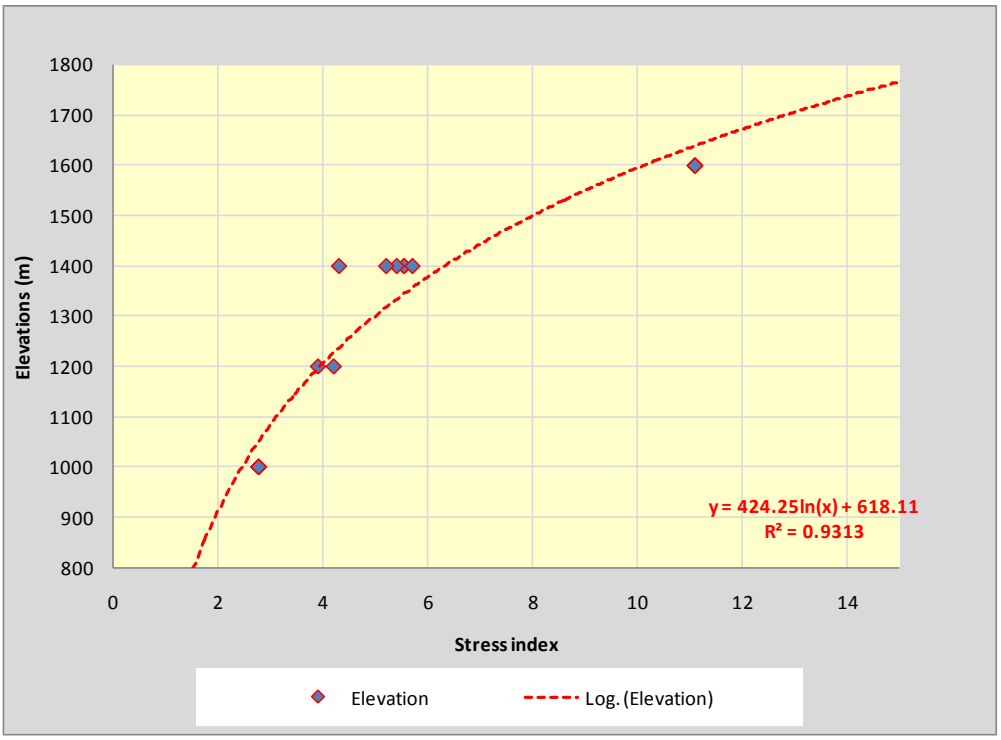


Figure 5-73 Graph showing correlation between elevation and stress index

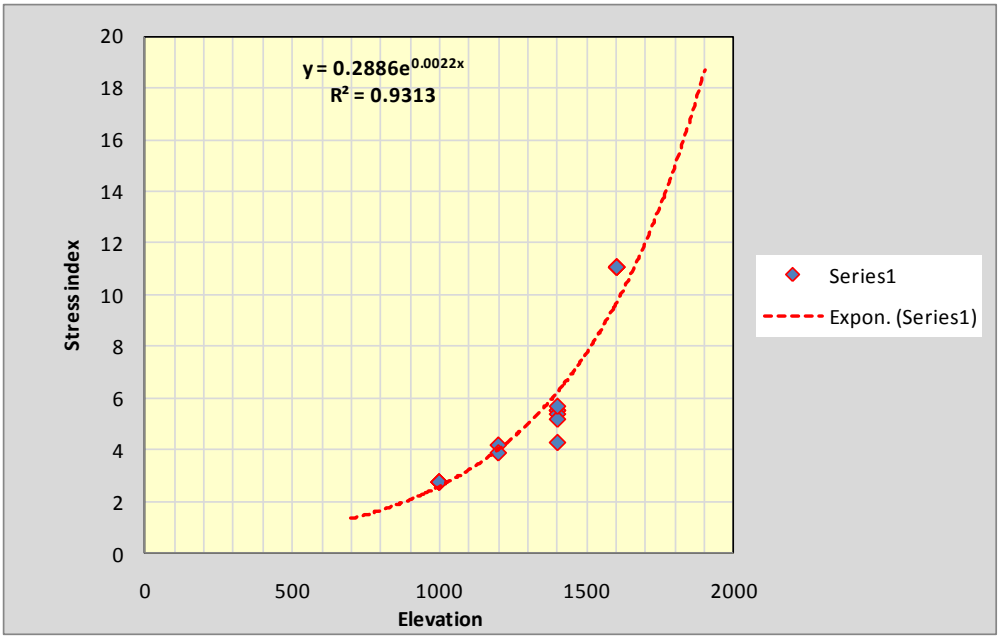


Figure 5-74 Graph showing correlation between stress index and elevation

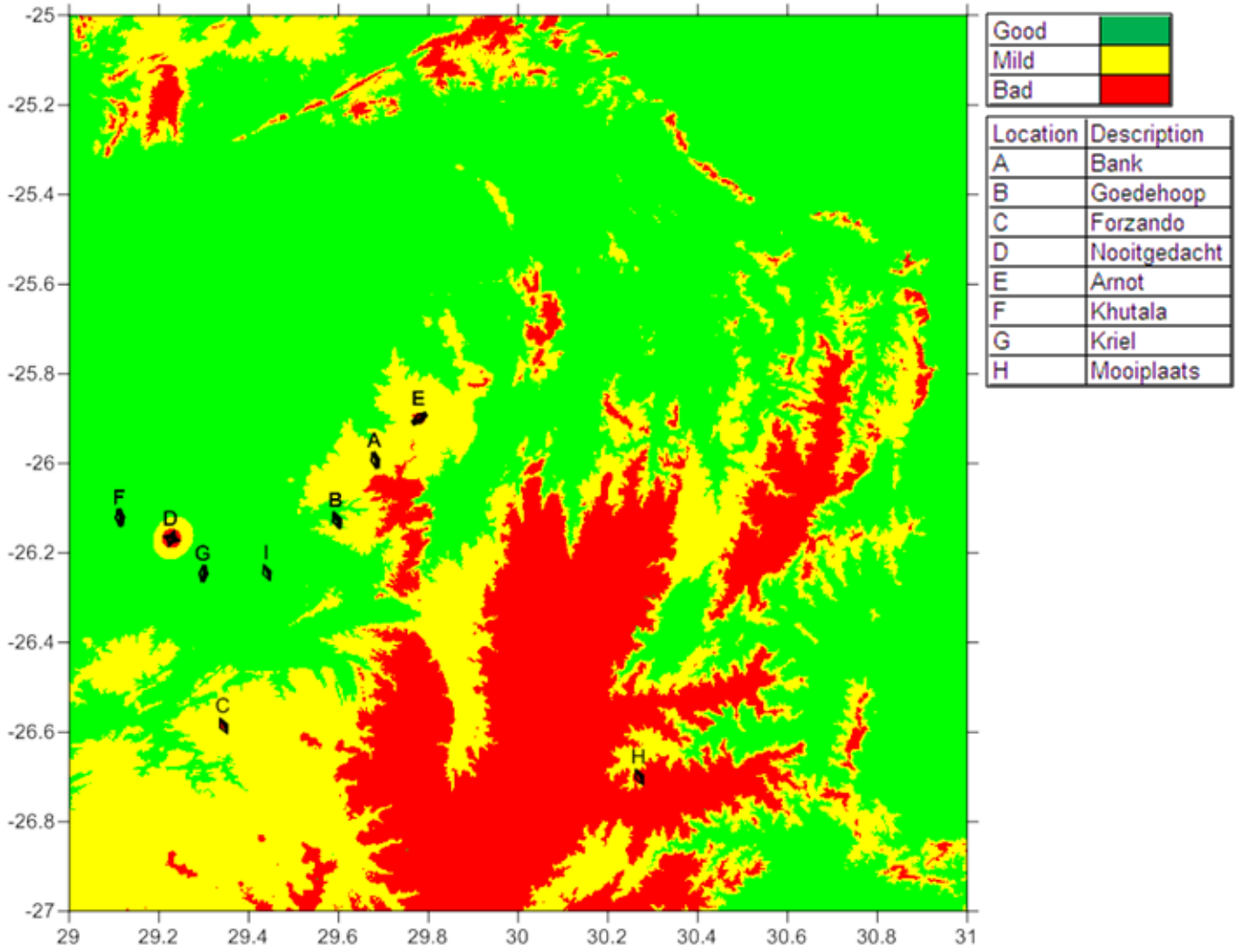


Figure 5-75 Hazard map as derived from topographical information and underground observations

5.3.6 Correlation with structural geology

Figure 5-76 shows the direction and magnitude of the maximum horizontal compressive stress overlying the map of the structural geology of the Witbank and Highveld coalfields. This map compiled by Andreoli (2011) illustrates lineaments (dykes or faults) and known faults within the Witbank and Highveld coalfields. Another important feature on the map is the presumed axis of buckling of the earth's crust in the southern Africa region. Geoscientists have observed that, under the thrust caused by the high values of the compressive horizontal stress, the earth's crust buckles. This buckling is too gentle to be perceived with an unaided eye (Andreoli 2011).

In Figure 5-76 it can be seen that there is a rough correlation between lineament directions and some of the directions of the maximum horizontal stress. For instance the expected direction of the maximum horizontal stress at Kenako (Nooitgedacht) is almost parallel to a lineament running close to the position of the mine. It can be speculated that this lineament which is probably a dyke, is responsible for the rotation of the stress regime reported by the in-situ stress measurements.

Likewise the anomaly of the maximum horizontal stress at Arnot in the northeastern part of the Witbank can be related to the presence of a lineament in the vicinity of the lease. However it is important to note also that the axis of buckling of the earth's crust (dashed blue line) runs very close to the Arnot lease and changes its direction in this region. The change of direction of this axis has often been associated with a rotation of in-situ stress regime from the Wegener stress direction (NNW-SSE) to the direction of movement of the Africa tectonic plate (NE) associated with the East African rift (Andreoli 2011). It is anticipated that this change of stress regime would be associated with an increase in seismic activity and the map seems to confirm this, a relatively high concentration of seismic events occuring around the Witbank-Highveld region. However, further studies on updated seismic data (focal mechanism solution) are needed to confirm this.

In Figure 5-76, a high concentration of lineaments that occurs around Mooiplaats was confirmed by the underground site visit. It is possible that the relatively high horizontal stress (guttering in a laminated sandstone roof) observed at this site, is associated with this high concentration of lineaments.

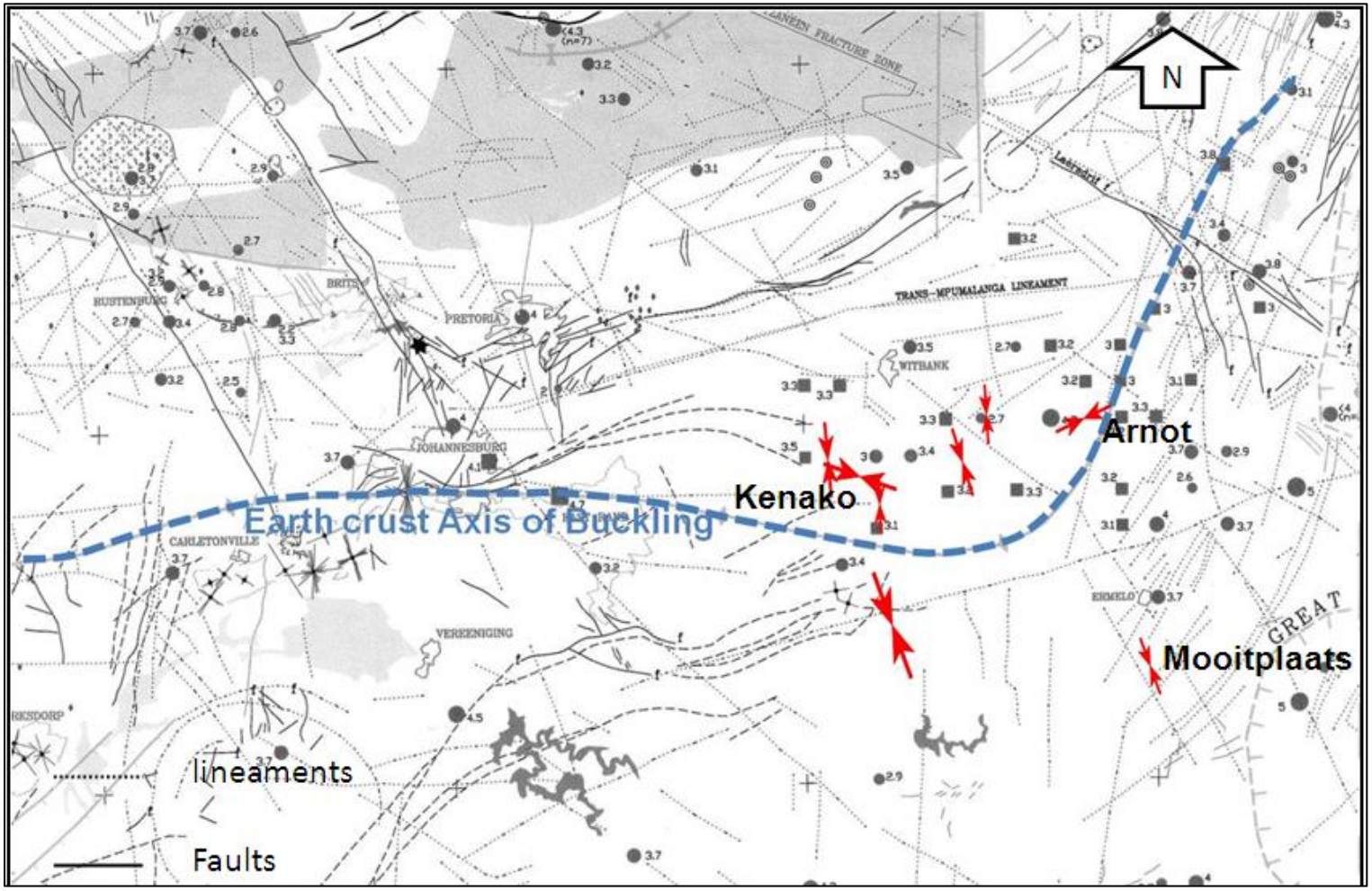


Figure 5-76 Map showing direction and magnitude of SHmax on a structural geology map (after the Andreoli, 2011)

5.3.7 Correlation with in situ stress measurement data from elsewhere

A compilation and grading of in-situ stress data around southern Africa was carried out by Stacey and Wesseloo (1998) using data from mines, civil engineering projects and other sources such as drillhole breakouts. Figure 5-78 illustrates directions of principal horizontal stress within the southern Africa region when data from Stacey and Wesseloo (1998) are combined with data collected in the Witbank and Highveld coalfield.

Following the anomaly observed in the stress direction at Arnot Colliery and the hypothesis that this anomaly could be due to the East Africa rift, combined in-situ stress data (data from Stacey and Wesseloo with those from the Witbank and Highveld coalfields) offered an opportunity to see if such an anomaly extends throughout the rest of the northeast part of southern Africa. Therefore, the southern Africa region was divided as shown in Figure 5-77 into two parts, a north-east region and a southwestern one. The fictitious axis (red axis on the map) which divides the region was placed at a 45° angle so that it also split the coalfields into two corresponding regions; a northeast region around the Arnot lease and a southwest region covering the rest of the coalfields.

Analysis of the data suggests that for the North east part the most expected direction of the maximum horizontal stress is about 120° or NWW-SEE and that 50% of the population is concentrated in a range from 90° to 140° or E-W to NNW-SSE (Figure 5-78).These results show that the NE direction of maximum stress recorded at Arnot is not typical of the northeast part of southern Africa.

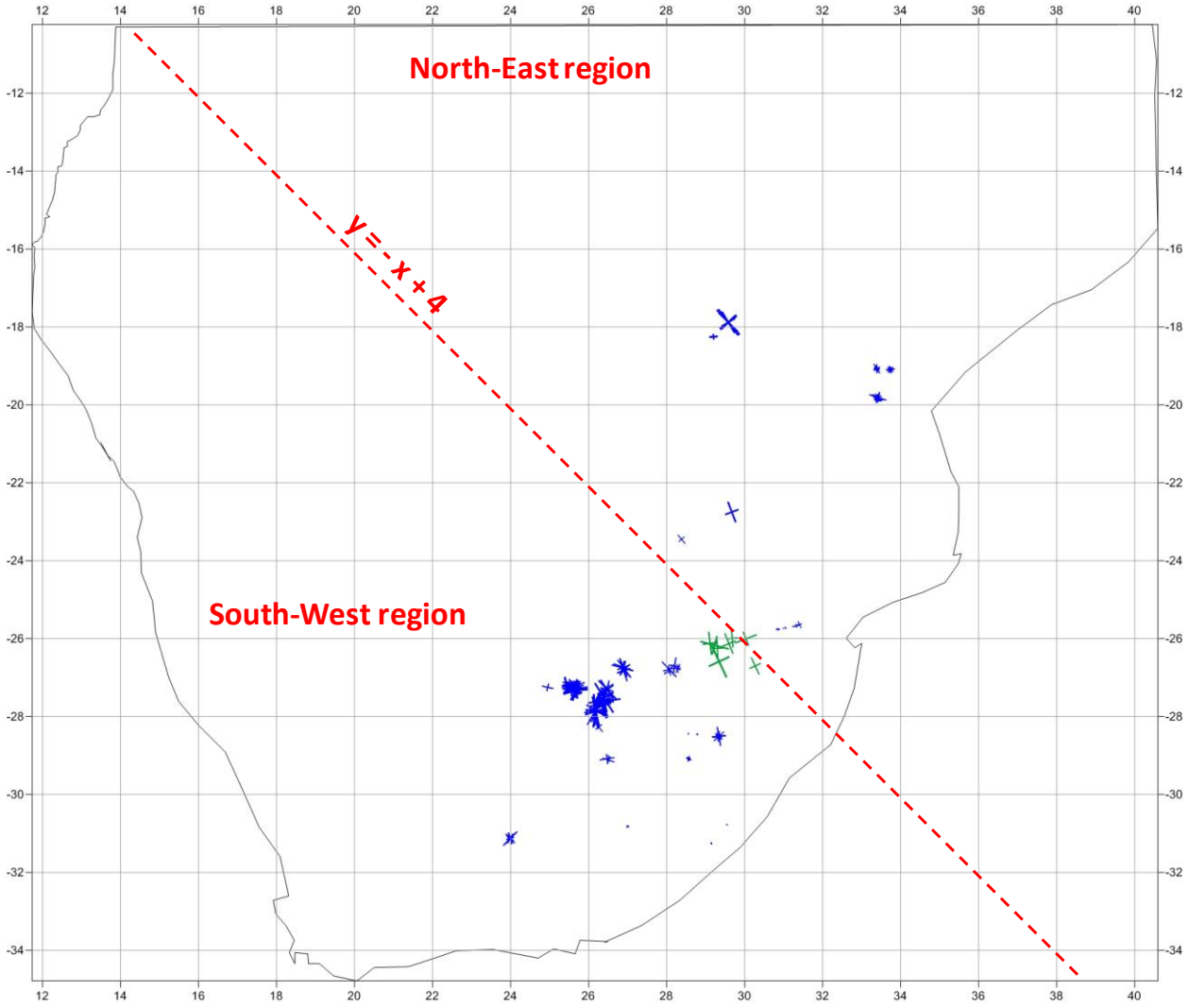


Figure 5-77 Map showing directions of principal horizontal stresses when combining data from Stacey and Wesseloo (in blue) with in situ stress data collected in the Witbank and Highveld Coalfield (in green)

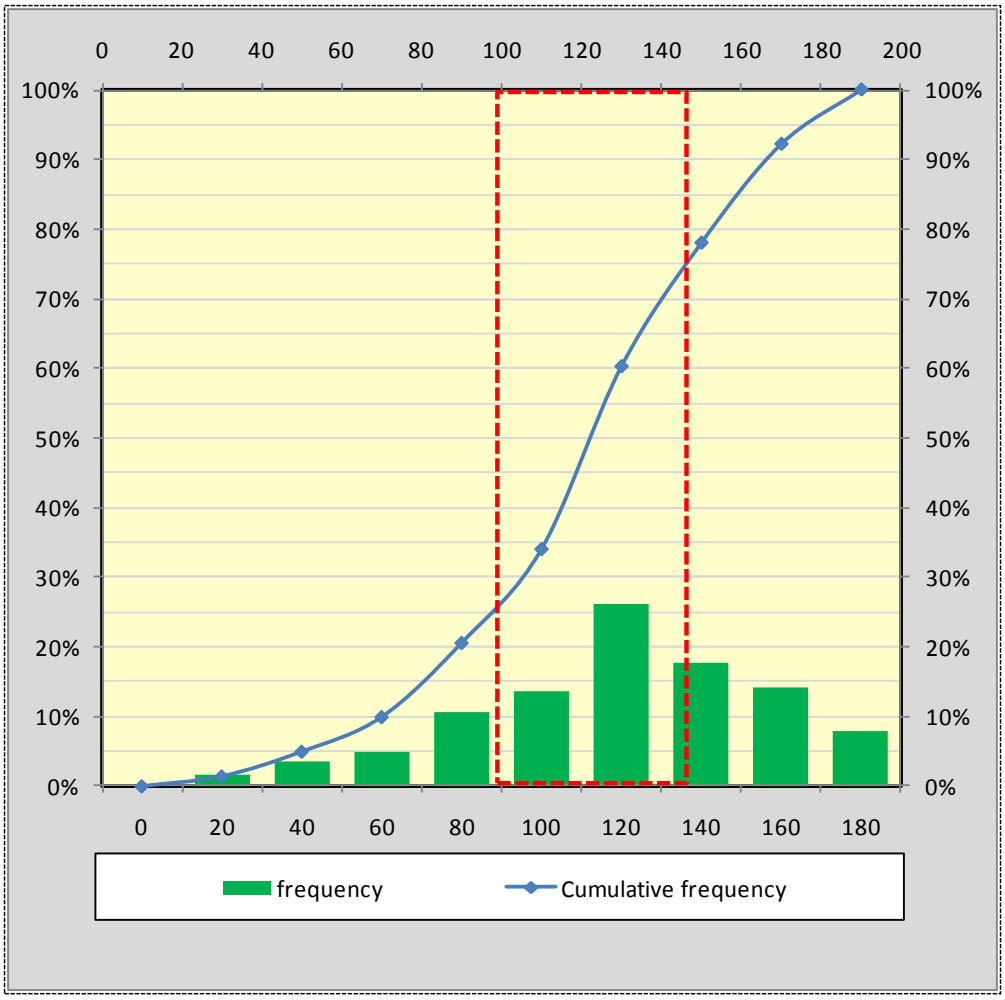


Figure 5-78 Histogram and cumulative frequency curve of major horizontal stress directions in the North East region

Figure 5-79 is the histogram of the directions of maximum horizontal stresses within the south-western part. The shape of the histogram suggests that two or more distinct populations have been combined into one and that two or more processes are in play in defining the stress regime of the region. However it can be seen that there is a significant number of maximum horizontal stress data which are oriented at 160° or NNW-SSE.

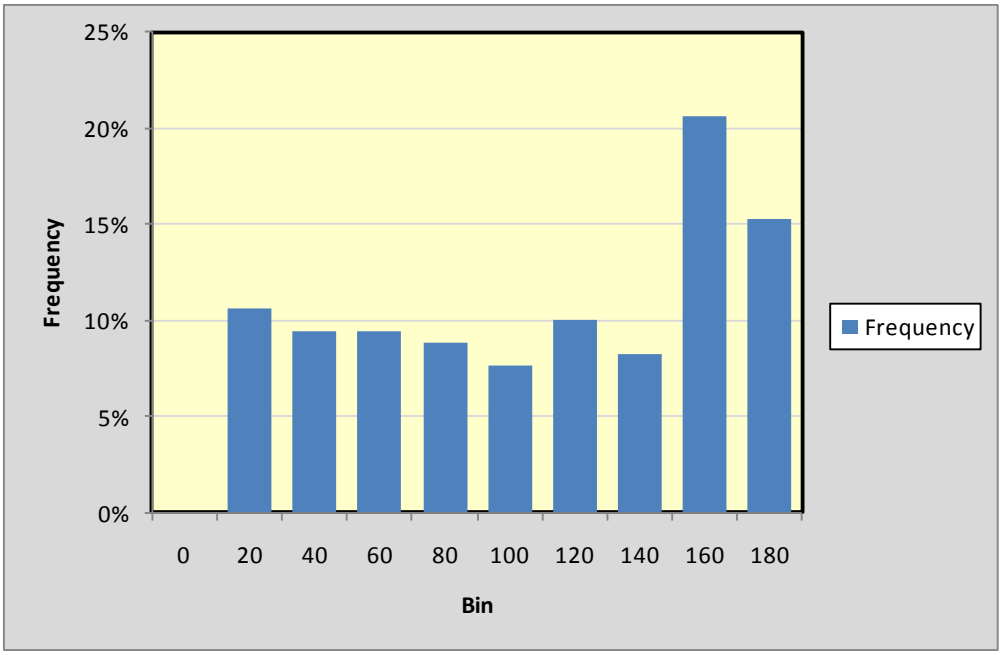


Figure 5-79 Histogram of major horizontal stress directions in the South west region

5.4 Review of stress mitigation strategies employed in the Coalfields

Various techniques are being used in order to combat the effects of stress. The more common are the following:

- Increase in roof bolt density and installation of area support such as straps,
- Increase in the stiffness of the roof by replacing mechanically anchored roofbolts by full column resin grouted roof bolts,
- Orientation of mining layouts in the direction parallel to the major horizontal stress,
- Use of a sacrificial road,
- Use of a slot cut in the roof,
- Undercutting, and
- Change of mining parameters such as road width and cut out distance

Some of these techniques are pro-active, meaning that they are implemented prior to any manifestation of stress, whereas others are purely reactive.

5.4.1 Increase roof bolt density

When guttering occurs, it is common practice to suspend the dead weight of the guttering to the competent roof overlying the guttered material. The density of roof bolts is often increased and an areal support such as straps is used to prevent the guttered roof from falling between tendons. However, in the presence of a thick laminated roof such as that shown in Figure 5-80, the conventional length of the bolts might be too small to provide an adequate anchorage of the bolt in the competent roof (about 60 cm in the competent roof). In this case roof bolts are not installed to suspend the dead weight of the gutter but rather to create a solid beam.

5.4.2 Change mechanical anchor bolts to full column resin grouted roof bolts

Most collieries have shifted from the old support system consisting of mechanical anchor bolts to full column resin bolts. Many collieries have reported an observed improvement in stress related problems as a result of this shift. In mechanical anchor bolting, holes are drilled at a diameter significantly greater than that of the bolt in order to accommodate the shell diameter. As a result an annulus is left between the bolt and the rock which in turn allows lateral sliding to take place when the roof sags under the influence of its own weight or horizontal stress. Therefore, such a system is soft and makes the creation of solid beams in laminated roof almost impossible. In contrast, full column resin bolts prevent such a lateral sliding from occurring since holes are drilled at diameter very close to that of the roof bolt and the annulus is filled with resin.

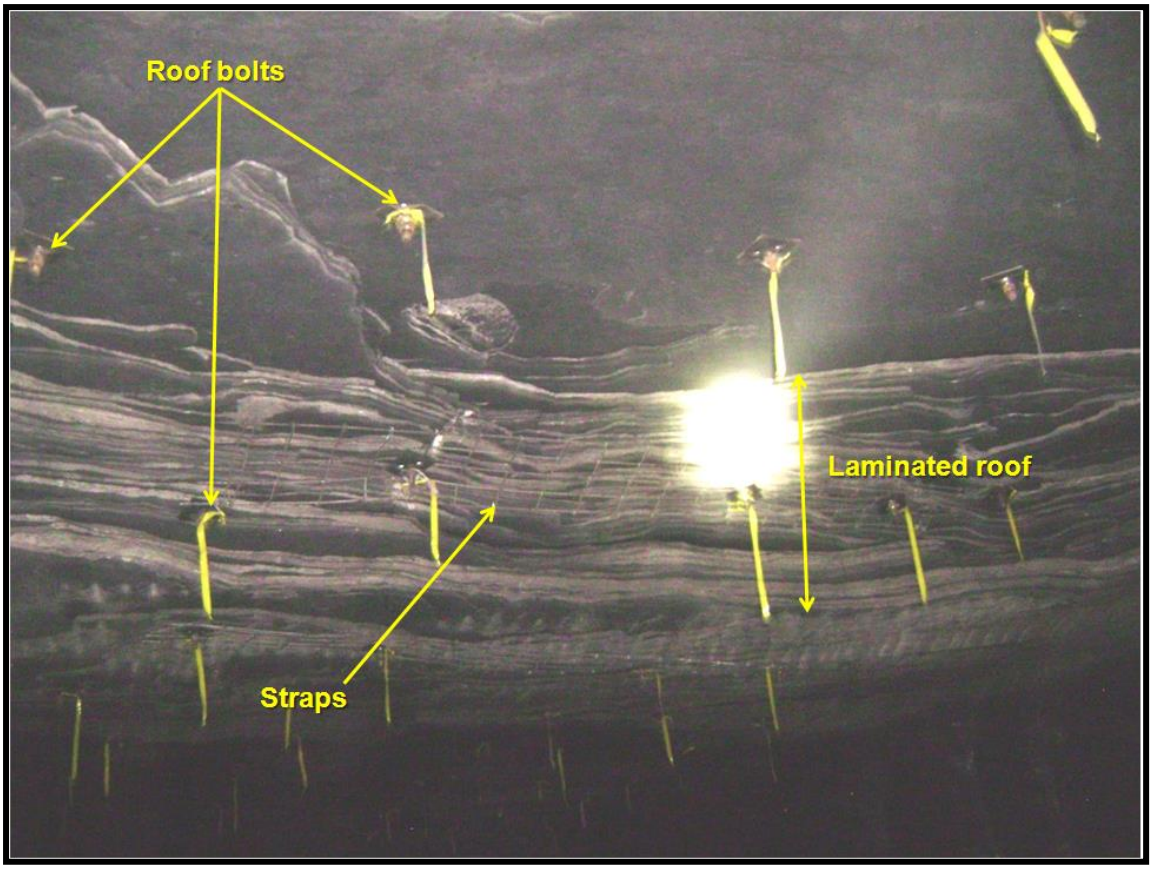


Figure 5-80 Picture showing guttering in a thick laminated roof and the support system composed of roof bolts and straps used to mitigate the hazard

5.4.3 Changed orientation of the panel with respect to the orientation of the major horizontal

Experience has shown that horizontal stress damage such as guttering is orientated along the minor horizontal stress axis or at a 90 degree angle to the maximum horizontal stress. This simply implies that when mining advances in a direction perpendicular to that of the major horizontal stress, most of the damage will be experienced in the roadways rather than the splits. Conversely, when mining is conducted in a direction parallel to the major horizontal stress, more problems are expected to occur in the splits than the roadways. In practice the latter scenario is preferred since roadways host valuable equipment such as transport equipment (conveyor belts...).

It is important to note that a change of orientation of panel as a way of mitigating the effects of horizontal stress can yield good results only when the difference between the major and minor horizontal stresses is significant. For instance, in Figure 5-81, this technique is more

likely to work at Bank and Goedehoop where the K1/K3 ratio is high than at Nooitgedacht where this ratio is relatively low.

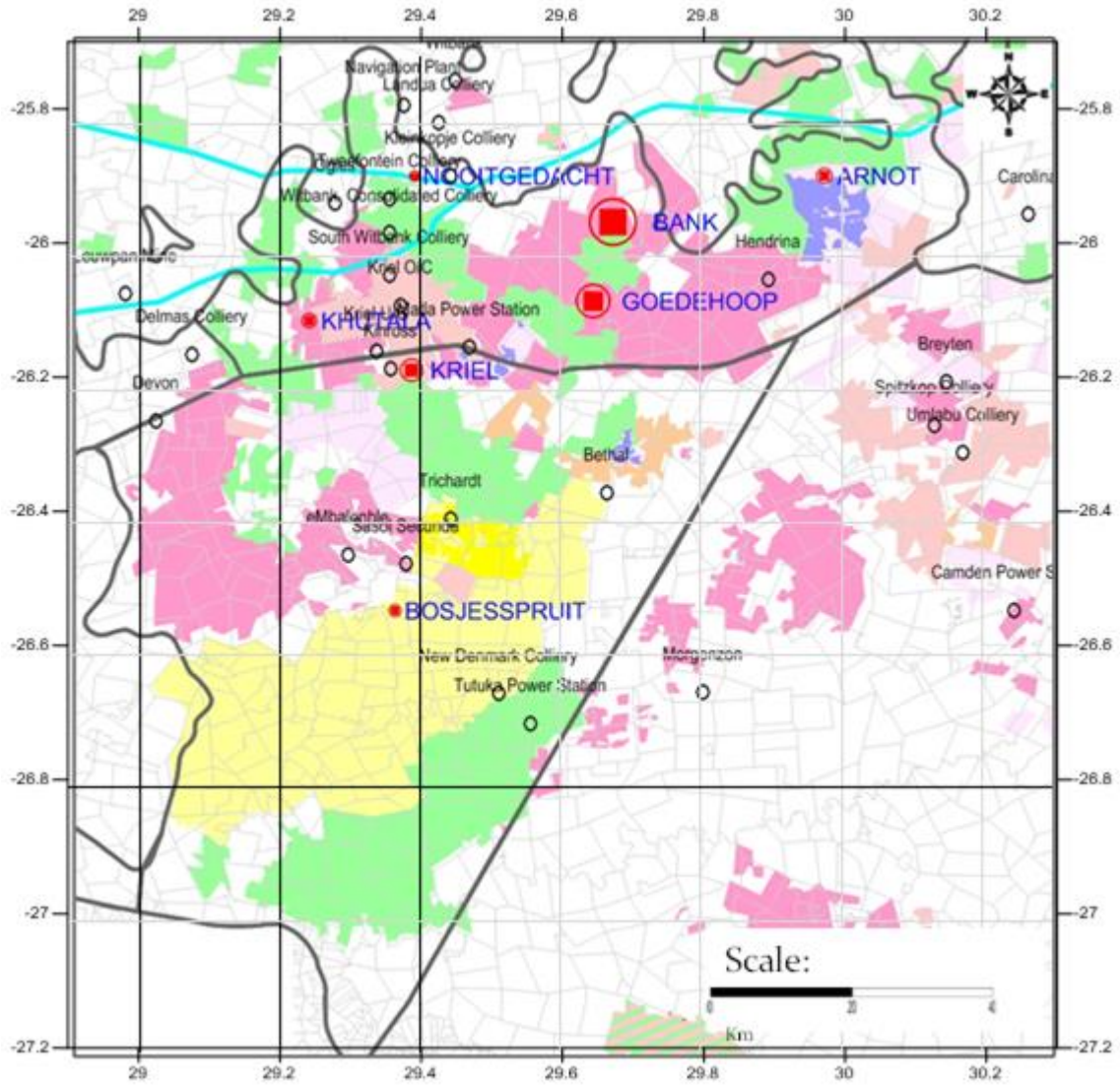


Figure 5-81 Map showing ratios of major to minor horizontal stress (K1/K3)

Another obstacle regarding this mitigation technique is the fact that orientation of mining layouts is chiefly dictated by orientation of geological features such as dykes. In essence, dykes are often associated with a set of joints running parallel to their strike, called sympathetic joints. Ideally mining should be conducted at right angles to the strike of the dyke and the splits in the vicinity of the dyke should be mined at angles rather than parallel to the dyke. In doing so, the likelihood of having joints running parallel to the roads or the splits is reduced and so is the probability of structurally controlled falls of ground.

5.4.4 Sacrificial road

This technique has been used successfully in the coalfield at places such as Arnot where guttering was once experienced in the chainroads (Minney and Munsamy, 2004). The technique consists of mining a roadway (sacrificial road) ahead of the rest of the faces where failure is expected to occur so as to relieve these roadways from stress.

This technique was trialed at Nooitgedacht without any success (Minney and Munsamy, 2004). The sacrificial road was mined first at one centre ahead of the rest of roadways without success, and then at two centres ahead of the rest of roadways, also without success. It was observed that the sacrificial road showed very little sign of stress,which was later confirmed by Sonic Probe extensometers installed in the roof, while the rest of roadways were experiencing stress damage through guttering as usual.

5.4.5 Use of a slot cut in the roof

Minney and Munsamy (2004) found using numerical modelling that by cutting a slot through the immediate shale roof up to the bedding plane, plastic strain reduces by 50%. However, attention was drawn to the fact that such a slot creates a cantilever beam and that adequate support to keep this cantilever from falling was required.

5.4.6 Undercutting

Many collieries within the Witbank area leave 0.5 m of coal in the roof. This practice, whereby a layer of coal is left in the roof, is referred to as Undercutting. The reasons why undercutting is practiced are many. Sometimes undercutting is used to seal off a layer susceptible to weathering such as shale or mudstone. However, it might also be that the roof is undulating or the top part of the seam is of poor quality and therefore undercutting is the only way to prevent dilution. In addition, undercutting can help create a solid beam in heavily jointed roof.

During various site visits it was noticed that collieries leaving 0.5 m coal in the roof experienced fewer horizontal stress effects compared with those where undercutting is not practiced. Therefore it was concluded that undercutting could be a potential mitigating factor for horizontal stress. In order to evaluate this, a series of numerical models was set up using the finite element code Phase2 of Rocscience as shown in Figure 5-82. Two scenarios were

run, the first scenario was run without coal in the roof whereas the second one was run with 0.5 m coal in the roof. For each scenario the k-ratio in the immediate roof was varied from 1 to 3. The number of yielded elements in the immediate roof was used as indicator of failure. Also, for simplicity only the immediate roof was assigned plastic properties while the rest of the model (overburden, coal seam, and floor) was maintained elastic. For the plastic material, a generalised Hoek-Brown failure criterion was used. Table 5-16 summarises the material properties used in the numerical modeling.

Table 5-16 Summary of material properties used in the numerical modeling

Properties	Immediate roof	Coal	Overburden
Initial element loading	field stress & body force	field stress & body force	field stress & body force
Unit weight	0.025 MN/m3	0.015 MN/m3	0.015 MN/m3
Elastic type	isotropic	isotropic	isotropic
Young's modulus	17607 MPa	17607 MPa	17607 MPa
Poisson's ratio	0.3	0.3	0.3
Failure Criterion	Generalized Hoek-Brown	Generalized Hoek-Brown	Generalized Hoek-Brown
Material type	Plastic	Elastic	Elastic
Dilation Parameter	0	5 MPa	5 MPa
Compressive strength	5 MPa	2.93725	2.93725
mb parameter	8.32221	0.108368	0.108368
s parameter	0.108368	0.500593	0.500593
a parameter	0.500593	None	None
Residual mb parameter	8.32221	0	0
Residual s parameter	0.108368		
Residual a parameter	0.500593		
Piezo to use	None		
Ru value	0		

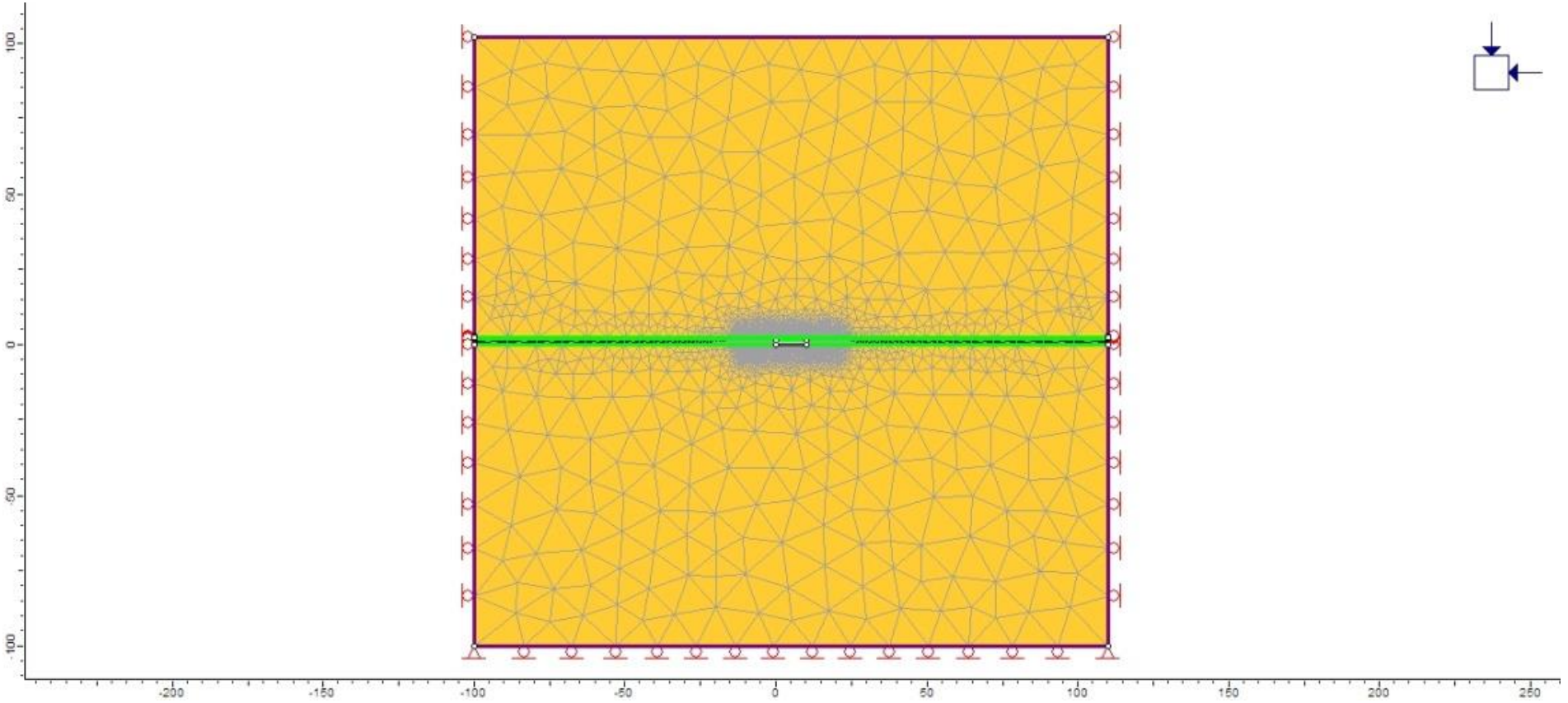


Figure 5-82 Phase2 Model set up to analyse effect of undercutting

The graph in Figure 5-83 illustrates variations of number of yielded elements as a function of k-ratio in the immediate roof. It can be seen that there is a marked difference between the scenario with coal and the one without coal for a k-ratio less than 2. Beyond a k-ratio of 2, almost the same amount of damage is caused to the roof in both scenarios. From this analysis it can be concluded that undercutting can reduce the risk associated with horizontal stress for relatively low values of horizontal stress. For higher values of horizontal stress, undercutting does not reduce risk associated with horizontal stress, but acts as liner around the roadway.

Undercutting can be viewed as a loss of coal. In some instances undercutting can even lead to ventilation problems in that it reduces the cross section of tunnels and therefore increases the hydraulic resistance. In addition, the coal left in the roof deteriorates over time and spalls off. This on its own can constitute a serious hazard especially in areas in which personnel and equipment have access. Results of Phase2 modeling are presented in Figure 5-84.

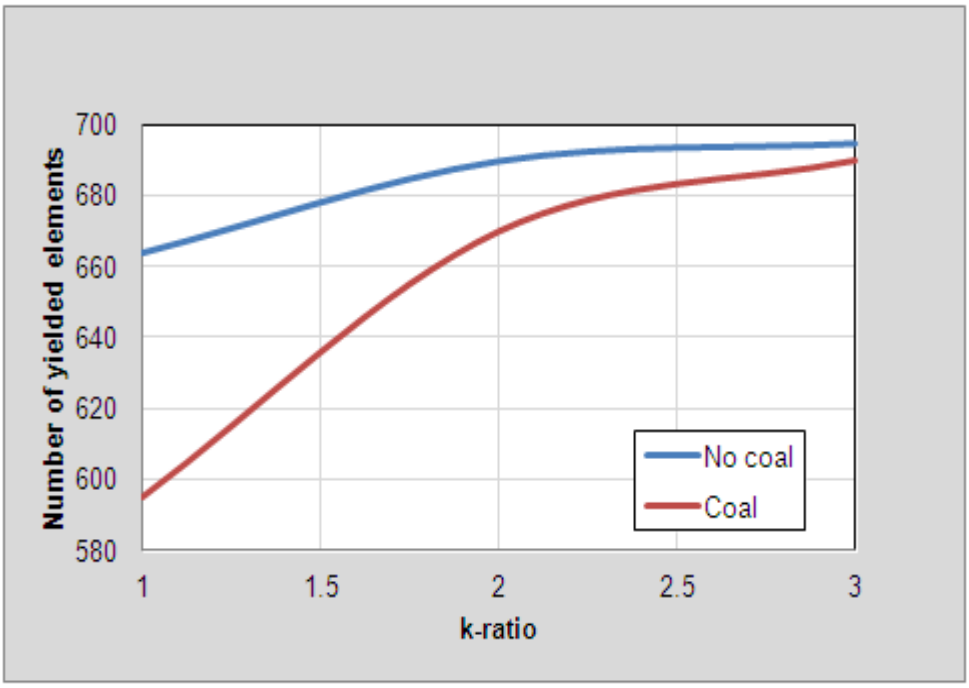
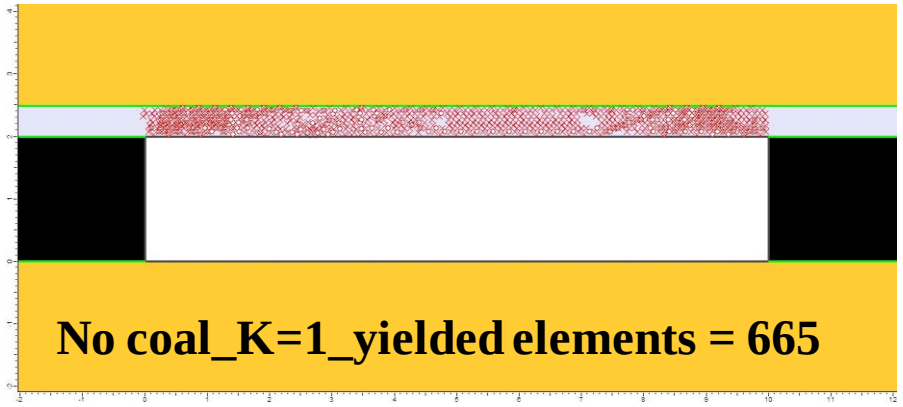
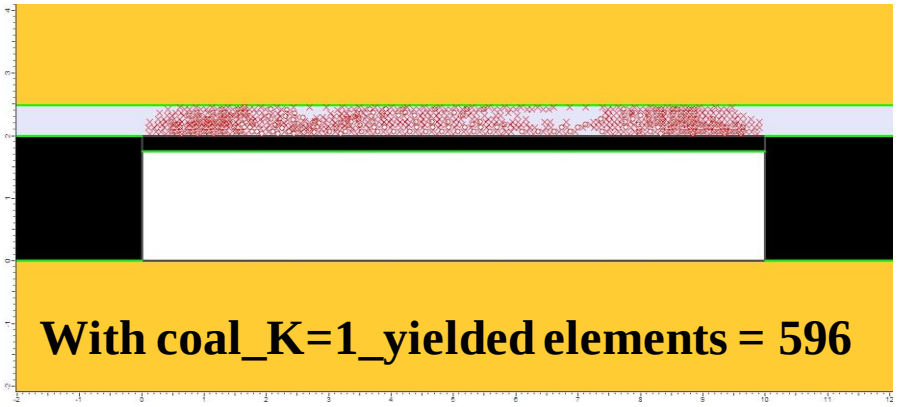
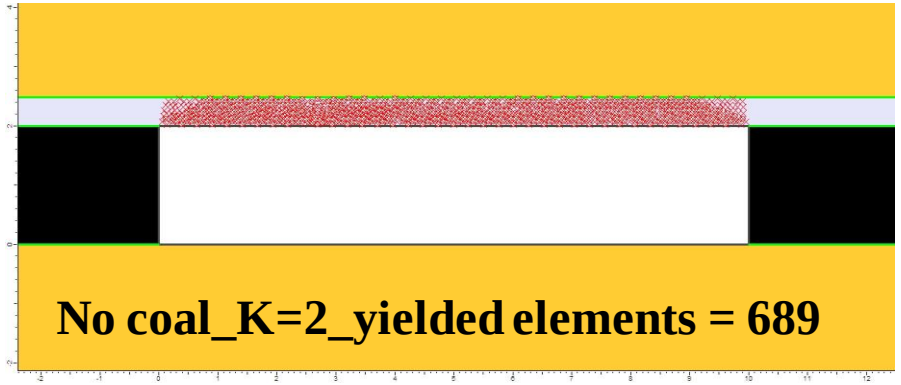


Figure 5-83 graph showing number of yielded elements versus k-ratio in the immediate roof







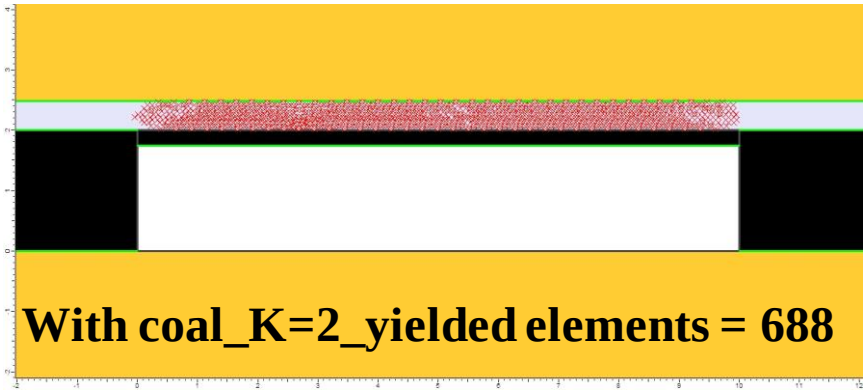


Figure 5-84 Results of the Phase2 undercutting Model

5.4.7 Change of mining parameters

Another operational way of coping with deleterious effect of horizontal stress in mining is by reducing mining parameters such as the cut out distance and the bord width.

Reduction of cut out distance

The safe cut out distance in South African mines has been studied by Canbulat and van der Merwe (2000). Underground experiments were conducted in 13 collieries, in four seams. A comprehensive database was compiled based on information collected from 350 panels. Geotechnical areas were defined based on roof and discontinuity ratings. From these results, it was found that South African collieries can be subdivided into five groups with the majority of South African production coming from one in particular.

A sonic probe extensometer was used to monitor the roof at the face and at the middle of the cutout. The roof was left unsupported for about 48 hours. From these observations, it was found that the most critical parameter in the derivation of the cut out distance is the bord width, which determines the amount of deformation that the roof will undergo. Similar results were confirmed by numerical analysis.

In addition, it was found that most of the maximum deformation in the roof was taking place before the ratio of the cut out distance to the bord width exceeds two. After a ratio of two, the maximum deformations stabilised considering that no geological and stress related factor influence the behaviour of the roof. Therefore it was recommended that the limitation to cut out distance for a given geotechnical condition should be based on detailed observations, roof hazard plans, geological information, roof lithology and support performance.

2D numerical modeling was carried to illustrate the effect of reducing the cut out distance on the stability of the roof in coal mines subject to high horizontal stress. In this analysis two cut out distance scenarios were chosen, 3 and 15 m. The first step in this analysis consisted of calculating internal pressures which simulate the support provided by the face at 3 and 15 m. The second step consisted of varying the horizontal stress (K-ratios) in the two scenarios and evaluating the condition of the roof.

a. Internal pressure

Phase2, the Rocscience 2D finite element program used for the analysis, allows internal pressure to be applied to excavation surfaces as a fraction of the initial field stress. Therefore, in this part of the analysis, the aim was to determine the fractions of the initial field stress

which correspond to situations of 3 and 15 m from the face. The curve of displacements as a function of distance from the face presented in Figure 5-85 was used. By applying a support pressure, the modeling of the tunnel, which is a three dimensional problem in nature, was reduced to a 2D problem.

In Figure 5-85, the x values corresponding to 3 and 15 m were determined using a tunnel diameter equal to the diagonal of the cross section of the roadway being modelled (D= 10.2 m). This resulted in x values of 0.3 m and 1.5 m for 3 and 15 m from the face respectively. The corresponding values of y (wall displacement/maximum displacement) were read off the graph and validated by using the formula in Figure 5-85. Values of 0.46 and 0.9 were obtained as y values for 3 and 15 m respectively. The maximum displacement was obtained by running an elastic Phase2 model with zero internal pressure to simulate a situation at an infinite distance from the face. A hydrostatic state of stress (k-ratio equal to 1) was used as field stress. The maximum displacement was found to be 0.0015 m. The wall displacements at 3 and 15 m from the face were calculated by multiplying the maximum displacement by the corresponding y values of 0.46 and 0.9. Values of 0.0007 and 0.00135m were obtained for 3 and 15 m from the face respectively.

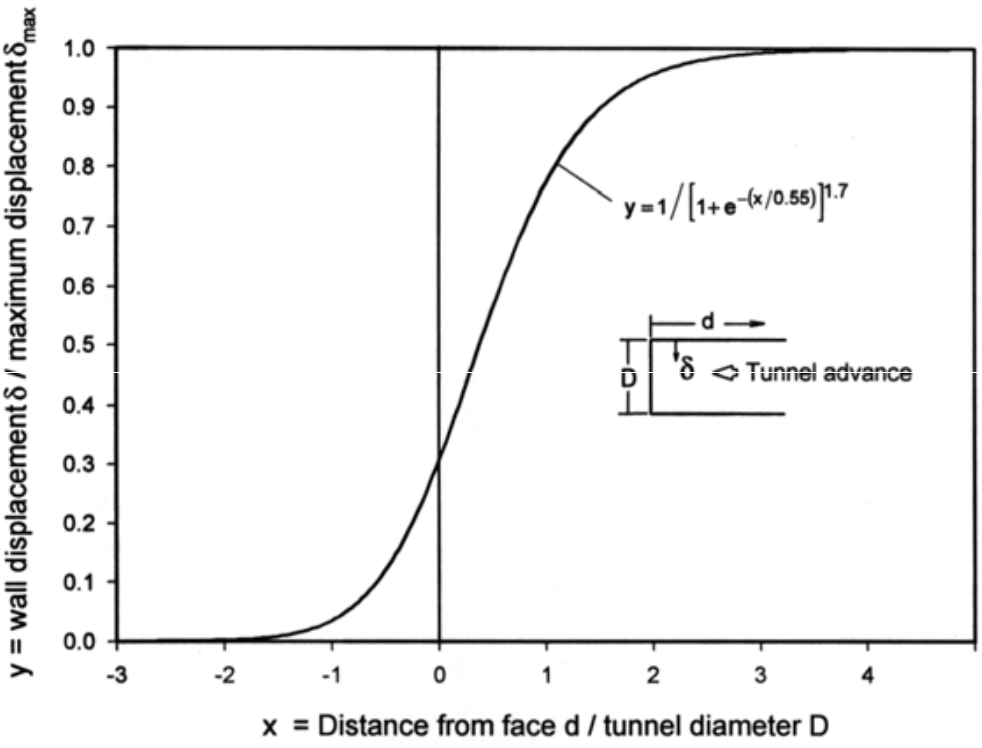


Figure 5-85 Tunnel wall displacements as a function of distance from the face (after Hoek 1999)

To finally determine the fraction of the field stress to apply to the surface of the roadway in the 2D model in order to simulate the face advances of 3 and 15 m, the relationship between the wall (roof) displacement and the internal support pressure as a fraction of the field stress was determined. This relationship was determined by running a Phase2 model in which various fractions of the field stress were, in turn, applied as internal pressures. From this

analysis, the relationship in Figure 5-86 was obtained. It was found that the wall (roof) displacements of 0.0007 (3m from the face) and 0.00135 m(15 m from the face) correspond to 50% and 11% of the initial field stress respectively. Therefore, an internal pressure of about half (50%) of the field stress was to be applied to the excavation boundary in the 2D model to simulate a 3 m face advance and 11%, a 15 m advance. Those factors (0.5 and 0.11) were used in the remainder of the numerical modeling.

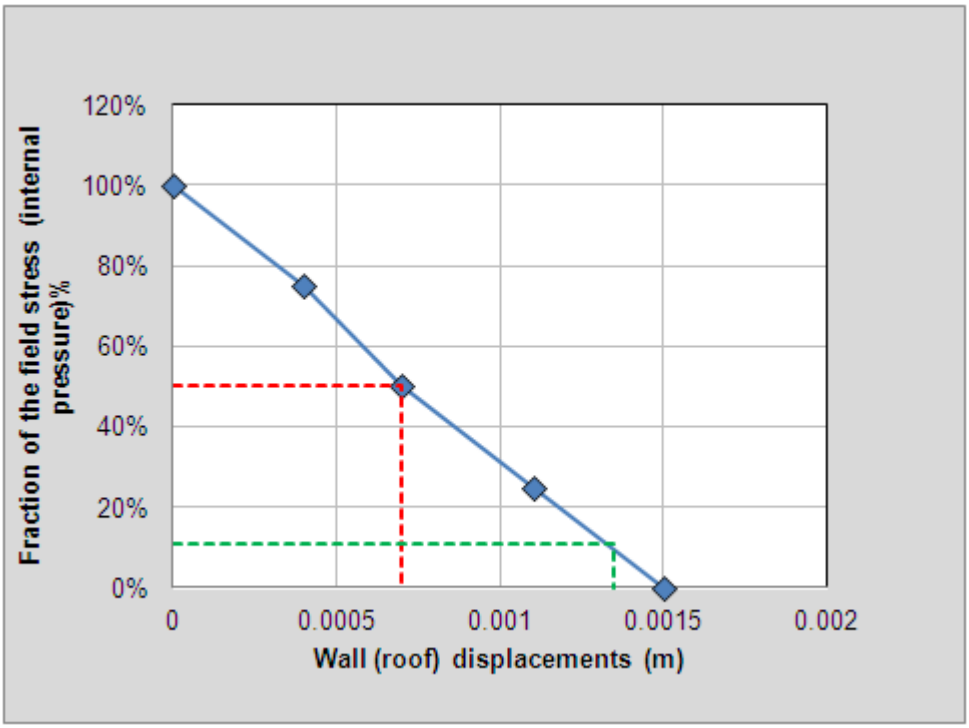


Figure 5-86 Numerical modeling result showing wall (roof) displacement (m) as a function of % of field stress

b. Change of horizontal stress (k-ratio)

The k-ratio was increased from 1 to 6 to simulate cases of lower and higher horizontal stresses. The Hoek-Brown criterion was used as the failure criterion. Scenarios at 3 and 15 m from the face were run for the k-ratio varying from 1 to 6. In each model, the number of yielded elements was monitored and used as stability indicator. The result of the analysis is presented in Figure 5-87.

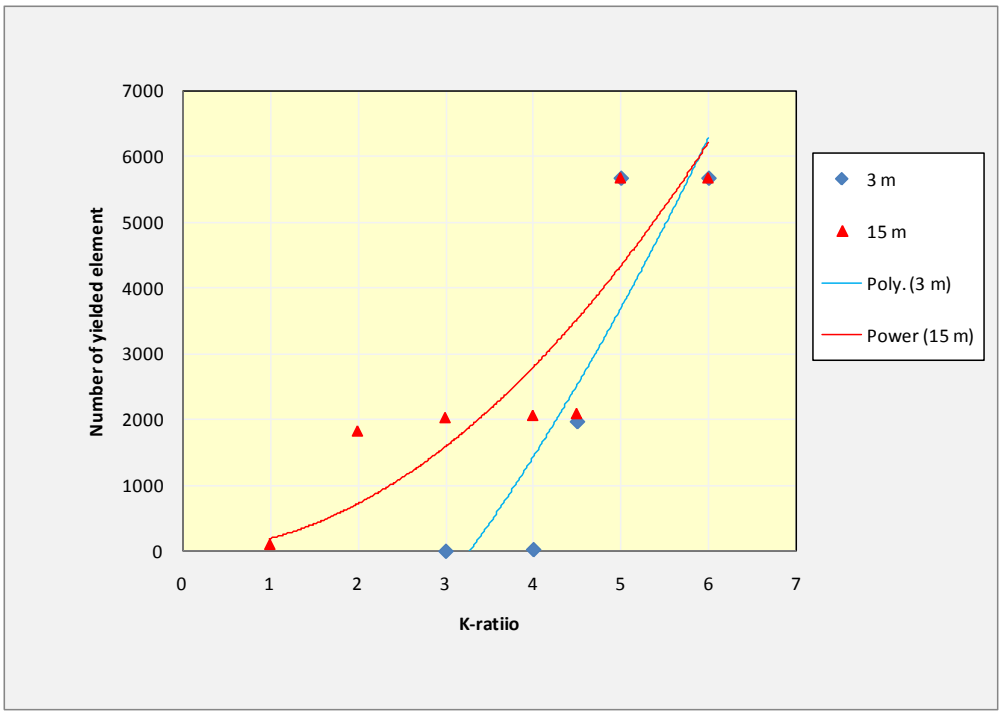


Figure 5-87 Graph showing number of yielded element in the roof versus k-ratios at a distance of 3 m from the face and 15 m from the face

The graph in Figure 5-87 indicates the following:

In both cases (3 and 15 m face advance), there is a probable increase of instability as the k-ratio (horizontal stress) increases;

A change of cut out distance from 15 m to 3, improves significantly the stability of the roof at lower values of k-ratio (less than 4); and

For higher values of k-ratio, the improvement in stability as a result of change in cut out distance reduces significantly. Beyond a k-ratio of 6 there is no difference between the two scenarios.

The reduction of the bord width is used as an operational technique to counter high horizontal stress effects. In essence, the portion of the roof between two pillars can be likened to a clamped beam. Thus, reducing the bord width implies a stiffer system and therefore less stress damage.

5.5 Conclusion

Observations made underground have confirmed the NNW-SSE orientation of the major horizontal principal stress in the Witbank and Highveld coalfields. These observations have also indicated that some collieries experience damage due to stress, while others also have stress related issues.

Stress measurement data collected from collieries where in situ stress measurements were carried out was gathered into a comprehensive database and analysed. Various trends such as K-ratio as a function of depth were identified and proposed for use in the design. However, at this stage, no clear correlation has been identified between the values of horizontal stress and the stiffness of the rock in which the stress measurement was conducted.

A stress map has been developed based on underground observations and the stress measurements. In the process, more importance was given to underground stress observations compared to the stress measurements. This was due to the low correlation obtained between stress measurements and actual stress related damage underground. The map derived predicted that the south-east part is more prone to stress related problems than the rest of the coalfields.

Methods to combat the deleterious effect of stress were identified. Numerical modelling was used to assess the relevance of some of these methods in a relatively highly stressed environment.

CHAPTER 6

Conclusions and Recommendations

Research in coal mines around the world has indicated that horizontal stress can manifest in form of guttering or buckling. Sometimes, the failure is associated with the presence of structural features such as slips and joints.

Numerical modelling has shown that the effect of horizontal stress depends largely on:

- the geological contrast of the roof (contrast in stiffness);
- the difference in magnitude between horizontal and vertical stresses; and
- Strength of coal compared to the strength of roof.

Sometimes, horizontal stresses have a stabilising effect. In this case, failure occurs where the clamping forces due to high horizontal stress decreases.

High horizontal stress can have various origins such as:

- Poisson's effect, where horizontal stresses build up as a result of restricted lateral deformation in the ground.
- Tectonic effect, where horizontal stress is considered to be generated as the result of moving tectonic plates which push against each other.
- Residual effect, where an unusual k-ratio observed at shallow depth is the result of thousands of metres of ice and magma covering some parts of the earth, which were eroded during geological time. As a result, the vertical stress was relaxed, whereas the horizontal stress remained locked in.
- Magmatic intrusion effect, where localised increase of horizontal stress can be the result of the intrusion of a magmatic body such as a dyke.

As part of this research, numerical analysis was conducted to illustrate how the erosion of the large thickness of sediments associated with the formation of the coal has resulted in high k-ratio observed at shallow depth. The effect of weathering on horizontal stress was also investigated through elasto-plastic analytical and numerical modelling. It was shown that both depth of weathering and the contrast in stiffness between the weathered horizon and the competent rock beneath it are major contributors to high horizontal stress. Indications of high

horizontal stress associated with weathering was observed in the Highveld coalfield on the national road N17.

Finite element analysis was also used to illustrated stress distributions around topographic features such as hilly districts and basins. This analysis has shown that for hilly districts formed either by erosion or filled by sedimentation, higher k-ratios form on top and in the valleys on both sides of the hill, while a zone of relatively low k-ratio forms at the core of the hill. However, this effect is more significant when the hilly district is formed by erosion than by sedimentation.

Finite element analysis has also shown that for a basin formed by erosion, the magnitude of horizontal stress around the edges of the basin is higher than in the centre. The magnitude of the maximum horizontal stress is a function of the basin width. The distance at which the maximum stress occurs was found to be the same for various basin widths. The same observation was made for basins with sediments.

Boundary element analysis was carried out to analyse stress distributions around simple excavations. As one would expect, the horizontal stress component concentrated in the roof and floor, whereas the vertical component concentrated in the side walls. However, the level of concentration depends on the shape of the concentration. Four different shapes of excavation were considered in this study even though openings in South African coal mines are almost always rectangular.

The mining methods commonly used in the Witbank and Highveld coalfields are:

- Bord and Pillar mining;
- Longwall mining;
- Pillar extraction; and
- Multiseam mining.

The impact of each of the mining methods on the stress regime depends mainly on the damage to the rock mass that this method produces and the volume of void left after mining. As a result, total extraction methods (Pillar extraction and longwall) will tend to have greater impact on stress than the conventional bord and pillar mining method.

In the Witbank and Highveld coalfields, over many years, bord and pillar has been the most used mining method. The most popular methods of design of bords and pillars have been summarised as part of this research. However, with the increasing depletion of reserves in these two coalfields, pillar extraction is practised more and more in spite of operational and safety issues associated with the method. Wherever conditions are suitable, other high extraction mining methods such as longwall mining are also used.

Multiseam mining is a common reality in the Witbank coalfield and requires a different design approach. Sometimes the two coal seams are mined simultaneously, but sometimes, there is one seam which was mined in the past and the actual mining is carried out above or underneath old mine workings.

Observations made underground have confirmed the NNW-SSE orientation of the major horizontal principal stress in the Witbank and Highveld coalfields. These observations have also indicated that some collieries experience damage due to stress, while other do have stress related issues.

Stress measurement data collected from collieries where in situ stress measurements were carried out was gathered into a comprehensive database and analysed. Various trends such as K-ratio as a function of depth were identified and proposed for use in the design. However, at this stage, no clear correlation has been identified between the values of horizontal stress and the stiffness of the rock in which the stress measurement was conducted.

A stress map has been developed based on underground observations and the stress measurements. In the process, more importance was given to underground stress observations compared to the stress measurements. This was due to the low correlation obtained between stress measurements and actual stress related damage underground. The map derived predicted that the south-east part is more prone to stress related problems than the rest of the coalfields.

Methods to combat the deleterious effects of stress were identified. Numerical modelling was used to assess the relevance of some of these methods in a relatively highly stressed environment.

Although very useful, this study was based on limited data. It is therefore important to update the database in order to increase the level of confidence. It will be interesting for further studies to be aimed specifically at understanding better the Wegener anormally and how it affects stress orientation in the Witbank and Highveld area. In this study, it was envisaged that this not well understood tectonic phenomenon might have a significant influence on the pattern of stress as observed in the Witbank and Highveld.

In addition, it is envisaged that a map of weathering across the Witbank and Highveld coalfield will be a valuable contribution to the evaluation of risk associated with stress. This map could not be constructed as part of the present research because of lack of borehole data. It is therefore suggested that further studies be geared towards the collection and analysis of weathering data across the coalfields.

References

ADAMS, D. (2002). Final Project Report - Survey of Horizontal Stress in Coal Mines from Available Measurements and Mapping. Johannesburg: SIMRAC.

ALAN, B., and JOHN, C. (2003). "Tensile Roof Failure arising from horizontal compressive stress and geological slips." *22nd International Conference on Ground Control in Mining.* Morgantown, WV: Coal Industry Publishing Co.

ANDREOLI, M.A.G (2007) "Intraplate stress, seismicity and neotectonics in western southern Africa: a link to the African Superplume." 10 th SAGA Bennial Technical Meeting and Exhibition, October 24-26, pp 1-4.

ANDREOLI, M.A.G.; DOUCOURE, M; VAN BEVER DONKER, J; BRANDT, D and ANDERSEN, N.J.B. (1996) "Neotectonics of southern Africa - a review." Africa Geoscience Review, pp 1 - 16.

ANDREOLI, M.A.G, interview by Joseph Muaka and Nielen v d Merwe. Personal Communication (May 04, 2011).

ARNOT COAL (2009). Code of Practice to combat roof fall accidents in Underground Coal Mines. Rock-001, Geotechnical Services,.

ATLAS COPCO (2008). Mining Methods in Underground Mining. Sweden: Ulf Linder.

BAEK, S-H; MOON, H.K.; PAR, S.G.; MOON, S.H.; KIM, C.Y., and KIM, K.Y. (2006) "Analysis of the distribution of rock stress ratio and its influence on the behaviour of underground opening." In situ Rock Stress Measurement , Interpretation and Applications. London: Taylor & Francis Group, pp 279-287.

BEUKES, J.S. (1990). *Stooping Practices in South Africa Collieries.* Reference Report No. 43/90, Chamber of Mines Research Organisation of South Africa.

BIENIAWSKI, Z.T., and. VAN HEERDEN, W.L. (1975) "In Situ Tests on Large Rock Specimens." Int. J. Rock Mech, Min. Sci.t Geomech. Abstr.,

BIRD, P.; BEN-AVRAHAM, Z.; SCHUBERT, G.; ANDREOLI, M.A.G. and VIOLA, G. (2006) "Patterns of stress and strain rate in southern Africa." Journal of Geophysical Research, 111p.

BRADY, B.H.G, and BROWN, E.T. (2006). Rock Mechanics For Underground mining. Dordrecht: Springer,.

BUCHAN, I.F.; ENGELBRECHT, C.F.; ERASMUS, B.J., FAUCONIER, C.J.; INCH, J.D.; and WAGNER H. (1981). "Paper E." SAIMM Vacation School (SAIMM).

CANBULAT, I., AND J.N. VAN DER MERWE. Safe mining face advance and support installation practice in mechanical miner workings under different geotechnical conditions. COL 609, 2000-0154, SIMRAC, 2000.

CARTWRIGHT, P.B. (1997). "A Review of Recent In-situ Stress Measurements in United Kingdom Coal Meausres Strata." Proceedings of the International Symposium on Rock Stress. Kumamoto, Japan, pp 469-474.

CHU, D, and GORDON, R. G. (1999). "Evidence for motion between Nubia and Somalia along the Southwest Indian ridge." Nature 394, pp 64-67.

COAL MINE.ART. Britannica Online Encyclopedia. 2011. http://www.britannica.com/EBchecked/media/113913/Schematic-diagram-of-an-underground-coal-mine-showing-surface-facilities (accessed june 17, 2011).

COLWELL, M.; FRITH, R. and MARK, C. (1999). "Analysis of longwall tailgate serviceability (ALTS): a chain pillar design methodology for Australian

conditions." Edited by C Mark, K.A Heasley, A.T. Iannocchione and R.J. Tuchman. *Workshop on Coal Pillar Mechanics and Design.* Pittsburgh: NIOSH, pp 33-48.

COOK, N.G.W. HODGSON, K. and HOJEM, J.P.M. (1971) "A 100 MN Jacking System for Testing Coal Pillars Underground." Journal of South African Inst. Min Metall., pp 215-224.

DICKINSON, W.R. (1974). "Plate tectonics and sedimentation." Publ. Soc. Econ. Paleontol. Miner, pp 1-27.

DOHM, C. "Statistical Techniques in mineral valuation." Johannesburg, April 2010.

DOUGALL, A.W. (2010). A review of current and expected underground coal mining method & profiles with an evaluation of the best practices associated with these. MSc (Eng) dissertation, Johannesburg: University of the Witwatersrand,.

DU PLESSIS, P. (2008). The relationship between geological structures and dolerite intrusions in teh Witbank Highveld Coalfield, South Africa. Magister Scientiae, Blomfontein: University of the Free State, 165p.

ESTERHUIZEN, G.S.; DO LINEAR, D.R. and IANNACCHIONE, A. (2008). "Field Observations and Numerical Studies of Horizontal stress effects on roof stability in US Limestone Mines." Ground Support in mining and Civil engineering construction. Cape-town: SAIMM,. 103-118.

GOLDEN SOFTWARE. Using Shuttle Radar Topography Mission (SRTM) Data in Surfer. 2011. www.goldensoftare.com/newsletter/Issue52.shtml (accessed febuary 15, 2011).

GREENSHIELDS, H.D. (1986). *Eastern Transvaal coalfield.* Edited by C.R. Anhaeusser and S. Maske. Vol. I and II. Johannesburg: Mineral Deposits of Southern Africa.

GRODNER, M.W. (2002). A regional, 3-D computer based sedimentological model of the Permian Witbank Coalfield, South Africa. MSc Dissertation, Johannesburg: University of Johannesburg.

GUANGYU, L; BAI, S. and JIGUANG, L. (1986) "Twenty years of experience on in-situ stress measurements in China." Rock stress and Rock stress measurement. Stockholm: Centek Publishers, pp 79-87.

HEIDBACH, O.; TINGAY, M.; BARTH, A.; REINECKER, J.; KURFEß, D. and MÜLLER, B. (2008). Stress Map of the WSM 2008 release.. http://dc-app3-14.gfz-Potsdam.de/pub/stress_data/stress_data_frame.html (accessed Febuary 8, 2011).

HILL, R.W. (1994). Multiseam design procedures. Research report Col 026, Johannesburg: SIMRAC.

HOEK, E. (1999) interview by Rocscience. Personnal Communication.

HOEK, E. (1966). First report on the Testing of Large Scale Coal Specimens In Situ. MEG 452, CSIR.

JOHNSON, M.R. (1997). "The foreland Karoo Basin, South Africa." Edited by R.C. Selley. *Elsevier* (Sedimentary Basins of Africa), pp 269-317.

JOHNSON, M.R. (2006). "Sedimentary Rocks of the Karoo supergroup." The Geology of South Africa. Johannesburg: Geological Society of South Africa, Johannesburg & Council of Geoscience, Pretoria , pp 461-499.

KELLY, M; GALE, M. and CRAIG, S. L. (2002). "Integrating tools for longwall geomechanics." *Int. J. Rock Mech.Min.Sci.*, pp 661-676.

LEES, D. interview by Joseph Muaka. Personal communication (May 19, 2011).

LIND, G.H. (2005). "An Integrated Approach at Reducing The Risks Associated with Underground Coal Pillar Extraction of Bord and Pillar Development Areas in South Africa." The 19th International Mmmg Congress and Fair of Türke) IMCET200S. Izmir Turkey, pp 19-27.

MADDEN, B.J. (1991). "Re-assessment of Coal Pillar Design." South African Institute of Mining and Metallurgy, pp 27-37.

MARK, C. and ZELANKO, J.C. (2001). "Sizing of Final Stumps for Safer Pillar Extraction." *22th International Conference on Ground Control in Mining.* Morgantown, WV, pp 59-66.

MINNEY, D. and MUNSAMY, L. (2004). "Stress Damage at a Coal Mine Roof at Shallow Depth." Second International Seminar on Deep and High Stress Mining. Johannesburg: SAIMM, pp 293-312.

MINNEY, D. interview by J M Muaka. Palaeo floor (September 2010).

MINNEY, D. interview by Joseph Muaka. Personal communication (May 2011).

MURALI, M. and PENG, S. S. (2005)."Numerical simulation of cutter roof failure under weak roof conditions." SME Annual Meeting. Salt Lake City, Utah, pp 1-11.

NDLOVU, X and STACEY, T R. (2007)"Observation and analyses of roof guttering in a coal mine." SAIMM, pp 477-491.

ORAVECZ, K.I. (1973). Loading of Coal Pillars in Bord and Pillar workings. Ph.D Thesis, Johannesburg: University of the Witwatersrand,.

POULOS, H.G. and DAVIS, E.H. (1974). Elastic solution for Soil and Rock Mechanics. New York: Wiley.

ROCSCIENCE (2009). RocSupport: Rock support interaction and deformation. Tutorial Manual, Rocscience Inc,.

SALAMON, M.D.G.and MUNRO, A.H. (1967). "A Study of the Strength of Coal Pillars." J. South Afr. Inst. Min. Metall, pp 56-57.

SALAMON, M.D.G.and ORAVECZ, K.I. (1976). Rock Mechanics in Coal Mining. P.R.D. Series No.198, Chamber of Mines of South Africa.

SALAMON, M. and CANBULAT, I. (2006). "Seam-Specific Pillar Strength Formulae for South African Collieries." Golden Rocks 2006, The 41st U.S. Symposium on Rock Mechanics (USRMS), American ROCK MECHANICS ASSOCIATION, pp 1154-1160.

SASOL. (1998). "Code of Practice.".

SNYMAN, C.P. (1998). *The Mineral Resources of South Africa.* Edited by M.G.C. Wilson and C.R. Anhaeusser. Handbook 16 vols. Pretoria: Council of Geoscience.

WESSELOO, J. and STACEY, T. R. (2006). "Updated in situ sress database for Southern Africa." In situ Rock Stress measurement, Interpretation and Application. London: Taylor & Francis group, pp 467 -471.

STACEY, T.R. and WESSELOO, J. (1998) Evaluation and Upgrading of Records of Stress Measurement Data in the Mining Industry. Final Project Report, Johannesburg: SIMRAC.

STEPHANSSON, O. and AMADEI, B. (1997). Rock stress and its measurement. London: Chapman & Hall,.

STEPHANSSON, O. (2003). "Proceedings of the third international symposium on Rock Stress." Lisse: Swets & Zeitlinger, pp 49-59.

SWOLFS, H.S. and SAVAGE, W.Z. (1986). "Topographic modification of in situ stress in extensional and compressional tectonic environments." Rock Stress and Rock Stress Measurements. Stockholm: Centek Publishers, pp 89-97.

SU, W.H. and PENG, S.S. (1982) "Cutter Roof and its Causes." *Coal Mine Ground Control.* Mining Science and Technology, p 491.

TANI, M. E. (1997). "Virgin state of stress and discontinuities of rock masses." Environmental and Safety concerns in underground construction: 668-672.

THOMAS, E; SEELING, C.H., PERZ, F and HANSEN, M.V. (1948). "Control of Roof and Prevention of Accidents from Falls of Rock and Coal: Suggested Roof Supports for use at Faces in Conjunction with Mechanical Loading." USBM IC 7471,.

VAN DER MERWE, J.N.and OLIVIER, F.T. (1992). "The development of a crush pillar system for high extraction coal mining." *Journal of the South African Institute of Mining and Metallurgy*.

VAN DER MERWE, J.N. (1993). "Revised Strength Factor for Coal in Vaal Basin." J. S. Afr. Inst. Min. Metall, pp 71-77.

VAN DER MERWE, J.N. (1998). *Practical Coal Mining Strata Control.* 2nd Edition. Johannesburg: ITASCA Africa (Pty) Ltd,.

VAN DER MERWE, J.N. (2003). "New Pillar strength formula for South African coal." J. S. Afr. Inst. Min. Metall, pp 281-292.

VAN DER MERWE, N. and MADDEN, B. (2010). Rock Engineering of Underground Coal Mining. Johannesburg

VAN HEERDEN, W.L. (1975). "In situ complete stress-strain characteristics of large coal specimens." *Journal of the South African Institute of Mining and Metallurgy*, pp 15-20

VAN NIEKERK (1995). Geochemistry of dolerites and the intrusion mechanisms of two major sills in Secunda. MSc Dissertation, Capetown: University of Stellenbosh,.

VIOLA, G.M.; ANDREOLI, M.A.G.; BEN-AVRAHAM, Z.; STENGEL, I. and RESHEF, M. (2005). "Offshore mud volcanoes and onland faulting in southwestern Africa: Neotectonic implications and constraints on the regional stress field." Earth and Planetary Science Letters, 231, pp 147-160.

WAGNER, H and SCHUMANN, E.H.R. (1996). The effects of total coal seam extraction on the surface structures. Report 20/85, Chamber of Mines of South Africa Research Organisation,.

WAGNER, H. (1974). "Determination of the complete Load-Deformation Characteristics of Coal Pillars." Proceedings of the 3rd ISRM Congress. pp 1076-1081.

WHITTAKER, B.N. (1974). "An Appraisal of strata control practice." *Min. Engr.* pp 134: 9-24.

Appendix A Coalfields stress database

a_AVG	b_GG	c_IG	d_COUNT	e_PROVINCE		f_LOCALITY	g_SITE	h_LOCATION	LON	LAT	DATE	i_METHOD	j_DEPTH
			South afric	MP		ARNOT	ARNOT colliery	D1 South R3 stub	29.78	-25.9	19991123	CSIRO Hollow	53.4
			South afric	MP		ARNOT	ARNOT colliery	E5 belt drive stub	29.78	-25.9	19991119	CSIRO Hollow	53.4
			South afric	MP		ARNOT	ARNOT colliery	shaft 10	29.78	-25.9	19991129	CSIRO Hollow	51.5
			South afric	MP		KHUTALA	KHUTALA colliery	22/3-4 area_barrier pillar split 33	29	-26.12	20051114	CSIRO HI Thinwall Cell	71.7
			South afric	MP		KHUTALA	KHUTALA colliery	22/3-4 area_barrier pillar split 33	29	-26.12	20051115	CSIRO HI Thinwall Cell	71.7
			South afric	MP		KHUTALA	KHUTALA colliery	22/3-4 area_barrier pillar split 35	29	-26.12	20051118	CSIRO HI Thinwall Cell	71.7
			South afric	MP		KHUTALA	KHUTALA colliery	22/3-4 area_barrier pillar split 10	29	-26.12	20051123	CSIRO HI Thinwall Cell	78
			South afric	MP		BANK	BANK Colliery	5 SHAFT	29.46	-25.97	20000705	CSIRO HI Thinwall Cell	41.4
			South afric	MP		BANK	BANK Colliery	5 SHAFT	29.46	-25.97	20000712	CSIRO HI Thinwall Cell	27.1
			South afric	MP	VLAKLAATGE	GOEDEHOOP	GOEDEHOOP Colliery	Section 2, Panel 1220	29.43	-26.09	20010428	CSIRO HI Thinwall Cell	67
			South afric	MP	Hope	GOEDEHOOP	GOEDEHOOP Colliery	Section 5/6	29.43	-26.09	19990625	CSIRO HI Thinwall Cell	42
			South afric	MP	Hope	GOEDEHOOP	GOEDEHOOP Colliery	Section 5/6	29.43	-26.09	19990630	CSIRO HI Thinwall Cell	42
			South afric	MP		GOEDEHOOP	GOEDEHOOP Colliery	Block 11	29.43	-26.09		CSIRO HI Thinwall Cell	
			South afric	MP		GOEDEHOOP	GOEDEHOOP Colliery	Block 12	29.43	-26.09		CSIRO HI Thinwall Cell	
			South Afric	MP		KRIEL	Kriel Colliery	Sections A18	29.155	-26.195		CSIRO HI Thinwall Cell	
			South Afric	MP		KRIEL	Kriel Colliery	Section M24	29.155	-26.195		CSIRO HI Thinwall Cell	107.5528
			South Afric	MP		KRIEL	Kriel Colliery	Section P30	29.155	-26.195			107.5528
			South afric	MP	DRIEHOEK	BOSJESSPRUIT	BOSJESSPRUIT Colliery	Section 56	29.13	-26.56	20000131	CSIRO HI Thinwall Cell	190
			South Afric	MP		NOOITGEDACHT	Noitgedacht Colliery		29.16	-25.9			30
													40

a_AVG	b_GG	c_IG	d_COUNTR	e_PROVINCE		f_LOCALITY	g_SITE	w_BS1	x_BS2	y_BS3	z_DIPS1	1_DIPS2	2_DIPS3	3_S1	4_S2	5_S3	k_SOB
			South afric	MP		ARNOT	ARNOT colliery	69	159	338	0	8	82	5.7	2.9	1.2	1.2
			South afric	MP		ARNOT	ARNOT colliery	231	140	354	5	7	81	3.7	2.5	1.2	1.2
			South afric	MP		ARNOT	ARNOT colliery	42	307	180	18	15	66	6.4	3.5	1.7	1.2
			South afric	MP		KHUTALA	KHUTALA colliery	174	264	68	1	4	86	4.9	4.4	1.3	1.8
			South afric	MP		KHUTALA	KHUTALA colliery	354	264	96	1	6	83	5.7	4.5	1.4	1.8
			South afric	MP		KHUTALA	KHUTALA colliery	161	69	279	9	16	71	4.7	4.1	1.3	1.8
			South afric	MP		KHUTALA	KHUTALA colliery	186	93	282	4	34	56	4.8	3	1.3	2.0
			South afric	MP		BANK	BANK Colliery	156	326	58	65	24	4	1	0.7	0.2	1.0
			South afric	MP		BANK	BANK Colliery	175	85	278	1	3	87	4.3	3.8	1.5	0.7
			South afric	MP	VLAKLAATGE	GOEDEHOOP	GOEDEHOOP Colliery	336	224	77	16	53	33	5.69	1.36	0.51	1.7
			South afric	MP	Hope	GOEDEHOOP	GOEDEHOOP Colliery	340	223	83	10	34	54	5.2	1.1	0.7	1.1
			South afric	MP	Hope	GOEDEHOOP	GOEDEHOOP Colliery	334	232	79	12	42	45	5.4	1	0.5	1.1
			South afric	MP		GOEDEHOOP	GOEDEHOOP Colliery	338			10						
			South afric	MP		GOEDEHOOP	GOEDEHOOP Colliery	345			10						
			South Afric	MP		KRIEL	Kriel Colliery	300			11						
			South Afric	MP		KRIEL	Kriel Colliery	195	288	89	7	23	66	3.9	3	0.4	2.7
			South Afric	MP		KRIEL	Kriel Colliery	177	63	278	16	52	32	4.3	2.7	2.2	2.7
			South afric	MP	DRIEHOEK	BOSJESSPRUIT	BOSJESSPRUIT Colliery	156	270	62	10	68	20	9.3	5.5	4.1	5.13
			South Afric	MP		NOOITGEDACHT	Noitgedacht Colliery										0.75
																	1

a_AVG	b_GG	c_IG	d_COUNTR	e_PROVINCE		f_LOCALITY	g_SITE	q_SX	r_SY	s_SZ	t_SXY	u_SYZ	v_SZX	l_SH1	m_SH3	n_BSH1
			South afric	MP		ARNOT	ARNOT colliery	5.3	3.2	1.2	0.9	0.1	-0.2	5.699	2.86	-69
			South afric	MP		ARNOT	ARNOT colliery	3.3	3	1.2	0.5	-0.3	-0.1	3.6772	2.581	-52
			South afric	MP		ARNOT	ARNOT colliery	4.674353	4.649345	2.276302	1.306661	1.294395	0.564835	6	3.3	-45.2741
			South afric	MP		KHUTALA	KHUTALA colliery	4.391988	4.892308	1.315703	-0.0581	-0.08477	-0.20795	4.898966	4.385331	-353.463
			South afric	MP		KHUTALA	KHUTALA colliery	4.43	5.65	1.46	-0.12	0.07	-0.35	5.697696	4.461786	-355
			South afric	MP		KHUTALA	KHUTALA colliery	3.87	4.6	1.57	-0.13	-0.22	0.87	4.640108	3.857506	-350.278
			South afric	MP		KHUTALA	KHUTALA colliery	2.5	4.75	1.86	0.28	-0.28	0.73	4.785734	2.469161	-353
			South afric	MP		BANK	BANK Colliery	0.351568	0.60312	0.945312	-0.24174	-0.12184	0.01468	0.8	0.2	-328
			South afric	MP		BANK	BANK Colliery	3.8	4.3	1.51	-0.04	-0.02	0.12	4.3	3.8	-355
			South afric	MP	VLAKLAATGE	GOEDEHOOP	GOEDEHOOP Colliery	1.44422	4.675998	1.439781	-1.60117	0.959534	-0.84122	5.4	0.8	-338
			South afric	MP	Hope	GOEDEHOOP	GOEDEHOOP Colliery	1.712941	4.2	1.087056	-2.11933	1.218401	-0.60448	5	1	-340
			South afric	MP	Hope	GOEDEHOOP	GOEDEHOOP Colliery	1.533561	4.361864	1.004576	-1.63485	0.884722	-0.68599	5.1	0.8	-334
			South afric	MP		GOEDEHOOP	GOEDEHOOP Colliery									-338
			South afric	MP		GOEDEHOOP	GOEDEHOOP Colliery									-345
			South Afric	MP		KRIEL	Kriel Colliery									-300
			South Afric	MP		KRIEL	Kriel Colliery	2.6	3.8	0.8	0.2	-1	-0.1	3.86	2.589	-195
			South Afric	MP		KRIEL	Kriel Colliery	2.354327	4.156855	2.688819	-0.03547	-0.44978	0.245237	4.157552	2.353629	-177
			South afric	MP	DRIEHOEK	BOSJESSPRUIT	BOSJESSPRUIT Colliery	5.137244	8.217957	5.4448	-1.87695	-0.78564	-0.13663	9.2	4.3	-335
			South Afric	MP		NOOITGEDACHT	Noitgedacht Colliery			5.8				10.7	7.44	-20
										1.6				7.5	5.4	-105

a_AVG	b_GG	c_IG	d_COUNTRY	e_PROVINCE		f_LOCALITY	g_SITE	o_K1	p_K3	6_KX	7_KY	8_NO	9_E	10_PR
			South africa	MP		ARNOT	ARNOT colliery	4.749167	2.383333	4.416667	2.666667	0	14.76	0.36
			South africa	MP		ARNOT	ARNOT colliery	3.064333	2.150833	2.75	2.5	0	9.23	0.29
			South africa	MP		ARNOT	ARNOT colliery	2.635855	1.44972	3.895294	3.874454	0	19.77	0.22
			South africa	MP		KHUTALA	KHUTALA colliery	3.723458	3.33307	3.65999	4.076924	23	6.07	0.42
			South africa	MP		KHUTALA	KHUTALA colliery	3.902531	3.056018	3.691667	4.708333	34	6.07	0.42
			South africa	MP		KHUTALA	KHUTALA colliery	2.955483	2.45701	3.225	3.833333	15	6.07	0.42
			South africa	MP		KHUTALA	KHUTALA colliery	2.572975	1.327506	2.083333	3.958333	4	17.32	0.45
			South africa	MP		BANK	BANK Colliery	0.846281	0.21157	0.292973	0.5026	0	12.3	0.28
			South africa	MP		BANK	BANK Colliery	2.847682	2.516556	3.166667	3.583333	0	7	0.27
			South africa	MP	VLAKLAATGE	GOEDEHOOP	GOEDEHOOP Colliery	3.75057	0.55564	1.203517	3.896665	0	21.6	0.22
			South africa	MP	Hope	GOEDEHOOP	GOEDEHOOP Colliery	4.599579	0.919916	1.575762	3.863647			
			South africa	MP	Hope	GOEDEHOOP	GOEDEHOOP Colliery	5.076769	0.796356	1.526575	4.341995			
			South africa	MP		GOEDEHOOP	GOEDEHOOP Colliery							
			South africa	MP		GOEDEHOOP	GOEDEHOOP Colliery							
			South Africa	MP		KRIEL	Kriel Colliery							
			South Africa	MP		KRIEL	Kriel Colliery	4.825	3.23625	3.25	4.75			
			South Africa	MP		KRIEL	Kriel Colliery	1.546237	0.875339	0.875599	1.545978			
			South africa	MP	DRIEHOEK	BOSJESSPRUIT	BOSJESSPRUIT Colliery	1.689686	0.789744	4.281036	6.848297	0	7.7	0.17
			South Africa	MP		NOOITGEDACHT	Noitgedacht Colliery	1.844828	1.282759				12.8	0.4
								4.6875	3.375				13.1	0.32

a_AVG	b_GG	c_IG	d_COUNTRY	e_PROVINCE		f_LOCALITY	g_SITE	11_ROCK	12_SEQUENCE	13_REFF	14_NOTES
			South africa	MP		ARNOT	ARNOT colliery	Sandstone/silstone	Karoo sequence	OS/SA/ARN/4620PC01	No2 seam
			South africa	MP		ARNOT	ARNOT colliery	Sandstone	Karoo sequence	OS/SA/ARN/4620PC01	No2 seam
			South africa	MP		ARNOT	ARNOT colliery	Gritstone	Karoo sequence	OS/SA/ARN/4620PC01	No2 seam
			South africa	MP		KHUTALA	KHUTALA colliery	Mudstone with Sand	Karoo sequence	OS/SA/RMTSA/050129REP01GW	No2 seam
			South africa	MP		KHUTALA	KHUTALA colliery	Mudstone with Sand	Karoo sequence	OS/SA/RMTSA/050129REP01GW	No2 seam
			South africa	MP		KHUTALA	KHUTALA colliery	Mudstone with Sand	Karoo sequence	OS/SA/RMTSA/050129REP01GW	No2 seam
			South africa	MP		KHUTALA	KHUTALA colliery	Mudstone with Sand	Karoo sequence	OS/SA/RMTSA/050129REP01GW	No2 seam
			South africa	MP		BANK	BANK Colliery	Gristone graded into coarse grained Sandstone	Karoo sequence	OS/SA/ANG/BANK4636PC01	No5 seam
			South africa	MP		BANK	BANK Colliery	Gristone graded into coarse grained Sandstone	Karoo sequence	OS/SA/ANG/BANK4636PC01	No5 seam
			South africa	MP	VLAKLAATGE	GOEDEHOOP	GOEDEHOOP Colliery	Sandstone	Karoo sequence	OS/SA/GOE/4677PC01	No4 seam
			South africa	MP	Hope	GOEDEHOOP	GOEDEHOOP Colliery	Carbonaceaous shale	Karoo sequence		No2 seam
			South africa	MP	Hope	GOEDEHOOP	GOEDEHOOP Colliery	Carbonaceaous shale	Karoo sequence		No2 seam
			South africa	MP		GOEDEHOOP	GOEDEHOOP Colliery				No2 seam
			South africa	MP		GOEDEHOOP	GOEDEHOOP Colliery				
			South Africa	MP		KRIEL	Kriel Colliery				No4 seam
			South Africa	MP		KRIEL	Kriel Colliery				No4 seam
			South Africa	MP		KRIEL	Kriel Colliery				No4 seam
			South africa	MP	DRIEHOEK	BOSJESSPRUIT	BOSJESSPRUIT Colliery	Gritstone	Karoo sequence	OS/SA/SAS/4628PC01	C4 Lower seam
			South Africa	MP		NOOITGEDACHT	Noitgedacht Colliery				

Appendix B Sasol Guttering database

ID	Mine	Date	Section	Nearest Peg	Guttering	Floor heave	Ride in side wall	depth of guttering	Tensile fracture
1	Brandspruit	20060401	17		Moderate	No			
2	Brandspruit	20070817	16		No	No			
3	Brandspruit	20070416	16		No	No			
4	Brandspruit	20061017	16		No	No			
5	Brandspruit	20060802	16		No	No			
6	Brandspruit	20071018	17		No	No			
7	Brandspruit	20070416	17		No	No			
8	Brandspruit	20070125	17		No	No			
9	Brandspruit	20060531	17		No	No			
10	Brandspruit	20060401	17		Moderate	No			
11	Brandspruit	20071219	18		No	No			
12	Brandspruit	20071121	18		No	No			
13	Brandspruit	2007023	18		No	No			
14	Brandspruit	20070315	18		No	No			Oblique to split
15	Brandspruit	20060624	18		No	No			
16	Brandspruit	20060126	18		High	No			
17	Brandspruit	20070806	29		No	No			
18	Brandspruit	20080102	29		No	No			
19	Brandspruit	20071128	29		No	No			
20	Brandspruit	20071025	29		No	No			
21	Brandspruit	20070116	29		No	No			
22	Brandspruit	20070201	29		No	No			
23	Brandspruit	20061017	29		No	No			
24	Brandspruit	20060917	29		No	No			
25	Brandspruit	20071018	30		No	No			
26	Brandspruit	20071002	30		No	No			
27	Brandspruit	20070724	30		No	No			
28	Brandspruit	20070510	30		No	No			
29	Brandspruit	20061010	30		No	No			
30	Brandspruit	20060116	30		No	No			
31	Brandspruit	20061011	30		No	No			
32	Brandspruit	20060714	30		Moderate	No			
33	Brandspruit	20071214	32		No	No			
34	Brandspruit	20071018	32		No	No			Planar tensile Cracks
35	Brandspruit	20071009	32		No	No			
36	Brandspruit	20070820	32		No	No			
37	Brandspruit	20061113	32		No	No			
38	Brandspruit	20060517	32		No	No			
39	Brandspruit	20060401	32		Moderate	No			
40	Brandspruit	20060210	32		No	No			
41	Brandspruit	20071219	87		Moderate	No			
42	Brandspruit	20060907	87		No	No			
43	Brandspruit	20060306	87		Moderate	No			
44	Brandspruit	20070914	87		High	No			Jagged cracked // to road
45	Brandspruit	20071219	87		Moderate	No			
46	Brandspruit	20060907	87		No	No			
47	Brandspruit	20060306	87		Moderate	No			
48	Brandspruit	20070914	87		No	No			
49	Brandspruit	20060306	87		Moderate	No			
50	Brandspruit	20070914	30		Moderate	No			
51	Brandspruit	20070717	71D		High	No			
52	Brandspruit	20070711	71A		High	No			
53	Brandspruit	20070524			Moderate	No			
54	Brandspruit	20061123	71D		No	No			Jagged cracked // to road
56	Brandspruit	20061219			No	No			
57	Brandspruit	20070911	Backholing 3E…		No	No			
58	Brandspruit	20070911	71B		No	No			
59	Brandspruit	20061201			No	No			
60	Brandspruit	20061010	71 Stonework		No	No			
61	Syferfontein	20060712			Moderate	No			
62	Syferfontein	200711029	1 stonwork		No	No			
63	Syferfontein	20071004	95		No	No			
64	Syferfontein	20070512	Back area		No	No			
65	Syferfontein	20070403	stonework 9		No	No			
66	Syferfontein	20060503	1 Stonework		No	No			
67	Syferfontein	20060515	span….		No	No			
68	Syferfontein	20060118	Pit3		No	No			
69	Syferfontein	20050510	15/4		No	No			
70	Syferfontein	20050425	92		No	No			
71	Syferfontein	20050315	stonework 9		No	No			
72	Syferfontein	20060807	1		High	High			Active Jagged cracked // to road
73	Syferfontein	20060617	1		Moderate	No		0.5	
74	Syferfontein	20060610	1		Moderate	No			
75	Syferfontein	20050315	1		No	No			
76	Syferfontein	20070309	3		No	No			
77	Syferfontein	20060124	3		Moderate	No			
78	Syferfontein	20050611	4		No	No			
79	Syferfontein	20050511	4		No	No			Planar tensile crack
80	Syferfontein	20061018	5		Moderate	No			Planar tensile crack
81	Syferfontein	20051130	5		High	No			
82	Syferfontein	20050222	6		No	No			
83	Syferfontein	200711006	Stonework 92		No	No			
84	Syferfontein	20071004	92		No	No			
85	Syferfontein	20070717	92		No	No			
86	Syferfontein	20061228	92 down….		No	No			
87	Syferfontein	20060407	old 92		Moderate	No			
88	Syferfontein	20051228	92		No	No			
89	Syferfontein	20050422	92		No	No			
90	Syferfontein	20071004	93		No	No			
91	Syferfontein	20061020	93		No	No			
92	Syferfontein	20080118	95		Moderate	No			
93	Syferfontein	20071113	95		No	No			
94	Syferfontein	20070306	95		No	No			
95	Syferfontein	20070112	95		Moderate	Moderate			

ID	Mine	Date	Section	Nearest Peg	Guttering	Floor heave	Ride in side wall	depth of guttering	Tensile fracture
96	Syferfontein	20060515	95		No	No			
97	Syferfontein	20060103	95		No	No			
98	Twisdraai east	20070518	South 4 Vent shaft area		No	No			
99	Twisdraai east	20061220	South 4 Vent shaft area		No	No			
100	Twisdraai east	20060531	DV55 Prim south	TW726					Single tension Crack
101	Twisdraai east	20060524	Frischgewaagd shaft		No	No			multiple tension crack
102	Twisdraai east	20051209	S4 Dam area		No	No			
103	Twisdraai east	20070531	81		No	No			Planar tensile crack
104	Twisdraai east	20070515	81		No	No			Planar tensile crack
105	Twisdraai east	20071213	81		No	No			
106	Twisdraai east	20060627	81		No	No			
107	Twisdraai east	20060511	81		No	No			
108	Twisdraai east	20060314	81		No	No			
109	Twisdraai east	20070329	82		No	No			
110	Twisdraai east	20070707	82		No	No			
111	Twisdraai east	20070518	82		No	No			
112	Twisdraai east	20070115	82		Moderate	No			
113	Twisdraai east	20061218	82		No	No			
114	Twisdraai east	20061114	82		No	No			
115	Twisdraai east	20060828	82		No	No			
116	Twisdraai east	20060106	82		No	No			
117	Twisdraai east	20051026	82		No	No			
118	Twisdraai east	20050929	82		No	No			
119	Twisdraai east	20051130	83		No	No			
120	Twisdraai east	20050518	83		No	No			
121	Twisdraai east	20061012	83		No	No			
122	Twisdraai east	20060617	83		No	No			
123	Twisdraai east	20060313	83		No	No			
124	Twisdraai east	20060221	83		No	No			
125	Twisdraai east	20060106	83		No	No			
126	Twisdraai east	20051129	83		No	No			
127	Twisdraai east	20070604	85		High	No			Planar tensile crack
128	Twisdraai east	20070515	85		No	No			
129	Twisdraai east	20071216	85		No	No			
130	Twisdraai east	20070124	85		Moderate	Moderate			
131	Twisdraai east	20061214	85		No	No			
132	Twisdraai east	20061213	85		No	No			
133	Twisdraai east	20061103	85		No	No			
134	Twisdraai east	20061020	85		No	No			
135	Twisdraai east	20060921	85		No	No			
136	Twisdraai east	20060804	85		No	No			
137	Twisdraai east	20060627	85		Moderate	No			
138	Twisdraai east	20060511	85		No	No			
139	Twisdraai east	20060304	85		No	No			
140	Twisdraai east	20060124	85		No	No			
141	Twisdraai east	20060106	85		No	No			
142	Twisdraai east	20051122	85		Moderate	No			
143	Twisdraai east	20060221	86		No	No			
144	Twisdraai east	20060106	86		No	No			
145	Twisdraai east	20050929	86		Moderate	No			
146	Twisdraai east	20070926	development		No	No			
147	Twisdraai east	20080122	81		No	No			
148	Twisdraai east	20080407	82		Moderate	No			
149	Twisdraai east	20080225	82		No	No			
150	Twisdraai east	20080122	82		No	No			
151	Twisdraai east	20071122	82		No	No			
152	Twisdraai east	20071003	82		Moderate	No			Jagged crack // the road
153	Twisdraai east	20070926	82		Moderate	No			
154	Twisdraai east	20070919	82		No	No			
155	Twisdraai east	20080110	83		No	No			
156	Twisdraai east	20070827	83		No	No			
157	Twisdraai east	20080407	85		No	No			
158	Twisdraai east	20080215	85		No	No			Planar tensile crack
159	Twisdraai east	20080110	85		Moderate	No			Planar tensile crack
160	Twisdraai east	20070827	85		Moderate	No			Planar tensile crack
161	Bosjesspruit	20080515	19		No	No			
162	Bosjesspruit	20080505	25		No	No			
163	Bosjesspruit	20070704	25		No	No			
164	Bosjesspruit	20070511	25		No	No			
165	Bosjesspruit	20070208	25		No	No			
166	Bosjesspruit	20061205	25		No	No			
167	Bosjesspruit	20080313	40		No	No			Planar tensile crack
168	Bosjesspruit	20071122	40		Moderate	No			
169	Bosjesspruit	20071031	40		Moderate	No			Planar tensile crack
170	Bosjesspruit	20070919	40		Moderate	No			Planar tensile crack
171	Bosjesspruit	20070802	40		No	No			
172	Bosjesspruit	20070518	40		No	No			
173	Bosjesspruit	20070403	40		No	No			
174	Bosjesspruit	20070417	40		No	No			
175	Bosjesspruit	20070113	40		Moderate	No		0.8	
176	Bosjesspruit	20061211	40		No	No			
177	Bosjesspruit	20080519	45		No	No			
178	Bosjesspruit	20070919	45		No	No			Planar tensile crack
179	Bosjesspruit	20070310	45		No	No			
180	Bosjesspruit	20061201	45		No	No			
181	Bosjesspruit	20061031	45		No	No			
182	Bosjesspruit	20080313	55		No	No			Planar tensile crack
183	Bosjesspruit	20080228	55		No	No			
184	Bosjesspruit	20071120	55		No	No			
185	Bosjesspruit	20070919	55		No	No			Planar tensile cracks
186	Bosjesspruit	20070227	55		No	No			
187	Bosjesspruit	20061211	55		No	No			
188	Bosjesspruit	20080222	56		No	No			
189	Bosjesspruit	20070531	56		No	No			

ID	Mine	Date	Section	Nearest Peg	Guttering	Floor heave	Ride in side wall	depth of guttering	Tensile fracture
190	Bosjesspruit	20061711	56		No	No			
191	Bosjesspruit	20061031	56		No	No			
192	Bosjesspruit	20080527	58		No	No	moderate		
193	Bosjesspruit	20080222	58		No	No			
194	Bosjesspruit	20080313	59		No	No			
195	Bosjesspruit	20080228	59		No	No			
196	Bosjesspruit	20071120	59		No	No			
197	Bosjesspruit	20070919	59		No	No			Planar tensile cracks
198	Bosjesspruit	20070821	59		No	No			
199	Bosjesspruit	20070529	59		No	No			
200	Bosjesspruit	20070227	59		No	No			
201	Bosjesspruit	20061211	59		No	No			
202	Bosjesspruit	20071206	68		No	No			
203	Bosjesspruit	20080527	68		No	No			
204	Bosjesspruit	20080219	68		No	No			
205	Bosjesspruit	20080104	68		No	No			
206	Bosjesspruit	20071218	68		Moderate	No			
207	Bosjesspruit	20070810	68		No	No	Moderate		
208	Bosjesspruit	20070419	68		No	No	moderate		
209	Bosjesspruit	20080605	91		No	No	moderate		
210	Bosjesspruit	20070911	91		No	No			
211	Bosjesspruit	20071011	South		High	No			Planar tensile cracks
212	Bosjesspruit	20071011	South		High	No			
213	Bosjesspruit	20070919	Irenedale shaft						Planar tensile cracks
214	Middelbult	20081028	35		Moderate	no			Planar tensile cracks
215	Middelbult	20081119	33 dyke exposed		No	No			
216	Middelbult	20080912	33		No	No			Planar tensile cracks
217	Middelbult	20080909	33		No	No			
218	Middelbult	20080930	36		No	No			
219	Middelbult	20081104	36		No	No			
220	Middelbult	20080624	36		Moderate	No			
221	Middelbult	20090103	37		No	No			Planar tensile cracks
222	Middelbult	20080818	37		Moderate				
223	Middelbult	20080814	37		No	No			
224	Middelbult	20080822	37		Moderate	No			Planar tensile cracks
225	Middelbult	20080702	37		No	No	Moderate		
226	Middelbult	20080709	37		No	No			
227	Middelbult	20080820	37		No	No	Moderate		
228	Middelbult	20080930	38		High	No	Moderate		Planar tensile cracks
229	Middelbult	20080912	38		Moderate	No	Moderate		Planar tensile cracks
230	Middelbult	20080617	38		No	No			
231	Middelbult	20080624	38		No	No			
232	Middelbult	20080923	41		Moderate	No			
233	Middelbult	20081230	41		No	No			
234	Middelbult	20080801	41		High	No			Planar tensile cracks
235	Middelbult	20080923	42		No	No			
236	Middelbult	20081230	42		No	No	Moderate		
237	Middelbult	20081108	42		No	No			
238	Middelbult	20080930	49		High	No			Planar tensile cracks
239	Middelbult	20080930	49		Moderate	No	Moderate		Planar tensile cracks
240	Middelbult	20081104	49		No	No	High		Planar tensile cracks
241	Middelbult	20080624	49		No	No			Planar tensile cracks
242	Middelbult	20081002	71		No	No			
243	Middelbult	20081129	Main shaft		Moderate	No			
244	Middelbult	20081028	34		High	No			
245	Syferfontein	20080627	3		High	No			
246	Syferfontein	20080709	97		No	No	Moderate		
247	Syferfontein	20090813	2		No	No			
248	Syferfontein	20090724	2		No	No			Planar tensile cracks
249	Syferfontein	20090604	2		No	No			
250	Syferfontein	20091209	92		Moderate	No			Planar tensile cracks
251	Syferfontein	20091202	92		moderate	No			
252	Syferfontein	20091113	92		No	No			
253	Syferfontein	20090404	92		No	No			
254	Syferfontein	20090223	92		No	No			
255	Syferfontein	20091113	95		No	No			
256	Syferfontein	20090805	95		moderate	No			
257	Syferfontein	20090223	95		No	No			
258	Syferfontein	20090930	97		Moderate	No	High		
259	Syferfontein	20090513	97		Moderate	No			
260	Syferfontein	20090825	section I storework		Moderate	No			
261	Syferfontein	20090612	Pit 7		Moderate	No	High		
262	Syferfontein	20090702	Stone work section 1		Moderate	No			Planar tensile cracks
263	Twisdraai Central	20090505	15		No	NO			
264	Twisdraai Central	20090605	20		Moderate	No			Planar tensile cracks
265	Twisdraai Central	20090320	20		No	No			
266	Twisdraai Central	20090211	20		No	NO			
267	Twisdraai Central	20090325	39		No	No	High		
268	Twisdraai Central	20090203	39		Moderate	No	High		
269	Twisdraai Central	20090605	51		No	no			
270	Twisdraai Central	20090417	61		moderate	NO			
271	Twisdraai Central	20090130	61		No	No			
272	Twisdraai Central	20090113	61		NO	NO			
273	Twisdraai Central	20090529	81		No	No	Moderate		
274	Twisdraai Central	20090223	81		No	No	High		
275	Twisdraai Central	20091113	15		NO	NO			
276	Twisdraai Central	20090922	15		No	No			
277	Twisdraai Central	20090824	56		moderate	No			
278	Twisdraai Central	20091110	50		No	No	High		
279	Twisdraai Central	20090724	50						
280	Twisdraai Central	20091118	51		No	No	High		
281	Twisdraai Central	20091113	61		No	No			
282	Twisdraai Central	20091120	61		Moderate	No			
283	Twisdraai Central	20090922	61		NO	No			
284	Twisdraai Central	20090711	61		No	No			

ID	Mine	Date	Section	Nearest Peg	Guttering	Floor heave	Ride in side wall	depth of guttering	Tensile fracture
285	Twisdraai Central	20090820	Stonework: west link		moderate	No			Planar tensile cracks
286	Twisdraai Central	20090807	Stone work: dyke area		No	No			
287	Twisdraai Central	20090706	Aircrossings NW2		No	No	High		
288	Twisdraai Central	20090708	Waterseals:west link		No	No			
289	Twisdraai Central	20091125	76		No	No			
290	Twisdraai Central	20090914	76		No	No	High		
291	Twisdraai Central	20091110	81		No	No	High		
292	Twisdraai Central	20090724	81		No	No			
293	Brandspruit	20091208	10		No	No	moderate		
294	Brandspruit	20090909	Waterseals:west link		No	No	High		
295	Brandspruit	20090910	71C Stonework		No	No	High		
296	Brandspruit	20080926	10		moderate	moderate			
297	Brandspruit	20090127	10		No	No			
298	Brandspruit	20090313	10		Moderate	No			
299	Brandspruit	20090421	17		No	moderate			
300	Brandspruit	20090506	32		Moderate	No			
301	Brandspruit	20090525	32		No	No			Jagged cacks paralled to road
302	Brandspruit	20090505	63		No	No			
303	Brandspruit	20090127	63		No	No			
304	Brandspruit	20090703	main 2 shaft		Moderate	No	High		
305	Brandspruit	20090420	71D Stonework		No	No	moderate		
306	Brandspruit	20090409	87		Moderate	moderate			
307	Brandspruit	20090409	87						
308	Brandspruit	20090606	30 stone works		moderate	No			
309	Brandspruit	20090207	87		moderate	No	High		
310	Bosjesspruit	20090907	19		No	No	High		
311	Bosjesspruit	20090708	19		No	No	High		
312	Bosjesspruit	20090907	25		No	No	High		
313	Bosjesspruit	20090108	25		No	No	High		
314	Bosjesspruit	20091015	26		No	moderate	moderate		
315	Bosjesspruit	20091127	27		No	No	No		
316	Bosjesspruit	20090702	27		No	No	NO		Planar tensile cracks
317	Bosjesspruit	20090514	27		NO	No			
318	Bosjesspruit	20091016	40		moderate	No			
319	Bosjesspruit	20090514	40		No	NO	High		
320	Bosjesspruit	20090702	45		No	No			Planar tensile cracks
321	Bosjesspruit	20091028	55		NO	No			Planar tensile cracks
322	Bosjesspruit	20091016	55		No	No	moderate		Planar tensile cracks
323	Bosjesspruit	20090904	55		moderate	No	High		
324	Bosjesspruit	20090424	55		No	No	High		Planar tensile cracks
325	Bosjesspruit	20090403	55		No	No			Planar tensile cracks
326	Bosjesspruit	20090403	59		moderate	No			
327	Bosjesspruit	20090617	Waterseals		no	No			
328	Bosjesspruit	20090708	19		No	No	High		
329	Bosjesspruit	20090617	27		No	No	High		
330	Bosjesspruit	20090928	Mutala conu 4		moderate	No			
331	Middelbult	20091117	35		NO	No			
332	Middelbult	20091008	35		High	No			
333	Middelbult	20090707	35		No	No	High		
334	Middelbult	20091019	33		NO	NO			Planar tensile cracks
335	Middelbult	20090807	33		No	No			Planar tensile cracks
336	Middelbult	20090530	33		No	No			Planar tensile cracks
337	Middelbult	20090418	33		No	No			
338	Middelbult	20091201	34		moderate	No			Planar tensile cracks
339	Middelbult	20091117	34		moderate	No	moderate		Planar tensile cracks
340	Middelbult	20091029	34		moderate	No			Planar tensile cracks
341	Middelbult	20090916	34		high	No			Planar tensile cracks
342	Middelbult	20090729	34		moderate	No			
343	Middelbult	20090801	34				moderate		
344	Middelbult	20090717	34				High		Planar tensile cracks
345	Middelbult	20090609	34		moderate	No			
346	Middelbult	20090804	36						Planar tensile cracks
347	Middelbult	20090304	36						
348	Middelbult	20090807	37				high		
349	Middelbult	20090418	37				high		
350	Middelbult	20091210	38				high		
351	Middelbult	20090804	38						Planar tensile cracks
352	Middelbult	20090304	38						Planar tensile cracks
353	Middelbult	20090604	41						
354	Middelbult	20090604	42						
355	Middelbult	20090903	49						Planar tensile cracks
356	Middelbult	20090903	49				high		
357	Middelbult	20090903	49		high	No	high		Planar tensile cracks
358	Middelbult	20090319	49				high		Planar tensile cracks
359	Middelbult	20090505	49						Planar tensile cracks
360	Middelbult	20090203	49				high		Planar tensile cracks
361	Middelbult	20091002	33						Planar tensile cracks
362	Middelbult	20091002	33						Planar tensile cracks
363	Middelbult	20090925	Back area 35		moderate		moderate		Planar tensile cracks
364	Middelbult	20090114	34		moderate				
365	Middelbult	20090525	71						

ID	rate of guttering	dyke	Goafs	Rivers	Folding	Faults	Change in dip	Roof Skin	Roof composition
1	Hours								
2		severe					Moderate		Massive SST
3		Moderate					None		Massive SST
4		Moderate							Massive SST
5									Massive SST
6		Moderate	Moderate						Massive SST
7		Moderate	Moderate	Moderate					Massive SST
8				Moderate					Mixed
9				Moderate					Massive SST
10	Hours	Moderate							Massive SST
11		Moderate	Moderate						Massive SST
12			Moderate						Masssive SST
13		High							Masssive SST
14		High	High	High					Massive SST
15		Moderate							Massive SST
16	Hours	High						Medium	SST
17		Moderate						Massive	
18		Moderate						Thin	Mixed
19		Moderate						Thin	Mixed
20		Moderate						Thin	
21				Moderate				Massive	SST
22		Moderate		Moderate				Medim	SST
23		Moderate	Moderate	Moderate				Massive	SST
24		Moderate	Moderate	Moderate				Medium	
25		High	High					Massive	SST
26		Moderate							
27		Moderate	Moderate					Massive	
28		Moderate	Moderate					Massive	
29		Moderate		Moderate				Thin	
30		Moderate						Massive	
31		Moderate						thin	
32	days	High						Medium	
33		High							SST
34		High	High						SST
35		Moderate						Massive	SST
36		High	High					Massive	SST
37		High		HIgh					SST
38		Moderate						Massive	SST
39		High						Medium	Shale
40		High						Medium	Mixed
41	years	High							SST
42		Moderate						Massive	SST
43		Moderate						Medium	
44	years					High			
45	years	High						Medium	SST
46		Moderate						Massive	SST
47	years	Moderate						Medium	
48						Moderate		Medium	
49	years	Moderate						Medium	
50	years	Moderate						Thin	
51	days	Moderate						Medium	Mixed
52	days	Moderate							
53	days					Moderate		Medium	
54		Moderate						Thin	
55	days	High						Thin	Mixed
56		Moderate							
57		Moderate							SST
58		Moderate						Medium	
59		Moderate							
60		High							
61									
62		Moderate						Massive	
63		Moderate							
64		Moderate						Medium	
65		Moderate						Massive	
66		Moderate							
67		Moderate							
68		Moderate							
69		Moderate							
70		High		High				Thin	Shale
71		Moderate							
72	Hours	Moderate							
73	Hours	Moderate						Thin	Shale
74	Hours	Moderate						Medium	
75		Moderate							
76		Moderate						Thin	Mixed
77	days	None						Medium	
78				Moderate				Medium	Mixed
79				Moderate					
80	days	None							SST
81	Hours	None						Medium	
82		High							Shale
83		Moderate						Massive	SST
84		Moderate						Massive	
85		Moderate						Massive	
86						Moderate		Massive	
87	Hours	High						Medium	Mixed
88		High				High		Medium	Mixed
89		Moderate						Thin	
90		Moderate						Massive	
91				Moderate				Massive	
92	days	High						Medium	
93		Moderate						Massive	
94		Moderate						Medium	Mixed

ID	rate of guttering	dyke	Goafs	Rivers	Folding	Faults	Change in dip	Roof Skin	Roof composition
96	Syferfontein	20060515	95		No	No			
97	Syferfontein	20060103	95		No	No			
98	Twisdraai east	20070518	South 4 Vent shaft area		No	No			
99	Twisdraai east	20061220	South 4 Vent shaft area		No	No			
100	Twisdraai east	20060531	DV55 Prim sou	TW726					Single tension Crack
101	Twisdraai east	20060524	Frischgewaagd shaft		No	No			multiple tension crack
102	Twisdraai east	20051209	S4 Dam area		No	No			
103	Twisdraai east	20070531	81		No	No			Planar tensile crack
104	Twisdraai east	20070515	81		No	No			Planar tensile crack
105	Twisdraai east	20071213	81		No	No			
106	Twisdraai east	20060627	81		No	No			
107	Twisdraai east	20060511	81		No	No			
108	Twisdraai east	20060314	81		No	No			
109	Twisdraai east	20070329	82		No	No			
110	Twisdraai east	20070707	82		No	No			
111	Twisdraai east	20070518	82		No	No			
112	Twisdraai east	20070115	82		Moderate	No			
113	Twisdraai east	20061218	82		No	No			
114	Twisdraai east	20061114	82		No	No			
115	Twisdraai east	20060828	82		No	No			
116	Twisdraai east	20060106	82		No	No			
117	Twisdraai east	20051026	82		No	No			
118	Twisdraai east	20050929	82		No	No			
119	Twisdraai east	20051130	83		No	No			
120	Twisdraai east	20050518	83		No	No			
121	Twisdraai east	20061012	83		No	No			
122	Twisdraai east	20060617	83		No	No			
123	Twisdraai east	20060313	83		No	No			
124	Twisdraai east	20060221	83		No	No			
125	Twisdraai east	20060106	83		No	No			
126	Twisdraai east	20051129	83		No	No			
127	Twisdraai east	20070604	85		High	No			Planar tensile crack
128	Twisdraai east	20070515	85		No	No			
129	Twisdraai east	20071216	85		No	No			
130	Twisdraai east	20070124	85		Moderate	Moderate			
131	Twisdraai east	20061214	85		No	No			
132	Twisdraai east	20061213	85		No	No			
133	Twisdraai east	20061103	85		No	No			
134	Twisdraai east	20061020	85		No	No			
135	Twisdraai east	20060921	85		No	No			
136	Twisdraai east	20060804	85		No	No			
137	Twisdraai east	20060627	85		Moderate	No			
138	Twisdraai east	20060511	85		No	No			
139	Twisdraai east	20060304	85		No	No			
140	Twisdraai east	20060124	85		No	No			
141	Twisdraai east	20060106	85		No	No			
142	Twisdraai east	20051122	85		Moderate	No			
143	Twisdraai east	20060221	86		No	No			
144	Twisdraai east	20060106	86		No	No			
145	Twisdraai east	20050929	86		Moderate	No			
146	Twisdraai east	20070926	development		No	No			
147	Twisdraai east	20080122	81		No	No			
148	Twisdraai east	20080407	82		Moderate	No			
149	Twisdraai east	20080225	82		No	No			
150	Twisdraai east	20080122	82		No	No			
151	Twisdraai east	20071122	82		No	No			
152	Twisdraai east	20071003	82		Moderate	No			Jagged crack // the road
153	Twisdraai east	20070926	82		Moderate	No			
154	Twisdraai east	20070919	82		No	No			
155	Twisdraai east	20080110	83		No	No			
156	Twisdraai east	20070827	83		No	No			
157	Twisdraai east	20080407	85		No	No			
158	Twisdraai east	20080215	85		No	No			Planar tensile crack
159	Twisdraai east	20080110	85		Moderate	No			Planar tensile crack
160	Twisdraai east	20070827	85		Moderate	No			Planar tensile crack
161	Bosjesspruit	20080515	19		No	No			
162	Bosjesspruit	20080505	25		No	No			
163	Bosjesspruit	20070704	25		No	No			
164	Bosjesspruit	20070511	25		No	No			
165	Bosjesspruit	20070208	25		No	No			
166	Bosjesspruit	20061205	25		No	No			
167	Bosjesspruit	20080313	40		No	No			Planar tensile crack
168	Bosjesspruit	20071122	40		Moderate	No			
169	Bosjesspruit	20071031	40		Moderate	No			Planar tensile crack
170	Bosjesspruit	20070919	40		Moderate	No			Planar tensile crack
171	Bosjesspruit	20070802	40		No	No			
172	Bosjesspruit	20070518	40		No	No			
173	Bosjesspruit	20070403	40		No	No			
174	Bosjesspruit	20070417	40		No	No			
175	Bosjesspruit	20070113	40		Moderate	No		0.8	
176	Bosjesspruit	20061211	40		No	No			
177	Bosjesspruit	20080519	45		No	No			
178	Bosjesspruit	20070919	45		No	No			Planar tensile crack
179	Bosjesspruit	20070310	45		No	No			
180	Bosjesspruit	20061201	45		No	No			
181	Bosjesspruit	20061031	45		No	No			
182	Bosjesspruit	20080313	55		No	No			Planar tensile crack
183	Bosjesspruit	20080228	55		No	No			
184	Bosjesspruit	20071120	55		No	No			
185	Bosjesspruit	20070919	55		No	No			Planar tensile cracks
186	Bosjesspruit	20070227	55		No	No			
187	Bosjesspruit	20061211	55		No	No			
188	Bosjesspruit	20080222	56		No	No			
189	Bosjesspruit	20070531	56		No	No			

ID	rate of guttering	dyke	Goafs	Rivers	Folding	Faults	Change in dip	Roof Skin	Roof composition
190	Bosjesspruit	20061711	56		No	No			
190				Moderate					SST
191				Moderate					SST
192		Moderate	moderate						
193			moderate						SST
194		High							SST
195		Moderate				moderate			Gritsone
196		High							SST
197		Moderate							SST
198		High	Moderate						SST
199		Moderate							SST
200			Moderate						SST
201		Moderate							SST
202		High							Mixed
203				Moderate					SST
204				Moderate					SST
205			Moderate						
206	years	High							SST
207		high	Moderate						SST
208		Moderate	Moderate						Shale
209		Moderate	Moderate						SST
210		Moderate							SST
211	days	moderate	moderate						
212	years								
213									SST
214	days	High							
215		Moderate							SST
216						High			
217						moderate			
218		Moderate							SST
219		Moderate							SST
220		Moderate							mudstone
221						moderate			
222						moderate			Mixed
223		Moderate							SST
224						high			Mudstone
225						Moderate			SST
226						Moderate			
227						High			SST
228	Hours								SST
229	Hours								SST
230		Moderate	Moderate						Mixed
231						High			SST
232		Moderate	Moderate						Shale
233		Moderate							Shale
234	Hours	Moderate							SST
235		Moderate							Mixed
236						Moderate			
237		Moderate		Moderate	Moderate				SST
238						High			SST
239	days					Moderate			SST
240									SST
241		Moderate							SST
242		Moderate							
243		Moderate							
244	Hours	Moderate		moderate					Mixed
245	Hours	Moderate							Mixed
246		Moderate							SST
247		Moderate				moderate			
248		Moderate							Mixed
249		moderate						uneven	
250	Hours	Moderate							
251	Hours	moderate							
252		Moderate							
253		Moderate							
254		Moderate							
255		Moderate							
256		Moderate							
257		moderate							
258						High			
259	Hours				moderate				
260	Hours	moderate							SST
261	days	moderate							Mixed
262		moderate							
263		Moderate							Mixed
264		moderate	moderate						Mixed
265		moderate		Moderate					
266		Moderate	moderate						Mixed
267		Moderate				moderate			SST
268						Moderate			
269		Moderate	moderate						SST
270	days	Moderate							Mixed
271		Moderate	moderate						Mixed
272		High							Mixed
273		Moderate	moderate			moderate			SST
274			moderate	moderate		moderate			SST
275		Moderate	moderate						
276		Moderate							Mixed
277		Moderate	moderate	moderate					Mixed
278			moderate						SST
279			moderate						SST
280		moderate	moderate						
281		Moderate	moderate						
282		Moderate	moderate						Mixed
283		moderate							Mixed

ID	rate of guttering	dyke	Goafs	Rivers	Folding	Faults	Change in dip	Roof Skin	Roof composition
284		Moderate							Mixed
285	days	moderate							Mixed
286		moderae							Shale
287									
288		moderate							
289		moderate	moderate						Mixed
290		moderate							Mixed
291			moderate						
292			moderate						SST
293		moderate							Mixed
294		moderate	moderate						
295		moderate		moderate					
296			moderate						SST
297		moderate							Mixed
298		moderate							
299		moderate	moderate						SST
300	days	moderate				moderate			Mixed
301									
302		moderate							Mixed
303		moderate	moderate						Mixed
304	days	moderate				moderate			Mixed
305		moderate		moderate					Mixed
306	days	moderate							Mixed
307		moderate							
308	days	moderate							
309	days	moderate	moderate			moderate			Mixed
310		moderate							
311		moderate							SST
312			moderate						SST
313			moderate						Mixed
314			moderate						SST
315						High			SST
316									Mixed
317		moderate							SST
318	days	High	moderate						
319		moderate	moderate						Mixed
320		moderate							Shale
321						moderate			Mixed
322									Mixed
323		moderate							Mixed
324		moderate				moderate			Shale
325		moderate							
326		moderate							
327		moderate							
328		moderate							SST
329		moderate							Mixed
330	days	moderate			moderate	moderate			
331		moderate				moderate			
332			high						Mixed
333		moderate							Mixed
334						high			SST
335									SST
336		moderate				moderate			SST
337		moderate				moderate			Mixed
338	days								
339	days	moderate				moderate			Mixed
340	days					moderate			
341	hours								
342									
343									mudstone
344						moderate			
345						High			Mixed
346									SST
347		moderate							
348		moderate							SST
349		moderate							
350		moderate							mixed
351									
352		moderate							
353		moderate		moderate					mixed
354						moderate			mudstone
355		moderate							
356		moderate							
357		moderate							SST
358		moderate				moderate			SST
359		moderate							
360		moderate							
361		moderate							
362		moderate				moderate			
363						high			Mixed
364		moderate							
365		moderate							SST